AEC RESEARCH AND DEVELOPMENT REPORT

ORNL-2457
Special

THE ORNL THERMONUCLEAR PROGRAM

OAK RIDGE NATIONAL LABORATORY
OPERATED BY
UNION CARBIDE NUCLEAR COMPANY
Division of Union Carbide Corporation
UCC
POST OFFICE BOX X · OAK RIDGE, TENNESSEE

[redacted]

ORNL-2457
Special

This document consists of 176 pages.
Copy 41 of 156 copies. Series A.

Contract No. W-7405-eng-26

SHERWOOD PROJECT

THE ORNL THERMONUCLEAR PROGRAM

Editoral Committee

P. R. Bell
J. S. Luce
R. J. Mackin, Jr.
E. D. Shipley
A. Simon

Other Contributors

C. F. Barnett
E. S. Bettis
D. S. Billington
C. W. Blue
R. E. Clausing
J. H. Crawford, Jr.
R. A. Dandl
J. W. Flowers
W. F. Gauster
D. T. Goldman
W. R. Grimes
E. Guth
R. J. Kerr
W. D. Manly
E. R. Mann
J. R. McNally, Jr.
C. D. Moak
R. V. Neidigh
C. E. Normand
M. Rankin
J. A. Ray
H. K. Reynolds
M. T. Robinson
P. M. Stier
C. H. Weaver
O. C. Yonts

DATE ISSUED

JAN 15 1958

OAK RIDGE NATIONAL LABORATORY
Operated by
UNION CARBIDE NUCLEAR COMPANY
Division of Union Carbide Corporation
Post Office Box X
Oak Ridge, Tennessee

[redacted]

[redacted]

ORNL-2457
Special

INTERNAL DISTRIBUTION

1. A. M. Weinberg
2. J. A. Swartout
3. A. H. Snell
4. R. A. Charpie
5. A. Simon
6. E. Guth
7. J. S. Luce
8. P. R. Bell
9. E. D. Shipley
10. R. S. Livingston
11. R. J. Mackin, Jr.
12. C. E. Normand
13. C. F. Barnett
14. C. W. Blue
15. W. R. Chambers
16. R. E. Clausing
17. R. A. Dandl
18. W. F. Gauster
19. R. P. Jernigan
20. R. J. Kerr
21. R. V. Neidigh
22. M. Rankin
23. H. P. Yockey
24. B. L. Cohen
25. M. J. Skinner
26. P. M. Reyling
27. J. H. Crawford, Jr.
28. E. R. Mann
29. J. R. McNally, Jr.
30. C. D. Moak
31. C. H. Weaver (consultant)
32. O. C. Yonts
33. E. S. Bettis
34. J. A. Ray
35. W. D. Manly
36. W. R. Grimes
37. D. S. Billington
38. M. T. Robinson
39. Sherwood Reading File (Virginia Glidewell)
40. Sherwood Reading File (P. R. Bell)

41-43. Central Research Library

44. ORNL – Y-12 Technical Library, Document Reference Section

45-144. Laboratory Records Department

EXTERNAL DISTRIBUTION

145-156. A. E. Ruark, AEC, Washington

[redacted]

[redacted]

CONTENTS

[redacted]

[redacted]

PART II. SUPPORTING PROGRAM OF BASIC RESEARCH

[redacted]

APPENDIXES

[redacted]

[redacted]

[redacted]

ABSTRACT

The Controlled Thermonuclear Reactor Program at the Oak Ridge National Laboratory is outlined. Trapping of a beam of 300-kev deuterons has been achieved in the Direct Current Experimental Facility (DCX). Construction and installation of the very-high-vacuum internal system has been completed. All parts of the internal system can be baked at 400°C, and a base pressure of 3×10^{-8} mm Hg has been attained. A liquid-helium pump is under construction to provide complete pumping for all gases, other than helium, and other types of pumps are being studied. The high-current carbon arc has been shown to act as a strong ion pump. The DCX ion source is being redesigned for higher current and pulsed operation in order to facilitate analysis. Improvement of the DCX magnetic field configuration is planned. Development work is proceeding on a 2-amp, 600-kv accelerator tube and power supply to provide a very large input of molecular ions. Many diagnostic techniques are being developed to study the hot plasma in DCX and in future devices.

DCX experiments are described, related to the design of a proposed new facility (ORION). This facility should be capable of producing a self-sustaining thermonuclear plasma. The machine, as now conceived, will be similar to DCX, but provision will be made to compress the trapped deuteron plasma by a step-function rise in the magnetic field. The final field will be strong enough to contain the charged products of thermonuclear reactions. Both molecular-ion injection and the injection of energetic neutral atoms will be utilized in this device. When built, ORION will be used to study the critical value of β for a self-sustaining reaction and the stability of a thermonuclear plasma under various conditions. Various methods of extracting power from the plasma will be investigated.

The successful operation of ORION would lead to the construction of an intermediate-sized reactor with which the scaling problems associated with large power-producing thermonuclear reactors would be studied. A description of a full-scale power reactor is outlined.

Part II of this report describes a strong basic program under way at ORNL to support and augment the experimental work on large devices. The characteristics of high-energy arcs are under investigation. Several kinds of energetic-molecular-ion sources are being tested in addition to an energetic-neutral source. A program of fundamental vacuum research is being carried out including continuing measurements on the sputtering rate of metals under energetic ion bombardment. Improvements are being made in diagnostic techniques, particularly in the use of probes and in spectrographic analysis. Metallurgical and radiation-damage problems are being studied.

The theoretical group is studying fundamental problems associated with the formation and behavior of a thermonuclear plasma ignited by the injection method used at ORNL.

[redacted]

Part I

THERMONUCLEAR REACTOR DEVELOPMENT PROGRAM

1. INTRODUCTION

The Thermonuclear Experimental Program at ORNL is directed toward the attainment of thermonuclear reactions through the injection of high-energy particles into a containing magnetic field. These particles are trapped within the field by a change of charge condition (e.g., from D_2^+ ions to D^+ ions, or from fast neutral atoms to D^+ ions).

This approach was made feasible by the discovery at ORNL of a new type of arc (Appendix E), a high-current vacuum carbon arc, which has a very high efficiency for dissociating energetic molecular ions which pass through it.

The accumulated trapped deuterons accomplish two things: they ionize, and thus facilitate the removal of, the residual neutral gas in the vacuum system; and, upon becoming thermalized, they produce a plasma whose temperature is above that required for the extensive production of thermonuclear reactions.

This report describes a series of experiments and developments directed toward the final attainment of a power-producing thermonuclear reactor. The high-energy injection methods can be applied to many containment geometries by suitable arrangements. In particular, the application to a toroidal geometry with helical windings seems almost as attractive as the use with a straight mirror machine.

Mirror geometry, although quite convenient, suffers from large losses through the mirrors. In view of these losses, a machine with a practical mirror ratio could maintain a self-sustaining reaction in a mixture of deuterium and tritium (Sec 10.2.1), but not in deuterium alone. By connecting the exit sides of the mirrors with a loop of Stellarator-like tubing whose magnetic field is as large as that between the mirrors, a great reduction of losses could be obtained, and operation on deuterium alone should be possible. Operation with deuterium has two major advantages: (1) The rigid neutron economy necessary to keep the tritium breeding factor above 1 would no longer be required. (2) A greater proportion of power could be extracted from the machine by field variation; thus, to some extent, the difficulties of a heat-electricity conversion could be avoided. However, because of its simplicity, only mirror geometry is considered in this report.

A schematic outline of the program is shown in Fig. 1.1.1. In this figure is shown the succession of experimental devices which it is believed will culminate in the construction of a full-scale thermonuclear generator of electrical power. The time scale on the left side of the figure is based on, among other things, an assumed level of effort which may appear wholly unrealistic within a very short time. The "major events" shown on the right mark the real dividing lines of interest between one instrument and the next. In each case, the final major event associated with a device represents the achievement of the goal for which that device was designed.

Although the diagram represents a single thread of development based on the change-of-state injection and trapping concept (Luce injection system), the present program does include other investigations of plasma phenomena which show possibilities of having thermonuclear applications (Sec 12). In fact, the greater part of the supporting research program described in Part II is sufficiently broadly based that it regularly discloses new information and insights of general thermonuclear interest.

At the present (January 1958), the experimental work is concentrated principally on the DCX equipment. This equipment, shown in Fig. 1.1.2 and described in Sec 2, achieves trapping of deuterons inside its mirror magnetic field by the dissociation of a 600-kev molecular deuterium ion beam with a high-energy vacuum carbon arc or a high-energy deuterium arc. Successful trapping was first accomplished in this equipment on August 21, 1957, and is considered the first major event in the program.

The vacuum conditions in DCX will be improved and the incoming beam current increased until the residual gas can be completely ionized by the incoming beam. When this condition (called "burnout")[1] is reached, the trapped ions will be lost much more slowly, and a plasma of hot ions and electrons is expected to form. The attainment

---

[1]A. Simon and M. Rankin, *Some Properties of a Steady State High-Energy Injection Device (DCX)*, ORNL-2354 (Aug. 26, 1957) (Appendix A of this report).

ORNL-LR-DWG 25991

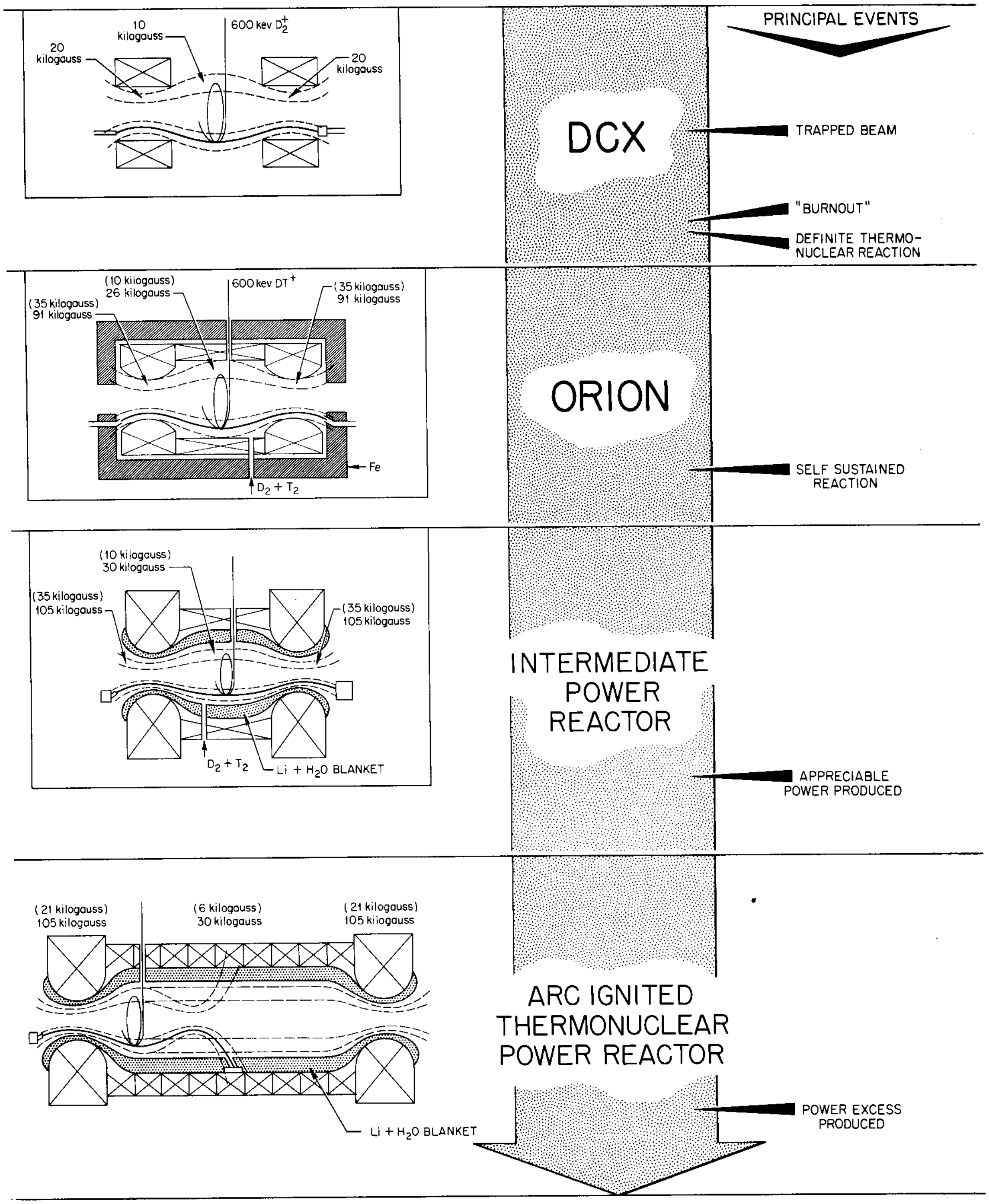

Fig. 1.1.1. ORNL Thermonuclear Program.

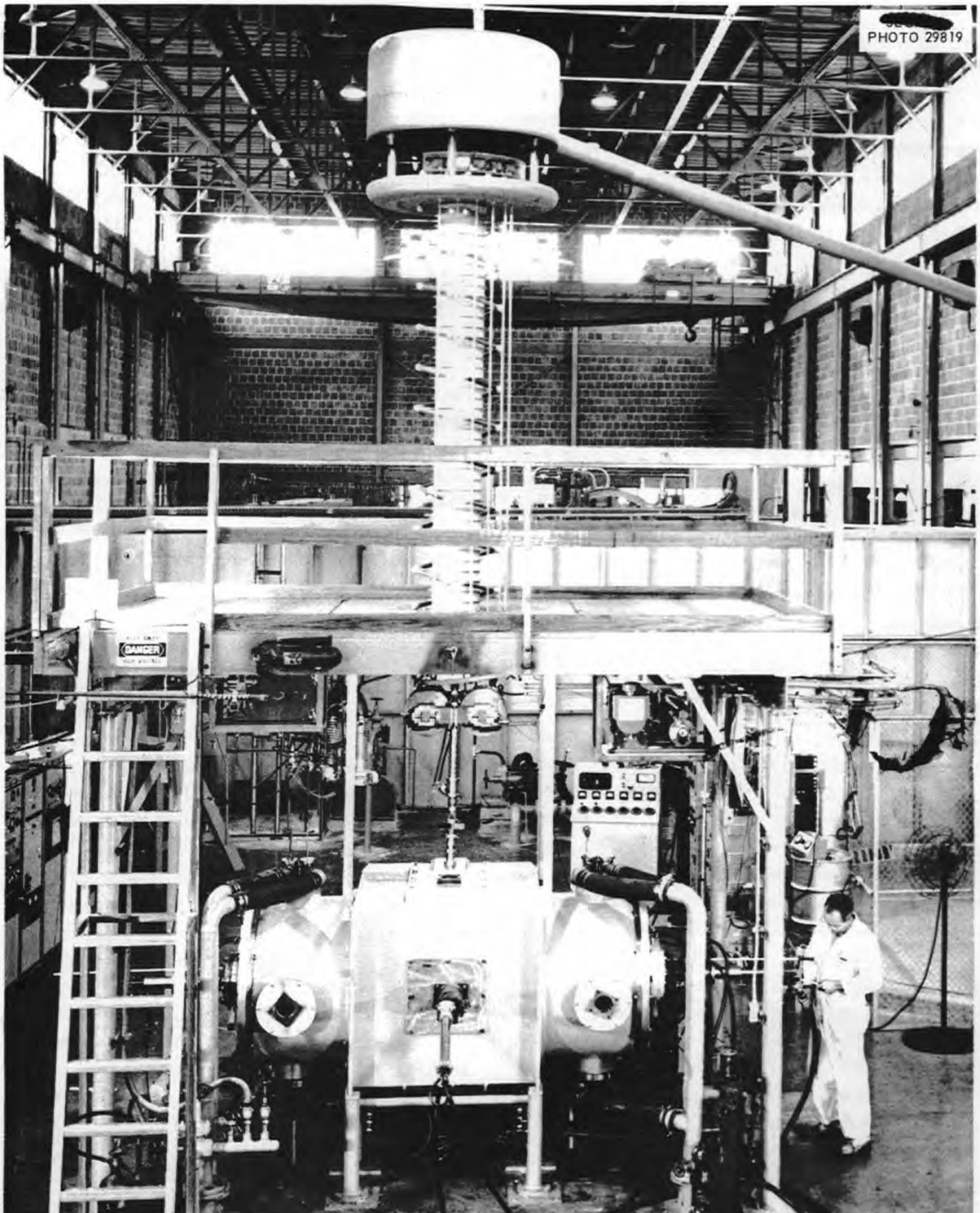

Fig. 1.1.2. DCX Facility.

of "burnout" condition will be our second major event.

The plasma formed after burnout is reached should have an effective temperature which may be as great as 250 kev,[1] and thermonuclear neutrons should be produced to such an extent that the neutron level, which before burnout will be principally produced in the walls and neutral gas of DCX, will rise by a factor of 10^4 to 10^5 (Sec 6.3). This distinct rise in neutron level will indicate the production of a definite thermonuclear reaction, which will be our third major event.

The magnetic fields in the DCX machine are too small to contain the reaction products of the thermonuclear reactions, and a self-sustaining reaction cannot be produced in it. Another facility must be constructed with a stronger magnetic field and a higher mirror ratio if a self-sustaining thermonuclear reaction, fed by cold gas, is to be demonstrated (Sec 10.2.1). This second machine, ORION (Fig. 1.1.1), will have a central field value of about 26 kilogauss and a mirror field of about 91 kilogauss. These fields in DCX are 10 and 20 kilogauss, respectively. The coils will be designed to permit increasing the field rapidly. The purpose of increasing the field is to compress the plasma associated with the trapped atomic ions, and to contain reaction products. It has been shown that molecular-ion injection must stop when the field is increased (Sec 7.2), and neutral-atom injection will then be used. It will be possible to use energetic neutrals if they are needed. These neutrals will be ionized by collisions in the compressed plasma.

When the plasma has reached its maximum density and impurities in the working volume have been "cleaned up," cold deuterium and tritium gas will be fed into the plasma and the energetic neutral beam stopped. A self-sustaining plasma, heated by thermonuclear reactions, is expected to result from this procedure. The system is extremely flexible, and several procedures will be tried. It may be possible to compress the trapped ions and inject cold gas immediately, thus eliminating the energetic–neutral injection phase.

When a self-sustaining plasma has been created, various schemes of power extraction will be studied. In addition to the power represented by the production of energetic charged particles, which most desirably would be converted directly into electrical power, that large amount of power that is dissipated by neutrons and radiation must be used. Many of the neutrons can presumably be trapped in a surrounding blanket containing lithium, for the further generation of nuclear power (about 5 Mev per neutron captured) and regeneration of the tritium burned in the reaction. A heat cycle will be necessary in order to convert power from these sources to a useful form. The problems associated with reactions in the lithium hydride blanket, radiation damage, shielding, huge copper coils, etc., must be resolved before a power-producing reactor can be built. These and other problems will be studied in the third device shown in Fig. 1.1.1, the Intermediate Power Producer.

When the problems outlined above have been solved, an actual power producer will be constructed. A description of the proposed reactor is contained in Sec 10. It is obvious that this reactor, to be practical, must be much larger than its predecessors. Filling this large volume with a plasma at thermonuclear temperature is a major problem. As described in Sec 10, the problem is to be solved by filling a small volume first. After burnout is achieved, the volume is slowly expanded until the entire reactor is filled. This slow filling is achieved by proper manipulation of the magnetic field. It is interesting to note that this method of filling could be used to fill reactors using toroidal or other geometries as well as those using mirror fields.

2. PRESENT STATUS OF DCX EXPERIMENTAL PROGRAM

2.1 DESCRIPTION OF DCX

DCX is a device designed to create a high-temperature plasma by dissociating energetic D_2^+ ions and trapping the resulting D^+ ions, whose path within the magnetic field will have only half the radius of the D_2^+ ion path. A 600-kev D_2^+ beam is injected into the reaction chamber of DCX by a vertically mounted 600-kv, d-c cascade accelerator (Fig. 1.1.2). The beam path lies in the plane which is the perpendicular bisector of the magnetic axis. A large fraction of the D_2^+ ions are dissociated ($D_2^+ \longrightarrow D^+ + D^0$) when they pass through a 300-amp high-energy carbon arc whose electrodes are mounted on plates at each end of DCX.

The atomic ions are trapped in a mirror magnetic field that is produced by two four-layer copper coils. Each coil is 12 in. long, with an outside diameter of 27½ in. and an inside diameter of 17¼ in. Each layer is constructed of edge-wound ¼ in. × 1 in. copper bar stock, and has 3/16-in.-dia holes, spaced 1 in. apart, drilled through the 12-in. length of the coil. Each coil is potted in Epon and enclosed in a ¼-in.-thick stainless steel case with water headers provided at each end of the coil. Direct current is provided for the coils by two 1750–kw generators connected in series. Three megawatts of power are used in the two coils.

A high-vacuum, bakable internal copper liner (Sec 3, Fig. 3.3.2, Fig. 3.3.3) is mounted between the coils, which are spaced 17 in. apart in DCX. The liner is evacuated by four oil diffusion pumps, each of which has a nominal pumping speed of 1400 liters per second. Appropriate water-cooled and liquid-nitrogen-cooled baffling is provided to act as an oil barrier and to create a very high vacuum in the interior of the liner. The liner can be heated to 400°C by superheated steam driven through the lines which are used for the cooling water during operation. The coils and the liner are mounted in a stainless steel housing, 7½ ft long and approximately 40 in. in diameter. This housing is also evacuated with four diffusion pumps, but cannot be baked out as can the internal system.

2.2 EXPERIMENTAL RESULTS TO DATE, AND CURRENT ACTIVITIES

The early operation of DCX has shown that a molecular deuterium ion beam can be injected into a mirror geometry in a plane perpendicular to the mirror axis, and that this beam can be dissociated with high efficiency and the resulting atomic ion beam trapped inside the mirror field.

No difficulty was encountered in injecting the molecular ion beam, and a good focus was obtained in the region of closest approach to the mirror axis. This good focus will allow a small-diameter arc to be used for breakup (dissociation and/or ionization), which will result in minimal contamination of the mirror region by ions and electrons from the arc.

The vacuum carbon arc operates very well in the mirror geometry with the cathode and anode inside or outside the mirror field maximum, and difficulties of operation are even less with the arc off the axis of the mirror system than on it. The troubles produced in on-axis operation, resulting from the considerable current of ions that miss the cathode and cause heating and electron emission from the cathode support assembly, are not present in off-axis operation. In this case, the ions follow flux lines that terminate on the liner, which is at a more positive potential than the cathode and thus does not emit electrons. Figures 2.2.1 and 2.2.2 are side and end views of the arc running in DCX.

Dissociation by the carbon arc has been found to proceed with a 25% efficiency for a 300-amp arc current. A high-energy deuterium arc has been tested and found to operate at comparatively low pressure and to produce appreciable dissociation of molecular ions. It is described in Appendix I.

A circulating trapped deuteron beam has been observed visually. The reaction volume was found to be filled with small carbon particles which became white hot upon passing through the ring formed by the circulating deuterons. When the number of these particles was reduced by baffling placed in front of the electrodes, the position of the ring was marked by a red glow, with a cross section of about 0.5 × 0.5 in. It is possible that

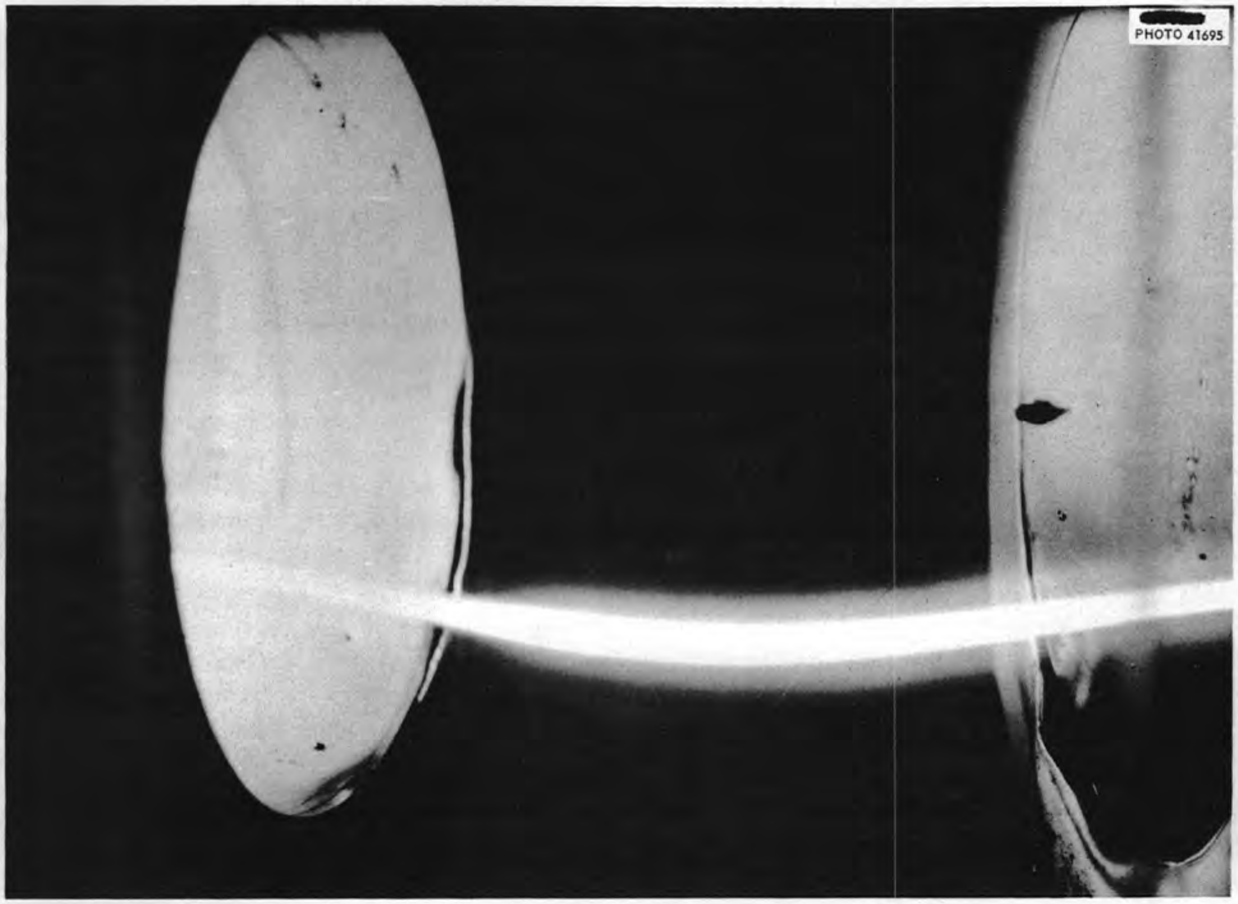

Fig. 2.2.1. Operation of the Carbon Arc in DCX. Side view.

the glow was produced by de-excitation of deuterium atoms formed by charge exchange.

In initial experiments with the inner liner, 400°C baking was performed for 24 hr. A base pressure of 3×10^{-8} mm Hg was achieved within the liner. Operation of the carbon arc at this pressure has not yet been attempted.

The condition of burnout, in which the residual gas in the machine is essentially all ionized, must be obtained before appreciable plasma density can be achieved. The necessary conditions for burnout (Appendix A) are not yet available, and our immediate program is directed toward satisfying these conditions in DCX. Considerably greater injection current and much better vacuum are required. For each value of residual gas pressure, there is a critical injection current required for burnout. For a pressure of 10^{-7} mm Hg, the critical dissociated ion current is about 8 ma for a molecular ion energy of 600 kev. If a lower pressure is attained, the critical current is lowered in direct proportion.

A major point of uncertainty in estimates concerning DCX is the ultimate pressure attainable in the presence of the carbon arc. In recent experiments in the long solenoid facility a pressure of 5×10^{-7} mm Hg was achieved in an unbaked chamber through which the arc passed. More details of the arc's vacuum properties are given in Sec 3.2.

Achievement of burnout presupposes the ultimate removal from the system of most or all of the low-energy ions which are produced. Various schemes for accomplishing this are under development and are described in Sec 3.

Much diagnostic equipment is being installed in order that good measurements of the plasma conditions in DCX may be made. Probes, neutron

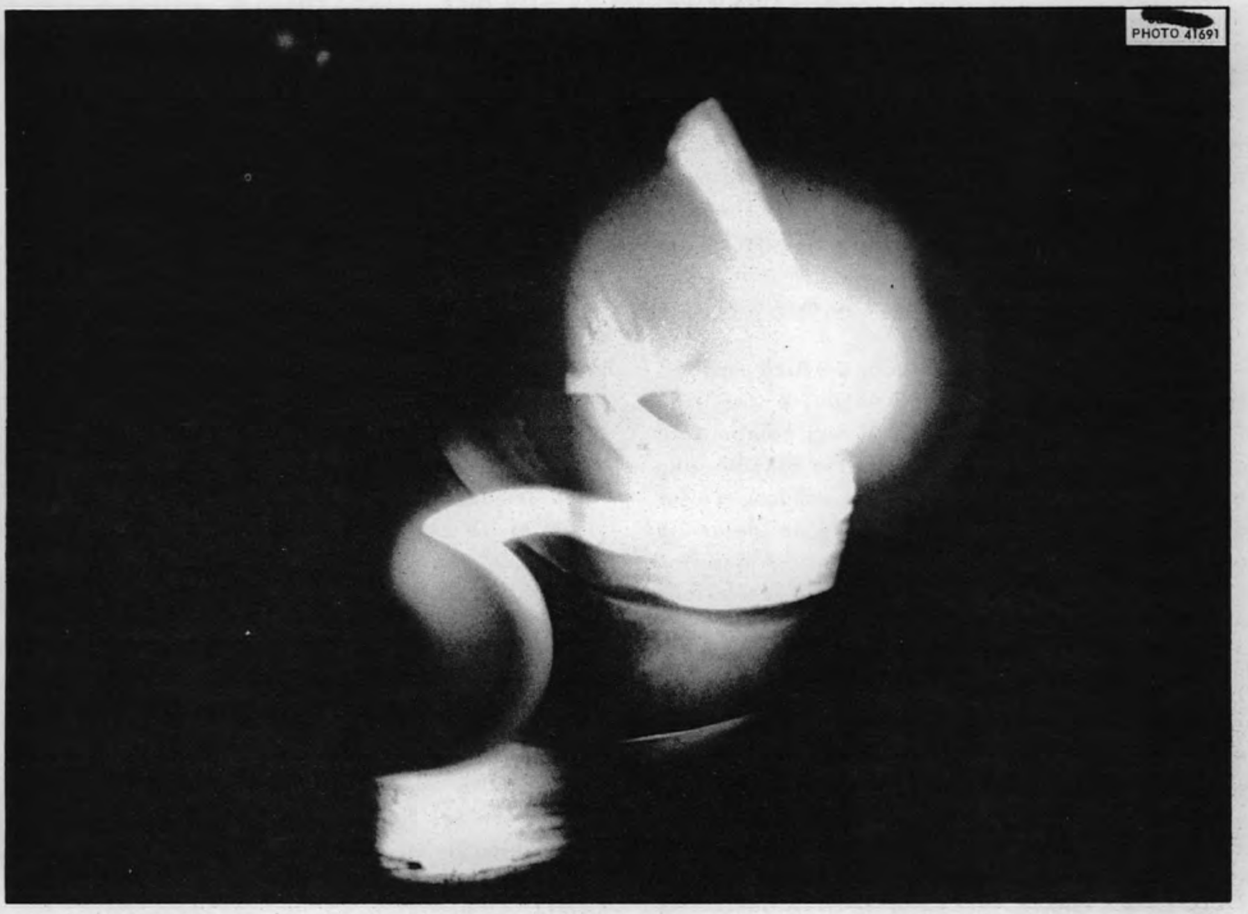

Fig. 2.2.2. Operation of the Carbon Arc in DCX. View from anode end.

counters, x-ray counters, microwave electron-density equipment, optical equipment, and spectrographs are among the devices already available. Clearly DCX represents an extremely difficult environment in which to conduct carefully controlled experiments. One response to this problem has been to provide for continuous monitoring and recording of a large number of supplementary data which might constitute relevant parameters of the experiment. Another response has been to conduct, wherever possible, parallel control experiments outside of DCX in order to determine the interactions between various components or to determine the otherwise uncertain performance of some device in DCX.

A more detailed description of the experimental program proposed for DCX for the fiscal years 1958 and 1959 follows.

3. LOWER PRESSURE FOR DCX

The criterion for burnout[1] is that the net rate of neutral gas removal from the plasma volume exceed the rate of influx. The influx is proportional to the pressure in the plasma region; hence the need to achieve the best possible vacuum. The rate of removal, taken to be the ionization rate by the trapped deuterons, is proportional to the input (trapped) current; hence the need to maximize this quantity.

There are, however, other factors which must be taken into account and which may play a vital role in determining the ease with which burnout is achieved. The first of these is the dissociating arc, whose possible effects on the vacuum, so far as these are known, are discussed in detail in Sec 3.2. The second arises from a consideration of the low-energy ions produced in collisions between the trapped deuterons and the gas molecules. In the original burnout calculations, these ions were regarded as removed from the system, as far as their subsequent effects are concerned. However, as pointed out by D. Alpert, it is necessary to recognize that they will quickly scatter into the mirror loss cone, strike the liner wall, become neutralized, and (in some fraction) return to the system. Minimization of the fraction of the ions which so return is a major aspect of the vacuum problem. It is discussed in Sec 3.7.

3.1 PRESENT STATUS OF DCX VACUUM

The DCX vacuum system consists of two chambers, one contained within the other. The outer one is a conventional high vacuum chamber of welded stainless steel construction with numerous rubber-gasketed closures. It is pumped by high-speed oil diffusion pumps with water-cooled and liquid-nitrogen-cooled baffling. The inner chamber, or liner, is of all-metal construction, and is designed to achieve pressures below 10^{-8} mm Hg.

The initial DCX experiments were conducted without the inner vacuum system. A temporary water-cooled liner was provided to protect the casings of the mirror coils from the heat of the arc (300 w/in.). These experiments gave the information necessary for the final design of the inner chamber, notably, the points of entry and exit of the molecular ion beam and the carbon arc, whose electrodes will be situated in the outer chamber. The pressures achieved during these operations were 6×10^{-6} mm Hg without the carbon arc and 9×10^{-6} mm Hg with the arc running.

The inner chamber has been installed and baked, and a pressure (without arc or beam) of 3×10^{-8} mm Hg has been achieved.

3.2 THE CARBON ARC

A major problem in the design of the high-vacuum liner is the disposition of the carbon arc. By virtue of its great ionizing power, the arc promises to provide considerable pumping action; however, for this to be effective, it is necessary to place the electrodes outside the liner. This is essential both because of the recombination of ionized gases at the electrodes and because of the great amounts of gas evolved there.

Estimates, using plausible cross sections for ionization by the primary electrons, suggest that the arc ionizes nearly all of the gas atoms which pass through it. This suggestion is strongly supported by the finding[2] that the arc has a 12% efficiency for removing the second electron from 20-kev nitrogen (N^+) ions. The effect for lower-energy ions would be expected to vary inversely as the ion (or atom) velocity, inasmuch as it probably is produced by energetic electrons and will be proportional to the time taken in passing through the arc.

Experiments to test this idea have been made in the long solenoid facility, and preliminary results indicate that the arc ionizes 85% of argon gas passing through it and 50% of air. Pumping by adsorption by deposited carbon was found to be strong for air and very weak for argon, in accord with previous experiments.[3] The base pressure achieved in these experiments, in a region corresponding to the DCX liner, was 5×10^{-7} mm

[1] A. Simon and M. Rankin, *Some Properties of a Steady State High-Energy Injection Device (DCX)*, ORNL-2354 (Aug. 26, 1957) (Appendix A of this report).

[2] J. S. Luce, *Ionization and Dissociation of Energetic Ions by a Carbon Discharge – Status Report*, ORNL-2219 (Jan. 1957); see also Appendix E of this report.

[3] C. E. Normand, O. C. Yonts, and C. W. Blue, p 462 in *Controlled Thermonuclear Reactions: A Conference Held at Berkeley, California, Feb. 20–23, 1957*, TID-7536 (Part 2).

Hg. The pressure in the region of the electrodes was a factor 20 higher. All evidence thus supports very strongly the expectation that the arc will contribute significantly to reducing the pressure in DCX.

An arc section 75 cm long and 2 cm in diameter, if completely absorbing, will have a theoretical pumping speed of 5500 liters/sec for deuterium gas. Its ionizing effect at 10^{-6} mm Hg will be equal to that of a 1-ma trapped deuteron beam. The latter figure is based on the ratio of approximately 32 to 1 between the ionization cross section[4,5] and the charge-exchange cross section for 300-kev deuterons bombarding deuterium (Appendix B.1). Each deuteron, on the average, will produce 33 ions during the time it is trapped in DCX. The figure for nitrogen is 29 ions per deuteron.

The ionizing power of the arc is also counted upon to isolate the very high vacuum region from the outer chamber. The arc will be run through a series of close-fitting carbon baffles mounted in the liner wall, so that any entering gas will be constrained to pass through the arc several times. An attenuation factor equal to the pressure ratio is necessary in order that these apertures will not act as leaks into the liner. Arc operation through close-fitting baffles has already been achieved in experiments in DCX.

The outgassing of the carbon electrodes will be drastically diminished by the following purification procedure:[6] The electrodes, while enclosed in a carbon capsule through which chlorine is flowed, will be heated to 2600°C and kept at this temperature until all foreign materials in the electrodes have been removed. The chlorine will then be replaced by a helium atmosphere in which the electrodes will be allowed to cool. The electrodes will then be placed in a vacuum furnace and the helium removed by heating to 1200°C. They will then be stored under vacuum until needed for DCX. The electrode assemblies are mounted through vacuum locks so that electrodes can be replaced without losing the vacuum in DCX.

A possible deleterious effect of the carbon arc may be the action of its intense, hard, ultraviolet radiation in releasing occluded gas from the liner wall. There seems to exist essentially no information on the magnitude of this effect.

An attractive substitute for the carbon arc appears to be the recently developed high-energy deuterium arc (Appendix I). Although it has not been operated at pressures below 5×10^{-5} mm Hg, there is no evident obstacle to lower pressure operation if the electrodes are situated in a separate volume.

3.3 THE VERY-HIGH-VACUUM LINER

Figure 3.3.1 is a schematic diagram of the DCX vacuum system. In making this drawing, various sections have been rotated about the center line so that they lie in the plane of the drawing. Figures 3.3.2 and 3.3.3 show the liner before installation of windows and ports.

The important design features of the liner and many of the obstacles to its achieving its purpose are evident in the figures. The following are among the more significant features:

a. There is provision for extended baking at high temperature (400°C) by combined use of the carbon arc and of superheated steam in the water lines. All surfaces which will be exposed to the very-high-vacuum region will be baked. Successful experiments with this system of baking have been conducted, and a pressure of 3×10^{-8} mm Hg has been achieved with the arc apertures plugged. (In this experiment, only one end of the inner chamber was pumped.) Stainless steel Sylphon bellows are used as thermal barriers between the surfaces to be baked and the walls of the outer chamber.

b. Use of a one-piece liner would entail removal of the mirror coils each time the liner was removed. To avoid this inconvenience, the liner was constructed in several individually removable sections. The joints had sliding metal-to-metal seals with a double overlap as shown in the following sketch.

UNCLASSIFIED
ORNL-LR-DWG 26267

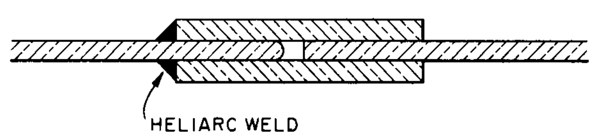

---

[4] H. K. Reynolds *et al.*, *Phys. Rev.* 92, 742 (1953).

[5] H. A. Bethe and J. Ashkin, *Experimental Nuclear Physics* (ed. by E. Segre), vol I, p 233, Wiley, New York, 1953.

[6] Purification process recommended by the National Carbon Co.

With expected tolerances and a pressure of 10^{-5} mm Hg in the outer chamber, the leak rate was not expected to be significant. Achieving these tolerances turned out to be difficult enough, however, that it was found expedient to close all but the end joints with Heliarc welds. Diagnostic apparatus may be inserted into the center section through access ports which use smaller sliding joints. These do not add a significant leak.

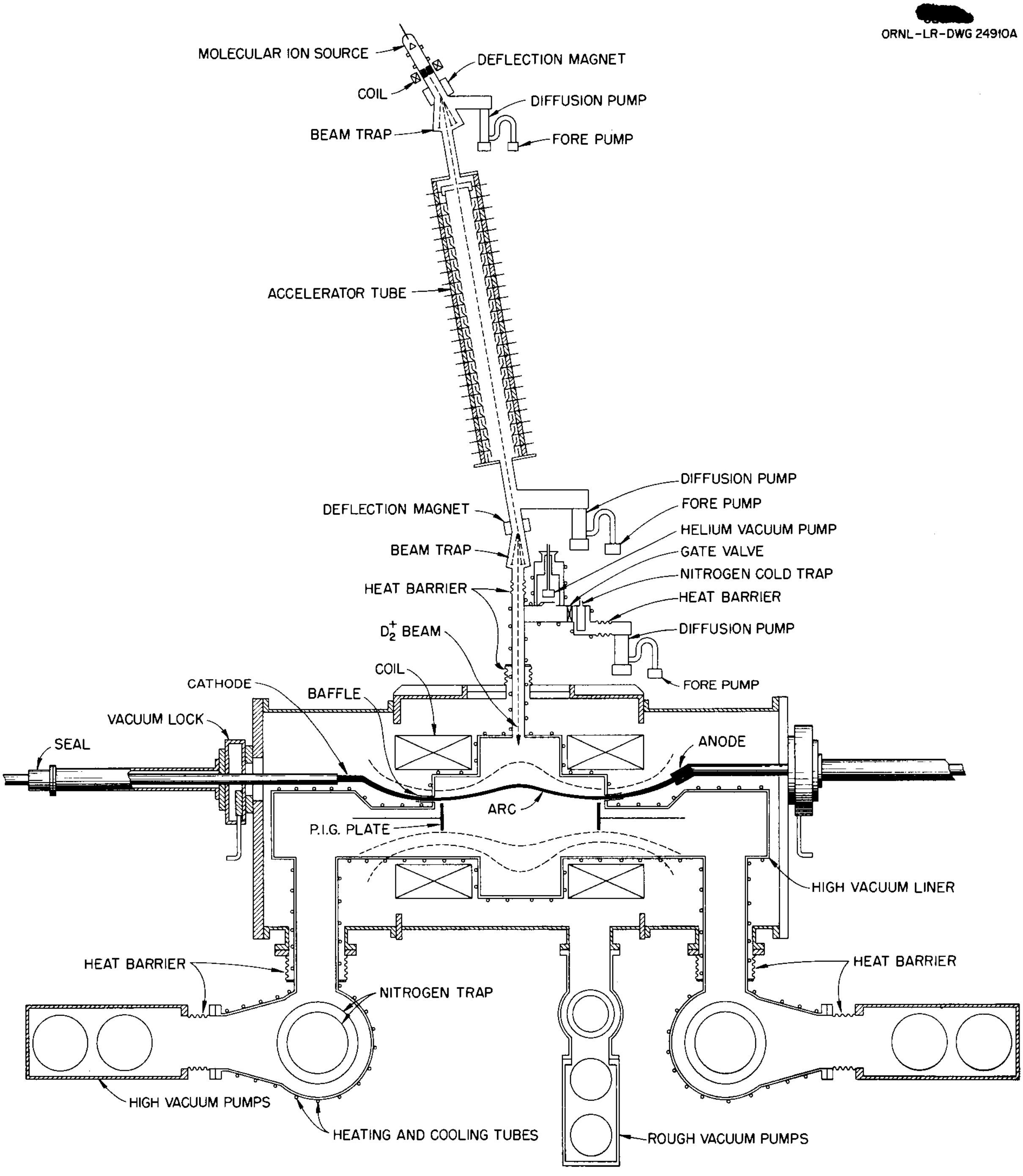

Fig. 3.3.1. Vacuum System of DCX.

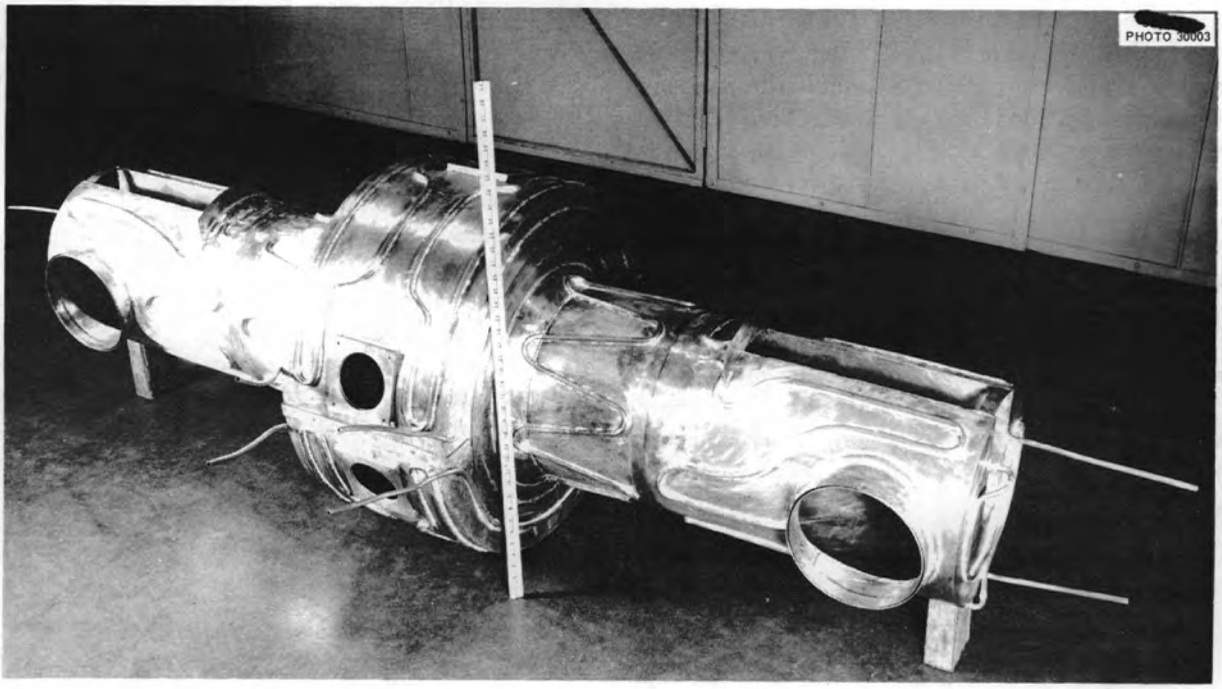

Fig. 3.3.2. High-Vacuum Liner of DCX.

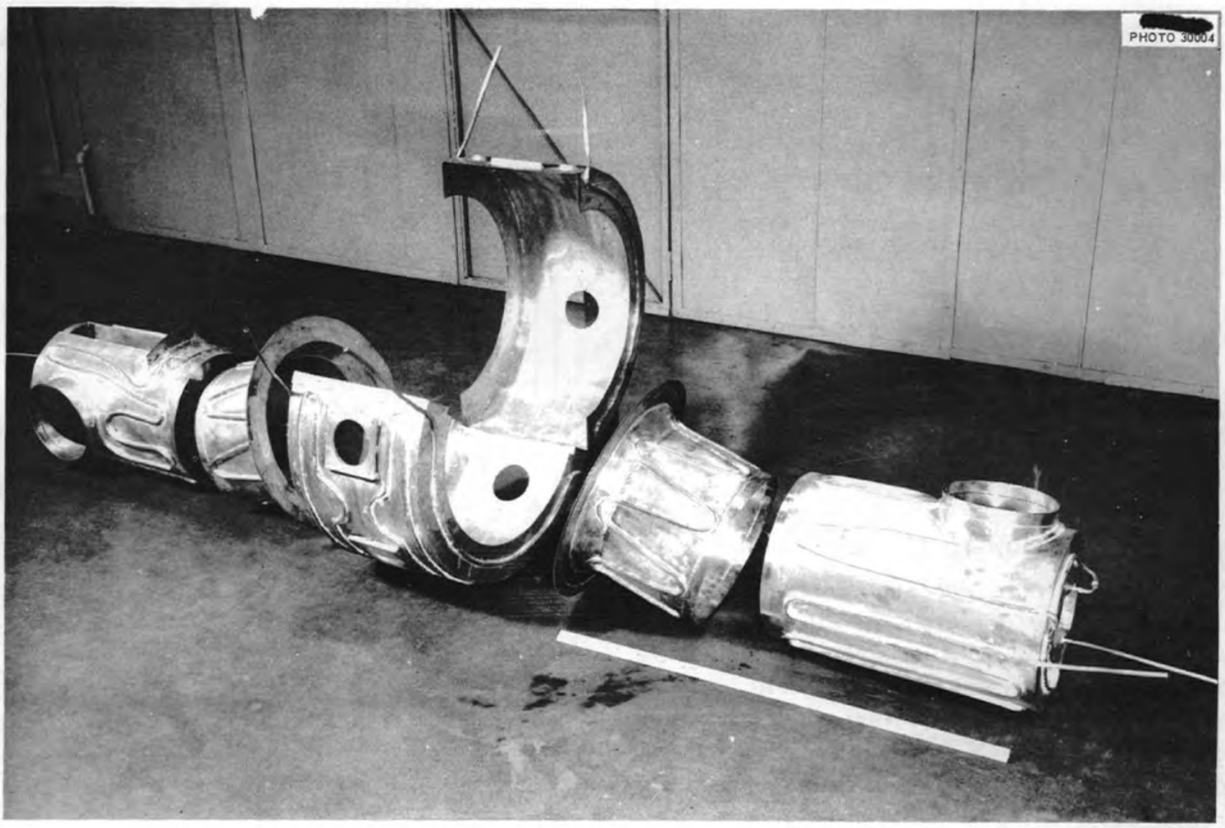

Fig. 3.3.3. High-Vacuum Liner of DCX, Unassembled.

[redacted] HIGH-VACUUM PUMPING SYSTEM

Oil diffusion pumps are used, mounted behind a liquid-nitrogen-cooled trap-baffle assembly which incorporates an oil creep barrier. The assembly is shown in Fig. 3.4.1. This type of pumping and trapping system was originated at UCRL, Livermore, and has been successfully applied there to achieve very high vacuum in large chambers. The essential points of the design are that no molecule will be able to pass through the trap without several collisions with a cold surface, and that no path will exist for oil creepage that does not cross a cold surface. The pumping speed of this system has been found to be only 300 liters/sec, however, and new trap designs are under investigation.

UNCLASSIFIED
ORNL–LR–DWG 24084

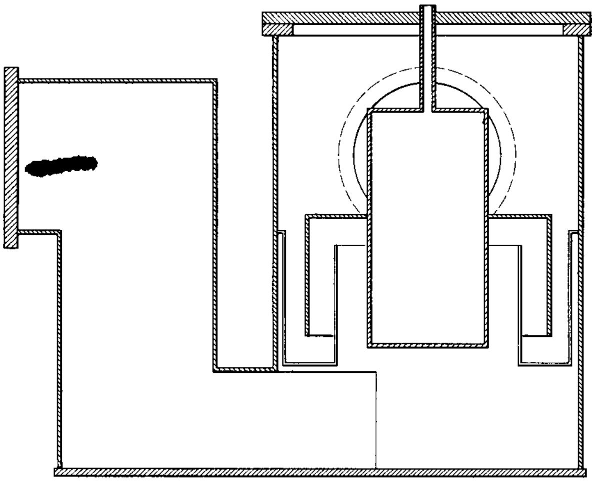

Fig. 3.4.1. Vapor Trap and Baffle, Liquid-Nitrogen-Cooled.

3.5 CONNECTION TO ACCELERATOR TUBE

The connection to the accelerator tube constitutes a major leakage path into the liner enclosure. As indicated in Fig. 3.3.1, it is planned to minimize this problem in several ways. Magnetic analysis before acceleration will prevent the evolution of gas just outside DCX by intense high-energy D_1^+ and D_3^+ beams. Dissociation in the background gas in the column will produce other extraneous beams (though weak ones) which will be removed by a second magnetic analyzer. The accelerator tube will be pumped at top and bottom; there will be a very-high-vacuum differential pumping system between the tube and DCX. To date, only the differential pumping system has been installed; other steps will be taken after its effectiveness has been determined.

A liquid-helium pump, now under construction, may turn out to be a key feature of the differential pumping system. It was designed in consultation with J. W. T. Dabbs of the ORNL Cryogenic Group. It is shown in Fig. 3.5.1. Successful operation of this pump may lead to the application of the principle to DCX itself. Preliminary designs have been completed for a 20,000-liter/sec model. It

UNCLASSIFIED
ORNL–LR–DWG 24085

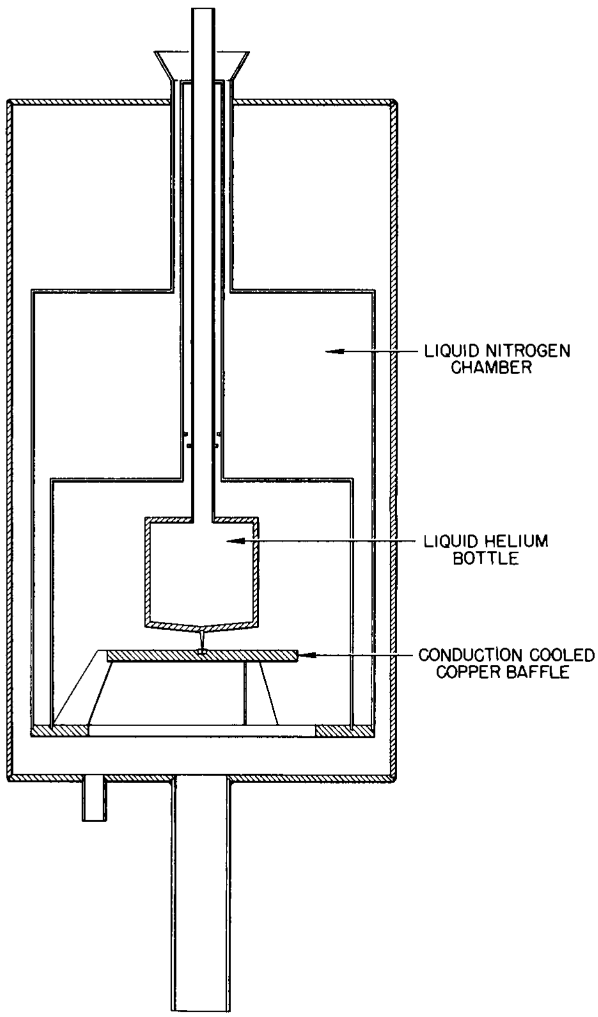

Fig. 3.5.1. Experimental Liquid-Helium Pump.

would have a 300-cm^3/hr liquid-helium consumption resulting almost entirely from heat radiation from the surrounding liquid-nitrogen jacket. The principal advantage of such a pump is that, in the absence of helium gas, it should have an ultimate pressure very close to zero. Problems of oil back-streaming, encountered when diffusion pumps are used, would be avoided through the use of a pump of this type.

3.6 ION BEAM DISPOSAL

The molecular ion beam itself constitutes a significant gas flow into DCX at the working pressure. For instance, a 1-ma beam constitutes an input of 16,000 liters/sec at 10^{-8} mm Hg. If permitted to recombine at the wall, it (and the dissociated D^0 flux) will reduce the net ionizing speed of the trapped beam by 30%. Perhaps a more serious difficulty is its heating effect on the wall, which may, in spite of the pre-baking, release large quantities of occluded gas.

There are two ways in which the problem is being attacked. The most attractive one is to increase the arc current until nearly complete dissociation (and ionization of D^0's) is achieved. At present, the arc current is limited by its power supply, which is being replaced by a larger one. The other advantages of increasing the arc current are so pronounced as to warrant its being done even if a certain amount of development is entailed. Notable among them are greater pumping speed of the arc itself, and as much as an eightfold increase in the input to the trapped ring.

If it is not possible to trap all of the incoming beam, it will be necessary to provide an exit channel for the residual ions with differential pumping between the collector and the liner. Such a channel has been designed with two-stage differential pumping, the stage nearest DCX being an all-metal system.

Even the trapped ions will eventually be driven into the wall after charge-exchanging. Since it will be of considerable advantage to prevent their returning to the system as neutral gas, studies are being made of various means to accomplish this.

The problem is lessened in the pre-burnout phase by the fact that the deuterons do not scatter or spread (axially) appreciably before suffering charge exchange (Sec 6.1). Thus, after charge exchange, they strike the liner wall in a narrow equatorial band. Proposed schemes for their removal are based on replacing the liner wall along this band by a thin foil (a few microns thick) or by a palladium strip clad with a thin layer of copper, which would permit the diffusion of the D^0 atoms into the outer chamber but not their return to the inner chamber. These techniques and the general problem of wall loading are under investigation by the ORNL Solid State Division (Sec 20).

3.7 FURTHER DEVELOPMENTS

The liner has been designed to permit the mounting, on the axis just behind the mirrors, of circular plates which can be charged to high voltage (Fig. 3.3.1). It is expected that the free electrons which are properly situated will oscillate between the regions of intense electric field and contribute significantly to ionizing the background gas and thus to achieving burnout. This is, of course, the mechanism of a Philips ion gage; hence the name PIG plates. Enhancement of the operation of the PIG plates may be accomplished by running them at emission temperatures.

The original burnout criterion was based on the tacit assumption that all of the ionized gas is removed from the system. Thus, if only a fraction f is removed, the ion current necessary to produce burnout (omitting the role of the PIG plates) will be increased by a factor $1/f$. In the present system, f is under 2%, and means are being developed to bring it up to nearly 100%. Those means which will be attempted include (individually or in combination) evaporating a getter over the entire liner end wall; burying ions in the PIG plates (which may require a sort of roller-towel arrangement to provide a constantly renewed surface); and use of an array of very-thin-walled tubes ("honeycomb") installed at the mirror field maximums with their axes parallel to the field lines. Cold ions, following field lines and possessing very small Larmor radii, will pass through the tubes with as much as 90% transmission. Molecules formed when the ions recombine at the liner walls will have their transmission back into the center chamber reduced by roughly a factor of 10. With the honeycomb, it appears feasible to raise f to 50% even with the present pumping system.

Finally, a continuing program of research on very high vacuum systems is being pursued in an attempt to provide a fundamental basis for the solution of many of the vacuum problems of DCX and its more powerful successors. This program is described in Sec 15.

4. HIGHER INPUT CURRENT FOR DCX

4.1 MODIFICATION OF DCX ACCELERATOR ION SOURCE FOR LARGER CURRENT

The ion source now in use, which delivers up to 0.5 ma of molecular ion current, is a slightly modified Moak-Good source.[1] The arrangement is shown in Fig. 4.1.1. The tapered iron exit-canal section is the principal modification. This change causes a considerable enhancement of the proportion of D_2^+ to D^+ over the value obtained with the aluminum canal. The ratio D_2^+/D^+ obtained was 2 at total currents of a few hundred microamperes, while the ratio D_3^+/D_2^+ was as large as 0.8.

The redesign of this type of source in order to yield 25 to 50 ma of D_2^+ seems difficult, and a source based upon the Philips ion gage (PIG) type is more attractive.[2] In such a source, the fast ionizing electrons are permanently trapped in electric and magnetic fields until they are released by collisions with gas molecules. The trapping effect thus allows a very low gas pressure to be used, which reduces both the gas leakage into the accelerator tube and the number of atomic ions produced in the source by multiple ionization. Furthermore, no extremely large electron source is required, because the electrons are not allowed to escape until they have been used profitably. Figure 4.1.2 shows the arrangement of a proposed modified PIG ion source. In PIG-type sources, ions are produced in the entire region where the electrons are trapped, and some ions will be lost on the side of the positive electrode away from the main ion acceleration region. By making the electron path as short as possible in this region and as long as possible on the other side, best ion economy is obtained, and less sputtering and other troubles in the source will result.

[1]C. D. Moak, H. Reese, Jr., and W. M. Good, *Nucleonics* 9(3), 18 (1951).

[redacted]

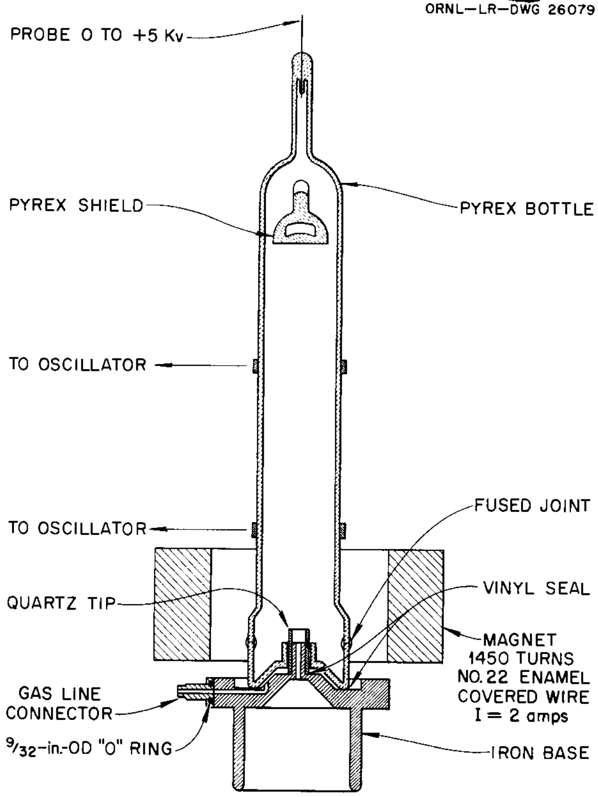

Fig. 4.1.1. Radio-Frequency Ion Source.

[redacted]

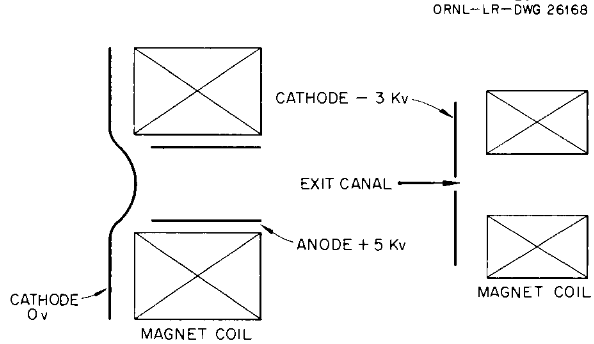

Fig. 4.1.2. Asymmetric PIG Ion Source.

Other sources are being studied (Secs 12.4 and 14), and the most promising of these will be used in DCX, if the modified PIG source does not meet our expectations.

At low current there is little need to remove unwanted ion species from the ion source beam before accelerating it to high energy, but with large currents, the heating and gas evolution

[2]C. F. Barnett, P. M. Stier, and G. E. Evans, *Rev. Sci. Instr.* 24, 394 (1953).

produced by these other ions which strike the walls of the entrance tube between the accelerator and DCX will be prohibitive. The ion source output will therefore be analyzed magnetically just after leaving the source and before entering the accelerator tube, and only the desired ions will be accelerated. The rejected ions will have energies of only 10 to 20 kev, and the power loss and neutron production will not be prohibitive. In order to reduce neutron production and outgassing troubles, the unwanted beams will be terminated on metal surfaces operating at relatively high temperature so that the retention of deuterium in them will be small.

4.2 HIGH CURRENT D-C ACCELERATOR

The current needed to achieve burnout is proportional to the pressure in the working volume (Appendix A). Since the lowest pressure that can be achieved is not known, the current needed to achieve burnout is also unknown. Several estimates of the magnitude of the needed current have been made. These vary from 1 ma to 400 ma of trapped atomic ions. If the latter estimate is correct, 1.6 amp of D_2^+ ions will be needed with a breakup efficiency of 25%.

Studies have been initiated which are directed toward the design of a system capable of the steady acceleration of 2 amp of molecular ions. These studies are based on the concept of using magnetic fields in such a way as to permit the application of an accelerating voltage to a beam containing equal numbers of electrons and ions, without permitting the electrons to drain to the electrodes.

There appears to be no basic reason why a space-charge-neutralized D_2^+ beam of 2 amp cannot be accelerated through a high-voltage tube. Low pressure is needed to prevent the formation of a secondary plasma inside the tube. By using standard vacuum techniques, particles can be accelerated to an energy of 600 kev with a particle flux of 100 ma/in.^{2}. An accelerator which uses 100-kev input particles has exceeded this particle flux by a substantial factor. Instantaneous currents exceeding 100 ma/in.^{2} have been achieved in several instruments.

The d-c accelerator proposed here will have a molecular ion source mounted in the high-voltage terminal. The beam will be accelerated initially to some intermediate energy and transmitted through a magnetic analyzer to remove unwanted ions. Before entering the accelerator, the beam will pass through at least one focusing magnet.

The accelerator tube will be a five-stage high-gradient device with appropriate magnetic coils. These coils will provide magnetic fields that will guide electrons out of the system and force them to drain into the electrodes before they can be accelerated to high energy. In this manner, loading of the high-voltage supply will be reduced. It may be possible to design the magnetic fields so they will tend to collimate the ions. Several magnetic configurations are being studied.

There appears to be no basic obstacle that will obviously prevent construction of a workable d-c accelerator capable of producing 2 amp of D_2^+ ions at 600 kev energy. There are, however, a number of unsolved engineering problems that must be investigated experimentally. This work will be carried out in the facility described in Sec 18.

4.3 THE HIGH-VOLTAGE SUPPLY

Compared with the difficulties encountered in the accelerator, it appears relatively simple to design a d-c power supply for 600 kv and 2 amp. The difficulties involved should not, however, be underestimated. A current of 2 amp is unusually large for this high voltage. Furthermore, the ripple must be no more than 2%, peak to peak, since the radius of the D_2^+ beam can only fluctuate by a distance which is much smaller than the diameter of the arc. Fortunately, the 13.8-kv, 60-cycle, 3-phase primary power supply of the laboratory is relatively stable, and it will not be necessary to provide a special automatic voltage regulator. In order to produce a constant voltage gradient along the accelerator tube, taps on the high-voltage supply would be useful. It is necessary to design the system so that an electrical breakdown at high voltage will not lead to major damage. Finally, it should be borne in mind that this high-voltage supply must deliver at least 1200 kw of power at high voltage, as well as considerable low-voltage power which is insulated from ground.

In view of these stringent requirements, three leading electrical manufacturers were contacted and given an opportunity to study the problems involved.

The three companies worked out preliminary proposals and each suggested a different solution. Representatives of the General Electric Company suggested a voltage multiplier with 50-kv steps. Germanium rectifier elements were recommended. A proposal from the Westinghouse Electric Corporation used a series connection of 6 double 3-phase bridges. The rectifier elements were high-vacuum rectifier tubes, type ML-5576/200, rated at 150-kv inverse voltage and 2.5-amp peak anode current. The Allis-Chalmers Manufacturing Company's proposal has a cascade rectifier circuit employing minimum steps of 100 kv. The cascade units constitute a 3-phase, full-wave bridge rectifier, built up from single-phase units into three vertical columns. Series strings, each consisting of a sufficient number of silicon diodes, allow a large safety factor for the peak inverse voltage of the diodes. The proposals are being studied and the detailed requirements of the ion source and accelerating tube are being determined.

5. IMPROVEMENT OF DCX MAGNETIC FIELD SHAPE

The existing design of DCX would allow the insertion of eight flux bars through holes in the end plates which support the liner, the arrangement of a cylinder 7/8 in. thick and 42 in. long around the two coils, and the location of end plates of whatever thickness is needed outside the coils. Altogether, a cross section of about 160 in.^{2} could be provided for the return path of the magnetic field lines through ferromagnetic material (mild steel). This is about one-third of the average area of the flux inside the liner.

End plates outside the mirror coils produce greater improvements of field strength than the cylindrical section. The effects of plates 34 in. in diameter and 7 in. thick, with 15½-in.-dia central holes, have been tested in a model magnet. Preliminary results indicate an 18% increase in the midpoint field, a 6% increase in the mirror ratio, and, most important, a 50% decrease in the average midplane field gradient.

Since these measurements were made, vacuum considerations have made impractical, for the present, use of extensive quantities of iron in the region of the coil throats. The design of coils which will make more efficient use of the available generator power has been studied, and field increases up to 50% seem readily attainable. At present, this enhancement of the field represents only an aspect of operational flexibility which may be useful in post-burnout plasma studies. It will not make possible the containment of reaction products.

6. DCX DIAGNOSTIC PROGRAM

The diagnostic program for DCX contemplates several phases of operation, during each of which the "contents" of DCX have markedly different properties. An outline, showing the successive phases and the activities appropriate to each, follows. Phase 2 is regarded as a precaution against the extremely unlikely event that burnout does not lead directly to a hot, thermonuclear plasma.

1. Pre-burnout activities should include:
   a. demonstration of containment and stability,
   b. study of neutral impurities,
   c. measurement of approach to burnout.
2. Post-burnout, subthermonuclear-plasma activities should include:
   a. demonstration of stability,
   b. measurement of plasma configuration, density, and temperature,
   c. study and elimination of sources of cooling agents,
   d. study of mirror losses and diffusion losses,
   e. search for thermonuclear neutrons.
3. Post-burnout, thermonuclear-plasma activities should include:
   a. measurement of plasma density and temperature,
   b. studies related to the design of ORION.

It should be noted that activities with similar names, but appearing in different phases of operation, will involve quite different experiments. The following paragraphs describe in some detail these experiments as they are now envisioned.

6.1 CONTAINMENT AND THE CROSS SECTION OF THE CIRCULATING RING

An initial question to be asked of DCX is whether the circulating deuterons are contained until they are lost by some atomic collision. A second question concerns what volume they will fill. The answers to these questions will come most readily from observation of the ring glow (Sec 2.2) and from a study of the hole which the circulating ion beam burns in a thin aluminum foil. The latter technique has the obvious virtues of giving exactly the information desired and of being free from complications caused by arc radiation or secondary plasma. It was used to great advantage in first establishing unambiguously the presence of a substantial circulating beam in initial carbon arc experiments (Appendix E) and in demonstrating the beam's sharp focus.

It will be important to know the spatial extent of the circulating beam, not only to ensure that the behavior is understood and is proper, but to enable the design of various probe or pickup experiments which depend on the distance of certain objects from the plasma ring.

The DCX midplane magnetic field has considerable curvature, as can be seen in Appendix G, Fig. G.2.1. Particles which depart from the midplane thus experience an immediate, strong restoring force. It is not correct to think of them as spiraling away to the mirrors before being reflected; the mirrors are distributed right up to the midplane.

It is thus natural to use the perturbation techniques, familiar in the nuclear accelerator field,[1] to estimate the spreading of the concentric circulating deuteron ring caused by various disturbances expected to be found in DCX. A parameter frequently encountered is

$$n = \frac{-r}{B}\frac{dB}{dr} ,$$

where r is the radial coordinate and B is the value of the midplane magnetic field at r. To first order, restoring forces on particles in perturbed orbits are linear, and perturbations will produce simple harmonic oscillations. The angular frequency of the axial oscillations is given by $\omega\sqrt{n}$, and that of radial oscillations by $\omega\sqrt{1-n}$, where ω is the particle's cyclotron angular frequency. A final point is that, since the perturbation equations are linear, we may use superposition of the responses to a series of perturbations in order to find the net response. This will be made clear in the examples to come. At the equilibrium radius for a 300-kev deuteron in DCX, with a midpoint field of 9600 gauss, $n = 0.42$.

There follows a list of possible mechanisms for spreading or losing the beam, with estimates, where possible, of the effect of each.

[1]See, for instance, M. S. Livingston, *High-Energy Accelerators*, chap. 2, Interscience, New York, 1954.

6.1.1 Asymmetries in the Magnetic Field

The mirror coil windings are inevitably not perfect; there are cross fields from the current leads; and there is an iron platform on which the accelerator is mounted. These are, for the most part, almost certainly minute inhomogeneities, since they were very painstakingly minimized in the design of DCX.

The maximum radial displacement Δr, resulting from a field variation ΔB extending over a segment of path length L, is given by

$$\Delta r = \frac{1}{\sqrt{1-n}} \frac{\Delta B}{B} L \ .$$

If ΔB is oriented so as to produce an axial deflection, the maximum displacement will be

$$\Delta z = \frac{1}{\sqrt{n}} \frac{\Delta B}{B} L \ .$$

These both are expected to be very small displacements. However, we must consider the possibility that, in the course of many passages through the inhomogeneity, the deflections will add so as to produce a large cumulative displacement. An example, that of the axial oscillations, will show that this is in general not so.

Each deflection will produce an axial oscillation given by

$$\Delta z \sin \omega t\sqrt{n} \ ,$$

where t is measured from the time of the deflection, and Δz is independent of z. After N deflections, then, the resultant displacement is given by the sum of all N displacements, since each is independent of the rest. This is the "superposition" referred to above. If $\theta = 2\pi\sqrt{n}$, the resultant oscillation after N deflections is:

$$\Delta z_N = \sum_{m=0}^{N-1} \Delta z \sin (m\theta + \omega t\sqrt{n}) \ ,$$

where the mth term represents the oscillation produced by the $(N - m)$th deflection, and t is now measured from the last deflection. The series sums to an expression which can be shown to be limited, independent of N:

$$\Delta z_N < \frac{\Delta z}{2(1 - \cos\theta)} [(2 + \sin\theta) \cos \omega t\sqrt{n} + $$

$$+ (3 - \cos\theta) \sin \omega t\sqrt{n}\,] < 1.2\Delta z \ ,$$

where t has been taken to give the expression its maximum value. Similarly,

$$\Delta r_N < 1.5\Delta r \ .$$

The net displacements are reassuringly small.

A perturbation of another form is provided by a 5- to 10-gauss stray field (perpendicular to the DCX axis) from a nearby Calutron track. The result produced by this field (ΔB) is found to be a rotation of the orbit through an angle α, where

$$\alpha = \frac{\Delta B}{B_0} \frac{n}{1-n} \ .$$

This effect, like those of field inhomogeneities, is expected to be too small to detect.

6.1.2 Effect of Carbon Arc Magnetic Field

Each passage of a circulating ion through the magnetic field of the carbon arc has been calculated to produce an axial displacement of 0.26 mm. Within the approximation that the restoring force is linear, the displacements from successive passages through the arc may be added. With $\theta = 2\pi\sqrt{n}$ as before, the net displacement z_N after N rotations is therefore

$$z_N = z_0 \sum_{m=0}^{N} \cos m\theta$$

$$= z_0 \left[\frac{1}{2} + \frac{\cos N\theta - \cos (N+1)\,\theta}{2(1 - \cos\theta)}\right]$$

$$\leqq z_0 \left[\frac{1}{2} + \frac{1}{1 - \cos\theta}\right] \ .$$

For a midpoint field of 9.6 kilogauss, $n = 0.42$, $\cos\theta = -0.59$, and $z_N < 1.13$; $z_0 = 0.3$ mm. The magnetic field of the carbon arc, then, is not expected to spread the trapped energetic ions appreciably.

6.1.3 Electric Deflections

Both the steady electric fields and the radio-frequency fields along the arc must be considered. We may infer from the behavior of arc voltage as a function of arc length (Appendix C) that a field of 1.0 v/in. exists along the arc. The magnitude of the r-f fields is not known.

If the field E exists outside the arc, say for a distance $L/2$ on each side, a deuteron with kinetic energy T will suffer a deflection on each turn of $LeE/2T$. For $T = 300$ kev and $L = 20$ cm, this amounts to 13 microradians. The deflections may be summed in the same manner as in the previous paragraph. For the DCX field, the net deflection is thus found to be limited to less than twice the incremental deflection, or 26 microradians. A deflection of this size will produce a maximum axial displacement of only 0.3 microns. Evidently, electric fields along the arc will have to be quite substantial in order to affect the ion spread.

6.1.4 Scattering

Multiple scattering in the arc is a negligible source of beam spread. Slowing down, however, will contribute slightly to the radial spread. The stopping cross section is about 10^{-14} ev·cm^2 for carbon. For a density of 10^{14} carbon ions per cm^3 and a path length in the arc of, say, 3 cm, there will be an energy loss of 3 ev per turn, or 30 kev in 10^4 turns. The change in radius of curvature will be about 5%, or 0.3 in., for such an energy loss. This is generally less than the inherent radial spread resulting from dissociation in different parts of the arc, which should be something over an inch. Scattering and slowing down in the background gas will be negligible until burnout occurs.

6.1.5 Space Charge

Space charge, if it builds up, may spread the beam or produce oscillations which disperse it. It seems unlikely that this would happen in the presence of the carbon arc. However, this phenomenon would also very likely be prevented in the case of a foil-burning experiment by the foil itself, and so its investigation is apt to require other techniques. So far, observation of the ring glow shows no evidence of space charge blowup.

It appears then that there is no serious threat to containment in DCX, in the initial stages, and that a trapped concentric current ring should not be spread measurably before burnout occurs.

6.2 ION CURRENT MEASUREMENTS AND PROBE STUDIES

In the initial operation of DCX, it was necessary to detect the dissociated deuteron beam in order to determine whether the incoming molecular beam had passed through the arc, and then to measure it to determine the arc's dissociation efficiency. Because the beam position is very sensitive to several parameters, it is presently necessary to repeat this measurement each time the instrument is operated.

The detector developed for this purpose is an enclosed Faraday cup with suppressor ring, similar to that used in the first high-energy dissociation experiments (Appendix C). In the present case it has not been necessary to place a foil across the opening because the opening does not face the arc. It has been found necessary to water-cool the collector, even when it is some seven inches from the arc.

If the first attempts to achieve burnout are not successful, it will be of interest to measure the current in the accumulated beam. For a neutral pressure of 10^{-6} mm Hg, the mean residence time of an ion will correspond to approximately 10,000 turns, based on the charge exchange cross section (molecular nitrogen) given in Appendix B. This would produce circulating currents of the order of amperes with ion sources presently available. Experiments in which this accumulated beam is deflected electrically or magnetically onto a Faraday cup detector in one turn (0.15 μsec), or several turns, are attractive.

If the beam cross section does not exceed that observed in preliminary measurements, about $\frac{1}{2} \times 1$ in. (Sec 2), a 1-in. deflection should be adequate to achieve complete collection. This would require a readily attainable electric field of 15 kv/cm (axial) or 17 kv/cm (radial) applied to the beam over a length of 5 cm. It would require an axial magnetic field of 0.38 times the steady field, or 3200 gauss, applied over the same length – a less appealing prospect.

The analysis applied in Sec 6.1 suggests that very little would be gained by allowing for multiple passes through the deflecting field. It does seem feasible, however, to accomplish the deflection by applying a comparatively small r-f field tuned to the appropriate oscillation frequency. A slight de-tuning would enable the collection of all particles regardless of phase.

It should be noted that the inherent buildup (or decay) time of the beam will be about 1.5 msec and that mechanically moving a target across the beam is not entirely out of the question.

The determination of the lifetime of the circulating beam after the incoming beam is interrupted is equivalent to the measurement of circulating current. A fairly elaborate system is available for turning the input current off or on in about 1 μsec. It is described in Sec 6.4.

There are several methods of following the decay of the residual current. Experiments to follow the intensity of the neutron flux and various magnetic measurements are described in Secs 6.3 and 6.9.

A fast-neutral-atom detector of the foil-covered Faraday-cup type, described in Appendix C, appears to be ideal for tracing the current decay. From the circulating ring will come a uniform radial spray of neutrals produced by charge exchange. In steady state, the number will be equal to the input (trapped) current, say at least 50 μa. A detector $\frac{3}{4}$ in. long, placed at the liner surface, will intercept about $\frac{1}{2}$ μa of neutrals, which can be made at least ten times the background, even in the presence of the carbon arc.

This detector will, in fact, have a number of uses. It will effectively monitor the circulating beam in steady state, indicating the presence of possible instabilities which might cause the loss of large portions of the ring.

A similar detector will monitor the neutrals from the dissociation in the arc in order to detect accidental interruptions in the input. Finally, a very narrow (and probably elongated) neutral detector can be moved parallel to the magnetic axis to scan the axial distribution of the circulating current. (Burning foil experiments, described in Sec 6.1, can only show the beam envelope, and may suppress any space charge blowup.)

A portion of the experimental program whose importance is yet to be ascertained is the study, by means of probes, of the secondary plasma which surrounds the ring. It is unlikely that probe measurements will be possible within the ring itself. An active research program on the characteristics of probes in magnetic fields is under way. Its immediate aim is to provide empirical data which may be useful in interpreting DCX experiments, and its ultimate goal is to develop a theory of the operation of probes under the conditions met in DCX. This program is described in more detail in Sec 13.

With certain exceptions, initial probe experiments in DCX will be largely exploratory. They will be used to measure the extent of the plasma and to determine such properties as may be correlated in the empirical studies. It is hoped that by the time burnout is achieved, there will be a reasonably sound theory which enables the development of more well-founded information. In particular, it will be most valuable to be able to measure electron temperatures in the sub-kilovolt range in the (possible) period after burnout has been achieved and before thermonuclear neutrons are observed. During this phase, probe measurements may provide the least ambiguous measure of electron temperature possible.

One experiment of immediate interest will be the measurement of space potential in the plasma by means of the comparison of the voltage-current characteristics of hot and cold probes. A circuit has been developed for applying to the probes a sawtooth wave with several hundred volts amplitude and one-tenth millisecond rise time. The technique, suggested by that used in early Calutron studies,[1] has been successfully applied to deuteron beam studies in the magnetic track. The results in DCX are expected to give a measure of the completeness of space-charge neutralization and a rough indication of the electron temperature.

Because the successful operation of the "honeycomb" (Sec 3.7) will depend critically on the energy of the cold ions, a means of measuring this quantity by a gridded probe technique[2] is being adapted to DCX geometry.

Mention is made in Sec 13 of pulsed probe techniques. Their most valuable use in DCX might possibly be as mass spectrometers to determine the various ion populations in the plasma.

---

[1]B. Peters, A. C. Helmholz, and W. E. Parkins, *Natl. Nuclear Energy Ser. Div. I* **4**, 33 (1951).

[2]N. I. Ionov, *Doklady Akad. Nauk S.S.S.R.* **85**, 753 (1952); AEC translation 2857.

6.3 NEUTRONS AND BREMSSTRAHLUNG

The neutron flux from DCX is presently monitored by a long counter and a plastic phosphor scintillation spectrometer. For 100 μa dissociated input, 20% breakup efficiency, and background gas with partial pressure p_D of deuterium and p_N of nitrogen, the neutron production rate before burnout is expected to be as follows:

From the walls[1]	3×10^7 neutrons/sec (upper limit)
	10^6 neutrons/sec (lower limit)
From the gas	$\dfrac{2 \times 10^6\, p_D/p_N}{1 + 0.2\, p_D/p_N}$ neutrons/sec
From the carbon arc	None [energy is below threshold for C^{12} (d,n); cross section is negligible for C^{13} (d,n)]

As burnout is approached, and before slowing down is important, the yield from the gas will be increased over that given above by a factor of $(1 + F)$, where F is the ratio of ionized to neutral deuterium in the region of the trapped ring.

The neutron yield for a completely ionized cold gas ($T \sim 50$ ev) is expected to be

$$Y = \frac{2 \times 10^7\, p_D/p_N}{1 + 0.14\, p_D/p_N} .$$

This yield will go up as the temperature is raised, because of the decreased stopping power of hot electrons. After burnout, the neutron flux is expected to rise to almost 10^{13} neutrons/sec, due to thermonuclear reactions (Appendix A).

Before burnout is approached, the neutron flux may be used as an index of the circulating current for beam lifetime studies. The only necessary precaution will be to minimize, by its position, the response of the counter to the input beam. For this purpose, a circuit has been developed which displays, on an oscilloscope face, integrated counts as a function of time after switching.

Neutron spectrometers are not being developed because nearly all the neutrons observed will be produced by D-D reactions, whether in the plasma or in the chamber wall.

The modest resolution of the plastic scintillator, or of the LiI(Eu) crystal which is available, will be sufficient to distinguish between primary neutrons and those which are scattered before entering the crystal.

However, a neutron collimator and counter has been designed which will be able to distinguish between plasma (or gas) neutrons and those originating at the wall.

The neutron collimator employs a group of tapered holes in a shield made of limonite aggregate (hydrated iron oxide ore) with the spaces filled with water. The axes of the holes meet at a common point 14 in. beyond the face of the shield block. Behind the large ends of the holes is placed a block of paraffin moderator in which a group of BF_3 counters is imbedded. The moderator block is lined on sides and back by thick layers of the limonite and water shield. A collimator of this type[2] has been tested and is based on the widely used medical gamma-ray collimator developed at ORNL.[3] Total weight of this collimator will be approximately 10 tons.

Even when neutral atom burnout is achieved, it is conceivable that the resulting plasma may rise only very little in temperature, since it may be cooled by the influx of cold electrons from the arc or from photoemission at solid surfaces which lie on magnetic flux lines which cut the plasma. Granted that the primary electrons of the arc have energies of several tens of volts, slower electrons may be present in large numbers.

The arc may constitute a more potent cooling agent than was estimated by Simon and Rankin (Appendix A), since a particle orbit which cuts the flux tube along which the arc runs will precess so that the particle returns repeatedly to the arc and is thus able to lose considerable energy therein. This difficulty may be reduced by making the magnetic field more nearly uniform in the plasma region.

A further difficulty is that the plasma is apt to be contaminated by carbon and heavier ions. As Simon and Rankin have shown (Appendix A), this will affect the density more than it will the temperature, once the impurities are fully ionized.

[1]From empirical data on foil bombardment (C. D. Moak, private communication).

[2]A. Robeson, G. Burleson, and P. R. Bell, *Phys. Semiann. Prog. Rep. Sept. 10, 1955*, ORNL-1975, p 76.

[3]P. R. Bell and J. E. Francis, *Phys. Semiann. Prog. Rep. Sept. 10, 1955*, ORNL-1975, p 91.

A valuable index of the plasma condition, in case the neutron yield remains low (below 10^{10} neutrons/sec) and burnout is evident, is afforded by the bremsstrahlung spectrum. For an electron temperature T, the spectrum has the form:[4]

$$N(E)\,dE = 1.35 \times 10^{-16} Z^2 n_i n_e \times \sqrt{\frac{mc^2}{kT}}\, e^{-E/kT} \frac{dE}{E} .$$

To study the bremsstrahlung, we will use a scintillation spectrometer designed for low-energy photon studies. It consists of a 0.010-in.-thick NaI(Tl) crystal provided with a 0.013-in. beryllium window and mounted on a DuMont 6291 photomultiplier. It has been tested on the 4.51-kev $K\alpha$ line of titanium. Figure 6.3.1 shows the pulse-height distribution obtained. The photon peak is well resolved. Similar systems with larger crystals will be used when electron temperatures above a few kilovolts are achieved.

The counter will be operated in the DCX midplane, where magnetic shielding should be least difficult. Multilayer magnetic shielding will be used on both the photomultiplier and the preamplifier.

The major difficulty in the operation of the counter is expected to be the high background count rate produced by neutron-induced gamma rays in the crystal and its surrounding. Most of these counts, however, would produce pulse heights corresponding to energies greater than those of the x-ray spectrum. A special nonoverloading linear amplifier of ORNL design (type DD2) is being used in order to minimize the effect of large pulses on the response of the system to the pulses of interest, and to give good performance at very high counting rates.

The measured count rate of 3- to 7-kev bremsstrahlung at a plasma temperature of 5 kev is expected to be about 5×10^5 counts/sec. It will be necessary to reduce the count rate by collimation or by distance; and this will, in fact, permit scanning the density distribution of the plasma.

The absolute bremsstrahlung intensity, when correlated with the neutron data, will give a measure of the density of the plasma and its contamination level. This determination will be somewhat complicated in view of the anisotropic velocity distribution of the electrons producing the bremsstrahlung and of the difficulties of absolute counting of neutrons.

A 2-ft-thick water-filled wall has been constructed (but not yet assembled) to serve as a neutron shield around DCX when the flux in the experimental area exceeds a safe limit.

UNCLASSIFIED
ORNL-LR-DWG 25992

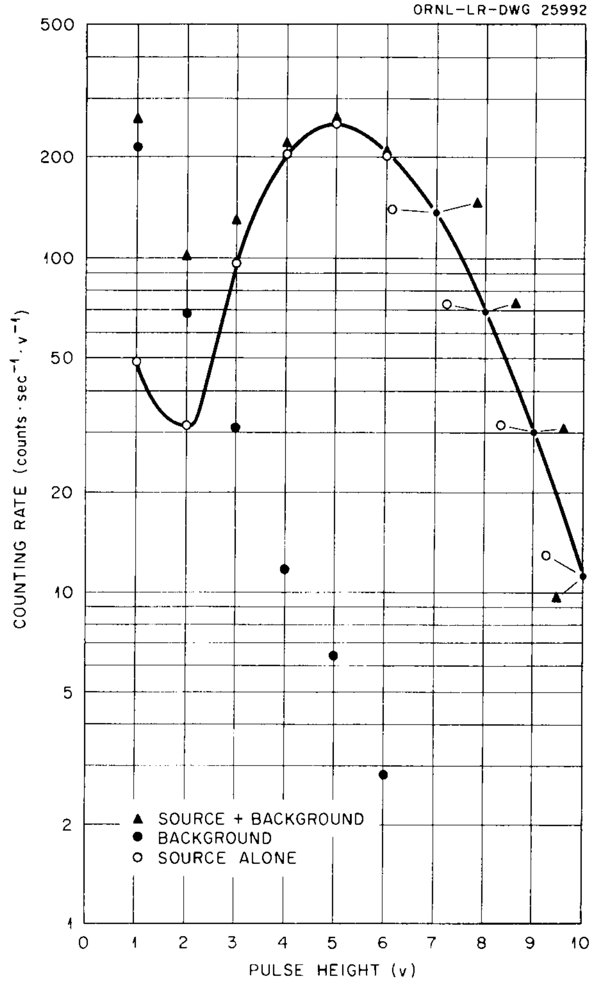

Fig. 6.3.1. Pulse-Height Distribution for the 4.51-kev $K\alpha$ Line of Titanium.

6.4 TECHNIQUE FOR FAST SWITCHING OF INJECTED BEAM

This section describes equipment which provides a way of studying buildup or decay of circulating ion current in DCX just after the injector is switched on or off, respectively.

A fast switching technique for the ion beam of an accelerator was recently developed at ORNL for neutron time-of-flight work. This technique

[4] J. E. Allen and W. R. Hindmarsh, *The Bremsstrahlung Radiation from Ionized Hydrogen*, AERE-GP/R-1761 (Sept. 21, 1955).

has been taken over directly to provide fast switching for the ions injected into DCX. The beam is switched in the region above the accelerator tube to avoid neutron background in the off periods. Switching is controlled by a radio link between the timing circuits and the high-voltage terminal of the injector.

The switching is accomplished by electrostatic deflection of the beam in a 5-in. tube between the ion source and the accelerating column. An Einzel lens system accomodates an ORNL r-f ion source to the extra drift length before acceleration.

The timer is simply a scale-of-100 scaler driven by a variable frequency oscillator. The injector is switched on when the scaler reaches zero counts, and is turned off N_1 cycles later. The detecting equipment waits N_2 cycles and then remains on for N_3 cycles. There is then another wait of $100 - N_1 - N_2 - N_3$ cycles and the injector turns on once again, beginning the next run. In this way, the detector is turned on after a constant, controllable delay after the injector is turned off. The total time duration of the 100-cycle runs can be changed widely by altering the frequency of the master oscillator.

The buildup or decay of circulating current may be followed by an energetic neutral detector (Sec 6.2), a neutron counter (Sec 6.3), or a magnetic pickup coil (Sec 6.9).

6.5 MICROWAVE MEASUREMENTS

Microwave diagnostics should be particularly applicable to DCX because it has constant mirror fields and its plasma-buildup times are relatively long. The machine arrangement is conveniently suited to microwave density measurements by either reflection or transmission.

Since the transmission method appears more promising, a two-path null system is being assembled. The experimental arrangement consists of a K-band (25 kMc) klystron feeding a matching T, which splits the energy between the plasma path and the null path. The transmission through the plasma will be accomplished by horns, or horns plus lenses if the radiation from the carbon arc makes narrower beams necessary.

The plasma densities contemplated in DCX are of the order of 10^{12} electrons/cm^3, which should result in a change of the free-space dielectric constant of approximately 10% at 25 kMc. Since the length of the microwave path through the plasma will be of the order of 15 cm, the effective change of the path length will be more than a free-space wavelength and therefore easily detectable. If DCX plasma densities become greater than 10^{12} electrons/cm^3, instrumentation for counting the nodes as the plasma builds up will be available. This instrumentation, combined with methods of processing the plasma-buildup data, should extend the density measuring limit to approximately 5×10^{12}. Diagnostic apparatus for 4-mm microwaves is also being developed in order to carry the density measurements through 5×10^{13} electrons/cm^3 and thus permit measurements in the breakup arc.

Use of microwave noise measurements is planned in an attempt to determine the electron temperature, although this measurement is expected to be complicated by radiation from the carbon arc. However, directional receivers and periodic interruption of the D_2^+ beam should help alleviate this difficulty.

Work is in progress to use a very narrow beam system to examine the region around and, if possible, in the carbon arc. These measurements will provide information concerning the background produced by the arc and possibly actual arc diagnostic information, such as arc radiation and electron densities.

6.6 OPTICAL MEASUREMENTS

The principal optical measurements to be made on DCX will be high-speed photographs of the plasma region. The light emanating from the plasma region will originate from excited atoms of background gas and emission following charge exchange; therefore, measurement of this light will probably be of interest during the initial stage of operation before burnout. However, useful trajectory information should nevertheless result. After burnout, the plasma can still be examined by studying the light from fast excited atoms produced by charge exchange, a process too rare to be seen in pulsed machines but useful in DC machines.

The high-speed viewing is based on the RCA C73435A electrostatically deflected image-converter tube. This tube is spectrally sensitive from 3500 to 5500 Å and will resolve 22 line pairs per mm. It should be possible to obtain six ½-in. frames per sweep on the 3-in. phosphor. The tube can be gated in 10^{-8} sec, which is less than one-tenth of the cyclotron period of a deuteron in DCX.

The same apparatus will also be used in carbon arc diagnosis, principally for the examination of the short-term motion of the carbon arc streamers.

6.7 HEAT AND POWER MEASUREMENTS

After burnout is achieved, it will be imperative to apply all sensible methods to determining the state of the resultant plasma. In most cases, the theory relating experimental data to plasma parameters is sufficiently inexact that believable numbers can be achieved only where there are several cross checks. A particularly useful instance of this will be the measurement of power radiated by the hot plasma and the correlation of the result with the various forms of data from which it may be inferred. Calorimetric techniques developed for high-energy arc studies will be employed to determine the energy flux of all types emerging in different directions from the plasma. There will, of course, be need for shadowing to insensitize the instruments to radiation from the carbon arc.

These data will be compared with bremsstrahlung, optical, and probe measurements. The power-balance calculation will thus determine whether all of the emerging power is in the form of electromagnetic radiation and energetic charged particles, and whether the total power output is equal to the beam power input. In either case, a negative result may indicate faulty data or incorrect interpretation of it. It may also, however, indicate unsuspected power sources or sinks. Among the many possibilities are the carbon arc, which may play either role, and plasma instabilities or turbulence which may cause bits of plasma to boil off. Only when all effects are accounted for will it be possible to make a significant analysis by means of the energy- and density-balance equations (Appendix A).

6.8 SPECTROSCOPIC INVESTIGATIONS OF DENSITY AND TEMPERATURE IN DCX

Attempts will be made to evaluate the properties of the DCX plasma by utilizing spectroscopic techniques. After burnout, it is expected that the deuterium spectrum can be observed only indirectly by using recombination or charge-exchange spectra of deuterium ions. In the region of the carbon arc, the impurities will, in general, reflect the properties of the arc; whereas, in the plasma region of DCX, the impurities will be expected to be low. It may be possible to use the radiative recombination probability ($D^+ + e \rightarrow D^0 + h\nu$) to obtain meaningful values of plasma density and temperature. The cross section is given by Bethe and Salpeter[1] and suggests measurable intensities for $T_e \gtrsim 50$ ev.

Doppler broadening resulting from random motion, as well as Doppler shift from ordered motion, will be used to determine the relative order and disorder in the system (see Fig. 6.8.1) and to give a measure of the plasma temperature. Mirror systems and image rotators are being used to examine

UNCLASSIFIED
ORNL-LR-DWG 24018

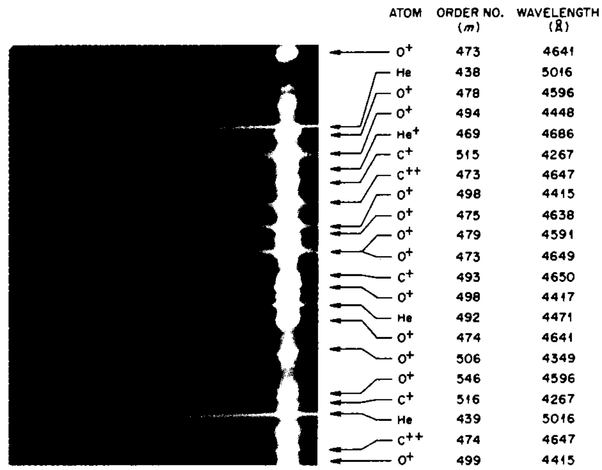

Fig. 6.8.1. Spectrograms at High Resolution of Mode I Discharge Showing Marked Ordered Motion of Ions (Doppler Slant Effect) About the Arc Column and Slight Disordered Motion (Line Broadening).

selected regions of plasma so as to exploit fully the Doppler effect. The expected Doppler shift due to ordered ion motion in the circulating ring is about 1.3% of the wavelength for deuterium atoms. The fractional line width for deuterons at temperature T (in ev) is

$$\frac{\Delta\lambda}{\lambda} = 0.55 \times 10^{-4} \sqrt{T} \ .$$

At temperatures above a few tens of electron volts, Doppler broadening will entirely mask Zeeman and Stark splitting and the various line broadening

[1] H. A. Bethe and E. E. Salpeter, p 408 in *Handbuch der Physik*, vol 35, ed. by S. Flügge, Springer-Verlag, Berlin, 1957.

effects which might otherwise give valuable information about the plasma. The Doppler effects illustrated in Fig. 6.8.1 correspond to several volts of energy.

The excitation of highly ionized (impurity) atoms of high Z can be studied in the vacuum ultraviolet region, both to determine the abundance of the impurity and to get a measure of its residence time or the electron temperature. Present theories of ionization levels[2] generally are based on the assumption that the system is in equilibrium with its radiation, but rough estimates can be made without this assumption.

For spectrographic observations of the vacuum-ultraviolet wavelengths, a spectrometer based on the Seya mounting[3] is being constructed. The grating mounting of the Seya spectrometer is different from other concave grating mountings (such as those of Wadsworth, Eagle, and Rowland) in that only one motion, rotation of the grating, is used in scanning over the full wavelength region. Seya found that if the angle between the incident and diffracted rays is set at about 70° 15′, it is not necessary to readjust the focal distance of the incident and diffracted rays to achieve focus when rotating the grating; for, in fact, the distance of the entrance slit from its "correct" position on the displaced Rowland circle is just the right amount to correct for the departure of the exit slit from the Rowland circle.

The mechanical simplicity of this arrangement makes it suitable for a portable vacuum-ultraviolet scanning spectrometer. Advantage can also be made of the astigmatism of the instrument. While the horizontal focus of the grating is on the entrance slit, the vertical focus, in a one-meter instrument, is a few feet beyond the entrance slit. It is planned to locate the plasma, or the discharge under study, at this secondary focus. Since proper imaging of the source will occur at the exit slit, analysis for Doppler shift and other spatial studies such as line profiles can be made in this way.

To obtain accurate profiles of spectrum lines for broadening and shift measurements, it is planned to use two moderate resolution (~40,000) Ebert spectrometers in a stacked arrangement. Dual optical and electronic channels will observe two spectrum lines in the same discharge. One channel will be used as a monitor and the other for scanning. If the intensity of emission is stable, the channels will be recorded separately, and corrections for drift in intensity can be readily applied. If, however, the intensity is erratic or fluctuating, the signals from the two channels will be fed into a ratio recorder, thus ensuring accurate and meaningful intensity data.

A similar arrangement may be used for spatial analysis of plasma or discharges. In this case, instead of wavelength scanning with one spectrometer, an external mirror will be slowly rotated in order to scan different parts of the discharge. Oscilloscopic observation with rapid scanning and with a rotating mirror will be used if the emission is very strong.

Study of spectra by use of time-resolved dispersion will be performed with the same optical equipment, but with revised electronics. It will be necessary to introduce gating circuits and correlating devices, such as a wide-band synchronous detector. Study will be given to Kerr cells and similar electro-optic modulators, but at present they do not appear to have enough contrast for high-resolution time-dispersion work.

If a quantitative study of the spectral distribution can be made, it will be of interest to extend the bremsstrahlung measurements into the vacuum-ultraviolet region as an independent determination of the temperature. The bremsstrahlung intensity in this region should exceed the recombination light intensity for temperature above a few tens of volts.

Spectroscopic studies to be conducted on high-energy discharges, as well as other basic studies, are described in Part 2, Sec 17. Most of the techniques described above are being applied to the carbon arc as well as to the DCX plasma.

6.9 MAGNETIC MEASUREMENTS ON TRAPPED BEAM AND PLASMA

Before burnout, it is expected (Sec 6.1) that the trapped deuteron beam will constitute a current ring about 10 in. in diameter with a cross section around $\frac{1}{4} \times 1$ in. Its time constant (the time for buildup or decay) will be about 1.5 msec at a pressure of 10^{-6} mm Hg, assuming air as the background gas. These features suggest magnetic pickup measurements as a natural means of studying

[2]G. Keller and R. E. Meyerott, *The Ionization of Gas Mixtures in Stellar Interiors: II. The Average Number of Electrons Occupying Various Shells*, ANL-4856 (July 1952).

[3]M. Seya, *Sci. of Light* 2, 8 (1952).

current buildup and decay. A system for rapid switching of the input beam is described in Sec 6.4.

Either a torus linking the ring or a comparatively small pickup coil of many turns placed at the center of the trapped ring appears to be the most attractive tool for studying beam changes. Either must be water-cooled and shielded from extraneous signals, although the former is essentially free from magnetic noise. If the trapped beam is as compact as indicated, the simplicity of either geometry will permit an absolute measurement of the circulating current. The value can be checked for consistency with the time constant of the circulating ring decay, which will also be determined. Instabilities and sharp changes in the input dissociated beam will give pronounced, characteristic signals which make possible the use of the coil as a beam monitor.

A toroidal pickup coil has been built and tested and is in process of being adapted for use in DCX. It is wound with 2000 turns of 24-strand Litz wire and potted in Epon. Double layer construction of the stainless steel casing will permit its surface to be baked while the coil itself is water-cooled.

The induced current in the toroid will be amplified in a field-insensitive, transistor, feedback preamplifier (Fig. 6.9.1). The preamplifier is designed to reproduce faithfully a signal which is proportional to the beam-current derivative.

A procedure by which all noise but that with the very lowest frequencies can be eliminated is to integrate the signal over the entire decay time, sacrificing the time-constant data. The integrated signal is, in fact, independent of the beam-interruption time, permitting a simpler beam switch if desired.

Another disturbance (in the case of the central pickup coil) is a 2-kc ripple of one part per million in the DCX field. It has been shown that this ripple can be essentially eliminated by shunting the DCX field with a sufficiently large capacitance (a few millifarads).

When limited partial burnout is achieved, the current change should depart from an exponential dependence on time. It is likely, however, that the shape of the ring (Sec 6.1) will be a more sensitive index of this condition.

Complete burnout will produce a hot randomized plasma in addition to the organized beam. It will be of marked interest to follow the exclusion of magnetic flux lines from this plasma as it grows. For this purpose, a coaxial pickup coil with diameter just less than that of the liner neck will be used. It is hoped that the different time rate of change of the plasma and the circulating beam

[redacted]
ORNL-LR-DWG 26229

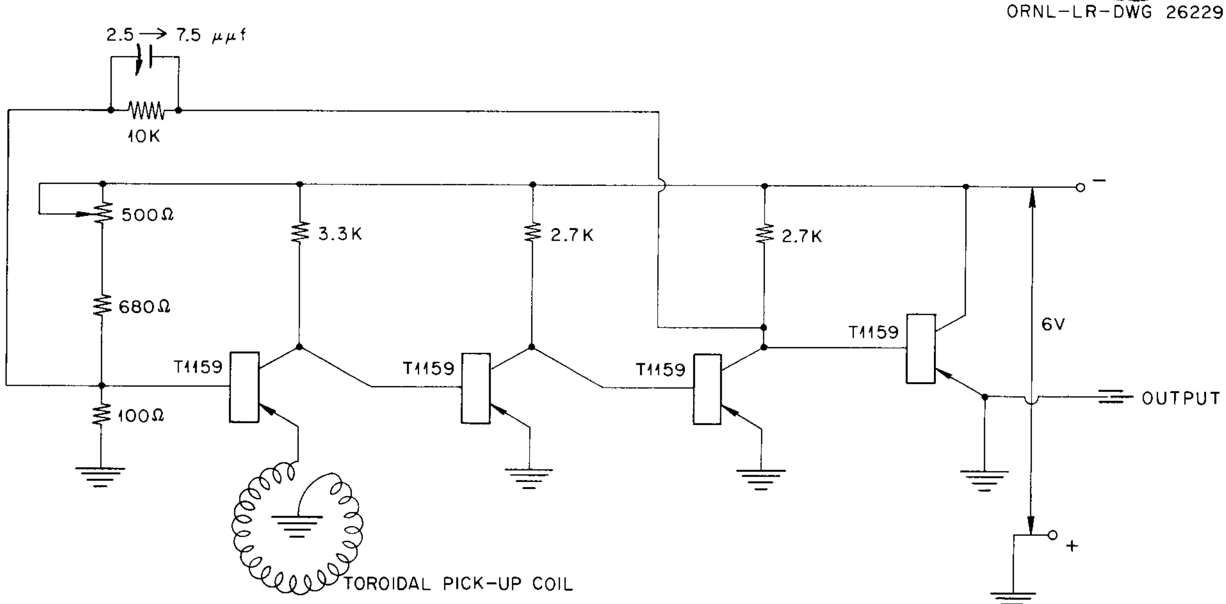

Fig. 6.9.1. Circuit for Measurement of Decay of Circulating Ion Beam with Magnetic Pickup.

will enable us to separate the flux changes resulting from each.

It should be noted here that after burnout, current (and plasma) growth will have a different time dependence than will their decay. Before burnout, unless space charge plays a role, the two are expected to follow the same exponential law.

Realistic design of more elaborate magnetic experiments must await a better knowledge of the plasma configuration which is produced in DCX.

6.10 INSTABILITY MEASUREMENTS

Instabilities which lead to the loss of major portions of the trapped ring or plasma will make their presence felt on the various counters and detectors with which DCX is being studied, if the response time of the instruments in question is faster than the time in which the plasma returns to equilibrium. In this sense, the response time of a counter would be that of its rate meter or indicator. Before burnout, the buildup time will be a few milliseconds; burnout time is expected to be at least several seconds.

Once the presence of instabilities is suspected, various types of electrical probes will be used to measure their configuration and rate of growth. In such measurements, it will be necessary to ensure in the circuitry a bandwidth which is adequate to represent the phenomenon accurately. When the natures of any instabilities have been determined, an attempt will be made to develop sensing circuits which may be used to activate suppression mechanisms of some sort. Some preliminary consideration has been given to the configurations involved, based on the hypothesis that the most likely instabilities will be long flutes.

6.11 MIRROR LOSS MEASUREMENT BY CONTAINMENT TIME AND PARTIAL EFFLUX

Before burnout, mirror losses in DCX are expected to be insignificant (see Sec 6.1). Only after burnout will the circulating particles become disorganized and scatter in appreciable numbers into the mirror "loss cone." "Loss cone" is used here in a generalized sense. In DCX, an energetic deuteron may be lost by a single large-angle scattering collision (Appendix C). This feature is common to most devices using Luce injection, but it generally constitutes a negligible addition to the accepted loss cone.

Direct measurement of the current emerging through the mirrors is expected to be complicated somewhat by the presence of the carbon arc and the PIG plates (Sec 3.7), and by the broad spread in energy of the emerging particles. However, foil-covered detectors (Appendix C) may be utilized to detect particles which are energetic enough to penetrate the foil, and it should be possible to make use of gridded probes (Sec 6.2) to sort out the rest.

An alternative measure of the loss rate of ions through the mirrors is given by the relaxation time of the plasma after the input beam is shut off. The decay rate of the plasma will be determined by charge exchange with the inflowing neutrals as well as by mirror losses. It can be shown, however, that the mirror loss rate (L_m) is related to the total loss rate (L_t) approximately by

$$L_m = \frac{L_t}{1 + (I_{crit}/I)},$$

where I_{crit} is the critical input current for achieving burnout (Appendix A) and I is the actual input current before interruption. Clearly, the correction may be as large as a factor of 2. This measurement appears most promising for the accurate determination of mirror loss rates.

7. EXPERIMENTS RELATED TO DESIGN OF ORION

The guiding purpose of ORION, the successor to DCX, will be the production of a self-sustaining thermonuclear reaction. To a far greater extent than DCX, ORION will have to be designed as a *system*. The stringent requirements imposed by the need to contain reaction products, by the larger mirror ratio (Sec 10.2.1), and by the desire to maintain maximum flexibility in operation and experimentation, are expected to necessitate considerable attention to the interrelations of the various components and the ways in which they must be accommodated to each other. DCX will constitute a valuable instrument for providing many of the data upon which firm requirements for the parameters of ORION components will be based. Some representative experiments for this purpose are described in the sections which follow. The thinking on these experiments and on ORION generally is in its early stages, and most of the considerations have not yet been analyzed quantitatively.

7.1 EFFECTS OF VARIATION OF INPUT ION ENERGY ON BURNOUT CONDITIONS

The Simon-Rankin calculations (Appendix A) of neutral atom burnout show that it occurs when the rate at which neutrals are ionized exceeds their influx. The latter quantity is highly uncertain. The former, where ionization is accomplished by energetic deuterons, is not, and it is only the former which enters the calculations of the relative efficiency of ions of different energies for achieving burnout. The number (R) of ion pairs produced per input deuteron is given by

$$R = \frac{\sigma_i + \sigma_{cx}}{\sigma_{cx}} .$$

The beam current necessary to achieve burnout at an energy E, relative to that necessary at 300 kev, is thus

$$\frac{I(E)}{I(300)} = \frac{R(300)}{R(E)} .$$

This is plotted in Fig. 7.1.1, in which a background of deuterium gas is assumed. It should be noted that protons having one-half the deuteron energy in each case will achieve the same result.

It is altogether possible that burnout will be accomplished entirely by the action of the carbon arc and/or PIG plates (Sec 3.7). If so, the above remarks will be of little interest. If only partial burnout is achieved by these means, Fig. 7.1.1 will still give the relative beam currents necessary to complete it.

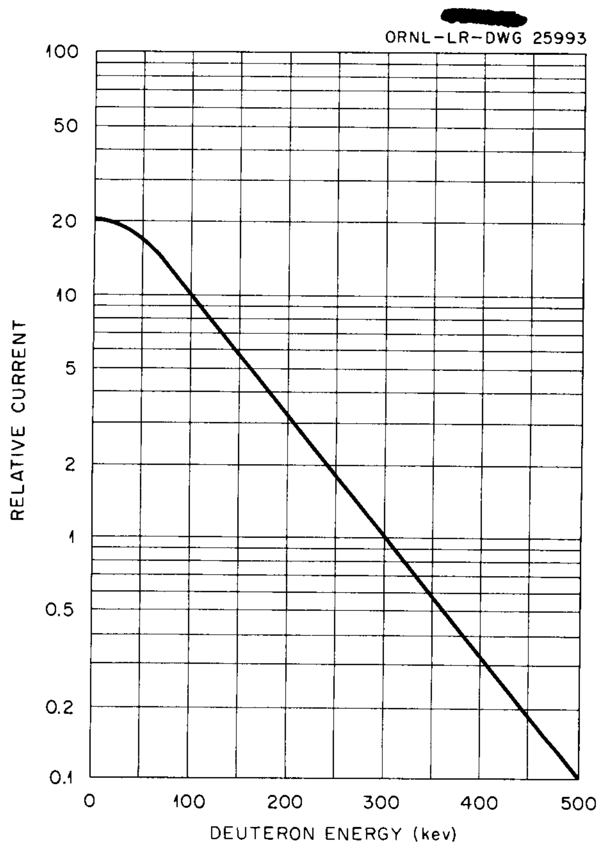

Fig. 7.1.1. Relative Trapped Current Necessary To Produce Burnout.

In preparation for the design of ORION, we will wish to verify not only the above relation to the extent permitted by the accelerator system, but also the calculations of the kinematics of the burnout process (Appendix I). By studying the state of partial burnout, it should be possible to make an accurate determination of the relative efficiencies of the arc, the PIG plates, and other pumping devices for removing neutral atoms.

It will be of particular interest to determine the current necessary to maintain burnout, once it is achieved. A significant reduction, which might occur as the result of the ionizing action of the secondary plasma, would have important ramifications for ORION design, notably the introduction of the possibility of achieving burnout with a very high-intensity pulsed source.

7.2 REACTION PRODUCT CONTAINMENT AND TWO-STEP IGNITION

In Sec 10.2.1 it is shown that the attainment of a self-sustaining D-D reaction is not possible in magnetic mirror machines without extremely high mirror field ratios. The fuel for ORION will therefore, of necessity, be deuterium and tritium in roughly equal parts. A mirror ratio of about 3.5 is required, and the magnetic field must everywhere be strong enough to contain most of the alpha particles produced in the D-T reaction. This requirement is somewhat more stringent than it would seem offhand, because the alpha-particle energies extend to quite high values. For instance, although D-T reactions occurring between particles with very small energy would produce 3.5-Mev alphas, the reactions between 300-kev deuterons and stationary tritons produce alphas with energies ranging from 2.5 to 4.85 Mev.

The calculations (Sec 10.2.1) which show that a mirror ratio of 3.5 is sufficient for "criticality" are based on the assumption that all of the alpha particles whose initial velocity vectors do not fall in the mirror loss cone are retained in the system. Further calculations show that the reactor becomes subcritical if less than 80% of the alphas remaining are contained by the field.

A detailed analysis of the marginal containment problem has not been attempted as yet. Clearly, it will involve an optimization of the field parameters, including over-all size of the reaction volume, field strength, mirror ratio, and midplane field gradient. An idea of the magnitudes involved is given by the example of a field with the spatial characteristics of DCX. For such a field shape, a midpoint field of 30 kilogauss is necessary for the containment of 5-Mev alpha particles emitted (in the midplane) at that point. Those whose orbit centers lie farther from the axis will not be contained. Because a D-T reactor with a mirror ratio of 3.5 will operate with mean ion energy near 100 kev (Sec 10.2.1), it is tentatively assumed that criticality can readily be achieved with a midpoint field of about 35 kilogauss.

Injection and axial dissociation in DCX for this field would require a D_2^+ energy of 1.7 Mev, a DT^+ energy of 1.36 Mev, or a D_3^+ energy of 1.1 Mev. It would require a T_2^+ energy of 1.1 Mev or a T_3^+ energy of 0.75 Mev. Trapping into an orbit whose center is on the axis would require a 25%-higher injection energy in each case. These numbers were determined by using the approach given in Appendix G.

It has been estimated that a 25% decrease in the central field will still permit adequate containment if the field in that region is made more nearly uniform. The necessary injection energies, however, would remain roughly the same.

The practical obstacles to such high injection energies recommend the use of a two-step ignition process. In the first step, molecular ion injection is used to create a hot plasma in a magnetic field with a strength of roughly 10 kilogauss. The field is then increased to the level necessary for containment, and molecular ion injection is is replaced by energetic neutral atom injection. The dynamics of the process have not yet been studied quantitatively, but a few of the requirements are evident, and plans to meet them are discussed in the succeeding sections.

The question of the cooling rate of a subcritical plasma has not yet been analyzed, and so it is still an open question as to whether a D-D plasma in ORION will heat a cold D-T fuel mixture to reaction temperature. If it is tentatively assumed that it will not, reacting D-T plasma is required in the first phase, and both species must be injected and trapped. This necessitates either the use of two accelerators (for D_2^+ and T_2^+), the use of one accelerator and two arcs (for D_2^+ and T_2^+), or the injection of DT^+ ions only. The last procedure is simplest in principle and is made feasible by the availability at ORNL of a supply of DT gas. Whenever tritons are accelerated, it will be desirable to reclaim those which are not trapped by collecting them on a palladium target.

Ideally, in the second phase, the injected fuel would be in the form of ordinary gas, which would be ionized and heated as it entered the plasma. A major obstacle is presented by the large coulomb-scattering cross section of cold ions, which causes most of them to be scattered into the mirror loss cone before being heated up to reaction energies. The low heating efficiency requires a much larger injection rate. There is thus a substantial drain from the system, not only of energy but also of density, since a fraction of the energetic ions already present will be lost by charge exchange with the fuel. The injection of cold ions instead of gas would remove the latter drain, but not the former one. The discussion in Sec 10.4.3 shows that fuel injection is a difficult problem in a full-scale mirror-type reactor, and one which is not entirely solved. In a small machine, it appears to be equally severe, and it may turn out to be one of the more difficult problems associated with ORION design.

The injection (and trapping by ionization) of energetic neutral atoms appears to provide one means of achieving a self-sustaining reaction in a small machine with a modest mirror ratio. The required minimum energy has not yet been calculated, but a plausible guess seems to be several kev.

The feasibility of producing an intense energetic-neutral beam by means of molecular ion dissociation in a high-energy arc is evident from the experiments reported in Appendixes C and E. The device might be arranged as shown in Fig. 7.2.1. As in phase 1, DT ions would be used. A molecular ion source with a 30-kev, 2.5-amp output has been built at ORNL, and the principles whereby still larger ones can be constructed are believed to be understood.

It would be preferable to rely on the compressed plasma itself as the trapping agent if this is feasible. Rough estimates of the ionizing efficiency of the expected plasma show very broad variations, and definite decisions regarding trapping means may have to await the results of plasma-density measurements in DCX.

If ionization of energetic neutrals by the compressed plasma alone is not feasible, a high-energy arc will be used as the ionizing agent. In preparation for this step, the apparatus and techniques described in Appendix C will be used to determine the ionizing efficiencies of the carbon arc and the deuterium arc for D^0's of various energies. In previous tests, 20% of a beam of 20-kev N^+ was converted to N^{++} in the carbon arc.

The behavior of the plasma during the magnetic-field increase will depend on several factors,

[redacted]

ORNL-LR-DWG 25994

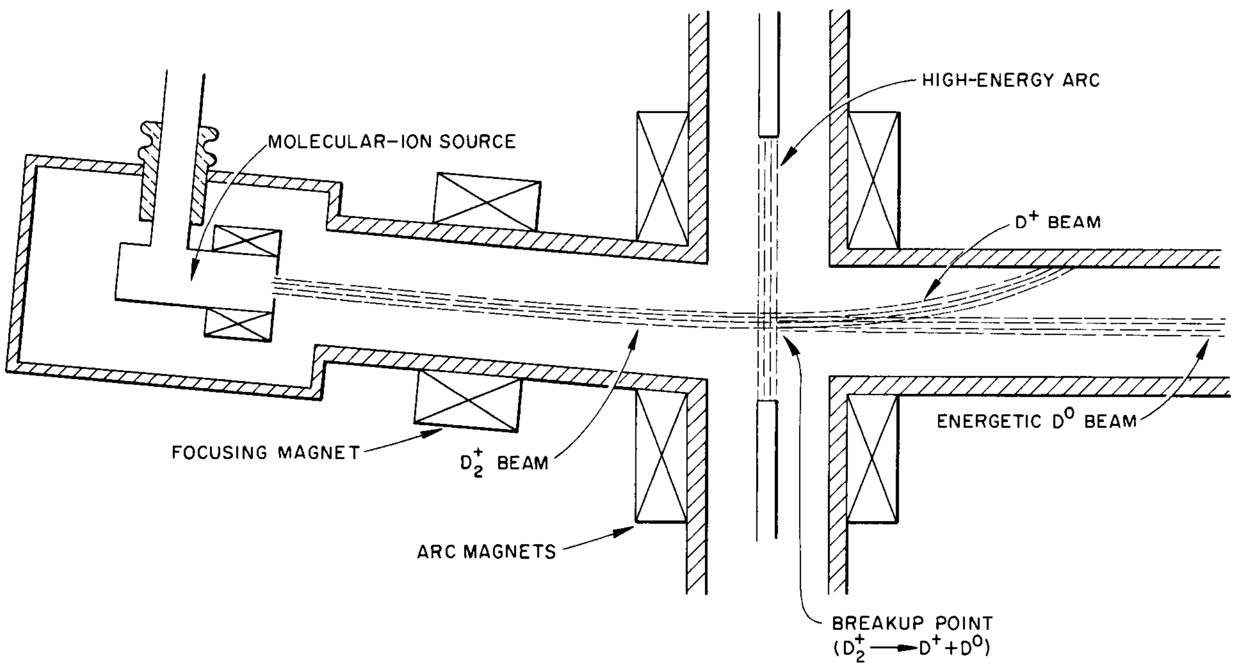

Fig. 7.2.1. Energetic-Neutral Source.

including the heating effect of the rising field and the energy and rate of trapping of energetic neutral atoms. It seems evident, however, that the heat production by the contained reaction products should be caused to start as soon as possible after the injection of molecular ions has, perforce, ceased. More accurately, the field increase should take place in, say, one-tenth of the containment time, which is expected to be a few seconds.

As a preparatory experiment, a field rise will be attempted with the DCX magnet coils by connecting them to a capacitor bank of about 1 farad capacity, charged to 800 to 1200 v. Figure 7.2.2 shows a tentative circuit arrangement. The measured coil inductance is 3.37 millihenrys. The measured resistance, including leads, is 0.077 ohm, not large enough to produce critical damping.

[redacted]

ORNL-LR-DWG 25995

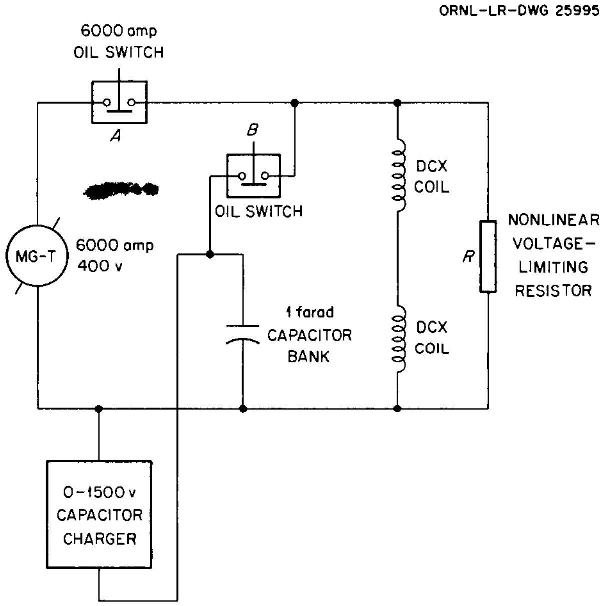

Fig. 7.2.2. Circuit To Produce Rapid Increase in Magnetic Field.

The schedule of operation is as follows: Initially the coils carry the usual current of 6000 amp; switch *A* is opened, the nonlinear voltage-limiting resistor *R* prevents the coil voltage from becoming excessive; switch *B* closes, connecting the charged capacitor bank to the coils. The current will rise to its maximum value in about 80 msec and decay to a low value in a similar time. "Crow-barring" the condenser voltage to zero may be employed, but it is not essential.

With the 1-farad bank, a field of approximately 20 kilogauss can be achieved, enough to contain most of the D-D reaction products and perhaps exhibit some plasma compression and heating effects.

The condenser suggested for this application would be a group of three series-connected electrolytic banks, of only moderate expense. To produce a field strong enough to contain the products of D-T reactions would require a 2.5-farad bank, and a decision has not been made regarding its use pending a more realistic appraisal of the potential information to be gained. A still stronger bank would be required in order to achieve both a field strong enough for containment and a mirror ratio great enough to produce a self-sustaining reaction.

7.3 EFFECTS OF CONTAMINATION ON SYSTEM

DCX, after burnout, is expected to provide unparalleled opportunities for the study of a steady-state thermonuclear plasma. Among the studies of interest will be the attempt to verify the Simon-Rankin calculations (Appendix A) on the effects of impurities on the plasma. According to these calculations, the major effect of impurities on a steady-state plasma in equilibrium with a constant fuel input is to reduce the density rather than the temperature.

A key idea in the high-energy injection concept is that contaminants, which enter with very low energies, will have very large coulomb cross sections and thus very short residence times before scattering into the loss cone or diffusing away from the active volume. They will have a very small probability of acquiring much energy before being lost, and their equilibrium density is expected to be low enough that they will not contribute significantly to the bremsstrahlung.

Recently, calculations by Post[1] have indicated that the chief power drain by contaminants will consist of the collision excitation of excited atomic energy levels and their subsequent de-excitation by radiation. His figures indicate that the presence of modest numbers of partially ionized

[1] R. F. Post, private communication.

contaminants cause the electron temperature to come into equilibrium at a very low value. However, this conclusion applies only if the plasma is being heated slowly, because, if the principal encounters are with particles so energetic that ionization competes strongly with excitation, the impurity atoms which remain long in the system will be stripped and the excitation process will no longer be possible. Therefore, this process is not expected to cause significant difficulty with high-energy injection.

Meaningful measurements to determine the validity of these conclusions are expected to be quite difficult. The experiment will require simultaneous measurement of at least two quantities (for instance, neutron intensity and mirror loss rate) to determine plasma density and temperature, and a third measurement (for instance, bremsstrahlung or optical spectral intensity) to determine the amount of impurity present.

Spectra from impurity ions trapped in the plasma will exhibit Doppler broadening and shifts characteristic of their motion. Thus, Doppler broadening in the optical spectra might be used to determine the mean temperature which the impurities achieve if they do not become completely ionized long before they scatter out. The probability of complete ionization before loss appears to be very small, except for the lightest molecules.

7.4 MEASURE OF β AND DETERMINATION OF CRITICAL β FOR INSTABILITY

A dimensionless parameter which characterizes the state of a plasma in a magnetic field is the ratio of plasma pressure to magnetic field pressure, β. It is generally used loosely in stability estimates which make no distinction between electron pressure and ion pressure or transverse and longitudinal pressure (relative to the field). Only rarely is it regarded as a continuous function of position. Generally, the imprecision of the estimates (for instance, of the critical value of β above which a plasma becomes unstable) is such that rough average values of the quantities involved determine β with an accuracy commensurate with the use to which it will be put.

Expressions for β (in terms of "averages") are:

$$\beta = \frac{nkT}{(B_0^2/8\pi)}$$

$$\beta = \frac{B_0^2 - B_i^2}{B_0^2} ,$$

where n is plasma density, T temperature, B_0 external magnetic field, and B_i internal magnetic field. The determination of β thus requires the measurement of two or three quantities. B_0 can be measured by some conventional technique. Density and temperature will be determined most easily from neutron flux and mirror loss rate in the case of a thermonuclear plasma, from bremsstrahlung spectrum and intensity if the plasma is somewhat cooler. If an alternative measurement is desirable, B_i (and B_0) may be determined by the trajectory of a beam of energetic ions through the plasma. Microwave measurements which yield the electron cyclotron frequency in different parts of the plasma appear to be feasible, but somewhat cumbersome to interpret. A pickup coil, coaxial with and closely surrounding the plasma, which will register the magnetic flux being excluded as the plasma grows, will be useful if it is found practicable to locate it close enough to the plasma.

Bernstein[1] has estimated that a plasma in a mirror field will be stable for β up to some value greater than 0.2. If it is presumed that means will be found to measure and control β, at least roughly, a number of significant experiments can be done which will be of general thermonuclear interest.

It will initially be necessary to determine the configurations of the instabilities. These configurations should be those of the normal modes of oscillation of the stable plasma. The procedure will then consist of inducing certain of these oscillations in plasmas with subcritical β's. This can be accomplished by means of current pulses in properly located external windings. The approach to criticality should be marked by progressively decreasing oscillation frequency for a given mode.

Most interesting among the experiments will be the verification of Bernstein's value of critical β, the measurement of the rate of growth of instabilities in supercritical plasmas, the study of various static and dynamic means of increasing the critical value of β, and the determination of the effects of nonlinear terms on plasma stability. The last experiment will be conducted by applying successively larger perturbations on a stable plasma

[1] I. Bernstein, private communication.

to determine whether instabilities develop above certain limits.

Note that the proposed plasma compression cycle (Sec 7.2) will not in itself change β. However, the heating effects of the D-D reaction products which are contained may be sufficient to raise it, particularly if energetic neutral atom injection is used. If the β before compression is marginal with respect to stability, this possibility could be sufficient to justify the compression experiment.

8. ORION DESIGN, CONSTRUCTION, AND EXPERIMENTATION. PRELIMINARY REMARKS

The design work on ORION has not yet begun, although many of its necessary and desirable physical characteristics are already rapidly emerging from preliminary experience with DCX and from the considerations of the design of a full-scale reactor given in Sec 10. The discussions of Sec 7 concerning DCX experiments relevant to ORION design indicate the general form envisioned for ORION and the expected range of its basic parameters.

Consistent with its purpose, which is to achieve a self-sustaining thermonuclear reaction, it is to be a magnetic-mirror plasma container with a mirror ratio of 3.5 to 1. As indicated in Sec 7.2, it would, if built to the scale of DCX but with improved field quality, have a 26-kilogauss central field and 91-kilogauss fields in the mirrors. About 7 Mw of power will be required for the production of this field. It may be found expedient to scale up the size somewhat and to operate with a smaller field and less power.

Initial operation will be conducted with a 10-kilogauss central field and with high-current DT molecular ion injection and trapping. An iron return path will be used for improvement of the field quality if vacuum considerations permit. After burnout and the establishment of a reacting plasma, the field will be increased to its final value and molecular ion injection will be replaced by cold gas feed or, if necessary, energetic neutral atom injection. Although the field increase might be avoided by the use of retractable magnetic shielding during the ion-injection phase, the plasma heating effects resulting from the field change are regarded as sufficiently desirable to justify it. In fact, operation with a much lower initial field may be found to be desirable.

ORION is naturally expected to open up an entire new range of possibilities for experimentation on plasma properties, reactor kinetics, and effects of intense radiations of various sorts. Its central function, however, will be to provide concepts and data for the design of its successor. Studies will be conducted on waste-gas disposal problems and on means of power extraction. Means of extraction currently considered include heat cycles, neutron utilization, magnetic field variation, and charge separation. Even though only 20% of the power from a D-T reaction is deposited in the charged reaction product, direct electrical conversion of this power with high efficiency can make its contribution to net salable power comparable with that produced by the neutrons.

A detailed design study of ORION is being planned for a forthcoming report.

9. DESIGN AND CONSTRUCTION OF INTERMEDIATE SCALE POWER REACTOR. PRELIMINARY REMARKS

As presently conceived, the Intermediate-Scale Power Reactor is to be built as a short section of the Full-Scale Power Producer. Presumably, by the time it is built, the basic physical phenomena of thermonuclear plasmas will be fairly well understood. It might then be considered a sort of engineering test device in which can be studied the numerous material, power extraction, and controls problems of the full-scale reactor. If the state of the art is sufficiently well advanced during its design period, it might be considered desirable that it be constructed to serve eventually as a component section of its successor. However, the extravagant use of copper, necessary to minimize power consumption where long-term economic considerations govern, would almost certainly not be carried over into the model. It should be borne in mind that a different system of plasma containment could be selected at any stage in the program.

A more detailed discussion of this reactor is being planned for a subsequent report.

10. DESIGN AND CONSTRUCTION OF AN ARC-IGNITED POWER PRODUCER

10.1 INTRODUCTION

The previous sections of this report have indicated how molecular breakup by the high-vacuum carbon arc, or other high-energy arc, will be used to grow a hot plasma in DCX. A second device, ORION, will then be built to proceed from this initial condition to a condition in which the plasma is self-sustaining and is being fed by neutral injection. The culminating step, after this point is reached, will be the construction of a device which is actually a power producer. This section will describe the rough requirements which must be satisfied by such a device. Needless to say, it will be expedient to construct an intermediate device between ORION and the full-scale power producer. However, it is most convenient, at first, to decide on the approximate dimensions of the ultimate goal and then scale down appropriately.

The present plans are for a device which operates on the D-T nuclear reaction with a 50% mixture of deuterium and tritium. Considerations of a D-D cycle have indicated that a device of that type is considerably poorer in its over-all economics than a D-T cycle. However, the D-D device is less dependent upon the solution of problems associated with the reprocessing of tritium and the utilization of neutrons in lithium blankets. In addition, direct conversion of the plasma energy into electrical energy becomes of great interest. It may be that these features will loom more importantly in the future. The present discussion, however, will be restricted to consideration of a D-T heat-cycle device.

The confining magnetic field of the proposed power producer is solenoidal with end mirrors having a mirror ratio of about 3.5 to 1. The field in the solenoidal region is taken to be 30 kilogauss, and it will be shown that the operating temperature is then about 40 kev (average particle energy 60 kev). The associated ion density is about 10^{14} per cubic centimeter, and the ions spend about 0.45 sec in the device before being lost out of the mirrors.

It is found that, with $\beta = \frac{1}{2}$, a plasma radius of 38 cm will produce twice as much electrical power as is needed to energize the magnetic field coils. The resultant salable power is 1.34 Mw per meter of length, and is thus 67 Mw for a device which is 50 m in length. The initial investment costs will be large ($322 per kilowatt for the copper alone).

Attention is paid to the problem of ignition and buildup in the subsequent sections of this report. An initial hot plasma is produced in a subvolume of the larger device by means of the breakup and trapping of molecular ions by a high-energy arc. This initial plasma is compressed until it is self-sustaining and is then fed by injection of cold neutral gas. After the subvolume is filled, the subregion is gradually expanded by electrical means with continuous feed of cold gas so as finally to fill the entire working volume. Operating and feed conditions can be chosen so that there is steady growth of the plasma with no change in temperature.

An important assumption is that the plasma will be stable for $\beta = \frac{1}{2}$. It is important to note that the field lines will be tied down by end plates on the outside of the mirrors. Theoretical calculations of stability carried out at New York University[1] have indicated that plasmas in mirror geometry will be stable for an upper limit of β which is at least greater than 0.05 if the field lines are tied down by a conductor at the ends. Calculations at Princeton[2] indicate stability for β as high as 0.2. The assumption will be made throughout this section that it will be possible to maintain the plasma in a stable condition with $\beta = \frac{1}{2}$.

Conservation of tritium requires that a very high percentage of the emitted neutrons be captured in the lithium of the blanket so as to produce tritium by an (n,α) reaction. It will be assumed that a blanket composed of lithium and water can be designed to accomplish this just as in the case of the proposed model D Stellarator.[3] The blanket thickness will be about 60 cm.

Heat will be extracted from the blanket and from the reaction tube surface by pumping pressurized water through a conventional heat exchanger and

---

[1] H. Rubin, p 193, in *Controlled Thermonuclear Reactions: A Conference Held at Berkeley, California, Feb. 20–23, 1957*, TID-7536 (Part 2).

[2] I. Bernstein, private communication.

[3] L. Spitzer *et al.*, *Problems of the Stellarator as a Useful Power Source*, NYO-6047 (Aug. 1, 1954).

electrical generating system. About 16% of the energy will emerge through the mirrors in the form of charged particles, which will be stopped at the end plates. The energy delivered to the end plate is removed in the same manner as above.

A sketch of the system is shown in Fig. 10.1.1. The relevant dimensions in the solenoidal region are shown in Fig. 10.1.2.

[redacted]
ORNL-LR-DWG 25996

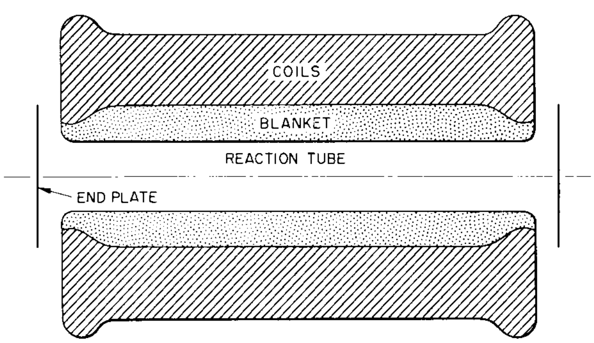

Fig. 10.1.1. Axial Section of Reactor.

[redacted]
ORNL-LR-DWG 25997

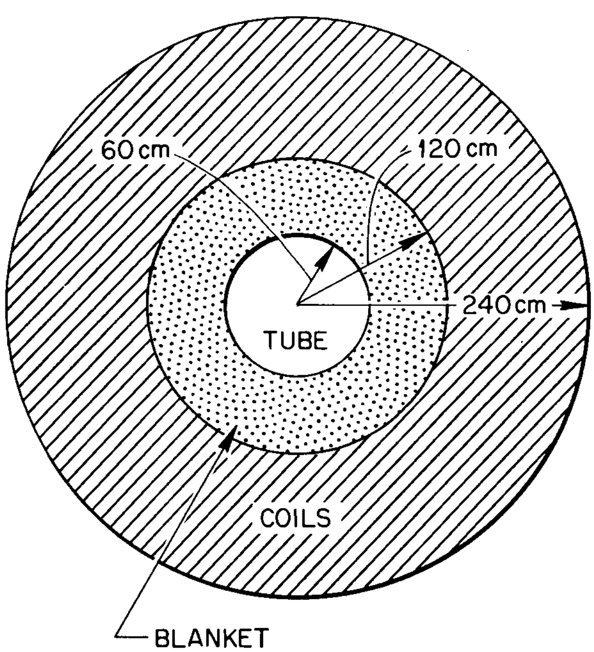

Fig. 10.1.2. Cross Section of Reactor.

10.2 STEADY-STATE PROPERTIES

Assume that the device has been ignited and built up to full density. What is the temperature which the plasma must have in order to maintain constant temperature? This and other parameters of the steady-state distribution are investigated in the following subsections.

10.2.1 Ignition Temperature

In order that the plasma maintain its own temperature, it is necessary that the energy deposited in the gas by the charged particles equal the energy lost by bremsstrahlung plus the energy needed to heat incoming cold gas particles to the temperature of the system. The energy deposited per unit volume per unit time is

$$P_{\text{dep}} = n_D n_T \sigma_{DT} v E_\alpha (1 - \wp) , \tag{10.2.1}$$

where

n_D = deuterium ion density,

n_T = tritium ion density,

σ_{DT} = nuclear cross section,

v = relative velocity,

E_α = energy of charged alpha particle (= 3.5 Mev),

$1 - \wp$ = probability that the alpha particle is not emitted into the mirror loss cone.

If the plasma particles are distributed according to a Maxwell-Boltzmann law, the quantities σ and v should be replaced by $\overline{\sigma v}$. This denotes the average of σv over a Boltzmann distribution. In a mirror machine, however, there will be a peaking of the distribution toward the higher end, owing to the preferential loss of colder ions through the mirrors. For this reason, σ and v will be calculated by assuming an isotropic one-velocity distribution of ions with an energy equal to the average energy of the plasma particles. In this case

$$\overline{v^2} = \frac{1}{2}\int_{-1}^{+1} (v_D^2 + v_T^2 - 2v_D v_T \cos\theta)\, d\cos\theta$$

$$= v_D^2 + v_T^2 .$$

Hence we choose

$$(10.2.2)\qquad \bar{v} \cong \sqrt{v_D^2 + v_T^2} = \sqrt{\frac{2\bar{E}}{M_D} + \frac{2\bar{E}}{M_T}} = \sqrt{\frac{10\bar{E}}{3M_D}}\ ,$$

where

$\bar{E}$ = average energy of an ion in the plasma,

M_D = deuteron mass,

M_T = triton mass.

By similar reasoning, the effective bombarding energy of the deuteron to be used in the cross-section curves[4] is

$$E_D \cong \bar{E} + \frac{2}{3}\bar{E} = \frac{5}{3}\bar{E}\ .$$

The power lost per unit volume due to bremsstrahlung is

$$(10.2.3)\qquad P_B = \frac{64 e^6 z^3 n^2}{3\sqrt{2\pi}\, m\hbar c^3}\sqrt{\frac{2\bar{E}}{3m}}\ ,$$

where

n = total ion density = $n_D + n_T$,

m = electron mass.

The power required to heat the incoming fuel is

$$(10.2.4)\qquad P_{fuel} = I_{in}\bar{E}\ .$$

Since at equilibrium the sum of the particle loss through the mirror and the loss by burning in the reaction must be equal to the input current, the input current per unit volume is:

$$(10.2.5)\qquad I_{in} = \frac{n^2 \sigma_c v \mathcal{P}}{2} + 2 n_D n_T \sigma_{DT} v\ .$$

The first term on the right accounts for mirror loss of fuel. Thus, σ_c is the coulomb cross section for scattering through 90 deg, and the mirror escape probability per 90-deg collision is denoted by $\mathcal{P}$. The second term accounts for fuel lost by nuclear reactions.

[4] N. Jarmie and J. D. Seagrave (eds.), *Charged Particle Cross Sections*, LA-2014 (March 1956).

A plot of the function

$$f = \frac{P_{dep} - P_B}{P_{fuel}}$$

is shown in Fig. 10.2.1. A 50-50 mixture of deuterium and tritium is assumed. This ratio is

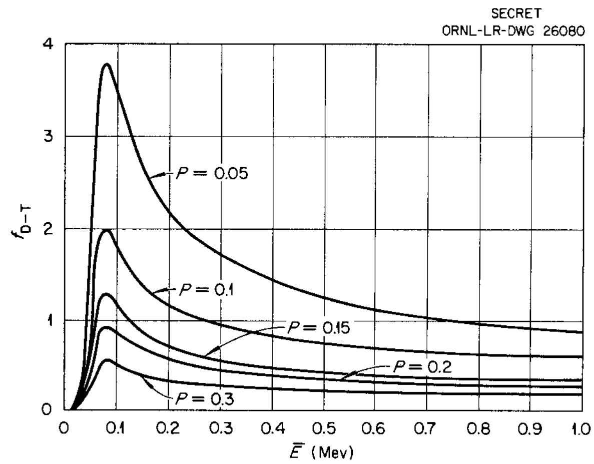

Fig. 10.2.1. Ratio of Net Power Generation to Power Input for Deuterium-Tritium Plasma.

then independent of the densities and is a function of $\bar{E}$ and $\mathcal{P}$ only. It should be noted that

$$(10.2.6)\qquad \sigma_c = 40\pi\left(\frac{e^2}{\bar{E}}\right)^2 = \frac{260 \times 10^{-20}}{\bar{E}^2}\ \text{cm}^2\ ,$$

where $\bar{E}$ is in kiloelectron volts and the assumption has been made that the usual logarithmic[5] term is about equal to 20. Five possible values of $\mathcal{P}$ are used for illustration. On the basis of the simple adiabatic mirror-loss formula,[6] and for a mirror ratio R,

$$(10.2.7)\qquad \mathcal{P} = 1 - \sqrt{1 - \frac{1}{R}}\ .$$

Hence,

$\mathcal{P} \cong 0.3$ for $R = 2$,

$\cong 0.2$ for $R = 3$,

[5] L. Spitzer, *Physics of Fully Ionized Gases*, p 72, Interscience, New York, 1956.

[6] A. Simon, *Nine Lectures on Project Sherwood*, ORNL-2285, p 104 (March 20, 1957).

$$\wp \cong 0.15 \text{ for } R = 3.5,$$
$$\cong 0.1 \text{ for } R = 5,$$
$$\cong 0.05 \text{ for } R = 10.$$

Note that a mirror ratio of 3:1 is too small to permit self-sustaining operation at constant density. For a mirror ratio of 3.5, however, self-sustaining operation at constant density is possible at either $\bar{E} = 60$ kev or $\bar{E} = 122$ kev. Now the lower the operating temperature of a thermonuclear system, the higher the density for fixed magnetic field strength ($nkT \cong B^2/8\pi$) and hence the higher the specific power in the plasma. This is normally desirable, since it results in smaller over-all devices and lower capital costs. For this reason, we choose the operation of our device to be at $\bar{E} = 60$ kev with a mirror ratio of 3.5:1. Note also that the point $f = 0$ is the true ignition temperature. The gas, at that temperature or above, will continue to burn (though at a decreasing rate) in the absence of cold feed.

For purposes of illustration, the function f has been calculated for the D-D reaction. This is shown in Fig. 10.2.2.

10.2.2 Ion Density, Residence Time, and Specific Power

Once the operating temperature of the system has been decided, the maximum density may be determined by specifying a value of the magnetic field. Assume that $B = 30{,}000$ gauss. Then

$$n_e kT_e + n_i kT_i = \beta \frac{B^2}{8\pi} , \tag{10.2.8}$$

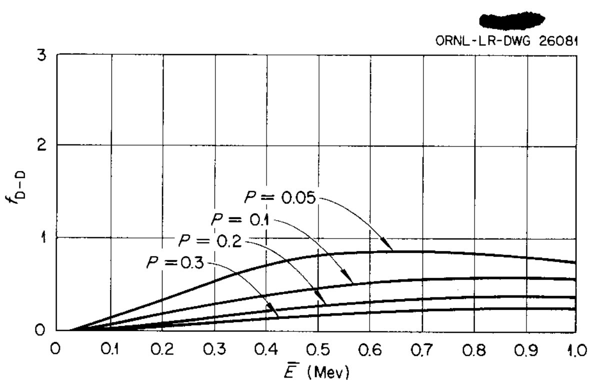

Fig. 10.2.2. Ratio of Net Power Generation to Power Input for Deuterium Plasma.

where β is the maximum ratio of material pressure to magnetic pressure. Assume, as mentioned in the introduction, that a maximum value of $\beta = \frac{1}{2}$ can be achieved. Now, if the electrons and ions are at the same temperature and have equal densities,

$$n_i = \tfrac{1}{2}\cdot\frac{B^2}{8\pi}\cdot\frac{1}{2kT} = \frac{B^2}{32\pi\cdot\frac{2}{3}\bar{E}} \tag{10.2.9}$$

$$= 1.35 \times 10^{14} \text{ cm}^{-3} .$$

The mean residence time in the mirror system is

$$\tau \cong \frac{1}{n_i \sigma_c v \wp/2} . \tag{10.2.10}$$

For $\wp = 0.15$, this yields

$$\tau = 0.45 \text{ sec} . \tag{10.2.11}$$

The specific power produced in the plasma is

$$P = n_{\rm D} n_{\rm T} \bar{\sigma}_{\rm DT} v E_{\rm DT} .$$

Now

$$E_{\rm DT} = 17.6 \text{ Mev} ,$$

and

$$\sigma_{\rm DT} \cong 5 \text{ barns}$$

at

$$E_{\rm D} = \tfrac{5}{3}\bar{E} = 100 \text{ kev} .$$

Hence

$$P = 42.2 \text{ w/cm}^3 . \tag{10.2.12}$$

Finally, the specific neutron production rate is

$$N = n_{\rm D} n_{\rm T} \sigma_{\rm DT} v = 1.5 \times 10^{13} \text{ cm}^{-3} \text{ sec}^{-1} .$$

10.2.3 Magnet Power

As the radius of the device is increased, the nuclear power yield per unit length increases as the square of the radius. On the other hand, the total magnet power required does not change as long as the ratio of outer coil radius to inner coil radius is kept fixed. Hence, there will be a minimum operating radius at which the power produced is sufficient to energize the coils. The minimum radius is calculated in this and the subsequent subsections.

We consider the device to be a long solenoid. This approximation should be valid, except near the mirrors. In that region, the actual magnet power will be somewhat larger than that calculated by this method.

The magnetic field in a solenoid is given by the relation

$$B = \frac{4\pi J}{10} , \quad (10.2.13)$$

where J is the number of ampere turns per unit length. If the inside and outside radii of the coils are denoted by r_1 and r_2, respectively, and s is defined as a space factor equal to the fraction of the gross cross section of the coil which is occupied by solid conductor, then

$$I = \frac{J}{(r_2 - r_1)\, s} ,$$

where I is the current density in the conductor. Hence

$$I = \frac{10B}{4\pi s\,(r_2 - r_1)} . \quad (10.2.14)$$

The ohmic power in the coils per unit length of the solenoid is then

$$P_m = I^2 \rho V , \quad (10.2.15)$$

where ρ is the resistivity of the conductor and V is the volume of the conductor per unit length of the solenoid. Now

$$V = \pi s\,(r_2^2 - r_1^2) . \quad (10.2.16)$$

Hence, by Eqs. 10.2.14, 10.2.15, and 10.2.16, the magnet power per unit length of the solenoid may be written as

$$P_m = \frac{25(r_2 + r_1)B^2\rho}{4\pi (r_2 - r_1)s} . \quad (10.2.17)$$

The resistivity of copper at 20°C is about 2×10^{-6} ohm-cm. In addition, as will be seen, the power density in the coils will be quite low. Hence, the space factor can be fairly large. We assume $s = 0.8$. The choice of r_2/r_1 is somewhat arbitrary. Large values of this ratio yield low values of the total magnet power, but at the expense of large capital investments in copper. We assume that $r_2/r_1 = 2$ will be a reasonable choice (note that a study by the model D group indicated the most favorable ratio to be about 3; however, 2 was chosen by them as being more practical from an engineering viewpoint).

For a field of 30 kilogauss, we obtain

$$(10.2.18) \quad P_m = \frac{25}{4\pi} \cdot \frac{3}{1} \cdot \frac{2 \times 10^{-6}}{0.8} \cdot (3 \times 10^4)^2$$

$$= 1.34 \times 10^4 \text{ w/cm}$$

$$= 1.34 \text{ Mw/m} .$$

10.2.4 Operating Radius

As we have seen previously, the specific power produced by the plasma was

$$P = 42.2 \text{ w/cm}^3 .$$

This number did not include the additional energy obtained from the (n,α) reaction in the lithium, which is 4.6 Mev. Hence, the effective power produced is 17.6 + 4.6 = 22.2 Mev per reaction, rather than 17.6 Mev. With this correction, the effective specific power production is

$$P = 53.2 \text{ w/cm}^3 . \quad (10.2.19)$$

The nuclear yield per unit length from a plasma of radius r is then

$$P_n = 53.2\pi r^2 \text{ w/cm} .$$

As has already been mentioned, this energy will be taken off in the form of heat from the blanket, tube wall, and end plates and will be put through a conventional heat cycle. Assume that this energy can be converted to electrical energy with an efficiency of 33⅓%. The electrical energy is then

$$P_E = \frac{53.2\pi r^2}{3} \text{ w/cm} .$$

We assume that we would like the device to produce as much salable electric power as is used in the magnet coils themselves. In this case, by Eq. 10.2.18,

$$\frac{53.2\pi r^2}{3} = 2 \times 1.34 \times 10^4 ,$$

or

$$r^2 = 4.8 \times 10^2 ,$$

and

(10.2.20) $r = 22 \text{ cm}$.

The actual radius of the reaction tube must be larger than this value for several reasons. For one thing, the above calculation was made on the assumption that the density of the plasma was constant and dropped suddenly to zero at the radius r. In actuality, the equilibrium distribution may be something like parabolic with the density falling smoothly to zero at the outer radius. (This is now regarded as a fairly pessimistic assumption.) Assume a distribution of the form

$$n = n_0 \left[1 - \left(\frac{r}{a}\right)^2\right] .$$

Here a is the actual outer radius of the plasma, and n_0 is the axial density, which will be equal to the density in the previous calculation. In order that the total power produced equal the amount calculated previously, it is necessary that

$$\int_0^a n^2 \cdot 2\pi r\, dr = \pi r^2 n_0^2 .$$

Hence

$$n_0^2 \pi a^2 \int_0^a \left[1 - \left(\frac{r}{a}\right)^2\right]^2 \frac{2r\, dr}{a^2} = \pi r^2 n_0^2 .$$

Therefore, we must choose

$$\frac{a^2}{3} = r^2 ,$$

or

(10.2.21)
$$a = \sqrt{3}\, r = 38.1 \text{ cm.}$$

In addition, the distance from the edge of the plasma should be large enough to ensure containment of the reaction product having the largest radius. In our case, this is an He^4 ion of 3.5 Mev, which has a radius of about 9 cm in a 30-kilogauss field. Thus, it is desirable to separate the plasma and the tube wall by at least the diameter, which is 18 cm.

Incidentally, it should be noted that the diffusion time across the plasma is very large compared with the containment time. The diffusion velocity is

$$v_D = \frac{1}{n} D \frac{dn}{dx} \cong \frac{D}{a} .$$

In this equation, D is the diffusion coefficient,

(10.2.22)
$$D = \frac{\lambda v}{3(\omega\tau)^2} ,$$

where

λ = mean free path in the plasma,

v = velocity of the electrons,

ω = cyclotron angular frequency of the electrons,

$\tau = \lambda/v$ = mean time between collisions.

The mean free path at 60 kev is

$$\lambda = \frac{1}{n_i \sigma_c} = \frac{1}{(1.3 \times 10^{14})(6.7 \times 10^{-22})}$$

$$\lambda = 1.1 \times 10^7 \text{ cm} ,$$

and

$$v \cong 1.36 \times 10^{10} \text{ cm/sec} .$$

Hence

$$\tau = \frac{\lambda}{v} = 0.80 \times 10^{-3} \text{ sec} .$$

Now

$$\omega = \frac{eB}{mc} = 5.8 \times 10^{11} ,$$

so that

$$(\omega\tau)^2 = 2.15 \times 10^{17} .$$

Thus

(10.2.23)
$$v_D \cong \frac{(1.1 \times 10^7)(1.36 \times 10^{10})}{3a(2.15 \times 10^{17})} = \frac{0.232}{a} \text{ cm/sec} .$$

The time to diffuse across the radius of the plasma is then

$$t_D = \frac{a^2}{0.232} = \frac{38.1^2}{0.232} > 100 \text{ min} \ .$$

On combining all these factors, it seems reasonable to choose the radius of the reaction tube so that the distance of the tube wall from the edge of the plasma is at least equal to the diameter of the orbit of an He^4 ion. We choose a tube radius of 60 cm.

The neutron flux at this tube surface is

$$F = \frac{1.5 \times 10^{13} \times \pi \times 22^2}{2\pi \times 60}$$

$$= 6.05 \times 10^{13} \text{ cm}^{-2} \text{ sec}^{-1} \ .$$

10.2.5 Blanket Thickness

The problem of tritium conservation in a D-T device requires that almost exactly one tritium atom be produced for every neutron produced in a 50-50 D-T mixture. It will, in fact, be desirable to breed extra tritium to the maximum extent possible, although the present blanket thickness appears marginal for this purpose. This would necessitate surrounding the reaction tube with a blanket consisting mostly of molten lithium. Unfortunately, it is difficult to use a pure lithium blanket because of the very large mean free path for 14-Mev neutrons and the consequent large age to capture. Blanket thicknesses of over 5 ft would be necessary.

Instead, we consider a blanket consisting of water, beryllium, lithium, and iron. The water is used to moderate the neutrons rapidly, while the beryllium produces extra neutrons by $(n,2n)$ reactions. The iron is used to contain the lithium and water separately.

No special analysis of this situation has been attempted. Instead, we use the results of the Stellarator analysis and assume for the present that a blanket of this sort which is 60 cm in width will be sufficient for the tritium conservation. More careful analysis is planned for the future.

Thus, our over-all thickness is now 60 + 60 = 120 cm, which is, then, the inner radius of the copper coils.

10.2.6 Copper Coil

As was mentioned earlier, the outer radius of the copper will be chosen to be twice the inner radius. Hence, the outer radius is 240 cm. The volume of copper per unit length of the solenoid is then

$$V = 0.8\pi \left(240^2 - 120^2\right) = 1.1 \times 10^5 \text{ cm}^3/\text{cm} \ .$$

The total magnet power was

$$P_m = 1.34 \times 10^4 \text{ w/cm} \ .$$

Hence, the specific power in the coils is 0.12 w/cm^3, which is quite small, as was stated earlier.

The total weight of copper per unit length is

$$W = 1.1 \times 10^5 \times 8.9 = 9.8 \times 10^5 \text{ g/cm} = 9.8 \times 10^4 \text{ kg/m} = 2.16 \times 10^5 \text{ lb/m} \ . \quad (10.2.24)$$

10.2.7 Total Electric Power and Investment

The total length of the device is somewhat arbitrary. It should certainly be reasonably large compared with the diameter of the coils. Since the outer coil diameter is 480 cm, we consider that a total length of 50 m is reasonable. Note, however, that there is no reason why an appreciably smaller length could not be chosen.

Now, since the salable power per unit length is equal to the magnet power, 1.34 Mw/m, the total salable power is

$$P = 50 \times 1.34 = 67 \text{ Mw} \ . \quad (10.2.25)$$

The total investment in copper is estimated by assuming that copper costs about \$2 per pound installed. Then

$$I = \frac{2 \times 2.16 \times 10^5}{1.34 \times 10^3} = \$322 \text{ per kilowatt} \ . \quad (10.2.26)$$

Since this represents the investment in copper only, it is clear that the total investment cost for such a plant will be very much higher than that for conventional systems.

10.3 IGNITION

The device described in the previous section is a steady-state device capable of running for long periods with appropriate injection of cold fuel. In practice, of course, frequent shutdowns and startups will be necessary, and therefore a suitable ignition scheme must be built directly into the device. The proposed scheme comprises two stages. In the first stage, a subvolume of the plasma cavity is partially filled with a hot plasma by use of high-energy molecular-ion injection and trapping. Compression then enables this subplasma to contain its own reaction products and become self-sustaining. The second stage involves injection of cold fuel and expansion of the subvolume. This will be discussed in Sec 10.4.

10.3.1 High-Energy-Arc Breakup

In the initial stage, a subvolume of the entire device is isolated magnetically by suitably energizing different sections of the coils. An additional mirror is produced about 1 m from one of the original mirrors and with the same mirror ratio $R = 3.5$. In addition, the entire field strength in this region is reduced to $\frac{1}{5}$ of its usual value. Thus, the field in the midplane of the subvolume is about 6 kilogauss on the axis and is 21 kilogauss in the coils. This is shown in Fig. 10.3.1. An additional feature is that the next section of field coils immediately following the temporary mirror is either reversed in current direction or reduced in magnitude. The purpose of these

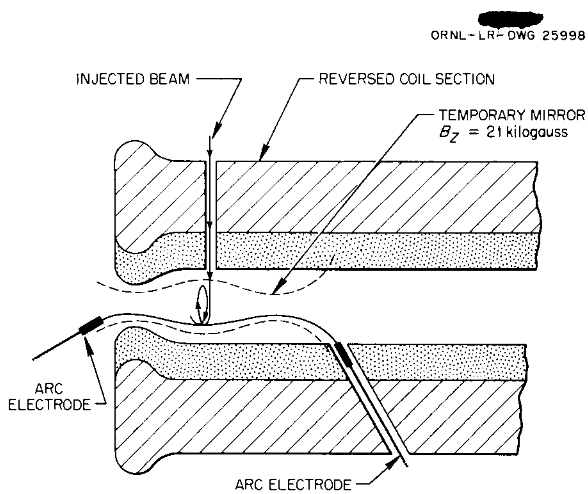

Fig. 10.3.1. Arrangement of Components for Arc Ignition.

changes is to produce a smaller region of the device which is itself a mirror machine. The current is reversed in the outer coil section in order to obtain some field lines which run up into the wall region.

A high-energy vacuum carbon arc or high-energy deuterium arc is now struck between the electrodes shown in Fig. 10.3.1. Note that the left-hand electrode is outside the main volume and that the right-hand electrode is recessed into the wall. It should be noted that a high-energy vacuum carbon arc has already been run in DCX far off-center and that it follows accurately a highly curved magnetic field line.

Once the arc has been struck, injection of molecular DT^+ ions (DT gas is already available at this laboratory) at energies of about 600 kev is begun by use of a cascade accelerator. The situation is very similar to that in DCX. If the two mirrors in Fig. 10.3.1 are separated by about 100 cm, the working volume to be filled is about equal to that of DCX ($\cong 10^5$ cm^3). The injected beam will be of the order of 1 amp, or greater, and a breakup efficiency of at least 25% is to be expected.

10.3.2 Burnout

The initial condition which must be attained is that of "burnout" (Appendix A). In this case, the pressure is low enough and the trapped beam is large enough so that the neutral particles which are flooding into the active volume are destroyed by ionization and charge exchange as fast as they enter. The neutral density drops, and the plasma begins to build up, thus burning out more neutrals. Hence, the system cleans itself up in short order. The injected current of 1 amp should be sufficient if the initial pressure is 10^{-6} mm. Any improvement over this pressure, of course, will produce a corresponding decrease in the current required for burnout.

Burnout in the subvolume will rapidly be followed by cleanup of the rest of the large device. This is because the wall emission ($\cong 10^{11}$ particles per square centimeter per second) yields an influx of particles into the working volume which is smaller than the influx from the vacuum manifold at a pressure of 10^{-6} mm by a factor of at least 10^3. Hence, once the trapped beam has been able to burn out a volume fed by a vacuum manifold influx corresponding to 10^{-6} mm, it should be able to burn out a volume fed by wall emission which has a surface area at least 10^3 times larger. Hence, in a short time, the entire volume will be reduced to a very low pressure.

The achievement of burnout will be immediately followed by the formation of a hot plasma in the subvolume. The resultant ion density is determined by the balance between trapped current and mirror losses, with the proviso, of course, that $\beta \leqq \frac{1}{2}$. It is easily shown that with $B = 10$ kilogauss, $\mathbb{P} = 0.15$, and with an input trapped current of 200 ma the particle density is limited by the $\beta = \frac{1}{2}$ condition for energies of the order of 100 kev or greater. Hence, the input current will be reduced immediately after burnout so as to end up with a plasma with a $\beta \leqq \frac{1}{2}$.

The final energy of the plasma is somewhat uncertain due to uncertainties in the calculations of the thermal conduction but should be of the order of 200 kev. At this energy, for example, the limiting density is

$$n = 1.1 \times 10^{12}\ \mathrm{cm}^{-3}$$

for $B = 6$ kilogauss.

10.3.3 Self-Sustaining Plasma

Immediately following the formation of the plasma, the magnetic fields in all regions (including the temporary mirror) will be increased by a factor of 5. Thus, the end mirror (and temporary mirror) rise to 105 kilogauss while the midplane field goes to 30 kilogauss. Simultaneously, the arc is shut off, high-energy injection is discontinued, and injection of cold fuel is begun.

The principal reason for this step is to reduce the Larmor radius of the He^4 reaction products sufficiently to enable them to avoid the walls. The radius of doubly ionized He^4 at 3.5 Mev is 9 cm in a field of 30 kilogauss. It should be noted that the radius of the input DT^+ ion is 40 cm for $B = 6$ kilogauss.

The addition of sufficient cold fuel causes the temperature of the plasma to fall. The injection continues until the temperature falls to 78 kev. At that time, the cold feed is adjusted to maintain the temperature at 78 kev and to increase the plasma density steadily until it fills the subvolume. The temperature $\bar{E} = 78$ kev is chosen because it is the optimum value for injection of cold fuel. The details of this mechanism will be discussed in the next section.

It should be noted that any impurities in the plasma that are due to the arc ignition technique will vanish rapidly after cold-fuel injection of pure DT gas is begun. It should also be noted that burnout might be achieved by use of pure D_2^+ beams, the subsequent 50-50 deuterium-tritium ratio being achieved by suitable injection of cold fuel. Another feature is that if the temperature is depressed too greatly by impurities, the injection of energetic neutrals may be used to maintain or raise the temperature until the impurities have been cleaned up.

10.4 BUILDUP OF THE PLASMA

If the average energy of the plasma is above the first steady operating point (Sec 10.2.1) and below the second steady operating point (between 60 and 122 kev for $\mathbb{P} = 0.15$), there is an intrinsic tendency for the plasma to heat itself up. On the other hand, if cold fuel is injected faster than it is being lost from the system, this has a tendency to depress the temperature of the plasma. By balancing these two effects, it is possible to maintain the average energy at a fixed level and to increase the total fuel in the volume steadily. The theory of this mode of operation is developed below. This technique will be used to fill the subvolume. The final step will then be the motion of the right-hand mirror to the right, with the consequent filling of the entire working volume. (See Fig. 10.3.1).

10.4.1 Time-Dependent Relations

Assume that the magnetic pressure remains constant and that the plasma pressure also is kept fixed. In this case, the rate of change of the number of particles in the plasma is

$$\text{(10.4.1)} \qquad \frac{d(nV)}{dt} = I - \tfrac{1}{2}n^2\sigma_c v \mathbb{P} - 2n_D n_T \sigma_{DT} v \ .$$

Here n denotes the total ion density ($n = n_D + n_T$), σ_c is the "coulomb cross section" for 90-deg scattering by repeated small-angle collisions, and v is the relative collision velocity. No distinction is made between D-T, D-D, and T-T collisions, although this small effect should be included in a more exact theory. The injected particle current of ions is denoted by I, and V is the total volume of the plasma.

Similarly, the time rate of change of the energy of the system, $\bar{E}$, is given by the equation

$$(10.4.2) \quad \frac{d(n\bar{E}V)}{dt} = Vn_{\mathrm{D}}n_{\mathrm{T}}\sigma_{\mathrm{DT}}v\left[E_{\alpha}(1-\wp)-2\bar{E}\right] - \frac{1}{2}Vn^2\sigma_c v\wp\bar{E} - P_{\mathrm{brems}}V - \frac{4}{3}n\bar{E}\frac{dV}{dt} \ ,$$

where $E_{\alpha}(= 3.5$ Mev) is the energy deposited in the gas by the He^4 reaction product and P_{brems} is the bremsstrahlung loss. The last term on the right represents the work done against the magnetic field by the plasma. The pressure, on the assumption that the electron and ion temperatures are equal, is $4/3n\bar{E}$. At constant pressure,

$$(10.4.3) \qquad n\bar{E} = \text{constant} \ .$$

Hence

$$(10.4.4) \quad \frac{7}{3}n\bar{E}\frac{dV}{dt} = V\left[n_{\mathrm{D}}n_{\mathrm{T}}\sigma_{\mathrm{DT}}vE_{\alpha}(1-\wp) - P_{\mathrm{brems}}\right] - \left[2n_{\mathrm{D}}n_{\mathrm{T}}\sigma_{\mathrm{DT}}v + \frac{1}{2}n^2\sigma_c v\wp\right]\bar{E}V = \bar{E}V(f-1)\left(2n_{\mathrm{D}}n_{\mathrm{T}}\sigma_{\mathrm{DT}}v + \frac{1}{2}n^2\sigma_c v\wp\right) \ ,$$

as follows from the definition of the function f in Sec 10.2.1. Thus, for fixed pressure, the volume will increase with time if $f > 1$ and decrease if $f < 1$.

Of course, this result is dependent on the conditions being consistent with Eq. 10.4.1. In particular, if we wish to keep both n and $\bar{E}$ fixed, this requires that

$$(10.4.5) \quad \frac{7}{3}n\bar{E}\frac{dV}{dt} = \frac{7}{3}\bar{E}\left(I - \frac{1}{2}n^2\sigma_c v\wp V - 2n_{\mathrm{D}}n_{\mathrm{T}}\sigma_c vV\right) \ ,$$

as follows from Eq. 10.4.1 by multiplication by $7/3\ \bar{E}$.

On comparison with Eq. 10.4.4, this shows that

$$(10.4.6) \quad \frac{I}{V} = \left[\frac{3}{7}(f-1)+1\right]\left(\frac{1}{2}n^2\sigma_c v\wp + 2n_{\mathrm{D}}n_{\mathrm{T}}\sigma_{\mathrm{DT}}v\right) \ .$$

Hence, neutral gas must be fed in at a rate specified by Eq. 10.4.6, which is greater than the loss rate if $f > 1$ and smaller if $f < 1$.

If we wish to increase the plasma volume at the maximum possible rate, we must operate at the peak of the f function. From Fig. 10.2.1, this peak occurs at about $E = 78$ kev for $\wp = 0.15$ and has the value $f = 1.3$. Hence, by Eq. 10.4.4

$$(10.4.7) \quad \frac{1}{V}\frac{dV}{dt} = \frac{3\times 0.3}{7n}\left(2n_{\mathrm{D}}n_{\mathrm{T}}\sigma_{\mathrm{DT}} + \frac{1}{2}n^2\sigma_c v\wp\right) \ .$$

The volume will increase exponentially with a time constant T which is

$$(10.4.8) \quad \frac{7}{3(f-1)}\tau = \frac{7n}{3\times 0.3\times\ 2n_{\mathrm{D}}n_{\mathrm{T}}\sigma_{\mathrm{DT}}v + \frac{1}{2}n^2\sigma_c v\wp} \ .$$

Naturally, by Eq. 10.4.6, the neutral feed will necessarily increase exponentially as well.

10.4.2 Buildup Time

For our conditions,

$$\tau \simeq 0.84 \text{ sec}$$

and

$$T = 6.5 \text{ sec} \ .$$

The total expansion of volume required to fill the entire device is of the order of 10^3. Hence, the time required is

$$T_{\mathrm{tot}} = 6.9T = 45 \text{ sec} \ .$$

Thus the entire device can be filled in about 45 sec.

This result also shows that the temporary mirrors will need no special windings, since a temporary overload of a section of winding for an interval of this duration should be of no consequence.

10.4.3 Stability Studies

Equations 10.4.1, 10.4.2, and 10.4.3 were simulated on the ORNL analog computer. The dependent variables n, V, and $\bar{E}$ were recorded on strip charts as various changes were made in both the independent forcing function I and in various system parameters. Details of these results will be published later in an ORNL report.

Some observations of a general nature were made, however. It was found that the two equilibrium points previously predicted ($\bar{E} \cong 60$ kev and $\bar{E} \cong 122$ kev) were both *stable* equilibrium points. Thus, when the analog computer was energized and the various dependent variables came into steady value, E always came to rest in the neighborhood of either 60 kev or 122 kev. For example, if the system was at the 122-kev point, a change in I resulted in a slow return to the 122-kev point. If I was changed by more than a critical value, however, the system then moved quickly to the 60-kev point. It would appear, in general, that there will be no severe problems of power regulation.

10.4.4 Injection Technique

In steady state, fuel will be injected as fast as it is being lost. This total rate is

$$\text{(10.4.9)} \quad \text{F.R.} = \frac{\pi r^2 L n}{\tau}$$

$$= \frac{\pi \times 22^2 \times 50.10^2 \times 1.35 \times 10^{14}}{0.45}$$

$$= 3 \times 10^{21}\ \text{sec}^{-1} \ ,$$

which corresponds to 1/10 liter of DT gas at NTP.

There is a considerable problem associated with the injection of the cold gas into the interior of the plasma. The mean life of the atom in the plasma, before ionization, is

$$t = \frac{1}{n\sigma v} \ ,$$

where

n = ion density,

v = ion velocity,

σ = ionization cross section.

Now

$$\sigma \cong 10^{-16}\ \text{cm}^2 \ ,$$

and thus

$$t \cong \frac{1}{10^{14} \times 10^{-16} \times 10^{8}} = 10^{-6}\ \text{sec} \ .$$

In other words, the incoming atom will be ionized in less than a microsecond, with the result that it does not penetrate into the plasma. It may be possible to operate in this fashion, although it is clearly inefficient.

Other possibilities include taking advantage of cooperative electric fields in plasma blobs. These fields enable blobs to cross magnetic fields quite readily,[7] and it may be that this mechanism will allow a jet of gas to continue on into the plasma after it is ionized. An alternative scheme is to use high-energy injection of neutral particles, although the economics of this would seem to be poor. Perhaps the best scheme is to inject neutral ions into the central plasma region through the mirrors. If the injection angle is chosen properly, the particle will be trapped after it is ionized.

[7] W. H. Bostick, *Experimental Study of Ionized Matter Projected Across a Magnetic Field,* UCRL-4695 (May 10, 1956).

10.5 SUMMARY

Steady-State Characteristics

Average plasma energy	60 kev
Mirror ratio	3.5 to 1
Fuel composition	50% D, 50% T
Ion density	1.35×10^{-14} cm^{-3}
Magnet field (solenoid)	30 kilogauss
β	1/2
Mean residence time	0.45 sec
Specific power	42.2 w/cm^3
Specific neutron production	1.5×10^{13} cm^{-3} sec^{-1}
Plasma radius	$\cong$ 38 cm
Reaction tube radius	60 cm
Flux on reaction tube wall	6.05×10^{13} cm^{-2} sec^{-1}
Magnet power	1.34 Mw/m
Blanket composition	Li, H_2O, Be, Fe
Blanket thickness	60 cm
Coil ID	240 cm
Coil OD	480 cm
Length	50 m
Total heat power	402 Mw
Total magnet power	67 Mw

Steady-State Characteristics		Startup Characteristics	
Salable electrical power	67 Mw	Injected current	1 amp
Total weight of copper	5.4×10^3 tons	Injection energy	$\cong$ 600 kev
Investment in copper	$322 per kilowatt	Filling time	$\cong$ 45 sec

Part II

SUPPORTING PROGRAM OF BASIC RESEARCH

11. STUDIES OF HIGH-ENERGY ARCS

For some time, experiments with energetic vacuum arcs have been made at the Oak Ridge National Laboratory. Some of the results of these investigations are discussed in Appendixes C, E, and I. A more complete systematic study is expected to reveal new and interesting phenomena, as well as a better understanding of those already discovered.

11.1 HOT PROBE

Experiments are under way to measure the space potential at different points in the carbon arc by means of a probe heated to emission temperature. The probe will be made to pass rapidly through the arc in order to prevent damage from energetic ions and electrons. In a feasibility test, a $\frac{1}{8}$-in.-dia carbon probe evaporated in 10 sec. A probe apparatus has been constructed which has been found to perform adequately. It consists of a tantalum loop mounted in a water-cooled shield box. The apparatus is arranged so that the loop can be moved rapidly through the arc. Provision has been made to pass current through the tantalum loop in order to heat it to emission temperature. The device is adjustable, so that readings can be made at arbitrary points along the arc.

Data processing will be done with sequential oscillographic pictures. Each picture will have a plot of the probe voltage as a function of the probe position as it moves through the arc. The probe potential and its location along the arc axis will be the parameters studied in the photographic sequence. These plots are necessary because of the heterogeneous cross section of the arc.

The carbon arc divides itself into small filaments that move constantly across the magnetic field and around the face of the cathode. The peculiar behavior of these columns places stringent requirements on the probe. It must be mechanically stable so as to prevent extraneous movements that result from forces produced by the arc. It must be thermally stable in order to prevent fluctuations in the readings. In addition, the probe must be well shielded in order to prevent pickup from electric fields and to prevent secondary particles from reaching it.

Preliminary data on floating potentials permit a few tentative conclusions. Most of the current seems to be carried in a channel whose diameter is equal to or smaller than that of the cathode. This current channel is surrounded by a region of positive space charge whose diameter increases with distance from the anode. Finally, in agreement with other data, there appears to be a sharp potential drop at the anode (~30 v) and a gradient of about 1 v/in. along the arc.

11.2 CALORIMETRIC MEASUREMENTS

It has been shown[1] that at least 50% of the power supplied to the carbon arc is dissipated through radiation in the column itself. There does not exist at present a complete quantitative understanding of the high-energy arc developed at ORNL. This is true of both the carbon and deuterium types, whose basic operational characteristics appear to be similar. Heat and power measurements should give a better understanding of these discharges. Measurements of this type will also be useful in studying the energetic deuterium plasmas formed in the various machines.

Calorimetric measurements will be made with 6-ft arcs in the long solenoid facility. A movable cylindrical probe will be used to determine whether the power radiated from the arc is constant along its length. In addition, independent measurements of the power dissipated at the anode and the cathode will be made. These measurements will provide data on the distribution of power radiated from all parts of the arc and its electrodes. In addition to measurements made with carbon and gas arcs, the same measurements will be made with combined gas and carbon arcs. These can be done by feeding into a carbon arc a measured amount of the desired gas and checking the effect on power dissipation. Concurrently, spectrographic data will be taken to determine the arc constituents. Spectrographic analysis will be made whenever feasible and correlated with calorimetric data.

In addition to probe and spectrographic measurements of the carbon arc, some of its other parameters will be studied. Some of these quantities are as follows: temperature of the anode and the cathode, formation of arc filaments and cathode spots, evaporation of the cathode and the anode under varying conditions, and analysis of the carbon particles and neutrals that are ejected from the cathode and the anode.

---

[1] Appendix E.

11.3 HIGH-ENERGY GAS ARCS

Recent experiments have shown that a deuterium arc can be made to operate in a mode very similar to that of the carbon arc (see Appendix I). The rotating hot probe, described above, will be very useful in studying these deuterium arcs. In addition, other gases will be used for test purposes. It is felt that these high-energy arcs are a new mode of operation independent of the gas used in the arc. Experiments with the high-energy deuterium arc are interesting because it has been shown that the arc can dissociate energetic molecular ions, which is impossible with conventional gas arcs. Impurities, such as tungsten, were present in the arc when breakup was achieved, but the spectrum appeared to be predominantly that of deuterium. If a deuterium arc could be made to operate at a pressure as low as that of the carbon arc and break up molecular ions effectively, then there would be a distinct advantage in using the deuterium arc. In particular, bremsstrahlung losses would be reduced due to the favorable ratio of the atomic number of deuterium to that of carbon.

The study of high-energy vacuum arcs is a comparatively new and fruitful field of research. New techniques will be needed to study these discharges because of their unusual characteristics. High-energy arc work is planned for the four facilities mentioned in Appendix E. While investigations will continue in the Beta track, the major experiments will be done in the other facilities, which permit better differential pumping and changes in the magnetic-field geometry.

12. MODE II AND COAXIAL ARCS

The Laboratory is pursuing a research program on two interesting types of arcs which show possibilities of producing a hot plasma capable of filling a thermonuclear device. Neither of these systems requires any electrodes in the working volume. At present, their applications extend outside the main line of the DCX program, and it is felt that they should be developed to the point where their usefulness can be quantitatively assayed. As with all such studies, their pursuit is providing a flow of new information and insights into the behavior of plasmas in magnetic fields.

12.1 INTRODUCTION TO MODE II

The characteristic arc behavior described in this section is called "mode II." The mode II arc is remarkable in its ability to transfer energy collectively from electrons to ions. Though not well understood, some of its characteristics and its ability to accelerate ions either parallel or perpendicular to the confining magnetic field are well known.[1]

It is at present thought of as a device which might be exploited in two ways. In the first application, it forms an ion gun suitable for use in injecting molecular ions into the working volume of DCX with energy and density sufficient to accomplish complete ionization and randomization of the plasma. In the second application, the arc is struck along the axis of DCX and accelerates atomic ions directly into the working volume and nearly perpendicular to the magnetic field. The ions are trapped by virtue of their possessing the greater portion of their energy perpendicular to the magnetic field. The arc is a virtual source; that is, there are no solid electrodes at the point of ion emission. Therefore the ions are not lost on their (eventual) return passage through their origin, which is within the confining volume.

12.2 MODE I AND MODE II CONTRASTED

The usual operation of an arc in a magnetic field is characterized by nearly uniform pressure along the length of the arc column. In the pressure range 10^{-4} to 10^{-2} mm Hg, the arc column is sharply defined and much brighter than the plasma surrounding it. Ionization in the plasma surrounding the central arc is 1% or less; ion diffusion out from the arc is by collisions between ions and neutral particles and is random. This condition is identified as mode I. Ion diffusion outward from the mode I arc has been analyzed previously.[2]

The mode II operation of the arc occurs only when there is a pronounced pressure gradient along the arc column and a floating plate is provided at the end of the central column as an electron reflector. The pressure gradient is accomplished by feeding gas directly into the hole which collimates the arc, as shown in Fig. 12.2.1. With a lower gas-feed rate than in mode I, the pressure in the vacuum chamber can be lowered to less than 10^{-5} mm Hg while the pressure in the collimating slot is 10^{-3} mm Hg or greater. The appearance of the arc changes discontinuously when the pressure reaches the required value. The central arc column becomes diffuse and nearly as dim as the surrounding plasma, which has suddenly become brighter. The arc column is still bright near the defining slot to which the gas is admitted, as shown in Fig. 12.2.2.

The following conclusions can be drawn from experiments with a mode II arc in which nitrogen or argon gas was used. Electrons accelerated from the heated cathode possess an energy spread much greater than in the usual arc. Ion energies increase linearly with hot-cathode bias. Time-varying electric fields exist in the central arc column which

[1] L. W. Johnston *et al.*, *Response of the Anthracene Scintillation Counter to Low Energy Electrons,* ORNL-2288 (April 16, 1957).

[2] A. Simon and R. V. Neidigh, *Diffusion of Ions in a Plasma Across a Magnetic Field,* ORNL-1890 (June 27, 1955); A. Simon, *The Influence of End Mirrors, High Density and Long Tube Length on Radial Diffusion,* ORNL-1960 (Sept. 9, 1955); R. V. Neidigh, *Some Experiments Relating Ion Diffusion in a Plasma to the Neutral Gas Density in the Presence of a Magnetic Field,* ORNL-2024 (June 15, 1956).

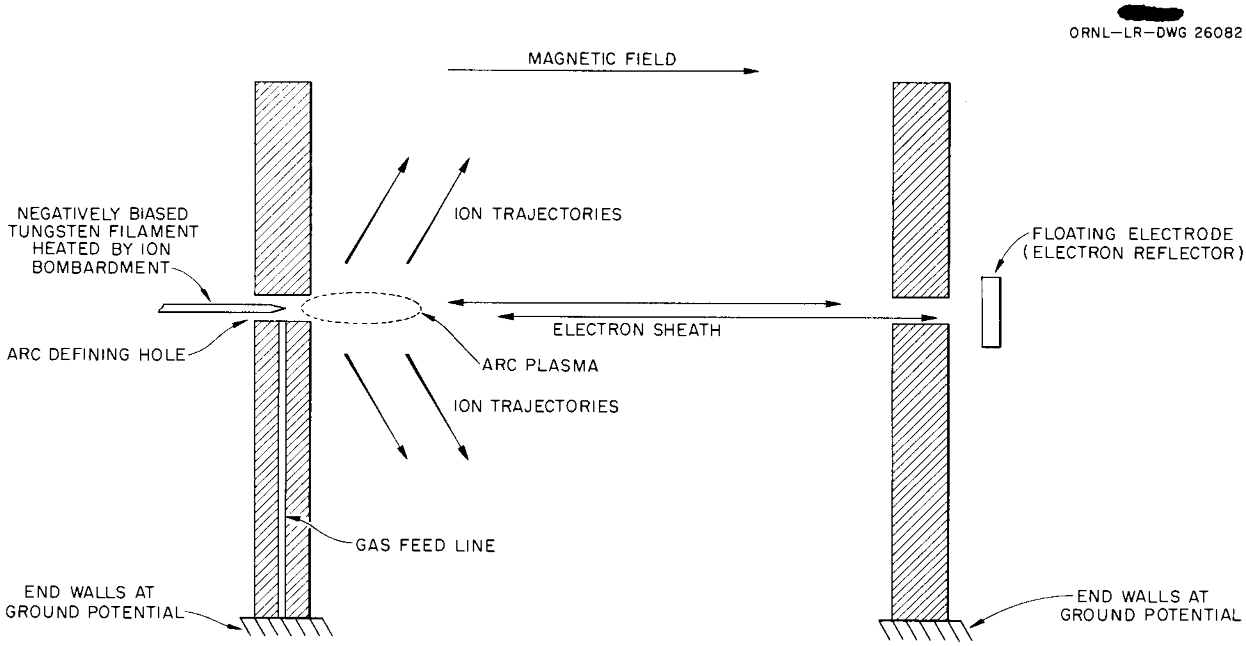

Fig. 12.2.1. Schematic Diagram of Apparatus for Production of Mode II Arc in a Uniform Magnetic Field.

accelerate some ions to at least twice the cathode bias. A degree of containment is effected for electrons. They are constrained to move along magnetic field lines; and the lines are bounded at one end by the heated cathode, at which there is a net electron flux in, and at the other end by a floating plate, which reflects all but the most energetic electrons. The potential of the reflector is always about double the potential applied to the heated cathode. The perpendicular component of the ion energy is comparable with and increases with increased reflector potential. This acceleration of ions is always associated with the pressure gradient in the arc column and occurs only when electrons are contained by the potentials at the ends of the arc and when the loss of ions is restricted by the extra large sheath dimension imposed by the low pressure.

The following conditions are typical of the mode II arc in the present state of development. The maximum deuterium ion energy observed has been 2.5 kv. The use of the heavier gases, nitrogen and argon, has produced a maximum ion energy of 5 kv. In each case the applied voltage was about half the ion energy. It was found that the electron source, formerly a heated tantalum filament, could be replaced by tungsten and heated by ion bombardment from the arc. The present bias is applied by means of a current-limited 35-kv supply. The arc current has been raised to 8 amp, which is the limit of this supply. The bias voltage is then determined by the resistance of the arc. The radial ion flux has not yet been measured with deuterium gas, but that of nitrogen gas has been found to be 200 ma. This work has all been in a uniform magnetic field, ranging from 2000 to 6000 gauss.

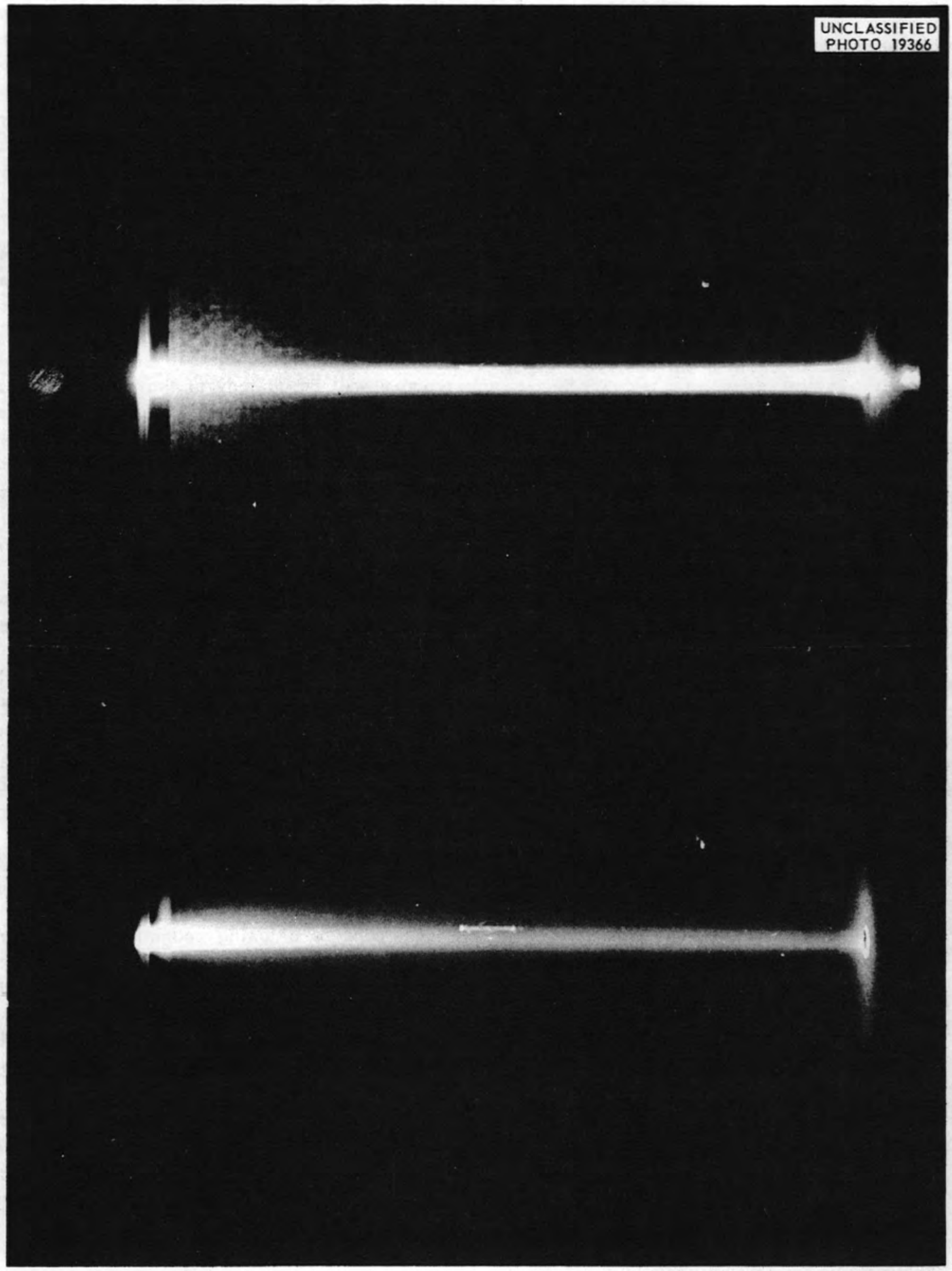

Fig. 12.2.2. Mode I and Mode II Arcs in a Uniform Magnetic Field. The upper photograph (Mode I) is the normal arc without a pressure gradient along its length. The lower photograph (Mode II) is the corresponding arc with the pressure gradient. All other parameters are the same. (Secret with caption)

12.3 ANALYSIS OF MODE II

Continuation of the analysis of mode II is planned, since experiments to determine the total energy distribution and the angular distribution of the ions emerging from the arc are already producing results of a quantitative nature. The rotation of the potential fields in the plasma surrounding the arc is known to be a function of the energetic ion trajectories, the total pressure of the ions and neutrals, and the end wall material. When the ion energies and trajectories become known, the total density of ions and neutrals can be determined from the decay time of the plasma. The decay time has already been observed experimentally (cf. Appendix H) and behaves as expected from present knowledge of the charge exchange and ionization cross sections.

Collective energy transfer from electrons to ions is known to be very efficient in the mode II arc. The ion energy is known to be comparable with and to increase with the reflector potential. An increase in the pressure gradient is also known to increase the ratio of the reflector potential to the cathode potential. An understanding of this mechanism of energy transfer is the goal of a part of the program. Once the mechanism is understood, it can be determined whether there are other applications of mode II to the various aspects of the Sherwood program. Both theoretical and experimental studies are to be made.

12.4 APPLICATION OF MODE II AS A MOLECULAR ION SOURCE

It is expected from first considerations that the principle of energy exchange in mode II can be applied to an ion gun which will shoot ions in dense beams parallel to the magnetic field. Various design and experimental studies will be made. It is also expected that the ion gun will be no longer than the present ion source now being used on DCX. Initial tests in this program have given strong evidence that the goal can be achieved.

12.5 APPLICATION OF MODE II TO A THERMONUCLEAR DEVICE

Ions from the mode II arc are projected at a large angle to the magnetic field. Achieving a predominance of ion current perpendicular to the field is somewhat difficult, and progress is slow because the mechanism of energy transfer is not understood. The efficiency of ion production is excellent. Greater than 90% of the input gas becomes energetic ions, and it appears that ionization will be even more efficient with the increase in applied potential. Since the perpendicular component of the ion energy increases with and is comparable with the reflector potential, and since the reflector potential is always some multiple of the cathode potential, the logical procedure is to increase the applied potential. This has been possible up to the level stated in Sec 12.2. An increase in the arc current lowers the applied potential but gives a corresponding increase in the current of energetic ions.

The immediate work with this phase of the program will be a study of the possibilities of increasing the applied voltage and thus the ion energy. Although it is not known at present how to achieve the same results with deuterium as with heavier gases, there is no reason to believe that it cannot be done. One line of attack is the alteration of the physical geometry of the apparatus in the present uniform magnetic field.

An alternative method is to operate the mode II arc in the magnetic field configuration which exists in DCX and attempt to raise the voltage in this kind of magnetic field, which will ultimately be used. Preliminary experiments on mode II injection into a mirror geometry have given encouraging results. It is hoped that the application of the results of the theoretical and experimental program will bring about a considerable increase in the ion density and energy.

12.6 COAXIAL ARCS

The concept of using coaxial arcs operating at different potentials as a means of heating the gas between them depends upon the establishment of a suitable potential distribution between the two arcs.[3] Experimentally, it has been shown that a 50-kv potential can be maintained between two deuterium arcs. One arc was in the shape of a hollow cylinder, and the other was a small round arc running through the center of the cylinder, hence the name coaxial arcs. The important question of the potential distribution between these arcs has not been resolved. It has been postulated that a field-free region exists between

[3]J. Luce, p 73 in *Conference on Thermonuclear Reactions, University of California Radiation Laboratory, Livermore, California, Feb. 7, 8, and 9, 1955*, WASH-289.

the two arcs, except in a sheath near the negative surface. There is evidence both to confirm and to refute this viewpoint. Probe potential measurements made in the long solenoid facility show that even at low density the gradient does exist primarily in a thin sheath at the negative surface. These plasma measurements suffer from the usual difficulties associated with the use of probes in a magnetic field. Contradictory evidence has been found in experiments where neutrons are measured in a coaxial system as a function of magnetic field and pressure.

In these experiments, a carbon cylinder was used in place of the outer cylindrical arc.[4] The cylinder adsorbs deuterium gas, which acts as a target for energetic deuterium ions. Neutrons are produced when the energetic ions strike the target. If a gradient exists throughout the volume, the ions will "wind up," and a circulating ion current will be created. If the ions wind up, a higher magnetic field would cause the ion orbits to be smaller and their energy to be lower so that they would make more collisions with particles in the volume. The ions give up energy when making collisions, so any increase in the number of collisions will reduce the energy the ions have when they finally strike the walls of the cylinder. The collision rate can also be increased when the magnetic field is held constant, by increasing the pressure in the system. Either raising the magnetic field or raising the pressure would degrade the energy of the ions if they were wound up in the volume. If the ions were accelerated across a thin sheath at the negative surface, no degradation of energy should occur when changes are made in either the magnetic field or the pressure. The cross section for neutron production decreases rapidly when the particle energy is decreased. Therefore, if the ions in the system are degraded in energy, they would produce fewer neutrons when they strike the walls of the cylinder. Experimentally, a very large decrease in neutron production was observed when either the magnetic field was raised or the pressure increased. The accelerating voltage and the current were held constant during these experiments. The concept of circulating ion currents accounts very readily for the effect of magnetic field and pressure on this change in neutron yield.

In summary, coaxial arcs must remain as a potential means for plasma heating unless a better understanding of potential gradients and sheath formation shows the obtainable density to be uninteresting.

[4]Currently, work is being done at Los Alamos (URP) with the same general geometry although at higher pressure.

13. STUDIES OF PROBES

A significant fraction of the present knowledge of glow and arc discharges has come from experimentation with Langmuir probes and analysis by means of the Langmuir theory and its various elaborations. There is, then, always the hope and expectation that probe techniques will prove to be valuable for assessing the state of the plasma in an embryonic thermonuclear reactor. That they have generally failed to live up to this expectation results mainly from the absence of any satisfactory theory of the behavior of probes – or plasmas – in magnetic fields. Even the process of diffusion in a magnetic field was very imperfectly understood until comparatively recently.[1]

A number of successful experiments have been conducted, however, with probes in magnetic fields. Neidigh's diffusion measurements[2] were based on the assumption that the saturation positive ion current is proportional to ion density. Bickerton and von Engel[3] have shown that under certain conditions the determination of electron temperature from the logarithmic derivative of the probe characteristics can be extended to use in magnetic fields. Their argument depends upon the electrons' suffering many collisions in crossing the positive ion sheath around the probe. Space potential measurements with probes heated to emission temperatures are valid in magnetic fields[4] and were found useful in early studies of ion beam plasma. Similar measurements have been made in deuteron beams in the Calutron Beta track facility, and the technique has been adapted for use in DCX.

The plasma conditions in DCX (after burnout) differ in many ways from those studied elsewhere. There will be almost complete ionization; there is a magnetic field gradient; there will be a plasma pressure gradient both along the field and across it; there is present intense ultraviolet radiation from the carbon arc; electron and ion velocity distributions will be anisotropic and will vary with position; and in the plasma core there will be a ring of trapped, organized, energetic ions. The plasma density may be 10^{11} or 10^{12}. Its temperature, at least during the first experiments following the achievement of burnout, is purely a matter for speculation.

It seems clear that a detailed theory of probes applicable to DCX will have almost no starting point in present theories, inasmuch as none of the conditions are met which permit an extension of the Langmuir-Tonks approach. In fact, radically different techniques of probe measurement may be called for.

One possibility under active consideration is the use of pulsed probes. The measurements would be made by applying, to a probe, step-function voltage changes with rise times of a few millimicroseconds and recording the subsequent transient currents. It is thus hoped that time dependence can be used to separate electron collection from ion collection; to separate collection along the magnetic field from cross-field collection; to trace the process of sheath formation or destruction; and possibly, eventually, to get a measure of the electron and ion velocity distributions.

The group is presently conducting experiments on the static behavior of probes in the secondary plasma around, and in, a ribbon-shaped beam of 20-kev ions moving perpendicular to a uniform magnetic field. These experiments are intended to verify and extend the ion beam plasma studies made in the Electromagnetic Separation Project.[4] The conditions are again different from those expected in DCX, but there are enough points of similarity that the empirical information being developed is expected to be a guide in the preparation of experiments for DCX. In particular, unambiguous space potential measurements have been made with emitting probes, and similar ones are under construction for use in DCX. Studies are also in progress on the measurement of ion and electron energies by the use of gridded probes,[5] a technique which appears promising.

[1] A. Simon, *Phys. Rev.* 98, 317 (1955); *Phys. Rev.* 100, 1557 (1955).

[2] A. Simon and R. V. Neidigh, *Diffusion of Ions in a Plasma Across a Magnetic Field*, ORNL-1890 (June 27, 1955); R. V. Neidigh, *Some Experiments Relating Ion Diffusion in a Plasma to the Neutral Gas Density in the Presence of a Magnetic Field*, ORNL-2024 (June 15, 1956).

[3] R. J. Bickerton and A. von Engel, *Proc. Phys. Soc.(London)* B69, 468 (1956).

[4] B. Peters, A. C. Helmholz, and W. E. Parkins, *Natl. Nuclear Energy Ser. Div. I* 4, chap. 2 (1951).

[5] N. I. Ionov, *Doklady Akad. Nauk. S.S.S.R.* 85, 753 (1952); AEC translation 2857.

14. ION AND NEUTRAL SOURCES

The need to inject molecular ions at very high energies (600 kev) into DCX has changed the ion source requirements from those originally envisioned. The grid sources formerly considered had accelerating potentials limited to about 30 kv and were operated in the same volume as was the trapped plasma, making it very difficult to achieve differential pumping. Furthermore, they produced a beam with a line focus rather than a point focus, which complicated considerably the problem of causing the entire beam to strike the dissociating arc.

The immediate requirement is for a source which will permit maximum exploitation of the present high-voltage supply, that is, a current capacity in the range 10 to 50 ma. The step to higher input current, say to 2 amp, requires a new approach to the acceleration problem and thus a coordinated study of both ion source and accelerating mechanism.

The feasibility of producing multiampere energetic D_2^+ ion beams was proved several years ago,[1] and a qualitative understanding of the process exists. Two of the basic requirements are low gas pressure in the ionizing arc and high-energy primary electrons. There are several ion sources under development that are expected to meet the essential requirements of the program.

14.1 HIGH-ENERGY-ARC ION SOURCE

This source will make use of the high-energy arc described in Appendix I. Experimentally, it has been shown that a 150-amp deuterium arc can be made to operate in the molecular state.[2] When these arcs are operated with long-cup anodes, a substantial electric field appears to exist in the arc. This internal field seems to accelerate ions, so that a well-defined ion beam should emerge from the hole drilled in the cathode.

Conventional ion sources depend upon applied electric fields for extracting the ions, which start with only thermal velocity. If a source can be constructed in which the ions are internally accelerated, higher currents and better beam definition should result.

In DCX, 20 amp of back-streaming ions from the carbon arc miss the cathode and are measured on an insulated plate. If a deuterium arc can be made to operate with internal acceleration, then the beam current should be comparable with that of the carbon arc. A source of this type is under construction, and testing will begin in the near future. If the electric field in the arc is insufficient for ion acceleration, the ions will still be accelerated across a sheath at the cathode, but the expected ion current will be greatly reduced. Electron utilization could be enhanced by placing a mirror coil at the end of the cup anode.

14.2 PIG SOURCES

PIG sources are inherently good producers of molecular ions, since they create energetic electrons and operate at low pressure (cf Sec 4.1). Comparatively small sources operated at the High Voltage Laboratory have produced up to 1 ma of D_2^+ ions. A larger model is under construction that is designed for 10 ma. Very little work has been done on these sources to minimize their atomic ion output, and it is thought that their performance can be improved.

The construction of a PIG source is simple: It contains two negatively charged reflecting electrodes with a positively charged ring between them. A magnetic field is directed parallel to the axis. The electrons oscillate between the negative electrodes and through the positive ring, producing ions which exit through a hole in the center of one of the negative electrodes. This simple construction and the inherent high efficiency are advantages when the ion source must operate at high voltage.

14.3 LINEAR ION SOURCE

A linear type of ion source is under construction. This source makes use of the "bucking coil" system designed by E. J. Lofgren of the University of California. Good focusing is inherent in the system because the ions emerge from a parabolic-shaped meniscus. The ion-producing arc employed in this source will be based on the molecular ion arc developed at ORNL. These arcs require large current supplies, since the primary electrons make only one passage through the arc. If a source of this type is used in high-energy machines, it will be necessary to operate power supplies rated at

---

[1] J. S. Luce, p 335 in *Conference on Controlled Thermonuclear Reactions Held at Princeton University*, Oct. 17–20, 1955, TID-7503.

[2] J. S. Luce, p 314 in *Controlled Thermonuclear Reactions; A Conference Held at Berkeley, California, Feb. 20–23, 1957*, TID-7536 (Part 2).

approximately 200 v and 300 amp in the high-voltage terminal. The power would probably be supplied by a gasoline engine and generator contained in the terminal.

14.4 NEUTRAL SOURCES

All energetic neutral sources depend upon initial acceleration of ions, which must somehow be neutralized after the desired energy is acquired. The most efficient known method of accomplishing neutralization is that of dissociation in an arc of energetic molecular ions, $D_2^+ \rightarrow D^+ + D^0$, as illustrated in Sec 7.2. Design work is under way on a system for testing the large-scale exploitation of this effect, and an assembly should be in operation in the near future.

15. VACUUM STUDIES

The unusual vacuum problems presented by DCX (Sec 3) and the uncertainty as to whether their solution lies within the realm of conventional techniques have necessitated the undertaking of a widely diversified program of developmental vacuum studies. Most of the devices and techniques to be used in DCX have their counterparts in experiments designed to determine and maximize the effectiveness of each under conditions that are more completely controlled than is possible in DCX.

In the category of conventional vacuum studies, a test is being made of various liquid-nitrogen-cooled baffle configurations, the aim being to achieve maximum pumping speed with acceptable backstreaming. Acceptable backstreaming for the present purposes is that which permits a base pressure of 10^{-8} mm Hg. The tenfold reduction in pumping speed imposed by the trap-baffle assembly presently mounted in DCX is about average for those currently used. It is hoped that these studies will lead to the formulation of a firm and realistic criterion by which future systems can be designed. A useful criterion might take the form: a satisfactory baffle system is one which cannot be traversed by an oil droplet, or molecule, without at least n collisions with a cold surface, where n is some empirical number. An ideal criterion would take the form: an oil droplet, or molecule, striking a cold surface has an $m\%$ probability of sticking. The present experiments seem more likely to yield a statement of the former type.

In the course of these experiments and others in which the system can be baked out, various baking temperatures will be set, and the time necessary for coming to equilibrium will be measured for each one. Various types of bakable seals and valves will be tried, including liquid and eutectic metal types.

The liquid helium pump now under study is described in Sec 3.5. Its pumping speed and ultimate vacuum will be measured for several gases. Experiments will be conducted with varying pressures above the helium reservoir, which will vary the helium temperature. Of particular interest will be the measurement of the quantity of gas necessary to saturate the pump.

Experiments on titanium vapor pumps are now under way and are being extended to include vapors of other metals. Yttrium is of chief interest currently, since a report was received indirectly from Iowa State College that its performance was superior to that of titanium. According to the report, its pumping speed not only was greater at room temperature but did not fall off at elevated temperatures as severely as that of titanium.

In DCX, it would be desirable to coat an entire liner end or PIG plate face (Sec 3.7) with a getter metal. This must be accomplished without permitting any material to enter the center section. Various evaporating techniques will be investigated to discover one which can be adapted to such selective vapor distribution. Experiments are being conducted to determine the effective pumping rate of titanium in the presence of the carbon arc.

Investigations of the vacuum behavior of the carbon arc have been under way for some time in the long solenoid facility. Recently a bakable liner has been inserted for the purpose of achieving a minimum pressure in the presence of the arc. Preliminary results, quoted in Sec 3.2, indicate that the arc acts as a powerful pump, both by its ionizing effect and by the gettering action of the carbon which deposits on the walls around it. A pressure of 5×10^{-7} mm Hg has been obtained in the liner without baking.

There exists the possibility, however, that the base pressure in the presence of the arc will be limited by recombination and by the action of the arc's intense ultraviolet radiation to release large quantities of occluded gas from the walls. Experiments with the baked liner are expected to determine the nature of the pressure limitations and to indicate the pressure which can be expected in DCX. A useful by-product will be information on whether a surface coated by carbon from the arc can be adequately cleaned up by baking after exposure to the air.

These experiments will be repeated with the deuterium arc, which should emit far less radiation and therefore may perhaps achieve a much higher vacuum.

The action of PIG plates is apt to be so complicated and so dependent upon various parameters not readily adjustable in DCX that an adequate study of their properties cannot be made there. Accordingly, a small chamber is being designed which will be used in conjunction with an existing set of mirror coils to study PIG plates and the various elaborations of them which may arise. Each coil has a 12-in. inner diameter and is capable of producing 4000 gauss at its center. High voltage will be supplied by the 100-kv supply (Sec 18). A certain amount of insight may be gained by study of related experiments at Livermore ("Plus One") and Los Alamos ("U.R.P."); however, the aim and the range of parameters of the presently contemplated experiments make the resemblance fairly superficial.

It is hoped that pumping can be achieved with the PIG plates by imbedding ions in the plate faces. The ionization rate produced by the action of the PIG plates will be measured, and various surface materials will be tested for their loading capabilities. Several schemes of surface regeneration will be tried, including selective evaporation and "roller towel" surface replacement.

Retractable emission points will be used to supply ionizing electrons, if necessary.

Sputtering of the plates by heavier gases threatens to be a problem if they are used as ion-burying pumps. Several solutions are evident, and they lend themselves to combination. One is to take advantage of the directionality of sputtering for low angles of incidence and to form the plates into overlapping, concentric, truncated conical surfaces – venetian blinds with circular symmetry. Another is to cover the surface with a "honeycomb" (Sec 3.7), a set of thin-walled tubes having their axes parallel to the magnetic axis. Sputtered atoms, produced at the bottom of the tubes, will have a reduced chance of entering the system.

Finally, if ion burying is found to be impractical, the plates can be constructed in the honeycomb form, and ions can be allowed to strike the chamber walls in the end sections. Those which recombine will have their passage back to the center section impeded by the honeycomb. It is hoped that experiments can be designed to test the honeycomb idea independently of the action of the PIG plates.

The magnetic field will be adequate for operating energetic arcs if it becomes desirable to make arc tests in the chamber.

Various means have been discussed (Sec 3) for preventing the return to the system of energetic deuterium atoms and ions which strike the chamber wall. A detailed study of wall loading will be conducted in the High Voltage Laboratory by members of the Solid State Division. This study is expected to lead into tests of some of the schemes of energetic particle removal which have been proposed.

16. SPUTTERING MEASUREMENTS

A major contaminant in a thermonuclear reactor might consist of material sputtered from the walls by neutrons and energetic ions. To gage the seriousness of this effect, an investigation of the sputtering of copper by 10- to 40-kev ions has been under way at ORNL for approximately 18 months. The aim of the program has been to provide data directly applicable to a broad class of thermonuclear devices and to lead to a basic understanding of the sputtering process.

The studies have been conducted by measuring the weight lost by a copper plate under prolonged bombardment by ions of hydrogen, deuterium, helium, and argon. Some of the results are reported in Appendix D.2.

The upper limit of the energy to which ions can be accelerated with the equipment presently used for sputtering studies is 40 kev. The limit can be extended to approximately 80 kev by modifications which permit the receiver and target to operate at equal and opposite high potentials. A high-voltage cage is under construction which will fit inside a standard Calutron tank. This cage will be operated at a negative potential of 40 kv. Ions leaving the source (operated at a positive potential of 40 kv) will be accelerated by two potential drops to a total energy of 80 kev. The ion monitoring equipment will all be at −40 kv with respect to ground. All of the required power supplies are now available in the high-voltage cubicles.

When the 100-kv power supply is installed (Sec 18), an extension of the measurements to 140 kev should be possible. Extensive ion-source development will be involved, and use of this equipment will not be possible for some time.

A unit which will permit operating with ions having small radii of curvature has been designed for the purpose of extending measurements below 6 kev. Electrical changes have been made in the high-voltage cubicles so that they will operate with voltages as low as 2000 v.

The immediate plans call for extending the argon-copper data (Appendix D.2) to cover the energy range from 2 to 80 kev.

The data obtained by bombarding copper with deuterium ions will next be extended to cover the same energy range as that of the argon-copper data. Sputtering studies on all of the metallic construction materials to be used in DCX will eventually be undertaken.

The very poor heat conductivity of a material such as stainless steel might make it incapable of withstanding intensive ion bombardment, even by low-energy ions, without an excessive rise in surface temperature. Two early attempts to conduct studies on stainless steel failed for this reason.

The ions to be used as bombarding agents will be mostly those expected to be encountered in DCX. A few ions of heavier gases may be included in order to verify present ideas about mass effects.

17. SPECTROSCOPIC STUDIES

Basic spectroscopic studies, bearing on the atomic and molecular species of importance in the various test devices and the DCX facility, must be carried out to implement the interpretation of data. Such studies include the further elucidation of atomic and molecular energy states of the constituent species in arcs and plasmas, the determination of the cross sections for excitation and ionization by photons and electrons, and the development of absorption and emission methods of evaluating the densities of neutral particles and ions. Several examples of such problems are summarized below.

17.1 ENERGY STATES OF THE HYDROGEN MOLECULAR ION

The study of the radiation absorbed or emitted by D_2^+ may lead to an experimental determination of bound states other than the ground state. Although no experimental observations have ever been made of the D_2^+ (or H_2^+) spectra, the theoretical calculations of Teller and others suggest shallow Franck-Condon potential minima for two highly excited states. For such studies it will be necessary to carry out spectroscopic studies in both the infrared and the vacuum ultraviolet and to develop light sources capable of selective excitation of the D_2^+ spectra.

Assuming the calculations of Teller[1] to be correct, experimental studies of H_2^+ emission spectra should reveal continua at about 1500 Å and 1300 Å. The actual position and shape of these and other possible emission (or absorption) bands in this region and at lower wavelengths will permit the evaluation of the transition structure and probabilities from the $3d\sigma$ and the $2p\pi$ states to the $2p\sigma$ repulsive state and the $1s\sigma$ bound state. Transitions to the $2p\sigma$ repulsive state represent spectra of the dissociation-continuum type. The breadth of each transition continuum will be dependent on the actual shape of the Franck-Condon potential energy curve. The deuterium arc is expected to provide an excellent opportunity to study the D_2^+ emission spectra.

[1]E. Teller, Z. *Physik* 61, 458 (1930).

17.2 OPTICAL CROSS SECTION

In high-density or highly ionized systems the shape of a spectrum line is grossly affected by the interaction with other particles in the gas.[2] The optical cross section for this interaction is determined by the self-absorption within the emitting source. The optical cross section may be evaluated in control experiments from the measurement of the total intensity and the contour of the line and from the density of emitters. Conversely, if one knows the optical cross section of individual spectrum lines, the density of the constituent atoms may be determined. Such cross sections have been determined for a number of lines of the elements such as Li, Na, K, Ca, Cu, and Fe; they vary from about 40×10^{-16} cm^2 to 300×10^{-16} cm^2. In terms of the cross section σ for broadening collisions, the collision width $\Delta\nu_c$ is given by

$$\Delta\nu_c = Nv\sigma ,$$

where N is the density of perturbers per cubic centimeter and v is the mean relative velocity of the two particles. The optical cross sections for excitation and ionization for as many as possible of the constituent particles in the DCX facility will be determined by appropriate experimental techniques.

17.3 ELECTRON EXCITATION FUNCTIONS

Electron excitation functions for the different plasma constituents should be determined in order to ascertain the electron energy in the plasma. In view of the importance of heat losses and of recombination losses of fast ions because of the presence of cold electrons, methods of determining the average electron energy and possibly other characteristics of the distribution must be developed. At Project Matterhorn, Princeton, N.J., the relative strengths of the singlet and triplet resonance lines of neutral helium are used for electron temperature determinations in a range expected to be below that encountered in DCX. Measurement of excitation functions for various

[2]A. C. G. Mitchell and M. W. Zemansky, *Resonance Radiation and Excited Atoms*, Macmillan, New York, 1934.

ionic lines will permit application of the technique at higher temperatures.

Probe experiments, especially in magnetic fields, are difficult and frequently of doubtful interpretation. Spectroscopic radiations, on the other hand, constitute an unperturbing multipurpose probe and can be an essential source of information on plasma properties, provided that the means for their interpretation can be developed. The excitation functions need to be determined with the use of controlled electron energies and densities together with controlled ion densities. The techniques of mass spectrometry can be used to advantage in these experiments.

Experiments are presently under way to determine maximum electron energies in different parts of the carbon arc by means of the detection of certain spectral lines requiring known electron energies for their production.

Inelastic collisions resulting in excitation, ionization, or dissociation can be used to measure the maximum electron energies on the assumption that metastable states are not involved and that single collisions are involved in the spectral excitation process. Table 17.3.1 illustrates the electron energies involved in the excitation of various important atomic energy levels of carbon, appropriately useful spectrum lines involving these upper states being listed for correlation purposes (1 ev = 8068 cm^{-1}). Thus, if the C III line at 4647 Å is observed, and if sufficient C^{++} ions exist in the discharge that only the excitation energy is required, then electrons having energies of at least 32.2 ev must exist in the discharge. In the vacuum carbon arc, copious quantities of carbon ions are required for maintenance of the discharge, and excitation of the 4647-Å line group of C^{++} is quite pronounced. Thus, significant numbers of electrons with energies in excess of 32 ev appear to be present. Observation of the excitation of higher states implies still more energetic electrons.

Electron energies in the carbon arc will thus be determined by utilizing excitation parameters for the allowed energy states in the carbon atom and its various ionic species. Improved studies of the spatial dependence of the C_2 bands as well as neutral-carbon lines appearing near the electrodes will permit a better understanding of the anode and cathode properties of the high-current vacuum carbon arc.

17.4 SPECTROSCOPIC STUDIES IN SPECIAL RESEARCH FACILITIES

The arc research, track, and solenoid facilities are especially useful for extremely refined experiments in which detailed processes may be investigated. The Doppler slant effect and axial

Table 17.3.1. Electron Energies Required for Excitation of Various States of Carbon

Atomic Species	Wavelength Excited (Å)	Excitation Energy (ev)	Ionization Energy (ev)	Total Ionization Energy (ev)	Total Energy (ev)
C I	1657	7.49	0.00	0.00	7.49
C I	2478	7.68	0.00	0.00	7.68
C II			11.26	11.26	11.26
C II	858	14.44	11.26	11.26	25.70
C II	4267	20.94	11.26	11.26	32.20
C III			24.38	35.64	35.64
C III	977	12.96	24.38	35.64	48.33
C III	4647*	32.19	24.38	35.64	67.83
C IV			47.86	83.50	83.50
C IV	1548	8.01	47.86	83.50	91.51
C IV	5802	39.67	47.86	83.50	123.17

*Observed in carbon arc.

ion drifts will be used to correlate and check independently phenomena that are observed by other methods such as probes. The improved vacuum system to be used in all projected facilities will require improvement of the spectroscopic detection methods. Instantaneous photoelectric methods are being developed to permit individual counting and time-gating of light pulses. These will make it possible to determine quantitatively the spatial and temporal dependence of the various excitation mechanisms. The rotational velocities of ions in Mode I and Mode II arcs will be accurately measured in this way.

The spectroscopic observation of the Mode II arc (Sec 12) is relatively more difficult because of the prolonged times required, often up to 3 and 4 hr. Although A^+ ions with energies of several kiloelectron volts have been reported in this system (Sec 12.4), it has been possible, so far, to photograph only the hydrogen spectra with sufficient intensity, and that by using a dispersion of about 7 Å/mm. The spectrograms show relatively broad H_α, H_β, and H_γ lines on which is superimposed the recombination spectrum of H ions. The recombination spectrum is shifted 1.7 Å in one direction at the top of the spectrum and 1.7 Å in the other direction at the bottom. This corresponds to an ordered velocity of rotation of the hydrogen ions of about 10^7 cm/sec, or an energy of about 50 ev.

The availability in the track facility (tank 629) of a steady magnetic field of 25,000 gauss in a 4-in. gap with a 2-ft radius will permit studies at greater field strengths. Preliminary data on Mode I arcs suggest strongly that the ion rotational velocities are significantly increased at 25,000 gauss. The approximately linear increase of ion velocity with magnetic field suggests that more exhaustive experiments be conducted at these higher fields.

The Doppler slant effect, so far observed only for ions moving transverse to the arc length, will be an important tool in evaluating mean ionic drift velocities along the arc and may lead to a reliable measure of the mean free path of ions in the direction of the magnetic field. Carbon arc experiments are now under way in the long solenoid facility, in which a spectrograph analyzes light emitted nearly parallel to the axis. Eventually, multidimensional spectroscopy requiring spatial, temporal, and chromatic determinations will be attempted by utilizing photomultiplier detection.

18. ION BEAM ACCELERATION STUDIES

To study the feasibility of injecting 2 amp of D_2^+ ions at 600 kev (Sec 4.3), it will be necessary to build a testing facility. The initial facility, now under construction, is designed to produce 5 amp at 100 kv. It is shown schematically in Fig. 18.1.1.

The use of 100 kv, instead of the 600 kv which is the ultimate goal, is based on economic considerations and considerations of time. It may result in some loss of flexibility in experimentation but not in the usefulness of the results for application to higher voltages.

Various ideas relevant to accelerating a space-charge-neutralized beam of ions will be evaluated in this facility. They are based on the following considerations. Excess electrons formed in the accelerator tube must be removed as soon as possible so that they cannot be accelerated back into the high-voltage terminal. It is proposed to use magnetic fields to trap and guide the electrons out of the tube. The magnetic field may also be useful in maintaining the collimation of the ion beam. Since the momentum of the ions is so much greater than that of the secondary electrons, they are able to pass through the fringing fields that trap and drain the electrons. There are several variations of this basic method, but some means of removing excess electrons and allowing the ions to pass through is needed.

The pressure in the tube must be kept as low as possible to prevent multiplication by the electrons and formation of a secondary plasma. A plasma in the tube will cause a sheath to form around the electrodes and will prevent acceleration of the ion beam. Since it is planned to accelerate the beam through many stages, formation of this plasma cannot be tolerated. A secondary plasma is a convenient means of neutralizing space charge in the ion beam. In the absence of the plasma, other methods of providing electrons to the beam may be needed.

In summary, the problems of ion beam collimation, electron drain, high vacuum, and space-charge neutralization will be studied. Other problems, such as the ion source (Sec 4), mechanical arrangement of magnetic coils around the tube, insulation of various components for high voltage (600 kv), etc., will also be investigated in the facility.

SECRET
2-02-015-425

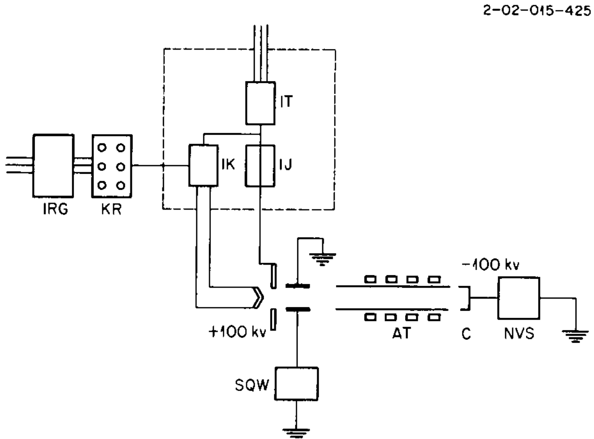

IRG — INDUCTION VOLTAGE REGULATOR, GE SERIAL NO. C714366, 3 PHASE, 220 kva, 60 cycles, 2400 v ±100 %

KR — KENOTRON RECTIFIER, GE SERIAL NO. C657070, 3 PHASE, 425 kva, 4800 v–85400 v Y, 100 kv AND 3, 5 amp d.c.

IK — INSULATED K–SUPPLY, 300 amp, 6 v
IJ — INSULATED J–SUPPLY, 2 x 10 amp, 250 v
IT — INSULATING TRANSFORMER FOR IK AND IJ
} EXISTING INSTALLED GROUP

SQW—HARD-TUBE SQUARE-WAVE GENERATOR FOR BEAM CURRENT MODULATION (RISE AND DECAY TIME 10^{-7} sec) OPTIONAL !

AT — ACCELERATOR TUBE

C — COLLECTOR

NVS—NEGATIVE VOLTAGE SOURCE, MADE UP FROM A FEW EXISTING M SUPPLIES WITH REGULATION FOR NEGATIVE POLARITY

Fig. 18.1.1. Proposed Ion Acceleration Research Facility.

19. METALLURGY

19.1 METALLURGICAL PROBLEMS ASSOCIATED WITH THE DESIGN AND OPERATION OF THERMONUCLEAR DEVELOPMENTAL DEVICES

DCX and the devices which follow will have a large number of complicated materials problems to be solved. The vacuum liner for such a device must be capable of maintaining a vacuum of 10^{-8} mm Hg or better and yet must operate at a temperature of 400°C during bakeout and perhaps even higher while being bombarded with energetic ions, neutral particles, x rays, and neutrons in large quantities. The vacuum liner must not contribute to the problem of maintaining a very high vacuum; on the contrary, it would be very desirable if it could be made of a material which would absorb a large portion of these particles and contain them until such a time as regeneration of its surface was possible. In addition to meeting these requirements, the liner must incorporate transparent windows for viewing and access holes for the insertion of probes and other devices. Needless to say, the preceding requirements are very severe, and the selection of metals, ceramics, and metal-to-ceramic sealants which will meet these requirements will be very difficult. Some of the general features of the experimental program leading to the construction of these devices can be outlined now. It should be noted that these are problems common to all Project Sherwood sites and that a system has been set up to facilitate general information exchange between them.

In the absence of sputtering data, an initial study will be made in order to select metals and ceramics which are capable of being fabricated into the shapes desired. Then the quantities of gas liberated by each of these materials in a high vacuum at temperatures up to and exceeding 400°C will be measured. This investigation will lead to a preliminary screening of the materials. Those ceramics and metals which appear promising after this test will then be joined by various welding and brazing techniques to form vessels which can be evacuated and tested for vacuum tightness and for outgassing at 400°C and higher. It may also be advisable to determine the permeability of these materials for various gases.

Methods for joining ceramic and metal bodies will be investigated, first for strength and integrity when subjected to repeated temperature cycles from room temperature to 400°C and above, and second for vacuum tightness and outgassing both before and after repeated cycles to 400°C. It is anticipated that the joining of these ceramic and metal components may require an extensive search for new materials and for methods capable of joining them.

The sputtering problem may under certain circumstances be quite serious. The wall which is struck should be selected to give off a minimum number of sputtered atoms and should not be seriously damaged by the collision. It may be possible for the liner to absorb the bombarding particles, but if the liner material absorbs these particles, they should be re-emitted only during a regeneration cycle. Materials which have been selected on the basis of the above experiments will be tested for sputtering in the experimental facility described in Sec 16. In the event that the materials previously selected prove to be unsuitable, a search will be made for suitable materials, and methods will then be developed for utilization of these new materials. It seems likely that the solution to the sputtering problem may lie in coating the liner surface with a layer of an appropriate material whose thickness is a fraction of the expected range of the bombarding ion.

Certain ingenious schemes for obtaining high vacua require the use of reactive metals. A study of the rates of absorption, rates of diffusion, and the absorbing capacities of the various promising metals will be made. It will be determined whether these materials may be regenerated and, if so, under what conditions. Some information is available in the literature; however, it is incomplete, and much of it has been calculated theoretically and needs experimental verification. It is also desirable to have more information available regarding the physical and mechanical properties of these reactive metals after they have absorbed significant quantities of impurities.

The proposed devices require the use of valves and gaskets which have extremely small leak rates and are capable of being freed of absorbed gases by baking at temperatures up to 400°C under a vacuum. These valves and gaskets will, in all probability, be all-metal, the sealing surfaces being metal-to-metal joints with very high contact pressures. The mating surfaces must be clean and must deform enough to make a good seal, but it is important that they do not gall or weld under operational conditions. It will be useful to examine the materials presently used for experimental components to determine whether more suitable combinations may be found. This may involve a fundamental analysis of the behavior of metals in intimate contact with each other at high pressures and moderate temperatures. One interesting valve design involves making and breaking a brazed seal to close or open the valve. Preliminary feasibility studies have been made, and materials have been selected for use in the construction of an experimental valve.

The preceding paragraphs have described some of the problems which will arise during the building of the various experimental devices and which will necessarily be solved coincidentally with the construction and development of these devices.

19.2 METALLURGICAL PROBLEMS PERTAINING TO THE ULTIMATE PRODUCTION OF POWER FROM THERMONUCLEAR DEVICES

While it is true that a large number of the materials problems arising when a successful thermonuclear device is converted into a practical source of power cannot be foreseen before the actual construction of such a device is begun, it is already possible to foresee a few problems which will be extremely difficult to solve. If these problems are not to be serious stumbling blocks to the construction of a practical source of power, it might be well to initiate some research into them immediately.

In most schemes presently considered, a thermonuclear reactor which burns tritium is much more attractive than a reactor fueled on deuterium alone. It is probably necessary that the tritium-burning reactor be surrounded with a blanket containing lithium, whose purpose is to react with the neutrons evolved from the thermonuclear reaction in order to create tritium. The tritium thus formed is recovered and is subsequently burned in the reactor.

A sizable portion of the useful energy from thermonuclear reactions may be obtained by utilizing the heat resulting from the slowing-down of energetic neutrons and from the heat of reaction of slow neutrons with lithium. This objective must be accommodated to the tritium generation and recovery function. Thus, immediately surrounding the evacuated chamber containing the plasma there must be a blanket serving to recover the fast-neutron energy and breed tritium.

A number of blanket schemes are currently under consideration. The scheme presented below seems to provide one of the most compact designs and a wide freedom of choice as to the specific materials selected for the various functions.

A very effective way of slowing energetic neutrons to intermediate energies is by inelastic scattering in a material such as tungsten. The cross section is quite substantial at high energies, and only a few interactions are needed to reduce the neutron energy to well below 1 Mev. The energy absorbed in such an interaction appears as gamma radiation, which is mostly absorbed in the tungsten and converted to heat energy.

The neutrons emerging from the tungsten have low enough energy that they may easily be thermalized in a hydrogen-containing moderator and may subsequently be absorbed in a lithium-bearing material.

If we consider the reaction vessel as a tube, the blanket might consist of concentric layers of coolants, inelastic-scattering materials, moderators, lithium-bearing absorbers, and perhaps neutron multipliers. [The term "neutron multipliers" as used here refers to materials (e.g., beryllium) which have large $(n,2n)$ cross sections for fast neutrons.] The total thickness might be considerably less than 2 ft; 2 or 3 in. of tungsten and perhaps 5 or 6 in. of moderator would seem to be adequate. The blanket could be cooled by circulating the neutron multiplier and lithium absorber in the form of liquid metals or fused salts.

Some consideration has been given to the use of metallic lithium as the neutron absorber. The use of lithium metal, which is liquid at the desired temperatures, may lead to mass transfer and other metallurgical problems unless it is contained in what might be considered exotic materials. Also, the power required for pumping a liquid metal through a magnetic field is much greater than the power required for pumping a nonmetallic liquid. Consideration should be given to the possibility of using lithium fluoride as the absorber rather than metallic lithium. This fluoride could be mixed with beryllium fluoride to produce a liquid having a fairly low melting point. The beryllium would produce some moderation, and the same salt might be used as a neutron multiplier.

Among the more promising moderator materials are water and the metal hydrides. Water has several important disadvantages for use at temperatures above 300°C, namely, its high vapor pressure and corrosiveness. Some metal hydrides, the hydride of zirconium for instance, have hydrogen densities comparable to the density of water and offer less serious containment problems. These materials should be evaluated as possible blanket components.

A large number of materials may be considered as inelastic-scattering media and as neutron multipliers. It is necessary to obtain nuclear data as well as physical and chemical property data in order that the most suitable of these materials may be chosen for use in the blanket.

The systems mentioned above should be investigated throughly, and other systems should be surveyed. Cooling by means of gas should be considered. These investigations should take the form of compatibility tests of the simplest type which would allow a screening selection of alloys, cermets, and ceramics useful in the blanket. On the basis of the results of the initial compatibility tests and other pertinent considerations, materials could be selected for testing under conditions more nearly simulating the operational conditions. Upon the completion of these tests, it should be possible to select the most promising scheme for the utilization of heat and the production of tritium. An important portion of this work would consist of the determination of the properties of the container materials at the temperatures expected in service, with special reference to long-time stability at high operational temperatures.

It is quite possible that container materials which have suitable corrosion resistance and strength properties will not be ideally suited to fabrication of heat exchangers and other reactor components. It will thus be likely that a sizable effort will be devoted to the development of fabrication technology, including not only the mechanical forming of the selected materials but also the joining of these materials to themselves and perhaps to dissimilar materials.

Even though it may be a decade or more before a thermonuclear power-producing reactor is built, it does not seem too soon to start work on the materials problems to be anticipated in recovering power from the reactor. Corrosion resistance, fabrication technology, and mechanical properties at the operating temperatures pose serious problems in the selection of structural materials, and it may take years rather than months to obtain definitive answers to such problems. Because of past experience with high-temperature liquid-metal and fused-salt systems, ORNL is well equipped with respect to both personnel and facilities to study the problems associated with the tritium-producing blanket and the removal of heat.

Many materials problems should be examined in the immediate future. Some thought and subsequently some experimental effort should be devoted to the development of suitable neutron moderators and neutron shield materials. It may be possible to alter the properties of the copper used in the magnet coils to make it stronger without the loss of conductivity. Certainly it will be very important to study the effects of irradiation on the properties of structural materials and copper. Methods of recovering tritium from the system should be analyzed, and the permeability of high-temperature container materials to tritium should be experimentally determined.

The preceding paragraphs are intended not to be a complete list of the metallurgical problems seen at this time, but only to illustrate some of those which could profitably be examined coincidentally with the development of experimental devices.

20. RADIATION DAMAGE OF STRUCTURAL AND CONTROL COMPONENTS

20.1 INTRODUCTION

In addition to the various materials problems relative to mechanical stability, corrosion resistance, fabrication, etc. discussed in Sec 19, one of the principal factors determining the choice of materials for structural components of a large-scale thermonuclear machine, and to some extent, the final configuration of components, is their instability under continuous exposure to the energetic radiation produced in the fusion reaction. The relative importance of radiation damage to the various components will be critically dependent on the nature of the material in question, on the intensity of the radiation field in which it is located, and, therefore, on the ultimate design of the machine. However, there are certain critical areas which are to a large extent independent of the final choice of configuration, and it is essential that these be examined to ascertain the extent and seriousness of the radiation aspect of the materials problem. Moreover, since the behavior of structural components when exposed to radiation may have an important bearing on the ultimate design, it is highly desirable that materials development studies be parallel to but integrated with the mainstream effort of the project.

The critical regions in which aggravated radiation effects may be expected are (1) the walls of the reaction chamber, (2) the blanket container, and (3) any components within the reaction chamber and the blanket region. In addition, depending on configuration, more or less extensive effects may be expected in electrical and electronic components, in particular, electrical insulators, temperature-sensing elements, and other auxiliary equipment, which must be placed in the more intense portions of the radiation field. The radiation effects will result from three general processes: (1) displacement effects caused by fast neutrons and, in the blanket region, by alpha particles and tritons, (2) transmutation effects due to neutron capture, and (3) ionization effects resulting from absorption of energetic photons and electrons. The first factor will be a serious one for all types of solids; the second will be of consequence for certain types of alloys in which the burning-out of a constituent having a high cross section would cause deleterious changes in behavior; while the last process is of consequence only in nonmetals. In addition to these effects, bombardment of the walls of the reaction chamber with a high flux of ions and electrons will produce considerable surface damage leading to evaporation and sputtering, thereby constituting an additional problem which may have serious consequences.

A survey of the effects of the various damage processes on components located in the critical regions described above has revealed a number of specific developmental problems which require early attention. In certain cases an appreciable amount of relevant information has already been obtained in other applications; since the nature of the effects on various properties has already been indicated, it is merely necessary to extend the range of measurement to appropriate values of flux, dose, and temperature. In other cases, little work has been done previously, and here extensive studies will be required. The more important of the anticipated problems are enumerated below.

20.2. EFFECTS ON MECHANICAL PROPERTIES OF ALLOYS

One of the most important of these problems concerns the behavior of metals as possible container materials for use in the reaction chamber and the blanket assembly. Such an alloy must resist high temperatures and high fluxes of neutrons and must be nonmagnetic. Typical readily available materials are austenitic stainless steels and Inconel, in which possible radiation effects are radiation-enhanced creep rate and loss of ductility as a result of continuous bombardment by fast neutrons.

The available data on the mechanical properties of refractory, nonmagnetic alloys are limited, particularly at high values of dose rate and total exposure, but definite indications of accelerated creep rates have been observed. It should be pointed out that the temperature of irradiation is most important, since the creep rate may decrease at low temperatures. Therefore it is essential that experiments be carried out at the expected operating temperature if realistic information is required. In the past, most observations have been made at relatively low temperatures. However, small increases in creep rate have been observed at irradiation temperatures near the temperature limit of the material. Therefore, it is necessary that extensive in-pile creep experiments be undertaken to determine the maximum increase in creep rate that might be expected under extreme operating conditions. Needless to say, the dose rate or flux of damaging neutrons is a most important parameter.

In addition to creep, other changes such as loss of ductility during creep are problems causing some concern. Such a ductility loss would cause the material to rupture after much lower extensions than in the absence of radiation. This phenomenon has not yet been observed, but the general loss of ductility observed in most irradiated metals and alloys indicates that such an effect may well exist, particularly after high intensity exposures.

Because of the interdependence of composition, prior history, and temperature of irradiation in determining the mechanical behavior of alloys, considerable research effort will be required for a satisfactory resolution of this problem.

20.3 DECOMPOSITION OF METASTABLE ALLOYS

In addition to the effects on the mechanical properties of alloys produced by the displacement of atoms by fast neutrons, the enhanced microdiffusion resulting from the radiation-produced lattice defects may cause decomposition of these alloys, many of which are in a metastable condition as far as their radiation behavior is concerned. The precipitation of a second phase may have serious consequences for the application considered. For example, in the case of the austenitic stainless steels, precipitation of magnetic ferrite is a distinct possibility. Evidence for the precipitation of ferrite under irradiation is scanty but has been obtained by several groups. Moreover, the effect has been observed even at relatively low fluxes. In the past, this problem has received attention because of the reduction of corrosion resistance that ferrite precipitation brings about. However, if such a radiation-induced process occurred in the walls of the reaction chamber or the blanket assembly of a thermonuclear machine, perturbation of the magnetic fields by the ferromagnetic precipitate particles might have serious consequences. The temperature dependence of this process is not well understood, but the precipitation rate is expected to increase at elevated temperatures and large fluxes. In other metastable structural alloys, induced precipitation reactions may impair the strength and, therefore, the usefulness of these systems as structural components.

20.4 EFFECT OF TRANSMUTATIONS

Another long-range effect which has received little attention is the alteration of alloy composition by transmutation processes. Although such an effect may assume serious proportions only for extended application of alloys in high neutron flux fields, attention to this point is necessary for final design criteria. Stainless steels of certain compositions, and other alloys with functional solutes of appreciable capture cross section, may be affected deleteriously by alterations in composition. Because of its large thermal-neutron capture cross section the manganese in stainless steels is largely burned out after prolonged exposure, being replaced by iron, and chromium is replaced by manganese. The effects of transmutations in changing the composition of alloys in the solid state are difficult to predict, since the effects of alloying elements depend upon the local distribution as well as the amounts of alloying elements. Consequently, an experimental study involving exposure of alloys to large integrated fluxes is necessary to resolve this problem. Since such an effect requires large thermal-neutron fluxes, difficulty from this quarter is expected only in the region where the neutrons are moderated, namely, the blanket assembly. It should be mentioned that this effect may also assume some importance in certain nonmetals, as well as in alloys.

20.5 RADIATION CORROSION

Enhanced corrosion due to radiation may be a serious factor in the blanket assembly, where a high ionization intensity and a high rate of damage by displacement at the interface between the lithium-bearing liquid and the container material are engendered by the (n,α) reaction on Li^6. Studies of systems containing liquids in which fission reactions occur indicate that the problem is a real one. In addition to gross attack of the container, preferential leaching of one or more components of the alloy (or other material if the container is nonmetallic) may occur, thereby altering the composition of the alloy in the interfacial range. If this occurs, the engineering properties of the container material may be seriously altered.

Experience with several reactor projects has demonstrated that studies of corrosion processes of this type and screening of materials available to find those of suitable corrosion resistance in radiation fields are difficult, time consuming, and expensive. Consequently, this problem should be faced as soon as development in other areas of the project permits.

20.6 SPUTTERING AND SURFACE DAMAGE IN THE REACTION CHAMBER

A problem that is closely related to conventional radiation damage is the matter of surface effects produced by interaction of container walls with low-energy neutral and charged particles. The energy range between 10 and 100 kev is outside that previously studied in charged-particle radiation damage investigations. Moreover, in this energy interval, sputtering also becomes a factor; at the present time, this is the only aspect of the problem receiving attention. Since both sputtering and extensive surface damage may be considered to be manifestations of the same irradiation process, it appears desirable to carry out a detailed study of the nature of the lattice damage induced in the surface layer by ion bombardment. Such a study would aid considerably in understanding the mechanism of the damage produced by the interaction of the particle with the surface and, therefore, the nature of the sputtering reaction. Problems that should be studied are (1) the mechanism of interaction of the primary particle with the surface as a function of energy and charge, (2) the relation between surface damage and radiation-induced changes in surface properties (chemical activity, emissivity, electron work function, etc.), and (3) techniques for retaining the particles on a surface.

20.7. RADIATION DECOMPOSITION OF NONMETALS

One of the more sensitive components to be found in accessory electrical equipment which might be located within the critical region is refractory insulation material. Its properties may be affected by both fast neutrons and the intense ionizing radiation of the reaction chamber. Both types of radiation may be expected to alter the electrical and mechanical properties of refractory insulators. Almost no attention has been given this problem for the intense fluxes and high temperatures under consideration. Within the reaction chamber the effect of photons may be at least as great as that of fast neutrons. In the case of certain types of insulating solids, photolytic effects would tend to decompose the solid to some extent by removing the electronegative constituent.

Similar effects may be expected for certain ceramic structural members. It is well known that, when exposed to fast neutrons for a prolonged time, many refractory solids, such as quartz, zirconia, barium titanate, and diamond, undergo extensive structural modifications leading to appreciable lattice expansion. Anisotropic dimensional changes, phase transformation, and complete loss of structure have been observed in a number of cases. Moreover, studies of ceramics have revealed appreciable modification of other physical properties. Appreciable decreases in thermal conductivity and increases in hardness have been observed. Consequently, it is evident that serious consideration should be given to the radiation behavior of any ceramic material contemplated for use in the final design of a thermonuclear device.

20.8 ONE APPROACH TO POWER EXTRACTION

Although some of them have received relatively little attention, the problems discussed above, all arising from the deleterious effect of energetic radiation on the useful properties of solids, are relatively well understood. In view of previous experience with this type of problem in connection with nuclear reactor technology, the research necessary for their solution will follow essentially standard paths. There is another solid-state research problem which may have important application to thermonuclear power in the future. This problem will require considerable departure from the usual course of materials development research for nuclear application. What is considered here is thermoelectric material to be employed for the removal of useful electric power rather than for the conventional thermometric application.

In several respects the thermonuclear reactor offers an unusual opportunity for escaping the usual inefficient conversion from thermal to usable energy which has, until the present, bound power generation to thermal means for power in any appreciable quantity. The pumped plasma concept is a most important step in this direction. Another possibility that is receiving increasing attention in other fields is the use of certain semiconducting thermoelectric elements which hold out some promise of efficient conversion of thermal to electrical energy. The growing interest in thermoelectric refrigeration by means of semiconductor elements is well known. Recently it has been pointed out that mixed-valency semiconductors, usually of transition-metal-oxide type, are effective in producing thermoelectric power even at elevated temperatures with an efficiency that is surprisingly high considering the small amount of development research that has been carried out.

Although, admittedly, investigation of the possible application of thermoelectric extraction of energy from a thermonuclear reactor is an extremely long-range endeavor and may appear premature at this stage of the project, the possibility is sufficiently attractive and the possible gains are so large that exploratory study seems warrented even at this early date. A research program should include exploratory investigation of a wide number of semiconductors with promising properties, and studies of the effects of radiation on the thermoelectric behavior of those compounds which are best suited for this application. Development research should be supported by basic studies, both experimental and theoretical in nature. The future course of such a program must be planned as successive results are obtained. However, a relatively modest research effort would be expected to indicate whether thermoelectric techniques are feasible in thermonuclear reactors.

21. CHEMICAL PROBLEMS IN THE THERMONUCLEAR PROGRAM

The success of the thermonuclear program will require solution of a wide variety of difficult chemical and materials problems. Since most of the proposed devices have features in common, it is possible to list several chemical problems whose solution would be of value to the program as a whole.

Each of the devices currently under study requires a pure high-temperature plasma of deuterons or deuterons and tritons. If a fuel mixture of deuterium and tritium is used, most of the reaction energy is released in the form of very fast neutrons. The problem of absorbing this energy as heat in a circulating coolant which will ultimately raise steam in boilers of conventional design is further complicated by the necessity for generation of sufficient tritium to sustain the fusion reaction. The functions of the blanket material outside the plasma envelope include (1) moderation of the fast neutrons, (2) absorption of the neutrons and evolution of tritium, (3) shielding of the magnet coils from harmful radiation, (4) cooling of the plasma envelope, and (5) transfer of the generated heat to the boiler system. It may be desirable, in addition, to incorporate neutron multipliers such as beryllium or bismuth in the blanket. Such a device, accordingly, poses problems in neutron economy not unlike those of a breeder reactor. Some aspects of the blanket problem have been discussed in earlier sections.

If the reactor is fueled by deuterium alone, as might be done in a toroidal geometry, most of the energy produced is retained with the charged particles. It is presumed that electricity could be generated from such a system by methods much more direct than the steam cycle. It will still be necessary to shield the magnets, and it may still be necessary to cool the plasma envelope. It is possible that this heat can be recovered at a usefully high temperature to raise steam in a conventional fashion. The system would have no dependence on neutron economy; however, the possibility of absorbing the evolved neutrons to increase the energy yield and to accomplish useful transmutations would of course be considered.

Chemical problems of immediate and of long-range interest to the program arise concerning (1) maintenance of a clean, hard dynamic vacuum in the plasma chamber, (2) development of optimum materials for the blanket and/or coolant, (3) recovery, purification, and handling of the tritium (if used), and (4) a possible purification recycle for the unburned effluent from the plasma chamber.

21.1 CLEANNESS OF THE VACUUM CHAMBER

The problems of most immediate importance to the program are concerned with optimum methods for outgassing the plasma chamber and for maintaining a high vacuum in the chamber under operating conditions. Chemical assistance would seem to include (1) testing of new and improved chemical getters, especially those with great affinity for the hydrogen isotopes, and (2) examination of the chemisorption of gases and vapors at very low partial pressures on metal and ceramic surfaces and the release of absorbed materials under bombardment with particulate and electromagnetic radiations.

21.2 DEMONSTRATION OF OPTIMUM BLANKET MATERIALS

The combination of materials in the blanket of a D-T system must be an efficient tritium generator as well as an excellent heat transfer medium. Much information is needed for evaluation of the possible ways of accomplishing these objectives. Several of the possibilities described briefly below seem to be worthy of study. Others have been discussed in Sec 19.

Tritium production could be accomplished in canned solid lithium-aluminum (or other) alloy bathed in a liquid coolant. Use of this scheme should permit recovery of tritium by well-known technology but would certainly complicate the problem of blanket fabrication. Such an assembly could be cooled by water or by a liquid metal such as sodium. If water were used, relatively low-grade steam or undesirably high pressures would result. If sodium were used, an additional moderator would be necessary.

Use of a separately canned hydride moderator or a heavy metal "reflector" for partial degradation of the neutron spectrum would seem to be possible. Such a reflector would probably have to consist of relatively thin sections in order to allow for adequate cooling.

Use of aqueous solutions of lithium compounds in a truly homogeneous blanket would not seem particularly valuable. While it might well afford the simplest blanket structure, the high pressures, radiolytic decomposition of the water, the relatively low-grade steam produced, and the required separation of tritium from enormous quantities of hydrogen would be serious disadvantages. Use of molten hydroxide mixtures containing lithium hydroxide would permit low-pressure operation but would add very serious corrosion problems.

With a suitable solid moderator or reflector, tritium could be produced in a coolant of lithium metal (or perhaps a liquid alloy) or in a coolant consisting of lithium fluoride in a molten fluoride mixture. Of these possibilities, molten lithium is the best heat transfer medium. However, corrosion by lithium is still serious, recovery of tritium at low concentrations from this metal may be difficult, and power losses to the metal from the magnetic field are likely to be important. On the other hand, molten fluoride mixtures containing lithium fluoride have been shown by extensive testing to be much less corrosive to several alloys than is metallic lithium. The molten fluorides are adequate heat transfer agents. They have low vapor pressures and are quite stable to radiation. The system lithium fluoride–beryllium fluoride shows usefully low melting points over a wide range of compositions, and it offers the advantage of a contained neutron multiplier.

The solubility of helium in similar fluoride mixtures obeys Henry's law and has the value 2×10^{-7} moles of helium per cubic centimeter of salt per atmosphere at 600°C. The solubility of tritium is unknown but is expected to be of this same order. The removal of contained tritium by pumping or by sparging should be relatively simple.

A molten salt mixture must maintain cation-anion equivalence even though the Li^+ or Be^{++} undergoes transmutation. Tritium fluoride, which might be expected to form, is (by analogy with hydrogen fluoride, for which experimental data are available) unstable to such container metals as iron or chromium. It is likely that a trace of dissolved metal (beryllium, for example) can be maintained in the molten salt to avoid the corrosion of the container metal which would otherwise be required to satisfy the excess F^- resulting from transmutation of Li^+. If the neutron multiplier is not essential, dilute solutions of potassium metal in lithium fluoride–potassium fluoride mixtures should certainly avoid difficulty of this sort.

If the device burns deuterium alone, the blanket problem is reduced to, at most, that of cooling the plasma envelope, shielding the magnets, and absorption of the neutrons for their energy and for the production of some salable material. It is conceivable that the production of polonium from bismuth, of U^{233} from thorium, of plutonium from U^{238}, or of low-cross-section isotopes of various elements might be practicable.

21.3 TRITIUM RECOVERY

It will be necessary to provide a recovery, purification, and storage system for the tritium and, presumably, a purification and recycling system for the tritium-deuterium mixtures recovered from the plasma envelope. However, the problems involved will depend on the blanket materials, the configuration chosen, and the pumping and trapping system chosen for the plasma envelope. In spite of the difficult standards of purity which will probably be required, there would seem to be no insurmountable problems in the handling of tritium and deuterium. Considering the relatively large volumes required, it seems likely that handling and storage of the materials as liquids would be justified. Liquefaction of the gases with low-temperature distillation and storage should suffice for purification. It might be more satisfactory, however, to recover the materials as D_2O and T_2O, purify and store them in this form, and subsequently electrolyze to provide the gases as required.

21.4 DEUTERIUM REPROCESSING

From a continuously operating system it will, presumably, be necessary to remove from the system unburnable particles such as nuclei of He^4. Such separations would presumably not be terribly difficult when applied to neutrals lost by various mechanisms from the plasma. For the deuterium burner, where charged particle economy is of extreme importance, it would be desirable to have a method applicable to charged particles lost from, but perhaps returnable to, the containing magnetic field.

APPENDIXES

[redacted]

Appendix A

SOME PROPERTIES OF A STEADY-STATE HIGH-ENERGY* INJECTION DEVICE (DCX)

A. Simon M. Rankin

ABSTRACT

DCX is an experimental Sherwood device utilizing high-energy molecular ion injection and trapping. It is shown that, if the input current of trapped deuterons exceeds a critical amount, there will occur a "burnout" of most of the neutral particles in the system. If this burnout does occur, the input ions will be degraded only slightly in energy before becoming disorganized in direction and forming a plasma. Some possible perturbing mechanisms are considered. Impurities are shown to have little effect on the temperature, although their presence decreases the plasma density somewhat. Heat conduction to the walls and to the arc is estimated, as well as the effect of cold electrons. It appears that, in the absence of plasma instabilities, the final temperature, with an input energy of 300 kev, can be as high as 280 kev or as low as 75 kev. A plasma density of 10^{12} per cubic centimeter or greater may be achievable with a 1-ma input.

A.1 INTRODUCTION

DCX is the name of the device which is being built at the Oak Ridge National Laboratory to exploit the molecular injection and trapping techniques developed by Luce.[1] The essential feature of the method is the injection of a D_2^+ molecular ion across a magnetic field and the subsequent dissociation of this ion into a D^+ ion and a D^0 atom or into two D^+ ions and an electron. In either case the resulting D^+ has half the momentum of the original molecule and hence half the Larmor radius in the magnetic field. Thus, if breakup occurs in the outer regions of the orbit of the molecular ion, the resultant D^+ is trapped and does not return to strike the injector. The scheme is sketched in Fig. A.1.1.

The success of this injection scheme is due to two advances made by Luce. The first was the development of high-current sources of molecular ions. The second was the discovery of the high-current carbon arc,[2] which can break up molecular ions with good efficiency (over 50% at 20 kev; about 10% at 600 kev). This composite injection scheme will be referred to as a Luce-type injection system.

DCX combines a Luce injection system with a containing geometry of the mirror type. This is the most convenient geometry to use, although not the only possible one. For example, it is perfectly possible to inject into a pinch device or a Stellarator. The present plans are to inject about 1 ma of D_2^+ ions at 600 kev by using the cascade accelerator which had been in use at the High Voltage Laboratory of ORNL.

---

*A. Simon and M. Rankin, *Some Properties of a Steady-State High-Energy Injection Device (DCX)*, ORNL-2354 (Aug. 26, 1954).

[1] J. S. Luce, *Molecular Ion Source*, ORNL CF-55-11-160 (Nov. 30, 1955).

[2] J. S. Luce, *Molecular Ion Breakup: Preliminary Note*, ORNL CF-56-7-119 (July 26, 1956).

[redacted]

ORNL-LR-DWG 26222

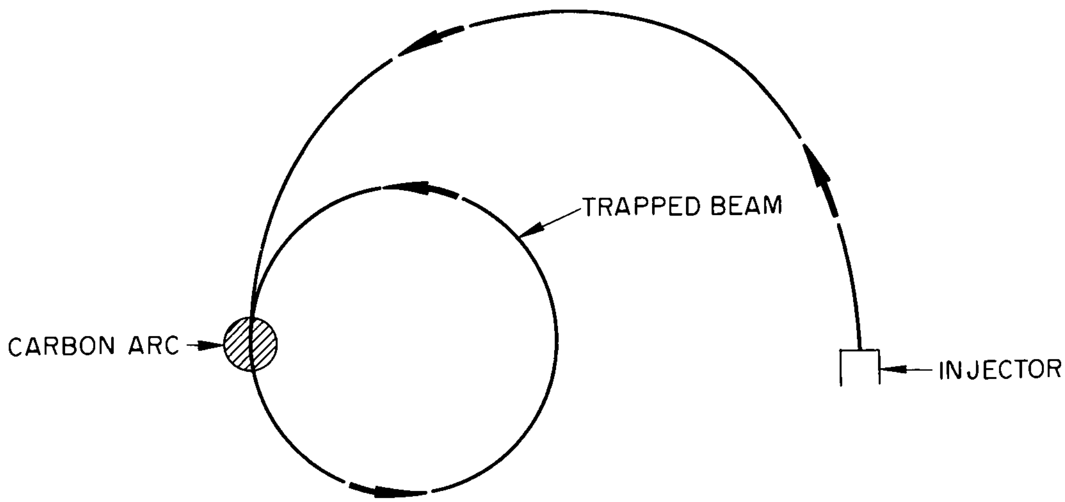

Fig. A.1.1. Luce Injection Scheme.

DCX differs in three fundamental respects from the other Sherwood devices. First of all, it makes use of the Luce injection scheme. Second, it is a completely d-c device; the injection, the magnetic field, and the arc are all steady-state. Finally, DCX grows a plasma by *working down* in energy rather than by working up.

The calculations in the subsequent sections are concerned with the properties which a device such as DCX will have. One question is the temperature at which the plasma is formed. This is investigated in Sec A.2. Neutral particles are damaging to the system because of their propensity toward charge exchange with the hot ions. It is found that there is a critical point at which the input ions "burn out" the neutrals. This is calculated in Sec A.3. Some additional effects which may be important are discussed in Sec A.4.

A.2 THE IDEAL DCX

In the first version of DCX the trapped beam of D^+ ions will be injected at a steady rate at an energy of 300 kev. In the steady state, there will be a plasma of cooler ions and electrons below the beam energy which immediately begins to degrade the beam energy by the usual energy loss processes. The cross section for this energy loss is somewhat larger than that for coulomb deflection. Hence, the beam tends to retain its original uniformity in direction and slowly spirals down in Larmor radius as the energy decreases. However, as the energy of the degraded particles approaches that of the plasma particles, the cross section for energy transfer drops below that for coulomb deflection, and the beam is then randomized in direction and goes into the plasma. The exact calculation of this behavior is a formidable task. Instead, an idealized model will be used to determine the approximate temperature of the plasma.

In this model the injected particles are assumed to stay organized in their motion until they enter the plasma. After entering the plasma, ions are lost through the mirrors in the usual fashion. Impurities and neutral particles are assumed to be absent. Energy is fed to both the ions and the electrons in the plasma by the ions which are slowing down. The electrons lose energy by bremsstrahlung. A schematic diagram of the model is shown in Fig. A.2.1.

[redacted]

ORNL-LR-DWG 26224

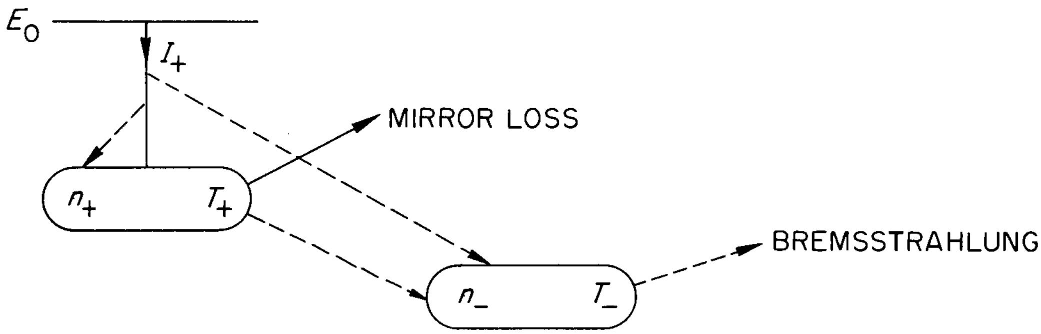

Fig. A.2.1. The Ideal DCX.

The dotted lines denote the direction of transfer of energy, while the solid lines denote particle paths. Note that no influx or outgo of electrons is assumed. Instead, the electron density is determined by the requirement of space-charge neutrality. The electrons are cooler than the ions by virtue of their bremsstrahlung losses.

There are four unknowns to be determined once the input particle current I_+ and input energy E_0 are specified. These are the ion and electron densities in the plasma, n_+ and n_-, and the temperatures of the plasmas, T_+ and T_-. These may be determined by the four equations resulting from the requirements of energy balance, ion conservation, and space-charge neutrality.

Energy Balance in the Ion Cloud

Let $N(E)\,dE$ denote the number of ions in the organized beam between energy E and $E + dE$. The rate at which energy is being fed into the ion cloud by the organized beam is then

(A.2.1) $$P_{in} = \int_{E_+}^{E_0} N(E) \left.\frac{dE}{dt}\right|_+ dE ,$$

where E_+ ($= \frac{3}{2} kT_+$) is the average energy of an ion in the plasma and $\left.\frac{dE}{dt}\right|_+$ denotes the the rate of loss of energy by an ion of energy E to a plasma at temperature T_+.

In steady state the energy flux of particles in the organized beam must be constant and equal to the input particle rate. Hence

(A.2.2) $$N(E) \frac{dE}{dt} = I_+ ,$$

where dE/dt represents the rate of loss of energy by the ions in the organized beam to all sources (i.e., both electrons and ions). Thus, Eq. A.2.1 becomes:

(A.2.3) $$P_{in} = I_+ \int_{E_+}^{E_0} \frac{\left.\frac{dE}{dt}\right|_+}{\frac{dE}{dt}} dE = I_+ \int_{E_+}^{E_0} \frac{\left.\frac{dE}{dt}\right|_+}{\left.\frac{dE}{dt}\right|_+ + \left.\frac{dE}{dt}\right|_-} dE .$$

A general expression for the rate of energy loss by coulomb collision from a particle of mass M to a Maxwell-Boltzmann distribution of target particles of mass m has been given by Chandrasekhar.[3] The result is

(A.2.4) $$\frac{dE}{dt} = -\frac{MA_D}{2\omega}\left[2x^2\left(1 + \frac{M}{m}\right)G(x) - \phi(x)\right] ,$$

where ω is the velocity of the particle of mass M, and l is defined by

(A.2.5) $$l^2 = \frac{m}{2kT} .$$

Here T is the temperature of the target particles. The quantity $x = l\omega$, the function ϕ is defined by

$$\phi(x) = \frac{2}{\sqrt{\pi}} \int_0^x e^{-y^2}\, dy ,$$

and

(A.2.6) $$G(x) = \frac{\phi(x) - x\,\phi'(x)}{2x^2} .$$

[3] S. Chandrasekhar, *Astrophys. J.* 97, 255 (1943).

Finally,

$$A_D = 8\pi n \left(\frac{zZe^2}{M}\right)^2 \ln \Lambda \ , \tag{A.2.7}$$

where the density and charge of the target particles are denoted by n and z, respectively, and Z is the charge of the incident particle. The logarithm results from the usual cutoff on the maximum impact parameter. This quantity is rather slowly energy-dependent, and in these calculations it will be taken to be a constant whose value is 20. Hence

$$\ln \Lambda \cong 20 \ . \tag{A.2.8}$$

Consider the rate of energy loss from ions to a cloud of electrons. Unless the electrons are extremely cold ($E_{elec} < [m/M]\, E_{ion}$), the velocity of the electron will be very much larger than that of the ions, and the quantity x is very small. If this assumption is made (as will be justified by the numerical results), a simplified expression is obtained for the loss rate to electrons. Since

$$\left.\begin{array}{l} G(x) \longrightarrow \dfrac{2x}{3\sqrt{\pi}} \\[2ex] \phi(x) \longrightarrow \dfrac{2x}{\sqrt{\pi}} \end{array}\right\} \quad \text{as } x \longrightarrow 0 \ , \tag{A.2.9}$$

it follows that

$$\left.\frac{dE}{dt}\right|_- = -\frac{MA_D}{2\omega} \cdot \frac{2x}{\sqrt{\pi}}\left(\frac{2Mx^2}{3m} - 1\right) \ .$$

On substituting from Eqs. A.2.8 and A.2.5,

$$\left.\frac{dE}{dt}\right|_- = -\frac{160\sqrt{\pi}\, n_- e^4}{M}\sqrt{\frac{m}{2kT_-}}\left(\frac{M\omega^2}{3kT_-} - 1\right) \ . \tag{A.2.10}$$

In the case of energy loss from ions to ions, the more general expression of Eq. A.2.4 must be retained.

Returning now to the energy loss to the ion cloud by the organized beam, we can rewrite Eq. A.2.3 by substituting from Eqs. A.2.4 and A.2.10. The result is

$$P_{in} = I_+ \int_{E_+}^{E_0} \frac{n_+[4x^2G(x) - \phi(x)]\, dE}{n_+[4x^2G(x) - \phi(x)] + n_-\sqrt{3m/\pi E_-}\,[(E/E_-) - 1]\sqrt{2E/M}} \ , \tag{A.2.11}$$

where $E_- = \frac{3}{2}kT_-$ and $x \equiv \sqrt{M\omega^2/2kT_+} = \sqrt{3E/2E_+}$.

In steady state the power delivered to the ion cloud must equal the energy lost by it to the electron cloud. Assume that all the ions in the cloud are at a single energy $E_+ = \frac{3}{2}kT_+$. The loss rate to the electrons is then, by Eq. A.2.10,

$$P_{out} = Vn_+n_- \frac{80\sqrt{3\pi}\, e^4}{M} \sqrt{\frac{m}{E_-}} \left(\frac{E_+}{E_-} - 1\right) , \tag{A.2.12}$$

where V is the volume of the plasma. More correctly, of course, P should be averaged over a Maxwell-Boltzmann distribution of the ions. The numerical results are insensitive to this, however, and this correction will be ignored. Upon equating the power delivery and loss, we obtain the first of the four equations that determine the densities and temperatures in the plasma:

$$\frac{I_+}{V} \int_{E_+}^{E_0} \frac{n_+[4x^2G(x) - \phi(x)]\, dE}{n_+[4x^2G(x) - \phi(x)] + n_- \sqrt{6mE/\pi ME_-}\, [(E/E_-) - 1]} = n_+n_- \frac{80\sqrt{3\pi}\, e^4}{M} \sqrt{\frac{m}{E_-}} \left(\frac{E_+}{E_-} - 1\right) , \tag{A.2.13}$$

where $x^2 = 3E/2E_+$.

Energy Balance in the Electron Cloud

Since all the energy lost by the ions in slowing down ultimately reaches the electrons, the power input to the electrons is simply

$$P_{in} = I_+(E_0 - E_+) . \tag{A.2.14}$$

Energy is radiated by bremsstrahlung at the rate

$$P_{out} = V \frac{64 n_+ n_- e^6}{3\sqrt{3\pi}\, mc^3 \hbar} \sqrt{\frac{E_-}{m}} . \tag{A.2.15}$$

Hence, the second of the four equations is:

$$\frac{I_+}{V} (E_0 - E_+) = n_+n_- \frac{64 e^6}{3\sqrt{3\pi}\, mc^3 \hbar} \sqrt{\frac{E_-}{m}} . \tag{A.2.16}$$

Ion Conservation

Mirror losses are the result of particle collisions which produce a scattered particle with its velocity vector in the escape cone. An approximate expression for the loss rate is:[4]

$$\frac{dn_+}{dt} \cong V \frac{n_+^2}{2} \sigma_c v_+ \mathbb{P} , \tag{A.2.17}$$

where σ_c is taken to be the coulomb "cross section" in the plasma for scattering by multiple small-angle collisions through 90 deg, v_+ is the rms ion velocity in the plasma ($= \sqrt{2E_+/M}$), and $\mathbb{P}$ is the probability of the velocity lying in the escape cone after a

[4] A. Simon, *Nine Lectures on Project Sherwood*, ORNL-2285, p 104, Eq. 6.7 (March 20, 1957).

random 90-deg collision. If $\wp$ is taken to be the ratio of the area in the escape cone to the total area, this is[5]

(A.2.18)
$$\wp = 1 - \sqrt{1 - \frac{1}{R}} \; .$$

The 90-deg "cross section" is[6]

(A.2.19)
$$\sigma_c \cong 8\pi \left(\frac{e^2}{Mv^2}\right)^2 \ln \Lambda$$
$$= 2\pi \left(\frac{e^2}{E_+}\right)^2 \ln \Lambda \; .$$

In steady state

(A.2.20)
$$\frac{I_+}{V} = n_+^2 \, \frac{20 \, \pi e^4 v_+ \wp}{E_+^2} \; ,$$

which is the third of the four equations.

Charge Neutrality in the Large

The electron density is determined by the condition that the total number of electrons equal the total number of ions, both in the plasma and in the beam that is slowing down. Hence

$$n_- V = n_+ V + \int_{E_+}^{E_0} N(E) \, dE \; ,$$

or

$$n_- = n_+ + \frac{I_+}{V} \int_{E_+}^{E_0} \frac{dE}{\left.\frac{dE}{dt}\right|_+ + \left.\frac{dE}{dt}\right|_-} \; .$$

Substitution from Eqs. A.2.4 and A.2.10 gives the fourth equation,

(A.2.21)
$$n_- = n_+ + \frac{I_+}{V} \cdot \frac{M}{80 \, \pi e^4} \int_{E_+}^{E_0} \frac{\sqrt{2E/M} \; dE}{n_+[4x^2 G(x) - \phi(x)] + n_- \sqrt{6mE/\pi M E_-} \, [(E/E_-) - 1]} \; ,$$

where $x^2 = 3E/2E_+$.

The requirement of space-charge neutrality in the large merits some discussion. If the input ions remain concentrated in a small region of the device until they become randomized, it would make more sense to require $n_+ = n_-$ in the remainder of the machine.

---

[5] *Ibid.*, Eq. 6.8.

[6] *Ibid.*, p 19, Eq. 2.9.

On the other hand, large precessions of the input ions may be expected because of the nonuniformity of the magnetic fields in DCX. Hence, an appreciable fraction of the volume may be filled with a "semiorganized" beam in the process of slowing down. In this case, the requirement of Eq. A.2.21 may be more sensible. The numerical results are insensitive to the choice between these two requirements.

Reduction to Two Equations

Upon substituting Eq. A.2.20 into Eq. A.2.16, we obtain an expression for the ratio n_+/n_- which is independent of input current. Thus

$$\text{(A.2.22)} \qquad \frac{n_+}{n_-} = \frac{16}{15\sqrt{6\pi^3}} \sqrt{\frac{ME_-}{mE_+}} \cdot \frac{e^2}{\hbar c} \cdot \frac{E_+^2}{mc^2(E_0 - E_+)\wp} .$$

Note that this ratio represents the fraction of the total ions which are actually in the plasma.

Equations A.2.22 and A.2.20 may now be substituted in Eqs. A.2.13 and A.2.21 so as to eliminate all dependence on plasma densities or input current. The resulting equations are:

$$\text{(A.2.23)} \qquad \int_{E_+}^{E_0} \frac{[4x^2G(x) - \phi(x)]\, dE}{[4x^2G(x) - \phi(x)] + (n_-/n_+) \cdot \sqrt{6mE/\pi ME_-}\,[(E/E_-) - 1]} = \frac{n_-}{n_+} \sqrt{\frac{6mE_+}{\pi ME_-}} \left(\frac{E_+}{E_-} - 1\right) \frac{2E_+}{\wp}$$

and

$$\text{(A.2.24)} \qquad \frac{n_-}{n_+} = 1 + \frac{\wp}{2(E_+)^{3/2}} \int_{E_+}^{E_0} \frac{\sqrt{E}\, dE}{[4x^2G(x) - \phi(x)] + (n_-/n_+)\sqrt{6mE/\pi ME_-}\,[(E/E_-) - 1]} ,$$

where $x^2 = 3E/2E_+$, and n_+/n_- is defined by Eq. A.2.22.

Equations A.2.23 and A.2.24 may be solved numerically for the two plasma energies $E_+ (= \frac{3}{2} kT_+)$ and $E_- (= \frac{3}{2} kT_-)$. The results then give directly the ratio of ions in the plasma to all ions, by use of Eq. A.2.22. Finally, the plasma density may be obtained from Eq. A.2.20 after the input current is specified.

Numerical Results

For an input energy $E_0 = 300$ kev and a mirror ratio $R = 2$, the following results were obtained:

$$E_+ \cong 0.944E_0 \cong 280 \text{ kev} ,$$

$$E_- \cong 0.71E_0 = 210 \text{ kev} ,$$

$$\frac{n_+}{n_-} \cong 0.97 .$$

With the assumption that the input current is 1 ma and the volume is 4×10^4 cm^3, the ion density is

$$n_+ \cong 1.1 \times 10^{13} \text{ cm}^{-3} .$$

Some preliminary calculations at $E_0 = 50$ kev yielded values of E_+ which were between E_0 and 0.98 E_0.

Discussion of Results

The numerical result that the plasma particle energy is close to the input energy is not unexpected. The reason for this is the fact that the energy fed down to the electrons is proportional to $E_0 - E_+$. The electrons must lose their energy by bremsstrahlung, which is a very slow $(e^2/\hbar c)$ process. Hence, equilibrium is reached at temperatures close to that of the source.

A more unexpected result is the fact that most of the energy loss by the organized ions is to the ion cloud and not to the electrons. This is the reverse of the situation when the electrons and ions are very cold $(< [m/M]\, E_0)$ compared with the organized ions. For comparable electron and ion temperatures, Eqs. A.2.4 and A.2.10 show that energy loss to the ions dominates by $\sqrt{M/m}$. This may also be seen from comparison of the two terms in the denominators of Eqs. A.2.23 and A.2.24. Hence, it is an excellent approximation to neglect this second term. In this case our equations become:

$$\text{(A.2.25)} \qquad \frac{E_0 - E_+}{E_+} = \frac{n_-}{n_+} \frac{2}{\wp} \sqrt{\frac{6mE_+}{\pi ME_-}} \left(\frac{E_+}{E_-} - 1 \right)$$

and

$$\text{(A.2.26)} \qquad \frac{n_-}{n_+} = 1 + \frac{\wp}{2(E_+)^{3/2}} \int_{E_+}^{E_0} \frac{\sqrt{E}\, dE}{4x^2 G(x) - \phi(x)} .$$

The solution of these simplified equations gives numerical results which are very close to the previous values.

Note that 97% of the ions are in the plasma and that only 3% are in the process of slowing down. This result also means that the characteristic slowing-down time is only 3% of the characteristic mirror-loss time.

One final remark should be made about the ion density quoted in the numerical results. The high value of this quantity is due to the high plasma temperature and the resulting low mirror losses. Therefore the value of

$$\beta = \frac{nkT}{H^2/8\pi}$$

for the plasma would be greater than unity in the DCX now coming into operation, since the center-plane field is about 9.6 kilogauss. Needless to say, one would be delighted to find that this phenomenon is the only one limiting the plasma buildup.

A.3 NEUTRAL BURNOUT

Any realistic device, particularly at startup, will have large numbers of neutral particles in it. These neutral particles will remove hot ions from the system because of the charge-exchange process. In this process, a hot ion strikes a neutral particle and picks up an electron, becoming a fast neutral. This neutral is lost to the system, while the cold ion left behind is itself readily lost through the mirrors. The cross section for charge exchange is a steeply decreasing function of the ion velocity above about 30 kev ($\sim 1/v^8$). However, even at 300 kev it has a value of about 3×10^{-18} cm^2, which is very much larger than the coulomb cross sections involved in energy loss and particle deflection. Hence, if any appreciable number of neutral particles remain in the system, they will remove the hot ions by charge exchange, and few, if any, ions will survive to form a plasma.

On the other hand, every charge exchange destroys a neutral particle. Furthermore, the ionization caused by the fast ion will remove many more neutrals by this means, since the cross section for ionization is more than 20 times as large as that for charge exchange at 300 kev. It seems reasonable that there will be a critical point for the input current, at which point the ions "burnout" the neutrals as fast as they are flowing into the plasma. Once this point is passed, the ions get ahead of the neutrals. The plasma builds up, hence burning out additional neutrals, and the system cleans out the neutrals in short order. Another way of saying this is that it is hard to see how any neutral particles can survive in any appreciable plasma at 300 kev or so.

This conjecture may be investigated numerically. Consider the rate of buildup of ion density n_+ in the plasma. The time-dependent equations are:

$$\frac{dn_+}{dt} = \frac{I_+}{V} - \frac{n_+^2}{2}\,\sigma_c v \mathcal{P} - n_+ n_0 \sigma_{cx} v \tag{A.3.1}$$

and

$$\frac{dn_0}{dt} = \frac{N v_0 S}{4V} - \frac{n_0 v_0 S}{4V} - n_0 n_+ (\sigma_i + \sigma_{cx}) v \ . \tag{A.3.2}$$

The first term on the right of Eq. A.3.1 represents the constant source input, with V being the plasma volume. The second term takes account of mirror losses, while the last term represents loss of fast ions by charge exchange.

The density of neutral particles, n_0, also varies in time, as given by Eq. A.3.2. It is assumed here that the plasma has a surface area S and that there is constant streaming of neutrals into the plasma from the external manifold through the surface S. If the *constant* density of neutrals in the manifold is denoted by N, there will be a steady kinetic streaming into the plasma at a rate of $Nv_0/4$ particles per unit area, where v_0 is the thermal velocity of the neutrals. Similarly, the neutrals in the plasma may stream out, as given by the [illegible]d term in the right of Eq. A.3.2. Finally, the effects of neutral burnout by ionization and charge exchange are represented by the last term on the right.

The results of Sec A.2 have shown that the ions do not lose much of their energy while slowing down into the plasma. Hence, it is a good approximation to assume all cross sections and velocities to be constant in Eqs. A.3.1 and A.3.2 at some value close to the source energy. The resulting equations may then be solved quite readily on an analog computer. Most of the numerical results to be described below were obtained by assuming values appropriate to an energy of 250 kev for the coefficients in Eqs. A.3.1 and A.3.2. There is one run at the energy $E_+ = 280$ kev that was found in Sec A.2.

The numerical results were found to be in agreement with a qualitative criterion for the critical current which could be guessed in advance. On the basis of the previous discussion, the critical current might be expected to occur at the point where the neutrals are being burned out just as fast as they are coming in. Now the number of neutrals that a fast ion destroys before being lost itself is clearly $(\sigma_i + \sigma_{cx})/\sigma_{cx}$. Hence, the critical input current should be

(A.3.3)
$$I_{crit} = \frac{\sigma_{cx}}{\sigma_i + \sigma_{cx}} I_0 ,$$

where I_0 is the total current of neutrals streaming into the plasma. The numerical results below have shown that there is indeed a burnout of neutrals. However, the event is not a sudden phenomenon but rather a smooth transition over a narrow range of current. It will be seen, however, that the relationship of Eq. A.3.3 gives the current at which most of the neutrals have disappeared and at which the plasma has built up to nearly full density.

Coefficients

The first version of DCX, which is now being built, has mirror coils with a 17-in. ID and a spacing between the inner faces of the coil of 18½ in. (see Fig. A.3.1). The volume of an inscribed cylinder whose rims just touch the inner edge of the coils is

$$V_{cyl} = \frac{\pi \times 17^2 \times 18.5 \times 2.54^3}{4}$$
$$= 6.9 \times 10^4 \text{ cm}^3 .$$

Since only part of this volume will be occupied by the plasma, the parameter V was taken to be

$$V \cong 4 \times 10^4 \text{ cm}^3 .$$

[redacted]

ORNL-LR-DWG 26225

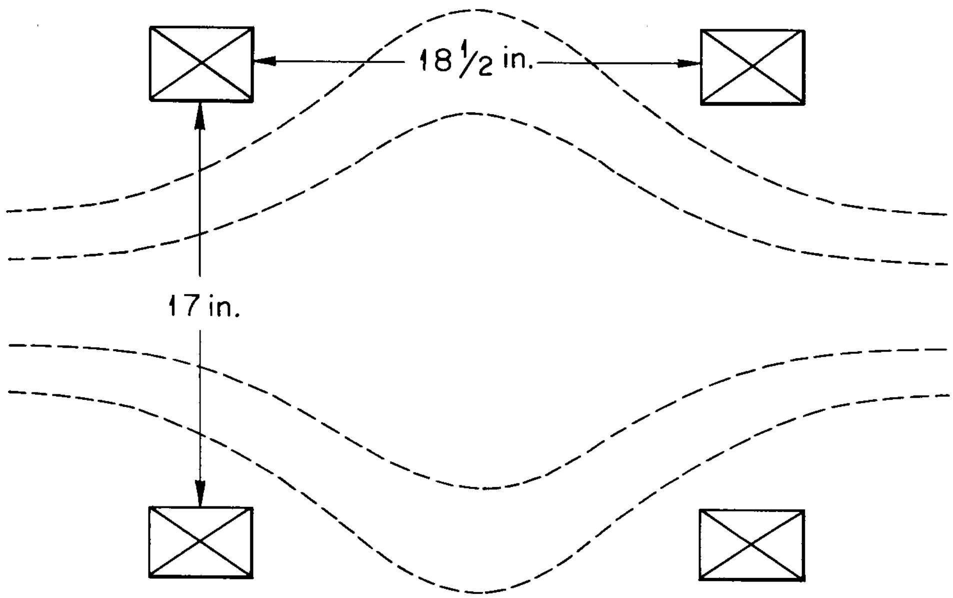

Fig. A.3.1. Dimensions of DCX.

Assume further that the plasma has a roughly spherical shape with a typical radius of about 8 in. In that case

$$\frac{S}{V} \cong \frac{3}{r} = \frac{3}{8 \times 2.54} \cong 0.15 \text{ cm}^{-1} ,$$

and thus

$$S \cong 6 \times 10^{3} \text{ cm}^{2} .$$

The thermal velocity of the neutrals was chosen to be that of a deuterium molecule at 300°K. Thus

$$v_0 = 1.9 \times 10^{5} \text{ cm/sec} ,$$

and the density N of the neutrals in the manifold is given by the manifold pressure. A mirror ratio of 2 was chosen throughout.

The coulomb "cross section" was chosen, as in Eq. A.2.19, to be

$$\sigma_c = 40\pi \left(\frac{e^2}{E_+}\right)^2 ,$$

while the ionization cross section at 250 kev was computed from the formula[7]

$$\sigma_i = 0.285 \frac{2\pi e^4}{|E_0|\, mv_+^2} \ln \frac{2mv_+^2}{0.048\,|E_0|}$$

$$= 1.0 \times 10^{-16}\ \text{cm}^2 \text{ at } 250 \text{ kev}$$

with $|E_0| = 16$ ev. Finally, the charge-exchange cross section was taken from the measured values of Stier and Barnett[8] for H^+ in hydrogen gas on the assumption that the deuteron has the same cross section at the same relative *velocity*. This value is 5.5×10^{-18} cm^2 at 250 kev.

Numerical Results

Equations A.3.1 and A.3.2 may be put in a more convenient form by defining the dimensionless quantities

(A.3.4) $$n_0' = \frac{n_0}{N}$$

and

(A.3.5) $$n_+' = \frac{n_+}{\sqrt{2I_+/\sigma_{cx} v\wp V}} \ .$$

Note that the initial values of n_0' and n_+' are 1 and 0, respectively, before the beam is turned on, and that if all the neutrals are burned out, n_+' rises to its maximum theoretical value of unity. In terms of these variables (the primes being dropped), Eqs. A.3.1 and A.3.2 become:

(A.3.6) $$\frac{dn_+}{dt} = A(1 - n_+^2) - Bn_+n_0 \ ,$$

(A.3.7) $$\frac{dn_0}{dt} = C(1 - n_0) - Dn_+n_0 \ ,$$

where

(A.3.8) $$A = \left(\frac{I_+\sigma_c v\wp}{2V}\right)^{1/2} \ ,$$

---

[7]H. A. Bethe and J. Ashkin, *Experimental Nuclear Physics* (ed. by E. Segre), vol I, Part II, Wiley, New York, 1953.

[8]P. M. Stier and C. F. Barnett, *Phys. Rev.* **103**, 896 (1956) (this report, Appendix B.1).

$$B = N\sigma_{cx}v \ , \tag{A.3.9}$$

$$C = \frac{v_0 S}{4V} \ , \tag{A.3.10}$$

$$D = \left(\frac{2I_+}{\sigma_c v p V}\right)^{1/2} (\sigma_i + \sigma_{cx})v \ . \tag{A.3.11}$$

Some typical analog computer runs are shown in Figs. A.3.2 and A.3.3. Figure A.3.2 shows a case for which the critical current is below the critical point. It is seen that the neutral density falls only slightly and that the ions do not build up appreciably in time. Figure A.3.3 illustrates a case well beyond the critical current. The neutral density falls rapidly in a time of the order of 50 milliseconds to 10% of its original value, and the ion density climbs almost linearly to a value close to the optimum.

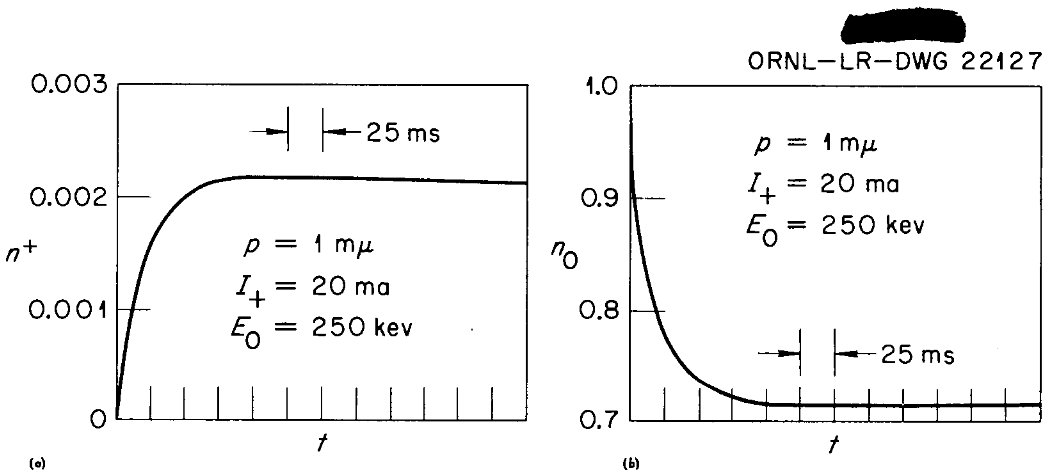

Fig. A.3.2. Density Variations for a Below-Critical Current: (*a*) Ion Density, (*b*) Neutral Density.

Focusing attention now on the equilibrium results, these are shown in Fig. A.3.4. These results show that the critical current varies linearly with the pressure as predicted by Eq. A.3.3. The arrows indicate the currents predicted by Eq. A.3.3 for each of the three pressures. Note the steep rise in equilibrium ion density with increasing current.

Discussion of Results

The first version of DCX, which is being built, may be expected to operate at a vacuum of about 10^{-6} mm. For this case, Fig. A.3.4 indicates that the critical current

[redacted]

[redacted]

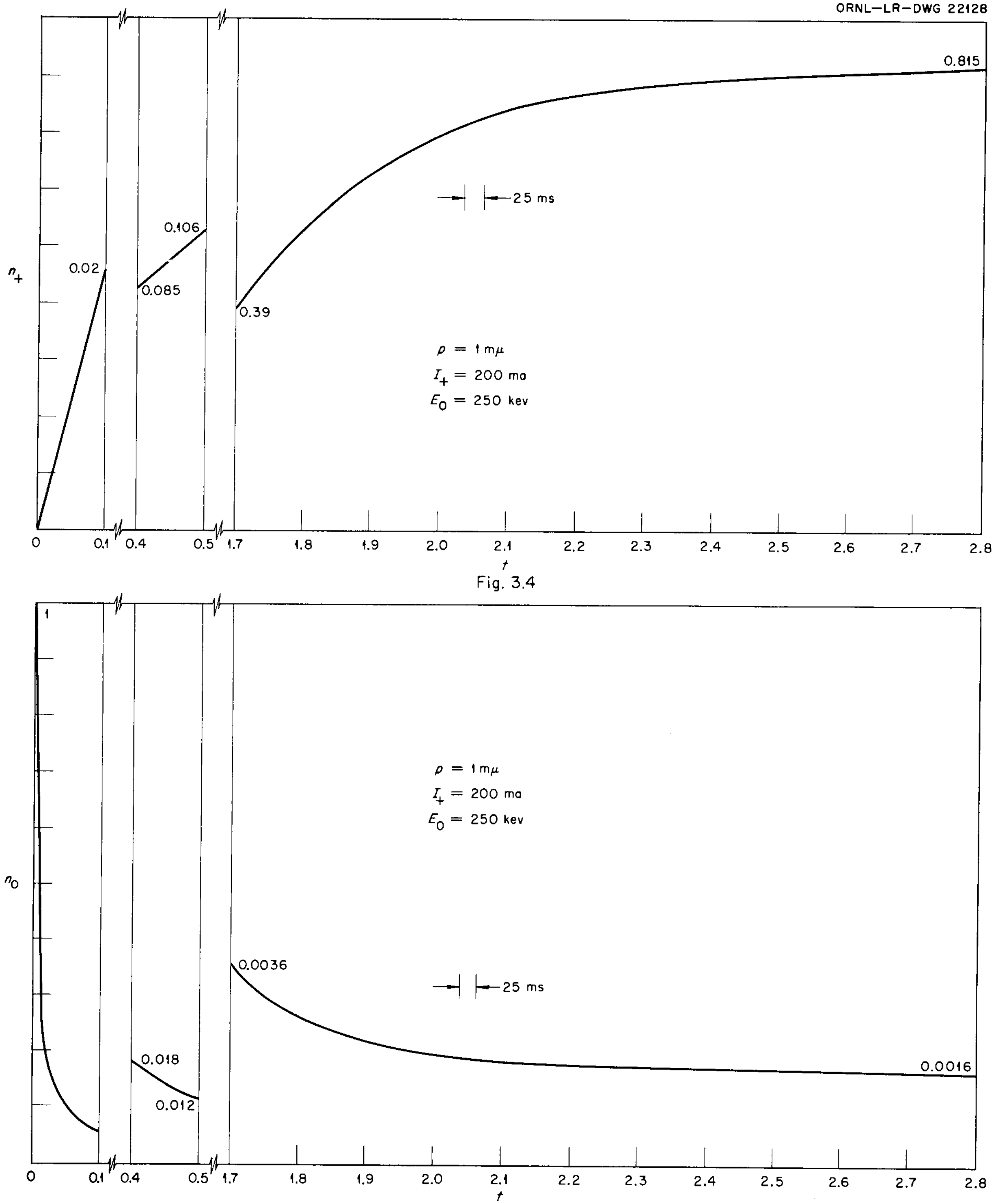

Fig. A.3.3. Density Variations for an Above-Critical Current: (*a*) Ion Density, (*b*) Neutral Density.

[redacted]

[redacted]

ORNL-LR-DWG 22130

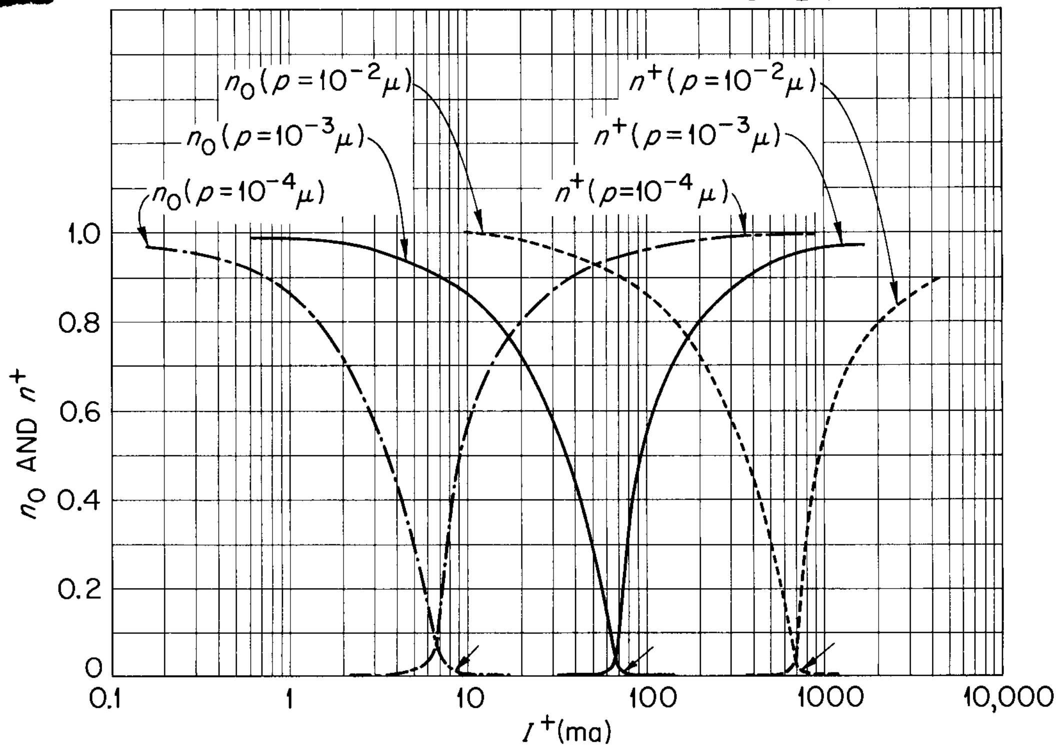

Fig. A.3.4. Steady-State Densities for 250-kev D^+.

is about 80 ma. Since this first device will only furnish about 1 ma, it would seem that neutral burnout will not occur.

This conclusion may be unduly pessimistic, however. At least one of the assumptions made in the calculation may be pessimistic by a factor of 10^3 or greater. This is the assumption concerning the rate of neutral influx into the plasma. At a pressure of 10^{-6} mm, $N \cong 3 \times 10^{10}$ cm^{-3}, and, since $v_0 = 1.9 \times 10^5$ cm sec^{-1}, the input flux is 6×10^{15} cm^{-2} sec^{-1}. On the other hand, Bell[9] has pointed out that the limiting influx of neutrals is not from the manifold but from emission by the walls. The Princeton Sherwood Group has listed some typical experimental values for the outgassing rate from a clean wall (with no baking). These are[10]

$$F = 2.13 \times 10^{11}\ \text{cm}^{-2}\ \text{sec}^{-1}\ ,$$

$$F = 0.96 \times 10^{11}\ \text{cm}^{-2}\ \text{sec}^{-1}\ ,$$

$$F = 0.53 \times 10^{11}\ \text{cm}^{-2}\ \text{sec}^{-1}\ .$$

---

[9] P. R. Bell, private communication.

[10] W. R. Farber *et al.*, *A Conceptual Design of the Model C Stellerator*, NYO-7309, p 48 (Feb. 1, 1956).

Hence, even though the effective wall area is somewhat larger than the plasma surface, it may be that the neutral influx has been taken too large by a factor of 10^3 or larger. If this is true, the critical current would be reduced by the same factor. Another unknown factor is the influence of the carbon arc itself on the burnout. Preliminary evidence indicates that the arc acts as an ion pump. A final point is that it may be necessary to go well above the critical current in order to bring the neutral density down to the point where charge exchange is small compared with plasma formation ($\sigma_{cx}/\sigma_c \cong 10^5$ at 250 kev). It should be noted that plans are well under way for the construction of a 1-amp 600-kev supply.

Asymptotic Relations

One check on the analog results is obtained by solving the steady-state equations for the case of currents which are well above the critical point. In that case

$$n_+ = 1 - \epsilon \ .$$

Keeping terms of first order in ϵ only in Eqs. A.3.6 and A.3.7, we find

$$\epsilon = \frac{CB/DA}{2 + 2(C/D) + (CB/DA)} \longrightarrow \frac{1}{2}\,\frac{Nv_0S}{4I_+}\left(\frac{\sigma_{cx}}{\sigma_i + \sigma_{cx}}\right)$$

and

$$n_0 = \frac{+ \quad 2C/D}{2 + 2(C/D) + (CB/DA)} \longrightarrow \frac{v_0S}{4(\sigma_i + \sigma_{cx})}\sqrt{\frac{\sigma_c \wp}{2I_+ vV}} \ .$$

A.4 ADDITIONAL EFFECTS

Impurities

The presence of the carbon arc will undoubtedly contribute large numbers of carbon ions to the plasma. It is often stated (rather loosely) that the presence of impurities in a plasma will increase the bremsstrahlung power loss by the factor z^3. This argument may be fallacious in the case of a steady-state mirror machine.

Owing to the fact that mirror loss is due to coulomb collisions, the more general form for the ion conservation equation in steady state for a mirror machine is

$$\frac{I_+}{V} = \frac{(\overline{z^2}n_+)^2}{2}\,\sigma_c v \wp \ , \tag{A.4.1}$$

where $\overline{z^2}$ is the average z^2 in the plasma and n_+ is the total ion density. All ion species are assumed to be at the same temperature, and the coulomb cross section with $z = 1$ is denoted by σ_c. The difference in velocity between the ion species is neglected here, and a common velocity is denoted by v. The essential point is that, with a constant source term, the product $\overline{z^2}n_+$ remains constant in a mirror machine.

On the other hand, the variation of the power radiated in bremsstrahlung is given by

(A.4.2) $$P_{\text{brems}} \sim \overline{z^2} n_+ n_- \ .$$

Hence, since $\overline{z^2} n_+$ stays constant, it is clear that the power radiated in bremsstrahlung rises no faster than z as impurities are added to a mirror machine.

For example, suppose that the plasma in DCX should contain 10% carbon ions. Since $z = 6$, we have $\overline{z^2} = 4.5$ and $\overline{z} = 1.5$. Thus the bremsstrahlung rate is increased by 1.5 and the ion density is decreased by the factor 4.5. The increased bremsstrahlung has a minor effect on the plasma temperature. Since the energy fed to the electrons goes out as bremsstrahlung, the value of $E_0 - E_+$ must be increased over its value for $\overline{z} = 1$ by a factor of about 1.5. Previously (see Sec A.2) we had $E_0 - E_+ \cong 0.06\ E_0$. Hence, we now require $E_0 - E_+ \cong 0.1\ E_0$, or $E_+ = 0.9\ E_0$, which is still an exceedingly hot plasma.

Heat Transfer to Arc

The arc itself, of course, represents a serious sink for heat, not only through excitation radiation but through the presence of cool ions and electrons in the interior. On the other hand, it may be no worse in this respect than the walls of DCX, since these are only one Larmor radius from the plasma. The calculation in the next section considers the effect of heat transfer to the walls and shows that, even under the most severe assumptions, the resulting plasma temperature is still high.

The arc may be even less troublesome than a wall, since it represents a "wall" at a rather high temperature ($\cong$ 100 v). In any event, if the arc holds down the full development of the plasma temperature, it may be possible to shut off the arc and to continue feeding ions by using the breakup due to the plasma that already exists.

Heat Transfer to the Walls

Up to this point, energy loss from the system has been assumed to occur by means of bremsstrahlung. Of course, heat transfer by means of the usual thermal conduction does also occur and may be quite important, particularly since the walls may be as close as one Larmor radius away. The power loss from a system per unit volume due to thermal conduction is

(A.4.3) $$P_{\text{cond}} = -\kappa \frac{d^2T}{dx^2} \ ,$$

where κ is the coefficient of thermal conduction in a magnetic field. Now

(A.4.4) $$\kappa = \frac{nk\lambda v}{2(\omega\tau)^2} \ ,$$

where n is the ion density, k is Boltzmann's constant, λ is the ion mean free path for collision, v is the ion velocity, ω is the ion cyclotron frequency, and $\tau = \lambda/v$ is the mean free time between ion collisions. If a parabolic temperature distribution is assumed,

$$\frac{d^2T}{dx^2} \cong -\frac{2(T_c - T_0)}{l^2}, \tag{A.4.5}$$

where T_c is the temperature in the center of the plasma, T_0 is the wall temperature, and l is the distance between these two points. The combined expression for the power loss by conduction becomes:

$$\begin{aligned} P_{\text{cond}} &\cong \frac{nk\lambda v}{(\omega\tau)^2} \frac{(T_c - T_0)}{l^2} \\ &= \frac{nkv^3}{\omega^2\lambda} \frac{T_c - T_0}{l^2} \\ &= n^2 \frac{\sigma k v^3}{\omega^2} \frac{T_c - T_0}{l^2}, \end{aligned} \tag{A.4.6}$$

where σ is the collision cross section. Now l should be chosen to be about one Larmor radius. Hence

$$l = r_0 = \frac{v}{\omega}$$

and

$$P_{\text{cond}} \cong n^2 \sigma v k T_c$$

if T_0 is neglected in comparison with T_c.

This expression is to be compared with the bremsstrahlung loss rate given in Eq. A.2.15 (divided by V). Using the value of σ given in Eq. A.2.19 with $\ln \Lambda = 20$ and with $kT_c \cong \frac{2}{3} E_+$, we find

$$\frac{P_{\text{cond}}}{P_{\text{brems}}} \cong \frac{39mc^2}{\sqrt{E_- E_+}},$$

which has the value 80 for the case that was discussed in Sec A.2, for which $E_+ = 280$ kev and $E_- = 210$ kev.

This very large ratio of conduction loss to bremsstrahlung may be quite spurious. It is very unrealistic to assume a smooth parabolic variation of temperature with radius when the wall is so close. This is particularly true in the case of a plasma consisting of very hot particles. The tendency for these particles upon striking a wall is to plow into the interior, with a small probability of return to the exterior with reduced energy. Recent results on sputtering by deuterium,[11] for example, show that the sputtering rate

[11] O. C. Yonts, Appendix D.2.

falls rapidly with increasing energy. This implies that there will not be a large number of cooler particles near the wall and that the plasma temperature stays fairly uniform until very close to the wall (if a "temperature" can be defined in that region at all!).

Perhaps the most important argument of all is to consider what effect the most pessimistic assumptions about heat conduction have on the temperature in DCX. Consider the following set of assumptions. Every ion within a Larmor radius of the wall transfers some fraction of its energy E_+ to the wall per collision. Now the number of collisions per unit volume is

$$N_c \cong \frac{n_+^2 \sigma_c v}{2} ,$$

and hence the total number of collisions per second within a Larmor radius of the wall is

$$N = \frac{n_+^2 \sigma_c v r_0 S}{2} ,$$

where r_0 is the Larmor radius and S is the wall surface area. If the fraction of energy transferred is denoted by E_+/f, where f is greater than or equal to unity, the total energy transfer to the walls is

$$E_{\text{out}} = \frac{n_+^2 \sigma_c v r_0 S E_+}{2f} .$$

In steady state, this must equal the energy input to the gas, which is $I_+(E_0 - E_+)$. Hence

$$I_+(E_0 - E_+) = \frac{n_+^2 \sigma_c v r_0 S E_+}{2f} .$$

On the other hand, by particle conservation,

$$\frac{I_+}{V} = \frac{n_+^2 \sigma_c v P}{2} .$$

Hence

$$E_0 - E_+ = \frac{r_0 S E_+}{V P f} ,$$

or

$$E_+ = \frac{E_0}{1 + r_0 S/VPf} .$$

Now the mirror escape probability is 0.3 for a mirror ratio of 2. In addition, $r_0 S/V$ is of the order of unity in DCX for the input ions. Finally, f is chosen to have its most unfavorable value, unity. In this case

$$E_+ \cong \frac{E_0}{4} = 75 \text{ kev} .$$

This result, although still constituting a plasma temperature of great interest, is undoubtedly extremely pessimistic. For one thing, the particle density, and hence the heat transfer rate ($\sim n^2$), should be reduced near the walls. A second point is that, as the plasma temperature drops, the ratio $r_0 S/V$ becomes smaller than unity, since the Larmor radius shrinks. Finally, it is unrealistic to assume loss of the entire energy of the particle to the wall upon collision. These considerations make it seem more likely that the effect of conduction to the walls is to reduce the temperature to something like $E_0/2$ or so. A more accurate value can be obtained by repeating the self-consistent temperature calculations of Sec A.2, with the use of the heat conduction formula of Eq. A.4.6 in place of the bremsstrahlung losses. This is now being done. It is clear, however, by the qualitative considerations above, that the result will be in excess of $E_0/4$. In addition, this calculation will still have the uncertainties regarding the value of n near the wall and the temperature profile.

Perhaps the most striking feature of these results is the fact that the most pessimistic assumptions still result in temperatures which are of extreme interest to Project Sherwood. This is a direct result of working down in energy.

Particle Diffusion to the Walls

Ions and electrons will reach the walls by means of coulomb collisions which deflect their orbits through appreciable angles. Since this is the very same mechanism which produces a leakage through the mirrors, it seems clear that this loss rate must be of the same order as the mirror losses. This is particularly so in one case, since for a mirror ratio of 2 the escape probability $\mathcal{P}$ is so high (≈ 0.3). Hence, diffusion to the walls should not decrease the plasma densities by any appreciable amount over the value calculated by simple mirror loss.

Effect of Cold Electrons

One sure way to depress the temperature of the plasma is to have large numbers of cold electrons around together with a continuous influx and outgo of cold electrons. The cross section for energy transfer to cold electrons can be very much larger than that for all other processes. On the other hand, if the total influx of cold electrons is of the order of magnitude of the hot-ion-particle current, this does not represent a serious energy drain from the system. For example, if one cold electron enters per hot ion, then, even if it stays in the system long enough to come to equilibrium with the ions, the resultant energy per particle is still $E_0/2$, which is 150 kev. More likely, since cold particles are preferentially lost through the mirrors, the electron only drains part of this energy before departing.

Where will these electrons come from? One possible source is the arc itself. In this case the electrons are not very cold ($\cong$ 100 v or greater) and do not play a very dominant role in the degradation of the energy of the ions. In addition, these electrons are localized in the region of the arc. In this sense, they play the role of a rather warm "wall" and should have a much smaller effect on the temperature than the actual walls themselves. There will be little tendency for the electrons to drift far into the plasma, owing to their small Larmor radius ($\cong$ 0.05 mm) and preferential loss through the mirrors.

A second source of cold electrons is the ionization of the D_2^+, thus, $D_2^+ \longrightarrow D^+ + D^+ + e$. It is clear that this source represents no more than one electron for every two deuterons trapped. Furthermore, these electrons also are localized in the immediate vicinity of the arc.

A third source of electrons is the ionization of the neutral particles at the critical current point. These could constitute about 20 electrons per hot ion injected (since $\sigma_i \cong 20\sigma_{cx}$ at 250 kev). However, above this current the ratio would fall off. Even a ratio of 20 to 1 would not be completely disastrous, since at equilibrium $E_+ \approx E_0/20 \approx 15$ kev. However, considerations of preferential mirror loss, failure to come to equilibrium, and higher injection currents make this less of a worry.

A fourth source of electrons is wall bombardment. Since the number of ions striking the wall is less than or equal to the input hot-ion rate in steady state and since the secondary-electron production is of the order of unity,[12] this does not represent a large influx of electrons. Besides, the electrons again are localized near the walls.

Another possible source of electrons is those which ride in on the input beam. There seem to be no quantitative data on this score, although it is hard to see how this rate could exceed the ion rate.

In summary, large numbers of cold electrons could severely decrease the temperature in DCX. It is difficult to see how such large inputs could be obtained unless by a deliberate intent to produce them. Nevertheless, the possibility exists. In this case, one possible countermove would be to inject large numbers of hot electrons into the plasma so as to make the plasma negative and thus inhibit the influx of other electrons. DCX is being built with this possibility in mind, and it will be possible to inject electrons through the mirrors if this should seem necessary.

Most of the considerations given above will apply as well to cold ions which could result from neutral ionization and wall bombardment.

A.5 SUMMARY

It appears that if the input current of trapped deuterons to DCX exceeds a critical amount there will occur a "burnout" of most of the neutral particles in the system. This

[12] H. S. W. Massey and E. H. S. Burhop, *Electronic and Ionic Impact Phenomena*, Clarendon Press, Oxford, 1952.

critical current is linearly dependent on the neutral pressure in the system and might be as high as 80 ma at a pressure of 10^{-6} mm or as small as a factor of 10^3 or greater below this value. The large variation in these predictions is due to the unknown action of the arc as an ion pump and to uncertainties in the magnitude of the neutral influx to the plasma.

If appreciable burnout should occur, and if bremsstrahlung is the chief mechanism of energy loss from the system, the input ions will degrade only slightly in energy before becoming disorganized in direction and forming a plasma. For an input energy of 300 kev, the ions would form a plasma at 280 kev. At this energy, the plasma density with a 1-ma input current could be as high as 10^{13} per cubic centimeter. Direct thermal conduction to the walls may represent a more serious energy drain from the system than does bremsstrahlung. Nevertheless, calculations of a highly pessimistic nature still yield ion temperatures no lower than 75 kev. More likely, this mechanism might drop the temperature to 150 kev or so.

Considerations of other possible perturbing mechanisms indicate that impurities should not seriously decrease the temperature, although the density will be decreased somewhat. The arc itself may have no worse an effect on the temperature in DCX than the walls. In any event, if the arc does retard the full development of the plasma temperature, it can be turned off and the breakup can be accomplished by the residual plasma. Cold electrons are also a possible source of temperature degradation. No large sources of cold electrons are present, and those which have been considered are not very much larger in particle input than the input ion current. At the worst, even if the energy is fully shared with these cold electrons, the resultant temperature would still be of the order of 15 kev or greater.

Of course, plasma instabilities could effectively stop the entire development of a hot plasma. These seem quite difficult to predict with any certainty at the present stage of the theory for a device such as DCX. In a sense, of course, this is one of the reasons for building DCX.

The very favorable temperature estimates which have been cited above are a direct result of working down in energy. It is hard to see how a device such as DCX can end up at an uninteresting temperature, from the Sherwood viewpoint. Of course, even if DCX should perform as well as is hoped for, it will be very far from a device which yields more power than is put into it. Achievement of this goal will require a considerably larger device. These points will be discussed in a later report.

Appendix B

COLLECTED ATOMIC CROSS SECTIONS MEASURED AT ORNL

B.1 CHARGE-EXCHANGE CROSS SECTIONS OF HYDROGEN IONS IN GASES[1]

P. M. Stier[2] C. F. Barnett

Abstract

Measurements are reported of the cross section for electron capture, σ_{10}, electron loss, σ_{01}, and electron detachment, σ_{-10}, for hydrogen atoms and ions traversing several gases (σ_{if} represents the cross section for charge transfer from initial state i to final state f). The kinetic energy of the particle was from 3 to 200 kev. The target gases used were H_2, He, N_2, O_2, Ne, and A. Cross sections were determined by measuring the attenuation of the hydrogen beam in a gas cell under the influence of an electrostatic or magnetic field. The fraction of the beam in each charge state after passing through a "thick target" was also determined. This latter measurement served as a test for internal consistency of the data, since the fraction is relatable to the cross section for entry to and exit from the charge state. The loss cross section, σ_{01}, increased monotonically at low energies, reaching a maximum at a velocity approximately equal to the orbital electron velocity. For the higher energies studied, the capture cross section could be represented by an expression of the form $\sigma = Ae^{-bv}$, where A and b are constants for each gas studied. The electron-attachment cross section, σ_{0-1}, was of the order 10^{-17} cm^2 per gas atom for the gases studied and attained a maximum between 5 and 20 kev. The cross section for the inverse transition, σ_{-10}, was approximately 10^{-15} cm^2 per gas atom in the energy range studied.

B.1.1 Introduction

This paper is the second of a series reporting experimental determinations of the charge-exchange cross sections for low-energy ions passing through gases. In the previous paper,[3] the ratios of the electron-loss to electron-capture cross sections were presented for each of the ions H^+, He^+, N^+, Ne^+, and A^+ passing through the gases hydrogen, helium, nitrogen, oxygen, neon, and argon. These were determined by observing the charge distribution in the particle beam after it had traversed sufficient gas for equilibrium to be established between competing electron transfer processes. The present paper reports several experiments in which the absolute cross sections were measured for electron capture and loss by a fast hydrogen atom or ion. The stopping gases were those listed above, and the energy range was from 3 to 200 kev.

The excellent reviews by Massey and Burhop[4] and by Allison and Warshaw[5] evaluate the charge-exchange cross-section measurements prior to their publication dates of 1952 and 1953, respectively. Several additional papers have appeared since these summaries. Whittier[6] has reported a study whose emphasis was on the behavior of fast negative ions in hydrogen gas. Stedeford and Hasted[7] have presented extensions

[1]P. M. Stier and C. F. Barnett, *Phys. Rev.* 103, 896–907 (1956).

[2]Now at National Carbon Research Laboratory, Cleveland, Ohio.

[3]P. M. Stier, C. F. Barnett, and G. E. Evans, *Phys. Rev.* 96, 973 (1954).

[4]H. S. W. Massey and E. H. S. Burhop, *Electronic and Ionic Impact Phenomena*, Clarendon Press, Oxford, 1952.

[5]S. K. Allison and S. D. Warshaw, *Revs. Modern Phys.* 25, 779 (1953).

[6]A. C. Whittier, *Can. J. Phys.* 32, 275 (1954).

[7]J. B. H. Stedeford and J. B. Hasted, *Proc. Roy. Soc. (London)* A227, 466 (1955).

of the work by Hasted[8] and by Keene,[9] and give results of measurements of the cross sections for the capture of an electron by a proton and the detachment of an electron from a negative hydrogen ion. Bates, Dalgarno, Griffing, and others[10–14] have presented a series of detailed calculations of the processes involved in inelastic collisions, particularly of charge exchange. Another theoretical calculation of the cross section for electron capture by protons in hydrogen gas has been given by Jackson and Schiff.[15] These more recent experimental and theoretical results of studies of electron capture and loss will be included in the graphs of the data reported in this paper.

In view of the rather wide discrepancies appearing in the literature of inelastic energy loss processes, a considerable number of overdeterminations were designed into the present set of experiments. It has been the hope that the additional labor would be worth while, in the sense that it would test for consistency and correctness of the data obtained.

B.1.2 Theory

The differential equations representing transitions between the possible charge states can be solved[16] for the fraction of the particle beam in each state as a function of the amount of stopping material traversed. For hydrogen ions at low energies three charge states are of importance, −1, 0, and +1. The fraction of the particle beam, ϕ_i, in charge state i after passage through sufficient gas for equilibrium between competing electron capture and loss reactions is:

$$\phi_{-1} = \frac{\sigma_{0-1}\sigma_{10}}{D_0} ,$$

$$(1) \qquad \phi_0 = \frac{\sigma_{-10}\sigma_{10}}{D_0} ,$$

$$\phi_1 = \frac{\sigma_{-10}\sigma_{01}}{D_0} ,$$

where

$$D_0 = \sigma_{-10}(\sigma_{01} + \sigma_{10}) + \sigma_{0-1}\sigma_{10} .$$

Here σ_{if} denotes the cross section for transitions from initial charge state i to final state f. The assumption is made that the cross section for transfer of two electrons in a single collision is considerably smaller than that for one-electron transfer, that is, σ_{-11} and σ_{1-1} are considered negligible.[17] It follows immediately that the ratio of the number of particles in adjacent states is the ratio of cross sections for transitions between these states:

$$(2) \qquad \frac{\phi_{-1}}{\phi_0} = \frac{\sigma_{0-1}}{\sigma_{-10}} , \qquad \frac{\phi_0}{\phi_1} = \frac{\sigma_{10}}{\sigma_{01}} .$$

The differential equations for the change in the flux n_i of particles in state i are:

$$(3) \qquad \frac{dn_0}{d\pi} = -n_0(\sigma_{0-1} + \sigma_{01}) + n_1\sigma_{10} + n_{-1}\sigma_{-10} ,$$

$$(4) \qquad \frac{dn_{-1}}{d\pi} = -n_{-1}\sigma_{-10} + n_0\sigma_{0-1} ,$$

$$(5) \qquad \frac{dn_1}{d\pi} = -n_1\sigma_{10} + n_0\sigma_{01} .$$

Here $\pi = Ll\xi P/RT$ is the number of atoms presented by the target gas per square centimeter, where L is Avogadro's number, l is the thickness

---

[8] J. B. Hasted, *Proc. Roy. Soc. (London)* **A212**, 235 (1952).

[9] J. P. Keene, *Phil. Mag.* 40, 369 (1949).

[10] D. R. Bates and A. Dalgarno, *Proc. Phys. Soc. (London)* **A65**, 919 (1952).

[11] A. Dalgarno and H. N. Yadav, *Proc. Phys. Soc. (London)* **A66**, 173 (1953).

[12] D. R. Bates and G. Griffing, *Proc. Phys. Soc. (London)* **A66**, 961 (1953).

[13] D. R. Bates and A. Dalgarno, *Proc. Phys. Soc. (London)* **A66**, 972 (1953).

[14] B. H. Bransden, A. Dalgarno, and N. M. King, *Proc. Phys. Soc. (London)* **A67**, 1075 (1954).

[15] J. D. Jackson and H. Schiff, *Phys. Rev.* 89, 359 (1953).

[16] Detailed solutions for several cases are given in the review article by Allison and Warshaw (ref 5). In view of this, only equations pertinent to the present experiments are given here.

[17] Experimental observations supporting this assumption will be given later in this paper (Sec B.1.4).

of the gas target, ξ represents the number of atoms per molecule in the gas which is at pressure P and absolute temperature T, and R is the gas constant.

If, by suitable experimental means, particles which change charge are removed, the integrals of these equations become simple exponential functions of the amount π of gas traversed. Thus, if a flux N_0 of fast atoms is incident on a region of gas, and ions are removed as formed, from Eq. 3 we find that the flux of atoms a distance l within the gas is given by

$$n_0 = N_0 e^{-\pi(\sigma_{01}+\sigma_{0-1})} \quad . \tag{6}$$

Similarily, from Eqs. 4 and 5, for incident negative and positive ion beams, we find

$$n_{-1} = N_{-1} e^{-\pi\sigma_{-10}} \tag{7}$$

and

$$n_1 = N_1 e^{-\pi\sigma_{10}} \quad . \tag{8}$$

It will be shown (Sec B.1.4) that for energies greater than approximately 30 kev the formation of negative ions is improbable and may be neglected, that is, $\sigma_{0-1} \cong 0$. Then Eq. 3 becomes

$$\frac{dn_0}{d\pi} = -n_0\sigma_{01} + n_1\sigma_{10} \quad .$$

Without ion removal, the fraction of the beam which is neutral after passage through a length l of gas is

$$\frac{n_0}{N_0} = (1 - \phi_0)\, e^{-\pi(\sigma_{01}+\sigma_{10})} + \phi_0 \quad , \tag{9}$$

using the condition that $n_0 + n_1 = N_0$. Thus ϕ_0 and $\sigma_{01} + \sigma_{10}$ are determinable from measurements of n_0/N_0 as a function of the amount of gas traversed.

B.1.3 Description of Experimental Apparatus and Procedures

As noted in Sec B.1.1, this paper reports the results of several separate experiments. The heavy-ion Cockcroft-Walton accelerator, described briefly in ref 18, furnished ions for the experiments over the energy range from 20 to 200 kev. Since intensity limitations precluded work at lower energies on this accelerator, a separate facility was assembled to extend the measurements to approximately 3 kev. In the Cockcroft-Walton work, the formation of negative ions was sufficiently improbable that they could be neglected. A significant number of negative ions were formed in the low-energy (3 to 30 kev) experiments, and their behavior was studied.

Different equipment and techniques were used in the separate experiments reported in this paper. Therefore, after a section of general experimental considerations, a section will be devoted to each phase of the work.

B.1.3a. General. – The ion source used for all of these experiments was a Philips ionization gage type.[19] After acceleration, the proton beam was selected by magnetic analysis. The energy for both the Cockcroft-Walton and the low-energy experiments was measured and stabilized as outlined in ref 18. For the Cockcroft-Walton work, the error in the particle energy measurement is believed to be less than 1%. In the low-energy experiments, the distribution in energy of the ions emitted by this type of ion source ($\sim$100 ev) can introduce an energy uncertainty of several per cent at 3 kev.

The target gases used in these experiments were good-grade compressed gases passed over cold traps maintained at liquid nitrogen temperature. In much of the work, additional purification procedures were used. Hydrogen was passed through a heated palladium barrier. Helium was passed through an active charcoal trap cooled to liquid nitrogen temperature. Neon and argon were passed over calcium and copper turnings, heated to approximately 600°C. In no case were the measured cross sections altered by the purification techniques, indicating that the feed gases were relatively pure and that the charge-exchange cross sections are not sensitive to the small contamination by gases not removed by liquid nitrogen traps. This results from the fact that the cross sections are of the same order of magnitude for the noncondensable gases.

---

[18] P. M. Stier, C. F. Barnett, and G. E. Evans, *Phys. Rev.* 96, 973 (1954).

[19] C. F. Barnett, P. M. Stier, and G. E. Evans, *Rev. Sci. Instr.* 24, 394 (1955).

The pressures in the charge-exchange chambers were monitored by a modified Alphatron gage[20] and were measured with liquid-nitrogen-trapped McLeod gages. Calibrations of the McLeod gages during construction are believed to have been correct to better than 1%. Three independently calibrated gages have been used interchangeably during the course of these experiments, indicating the reliability of these calibrations.

As a particle beam passes through a stopping material, the beam is broadened by multiple elastic collisions. The magnitude of this scattering is determined by the velocity of the particle and the relative masses of the incident and target atoms. It is evident that the hydrogen beam transmitted through a charge-exchange chamber such as shown in Fig. B.1.1 has been attenuated by elastic scattering. This is of no consequence provided the cross sections for elastic scattering of an ion and an atom by a target atom are the same or are small compared to the inelastic cross section of interest. In the present experiments the latter condition was not always met. To ascertain whether the scattering of an ion and an atom were the same, a comparison was made of the elastic attenuation of an initially atomic beam with that of an ionic beam. Within the experimental error, no difference in elastic scattering could be detected. The test was made considerably less sensitive by the fact that both incident beams rapidly approach charge equilibrium. Hence, for conveniently measured attenuations, both beams are at or near charge equilibrium over part of their range. More definitive tests for errors due to elastic scattering will be discussed in Sec B.1.3f.

The charge-exchange chamber in each of the experiments was a windowless, differentially pumped gas cell. The pumping speed and aperture sizes were chosen for approximately 100-to-1 pressure drop between the gas cell and external chamber. In each apparatus the pressure in the external vacuum system was in the range of 1 to 5×10^{-5} mm Hg. The effective path length for charge exchange will be discussed below for each experiment.

B.1.3b. High-Energy (20–200 kev) Measurements of σ_{01}. – A schematic diagram of the apparatus used for the measurement of the electron-loss cross sections is shown in Fig. B.1.1. The first gas cell, designated the neutralizer, converts a portion of the ion beam from the accelerator to fast atoms by charge exchange. The electrostatic deflection plates (electrostatic analyzer No. 1) removed all ions emerging from the neutralizer, so that the particle beam incident on the second gas cell could be entirely fast neutral atoms. Within the second chamber, ions formed by electron loss could be removed by the transverse electric field between the deflection plates. Since an ion must travel a finite distance in the electric field to be deflected enough to be removed by the collimating aperture, the effective length of the analyzing plates is slightly different from their geometric length. By segmenting the deflection plates and applying the field to successive sections, it was possible to determine the effective length of each section experimentally. Effective lengths determined in this manner agreed well with calculated values, and the presented cross sections have been computed using these effective lengths. The maximum difference between effective and geometric plate lengths was approximately 5% at 200 kev.

The detectors used were similar to the combination foil thermocouple and secondary-electron-emission detector described by Stier, Barnett, and Evans.[21] Most of the electron-loss cross sections presented here were measured using secondary-electron collection. Using the foil differential thermocouple as a charge-insensitive detector, the relative coefficients for electron emission due to atom and ion bombardment were determined for the detector used, and were the same as those reported[21] within the experimental error. Analyzer No. 6 in Fig. B.1.1 was used to measure the relative number of ions and atoms in the particle beam emerging from the charge-exchange chamber for purposes of this correction.

It is evident that the fraction of the particle beam which was neutral at equilibrium (π large) is readily measured with the apparatus. An equilibrium charge distribution could be obtained from the ion beam, either in the neutralizer or in the charge-exchange chamber. It was also possible to approach charge equilibrium from an initially atomic beam. Further, in accordance

[20]National Research Corp., Newton Highlands, Mass.

[21]P. M. Stier, C. F. Barnett, and G. E. Evans, *Phys. Rev.* 96, 973 (1954).

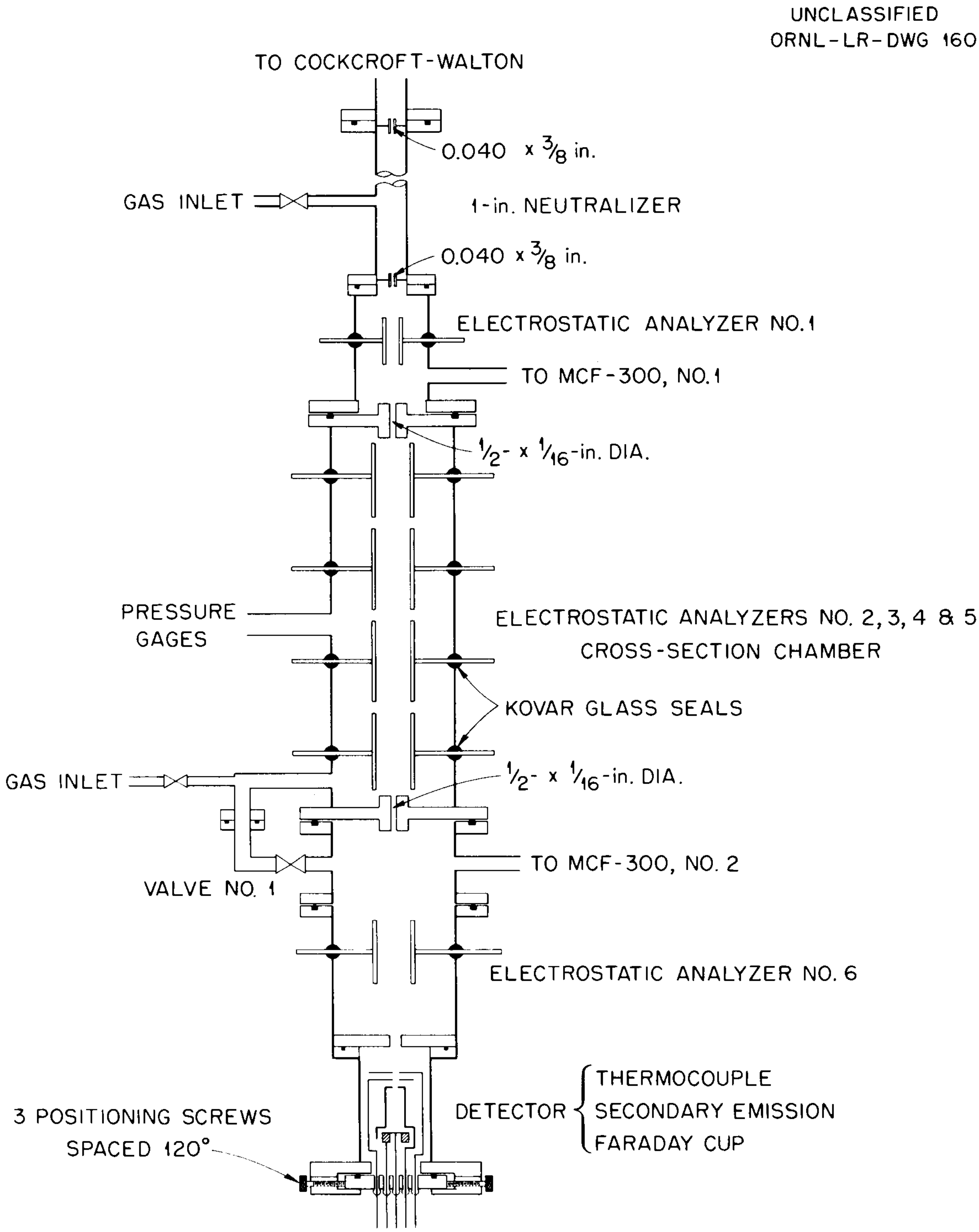

Fig. B.1.1. Apparatus for Measurement of Electron-Loss Cross Sections at 20 to 200 kev.

with Eq. 9, the sum of the cross sections, $\sigma_{01} + \sigma_{10}$, could be obtained.

B.1.3c. Low-Energy (3–30 kev) Measurement[22] of $\sigma_{01} + \sigma_{0-1}$, ϕ_{-1}/ϕ_{+1}, and ϕ_0. – The apparatus used for this phase of the work is shown schematically in Fig. B.1.2, and is similar in many respects to that described in Sec B.1.3b. Making use of charge exchange in the first differentially pumped gas cell, the particle beam incident on the second gas cell could be entirely atomic or could have an equilibrium distribution in charge. Application of the electric field within the gas removed ions as formed, and the cross section $\sigma_{01} + \sigma_{0-1}$ was computed from the observed attenuation of the transmitted beam. The bellows and the third pair of electrostatic deflection plates permitted measurement of the relative intensity of the positive, negative, and neutral components.

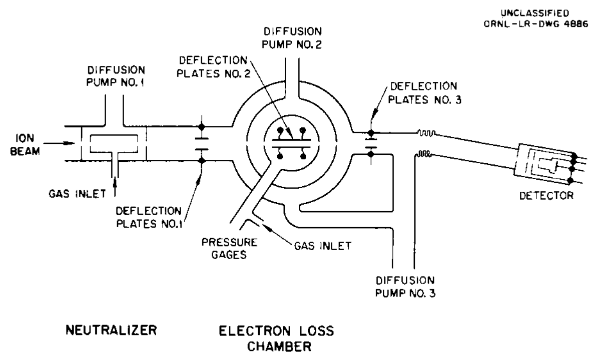

Fig. B.1.2. Apparatus for Measurement of Electron-Loss Cross Sections at Low Energies.

The detector, described in ref 21, was used as a Faraday cage for ion beams and as a secondary-electron-emission detector for atomic or mixed beams. The intensity of the transmitted beams was too small for convenient thermocouple detection. However, it was possible to avoid the problem of the possibly differing secondary-electron emission for ions and atoms by ensuring that only neutrals or only equilibrium charge distributions were incident on the detector. Thus measurements of ϕ_0 were made by equilibrating the beam in the first gas cell and then passing both the total beam and the neutral component through enough gas in the second cell to re-establish equilibrium. By this procedure, the secondary-electron emission was due to a particle flux with equilibrium charge distribution. Also, the attenuation observed for the computation of $\sigma_{01} + \sigma_{0-1}$ was the change in the neutral component at analyzer No. 3 caused by applying a field within the charge-exchange chamber. This was equivalent to recording the attenuation of a neutral beam incident on the second gas cell, in view of the fact that, for an equilibrium beam emergent from the neutralizer, the particle flux at the detector was the same whether electrostatic deflection plates No. 1 or No. 3 were energized. Both of these procedures require that the elastic scattering of ions and atoms be approximately the same. This will be shown to be sufficiently well satisfied in Sec B.1.3f.

The effective path length for charge exchange is taken as the distance from the entrance to the exit aperture. In the normal procedure, when potential was applied to deflection plates No. 2 in the gas, it was also applied to deflection plates No. 3. Consequently, an ion formed near the exit aperture and not removed by plates No. 2 will be removed by plates No. 3. It is, of course, possible for such an ion to experience an electron-capture collision before it reaches plates No. 3. Calculations show that, under typical conditions of this experiment, only a negligible number of the ions formed recapture an electron and reach the detector. Corrections for this effect have not been applied to the data since they necessitate a prohibitive number of numerical integrations.

B.1.3d. High-Energy Measurement of σ_{10}. – The equipment used for the Cockcroft-Walton measurements of the electron-capture cross section σ_{10} is diagramed schematically in Fig. B.1.3. The proton beam, after magnetic analysis, entered a differentially pumped gas cell and was deflected through an angle of 45 deg by a transverse magnetic field. In order to avoid attenuation of the ion beam due to small-angle elastic scattering and maintain the advantages of having the detector in a high-vacuum space, the ion beam was moved across an exit slit by a linear electrostatic sweep voltage. The emergent beam was integrated. Recorder traces of the detector current as the beam was moved across the slit demonstrated the amount of elastic scattering and the number

[22]Prof. R. A. Howard, of the University of Oklahoma, contributed substantially to the work described in this section while a summer participant at ORNL.

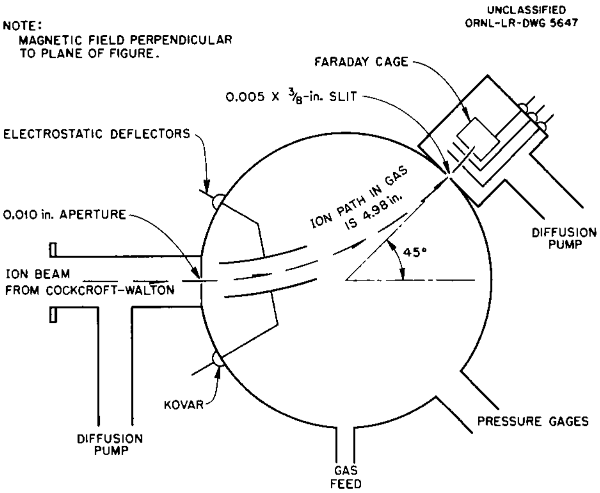

Fig. B.1.3. Apparatus for Measurement of Electron-Capture Cross Sections at High Energies.

of ions which suffered two charge-exchange events. For the energies and pressures used in these experiments a negligible fraction of the ions reaching the detector had captured and lost an electron. If this were not true, the measured cross section would have been pressure dependent and the strip-chart record of the proton current received at the detector as the electrostatic field was varied would have shown an asymmetric "tail" on the long-radius-of-curvature side. Experimentally, such a tail was observed to occur at considerably higher pressures than were used for the reported cross-section measurements.

The detector was a single Faraday cup with saturation bias voltages applied to the guard electrodes.

It is to be noted that this experiment differs from those described in Secs B.1.3b and B.1.3c in that the charge-exchange chamber was alternately at high vacuum and at a pressure of a few microns. A small change in the flux of protons which enter the chamber was caused by elastic scattering from the gas escaping through the entrance aperture. In order to avoid this error, gas was leaked outside the entrance aperture and exit slit so that vacuum conditions in these regions were the same with and without gas in the charge-exchange chamber. The differential pumping capacity was such that the pressure in these regions was from 1 to 5 $\times$ 10^{-5} mm Hg.

The path length was taken as the distance along the curve from the entrance to the exit aperture.

B.1.3e. Low-Energy Measurement of σ_{10} and σ_{-10}. – The measurements of the cross sections σ_{10} and σ_{-10} in the 3- to 30-kev region were very similar to the corresponding Cockcroft-Walton work. As diagramed in Fig. B.1.4, the proton beam was passed through a differentially pumped gas cell. The emergent beam was resolved into the -1, 0, and $+1$ components. The second chamber was equivalent to that described in Sec B.1.3d, except that electrostatic deflection was used instead of magnetic deflection. A small linear sweep voltage was superimposed to move the deflected beam across the exit slit, and the emergent beam was integrated as described above. In other respects the techniques discussed in Sec B.1.3d were employed.

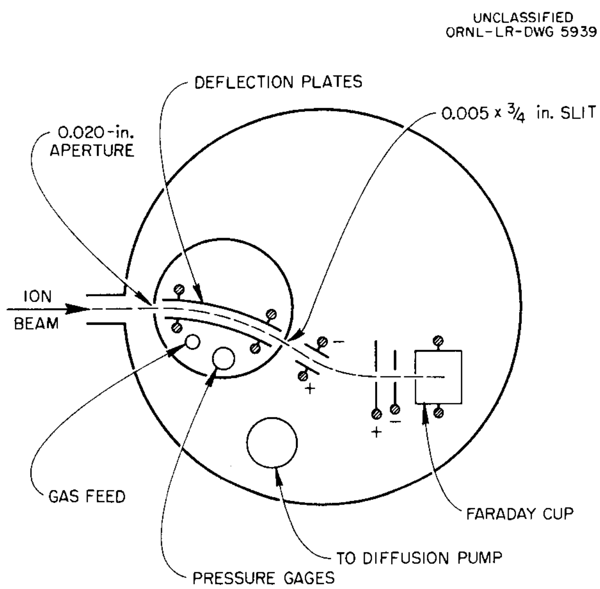

Fig. B.1.4. Apparatus for Measurement of Electron-Capture Cross Sections at Low Energies.

The entrance aperture was 0.020 and 0.040 in. for the σ_{10} and σ_{-10} measurements, respectively, and the exit slit widths were 0.005 and 0.015 in., respectively. The enlarged dimensions for the negative-ion work were dictated by the reduced intensities available, and were allowable in view of the lower chamber pressures needed for reliable measurements of the relatively large σ_{-10} cross sections. In all cases the differential pumping capacities were sufficient to maintain pressures of 1 to 5 $\times$ 10^{-5} mm Hg in the regions outside the charge-exchange chamber.

Calculations comparable to those indicated in Sec B.1.3c show that only a very small fraction of the atoms formed by charge exchange are reionized and reach the detector. The effective length is taken as the full path length in the gas.

B.1.3f. Low-Energy Measurements of $\sigma_{01} + \sigma_{0-1}$ and ϕ_0 by Integration.[23] – As was discussed in Sec B.1.3b, the deneutralization cross-section measurements described in Secs B.1.3b and B.1.3c require that the elastic-scattering cross section be the same for fast atoms and ions, or that it be small by comparison with the charge-exchange cross sections. This section describes further experiments designed to test this condition.

Upon completion of the measurements described in Sec B.1.3e, the apparatus was modified as depicted in Fig. B.1.5. Deflection plates were installed to establish an electrostatic field perpendicular to the beam axis, and a movable exit slit was installed. The slit was moved at a constant linear rate across the beam axis by a motor-driven shaft through the vacuum wall. The current through the slit was integrated as discussed in Sec B.1.3d. An additional set of deflection plates was installed between the exit slit and the secondary-electron-emission detector to prevent any ions formed near the exit slit from reaching the detector.

The deneutralization cross section was calculated from the attenuation of the integrated beam (1) as voltage was applied at constant pressure or (2) as target gas was introduced at constant voltage. Both of these measurements should be insensitive to elastic scattering. Thus, if the elastic-scattering cross section for ions was significantly different from that for atoms, the cross sections obtained in determinations (1) and (2) would differ from the results obtained by the procedure of Sec B.1.3c. The results of the various determinations are shown in Fig. B.1.6.

[23]Much of the work described in this section was performed by Mr. W. A. Bugg, while he was a summer employee at the Laboratory.

UNCLASSIFIED
ORNL-LR-DWG 11684

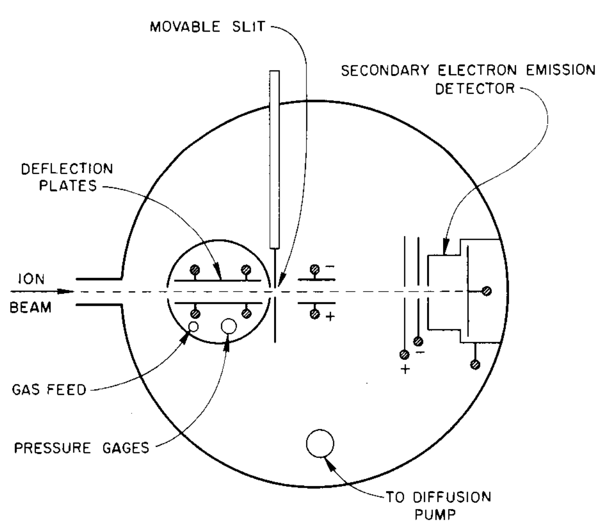

Fig. B.1.5. Apparatus for Investigation of Elastic Scattering Effects.

UNCLASSIFIED
ORNL-LR-DWG 10246

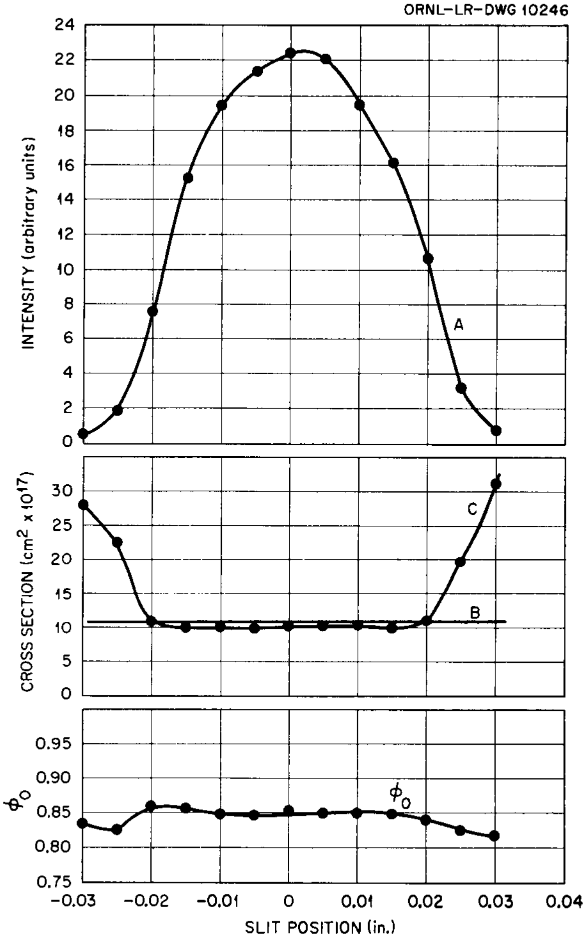

Fig. B.1.6. Variation of Intensity, Cross Section, and Neutral Fraction with Position in the Beam: H in Nitrogen at 4 kev.

In the top half of the figure (curve *A*), the envelope of the beam is plotted on an arbitrary intensity scale in order to orient the observed variations in cross sections. In the lower portion of the figure the values of the cross sections determined by integration in procedures (1) and (2) are shown as the horizontal line *B*. The variation of the cross section as a function of position in the beam is shown as curve *C*. These data were taken by moving the slit across the beam by increments, and at constant pressure, observing the attenuation as voltage was applied by the procedure of Sec B.1.3c. The cross section was independent of position near the center of the beam but rose sharply at the periphery (curve *C*, Fig. B.1.6). This interesting feature may be ascribed to electron-loss collisions in which elastic scattering occurs. Particles which were elastically scattered to form the periphery of the beam had usually undergone charge exchange. Hence the attenuation, or apparent cross section observed as the field was applied, was larger for these regions. However, only a few per cent of the beam was contained in this peripheral shell, and the cross section determined at the center of the beam was very nearly equal to the result obtained by integration. The data shown in the figure were measured at 4 kev, where the effects of elastic scattering are largest. No effect could be detected above 10 kev.

The curve ϕ_0 of Fig. B.1.6 depicts the variation of the neutral fraction of an equilibrium beam with position in the beam. The periphery of the beam was slightly deficient in neutral atoms, as would be expected from the observed increase in cross section.

B.1.4. Results and Discussion

The experimental results of this series of experiments are presented in Figs. B.1.7–B.1.19. Subsequent figures show the agreement of the present results with the more recent measurements by other workers.

The variation of the equilibrium fraction of the particle beam in each of the charge states is shown as a function of energy in Figs. B.1.7–B.1.12. These data were obtained by the methods described in Sec B.1.3c. The particle beam was passed through enough gas for equilibrium to be established between competing electron capture and loss reactions. In each of the figures, the open circles of the ϕ_0 curves represent the neutral fractions measured in the low-energy experiment, while the solid triangles on these curves are data taken in the Cockcroft-Walton experiment. In all cases good agreement is obtained between the low-energy data, data measured using the Cockcroft-Walton as described in Sec B.1.3b, and the results previously reported.[24] The ϕ_{+1} and ϕ_{-1} curves were computed from ϕ_0 and the measured

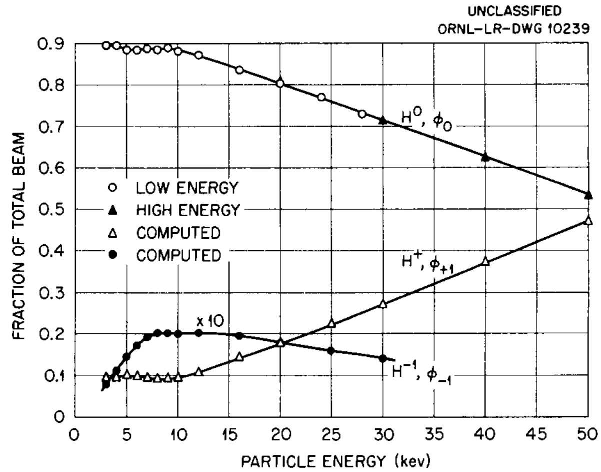

Fig. B.1.7. Fraction of Beam in +1, 0, −1 Charge State After Passage Through "Thick" Target: H in Hydrogen.

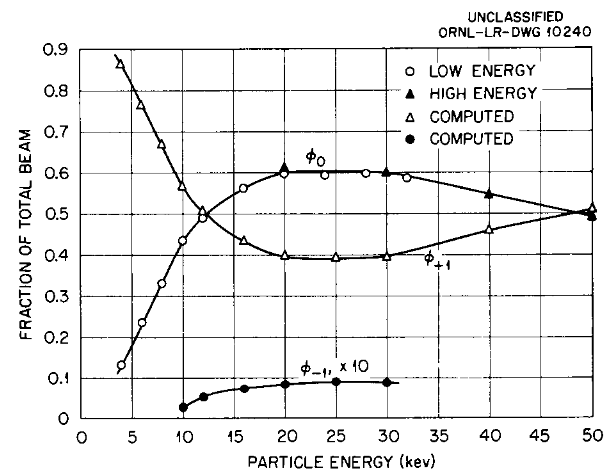

Fig. B.1.8. Fraction of Beam in +1, 0, −1 Charge State After Passage Through "Thick" Target: H in Helium.

[24] P. M. Stier, C. F. Barnett, and G. E. Evans, *Phys. Rev.* 96, 973 (1954).

ratio of negative to positive ion components, that is, ϕ_{-1}/ϕ_{+1}, with the requirement that

$$\phi_{-1} + \phi_0 + \phi_{+1} = 1 \ .$$

Attention is called to the fact that the ordinate for ϕ_{-1} is expanded by a factor of 10 in each of these figures for clarity in presentation. Referring to the figures, it will be seen that, at 40 kev, 1% or less of the hydrogen beam is H^-. Therefore, it has been neglected in computations at higher energies.

Two types of behavior are evident from the curves, exemplified by the neutral components in argon and helium. At the lower energies in argon, hydrogen, nitrogen, and oxygen, most of the fast hydrogens are neutral. By comparison, in helium at corresponding energies most of the beam is in the +1 charge state. These observations correspond to the fact that while passing through an easily ionized gas, for example argon, protons readily capture electrons. On the other hand, a proton has difficulty in removing an electron from

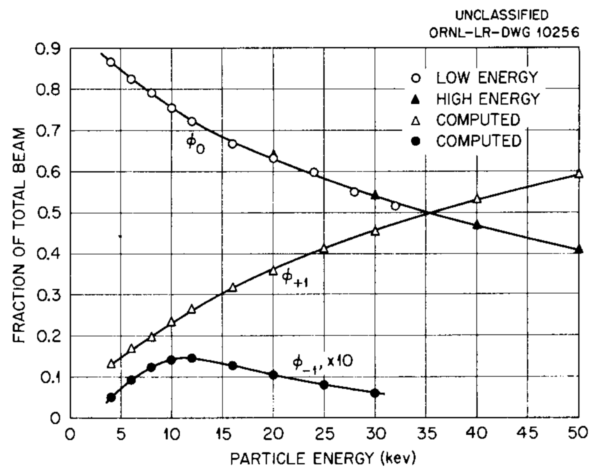

Fig. B.1.9. Fraction of Beam in +1, 0, −1 Charge State After Passage Through "Thick" Target: H in Nitrogen.

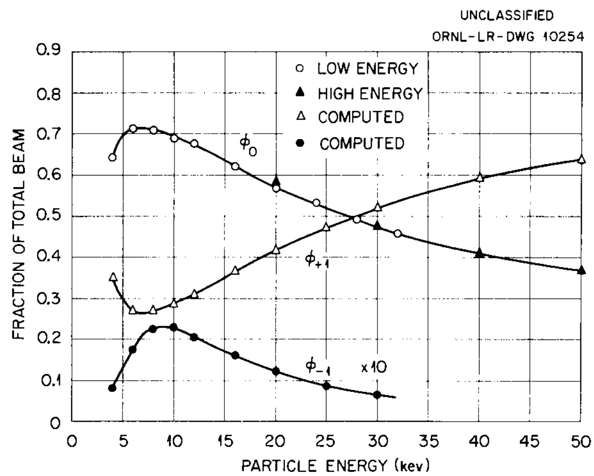

Fig. B.1.11. Fraction of Beam in +1, 0, −1 Charge State After Passage Through "Thick" Target: H in Neon.

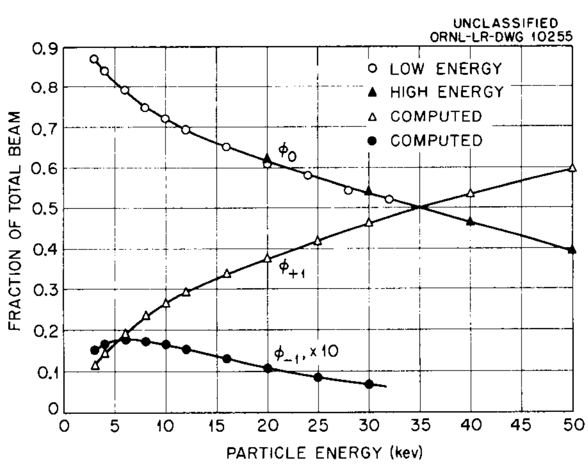

Fig. B.1.10. Fraction of Beam in +1, 0, −1 Charge State After Passage Through "Thick" Target: H in Oxygen.

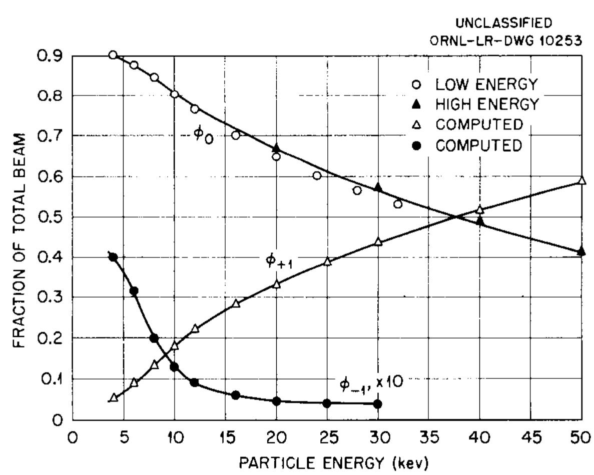

Fig. B.1.12. Fraction of Beam in +1, 0, −1 Charge State After Passage Through "Thick" Target: H in Argon.

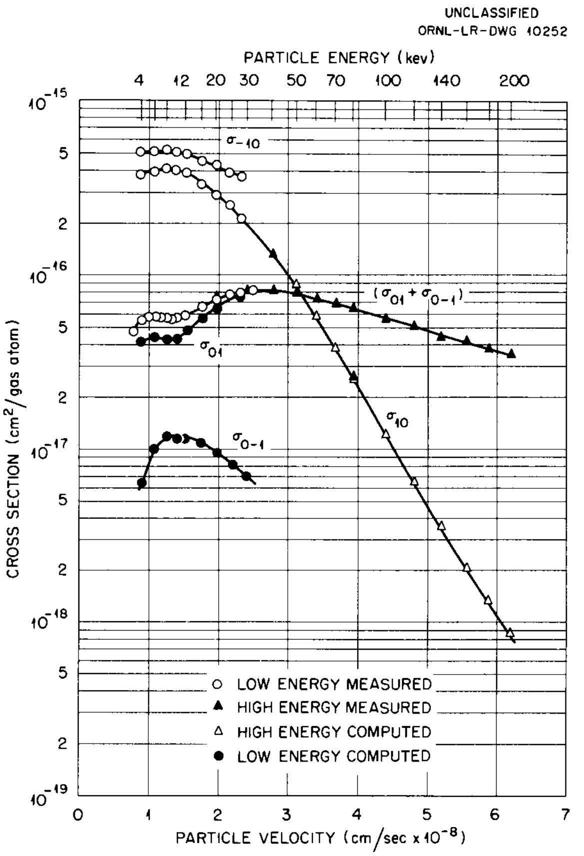

Fig. B.1.13. Charge-Transfer Cross Sections Per Atom of Gas Traversed as a Function of Particle Velocity or Energy: Hydrogen Atoms and Ions in Hydrogen Gas.

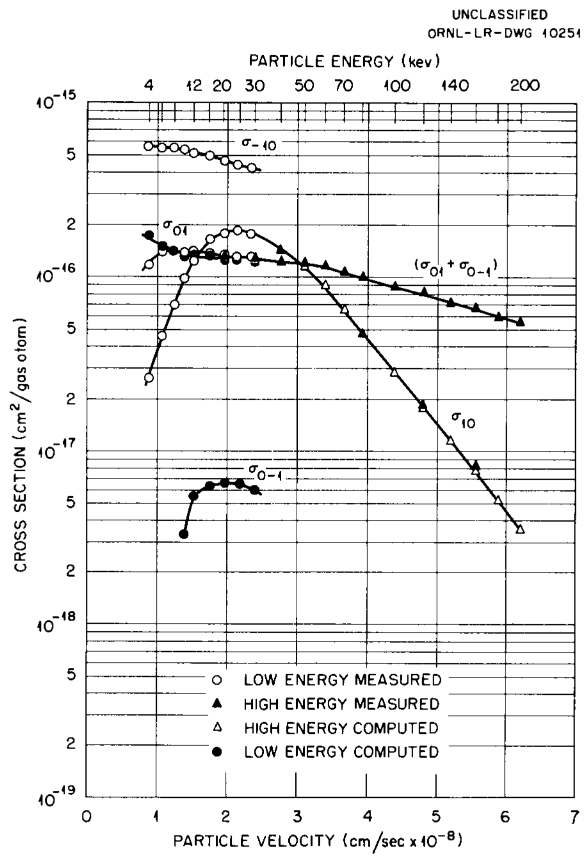

Fig. B.1.14. Charge-Transfer Cross Sections Per Atom of Gas Traversed as a Function of Particle Velocity or Energy: Hydrogen Atoms and Ions in Helium Gas.

the tightly bound helium atom, although a fast hydrogen atom may be ionized in a collision with a helium atom. The behavior in neon is intermediate between helium and argon. It is only at the lowest energies studied, that is, nearest to the adiabatic condition, that the proton is ineffective in removing an electron from the neon atom. It should be pointed out that this behavior is equivalent to that reported[24] for argon ions in helium and neon at considerably higher energies. These qualitative statements will be discussed in terms of the separate cross sections below.

Attention is called to the unique behavior of the ϕ_0 and ϕ_1 curves in hydrogen gas in the energy region 3 to 10 kev. Throughout this energy range, the neutral component is approximately constant and, in fact, shows a slight local minimum. As will be shown below, this results from a subsidiary maximum in the cross section for electron loss, σ_{01}.

The cross sections for charge transfer measured in this series of experiments are presented as functions of particle energy and velocity in Figs. B.1.13–B.1.18. For the curves representing σ_{-10}, σ_{10}, and $\sigma_{01} + \sigma_{0-1}$ the points are the average of the several measurements made at each energy, and the small scatter of the data around the smooth curves indicates the relative accuracy of the measurements. The open circles represent the results of the low-energy measurements (Secs B.1.3c and B.1.3e), while the triangle points represent the high-energy data (Secs B.1.3b and B.1.3d). The solid circles indicate values of the

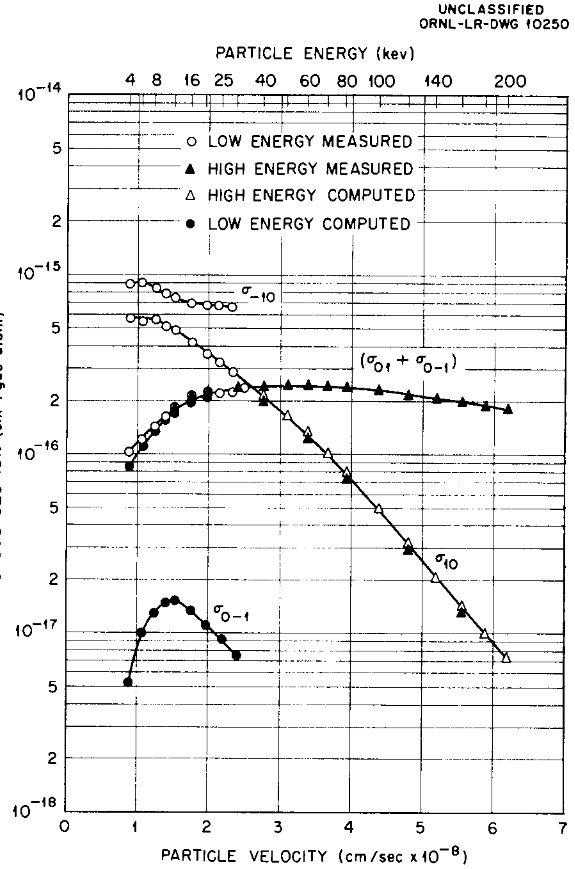

Fig. B.1.15. Charge-Transfer Cross Sections Per Atom of Gas Traversed as a Function of Particle Velocity and Energy: Hydrogen Atoms and Ions in Nitrogen Gas.

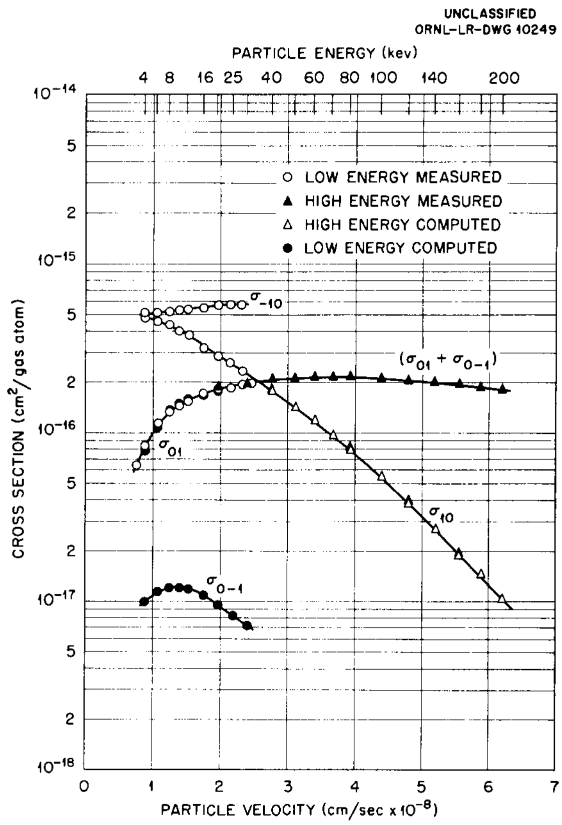

Fig. B.1.16. Charge-Transfer Cross Sections Per Atom of Gas Traversed as a Function of Particle Velocity and Energy: Hydrogen Atoms and Ions in Oxygen Gas.

cross sections σ_{0-1} and σ_{01} computed from σ_{-10} and σ_{10}, respectively, making use of the independently determined values of ϕ_{-1}/ϕ_0 and ϕ_{+1}/ϕ_0. The points designated as open triangles on the σ_{10} curve were computed from $\sigma_{01} + \sigma_{0-1}$, which is taken to be σ_{01} for energies in excess of 40 kev (see below). Excellent agreement is obtained between the separate low-energy and high-energy experiments, as is evident from the smooth joining of the curves between 20 and 30 kev. Internal consistency of the series of experiments is tested by the agreement of the sum of the computed σ_{0-1} and σ_{01} curves and the experimental $\sigma_{01} + \sigma_{0-1}$ curve. Reference to the figures shows that the agreement is well within the cumulative experimental errors. Explicitly, the computed deneutralization cross section is given in terms of the experimental measurables σ_{10}, σ_{-10}, ϕ_0, and ϕ_{-1}/ϕ_{+1} as

$$\sigma_{01} + \sigma_{0-1} = \sigma_{10}\left[\frac{(1/\phi_0) - 1}{1 + (\phi_{-1}/\phi_{+1})}\right] + \sigma_{-10}\left[\frac{(1/\phi_0) - 1}{1 + (\phi_{+1}/\phi_{-1})}\right] .$$

It is to be noted from the sequence of Figs. B.1.13–B.1.18 that the velocity behavior of the σ_{-10} cross section resembles that of the σ_{01}, while the σ_{10} and σ_{0-1} curves have similar shapes. This correspondence might be predicted, since σ_{10} and σ_{0-1} characterize electron-attachment reactions, while σ_{-10} and σ_{01} gage electron-loss processes.

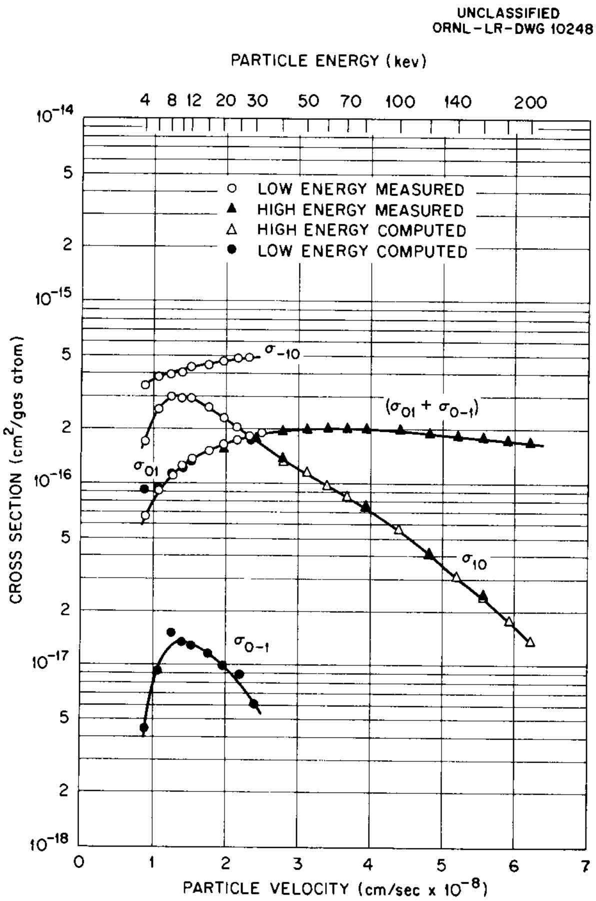

Fig. B.1.17. Charge-Transfer Cross Sections Per Atom of Gas Traversed as a Function of Particle Velocity and Energy: Hydrogen Atoms and Ions in Neon Gas.

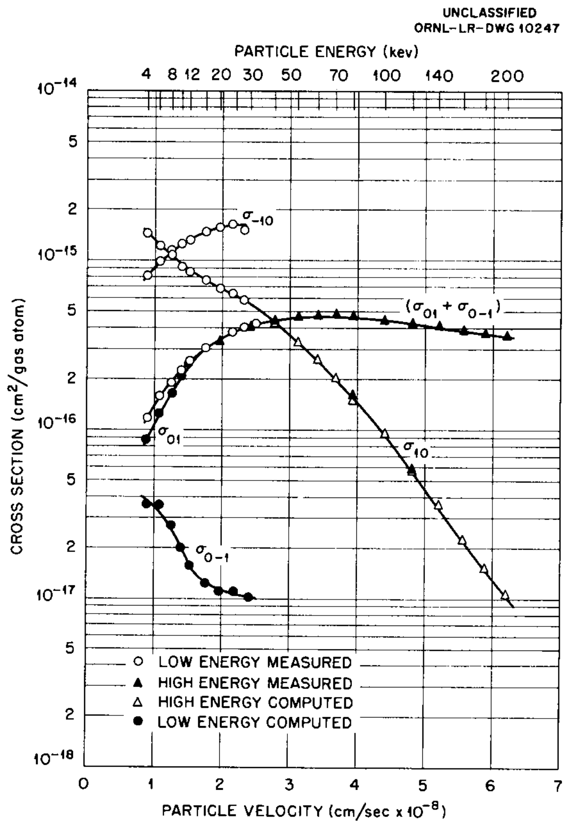

Fig. B.1.18. Charge-Transfer Cross Sections Per Atom of Gas Traversed as a Function of Particle Velocity and Energy: Hydrogen Atoms and Ions in Argon Gas.

In each of the gases studied, the cross section σ_{10} decreases at the higher energies very nearly as Ae^{-bv}, where A and b are constants for each gas. This behavior is most noticeable in hydrogen and helium. In the energy range studied, σ_{10} decreases by about three orders of magnitude in hydrogen gas, while the observed decrease in oxygen and neon was only about a factor of 50.

In contrast to the rapid variation of σ_{10}, the electron-loss cross section σ_{01} changes only by a factor of from 2 to 4 within this energy region. The most interesting feature of these σ_{01} curves is the subsidary maximum in the data for hydrogen gas. Although no detailed treatment of this feature can be given at the present, the structure is similar to that expected theoretically when double-transition collisions may occur. Bates and Griffing[25] have discussed the cross sections expected for collisions between two hydrogen atoms in which both atoms may undergo electron excitations. They find that at low energies (~10 kev) single-transition collisions predominate, but at higher energies, double-transition collisions are more important. Thus the curves of total cross section vs energy may show two maxima. In the present case, the reaction studied is an atom-atom collision in which the fast atom is ionized. The shape of the cross-section curve suggests two modes for the reaction: at low energies the stationary molecule is left in the ground state, whereas at higher energies it is likely that the stationary molecule will be left

[25]D. R. Bates and G. Griffing, *Proc. Phys. Soc. (London)* A66, 961 (1953).

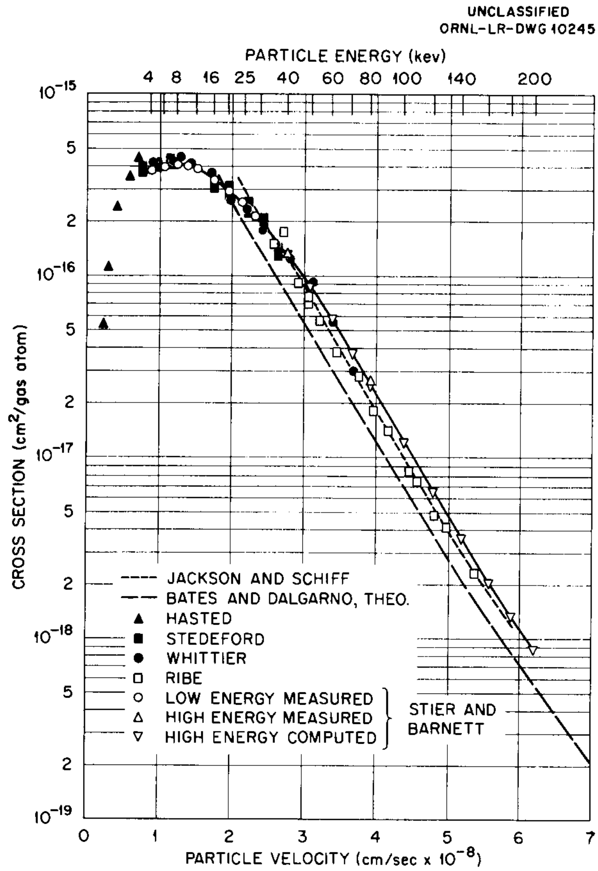

Fig. B.1.19. Electron-Capture Cross Section Per Atom of Gas Traversed: Protons in Hydrogen Gas.

in excited or ionized states. Similar behavior might be expected for other target gases. That double maxima are not observed must be attributed to overlapping of the single- and double-transition cross-section contributions, producing a single broad maximum.

Figure B.1.19 is a comparison of the present electron-capture cross section, σ_{10}, in hydrogen gas with recent experimental and theoretical values by other workers. The solid curve is drawn through the present data. The results of Whittier[26] and Ribe[27] were plotted from their tabulation, and the data points for Stedeford and Hasted[28] were taken from their published curve.

[26]A. C. Whittier, *Can. J. Phys.* **32**, 275 (1954).

[27]F. L. Ribe, *Phys. Rev.* **83**, 1217 (1951).

[28]J. B. H. Stedeford and J. B. Hasted, *Proc. Roy. Soc.* (*London*) **A227**, 466 (1955).

In view of the difficulty of the experiment and the diversity of techniques used by the various investigators, the agreement may be considered excellent. The similarity between the velocity dependence of the experimental cross section and the theoretical dependence obtained by Bates and Dalgarno and by Jackson and Schiff is also satisfying.

A similar comparison of the data for σ_{10} in helium is given in Fig. B.1.20. Again the solid curve has been drawn through the present data. Very striking agreement is again noted between this curve and the results of Stedeford and Hasted.[28] The theoretical curve of Bransden, Dalgarno, and King[29] shows an essentially identical dependence of the cross section on the velocity. As Griffing has pointed out,[30] the

[29]B. H. Bransden, A. Dalgarno, and N. M. King, *Proc. Phys. Soc.* (*London*) **A67**, 1075 (1954).

[30]G. Griffing, private communication.

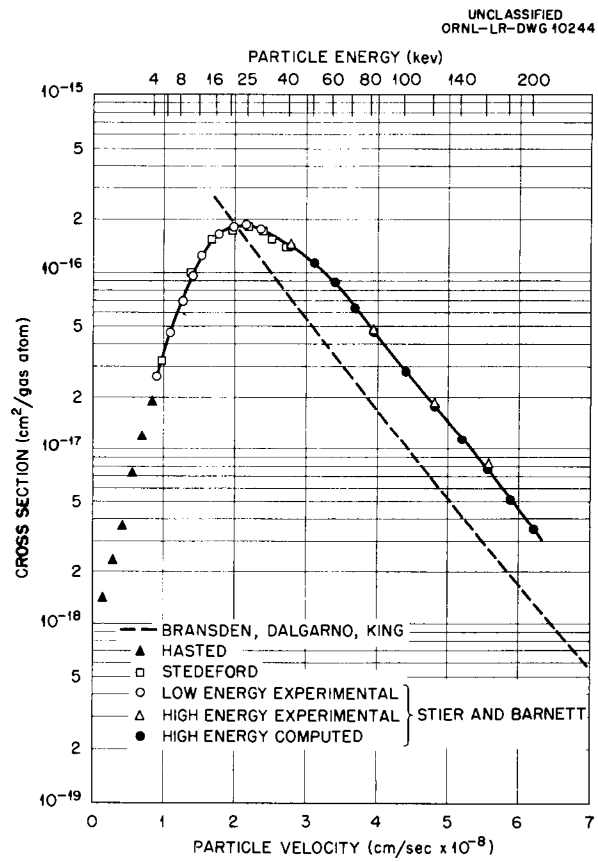

Fig. B.1.20. Electron-Capture Cross Section Per Atom of Gas Traversed: Protons in Helium Gas.

theoretical formulation is best tested by the velocity dependence of the cross section, although the amplitude may be in error by a small factor.

In Fig. B.1.21, the present values of σ_{10} for protons in neon and argon are seen to be in excellent agreement with those of Stedeford and Hasted. The capture cross section was found to vary slightly more rapidly with velocity in oxygen than in nitrogen, as shown in Fig. B.1.22. In this figure, the results of Kanner, who measured σ_{10} in air, are given for comparison.

Very few data are available in the literature for comparison with the cross sections σ_{01} or σ_{0-1} obtained in these experiments. Montague[31] and Kanner[32] have measured σ_{01} in hydrogen and in air, respectively. These experimenters obtained

[31]J. H. Montague, *Phys. Rev.* 81, 1026 (1951).

[32]H. Kanner, *Phys. Rev.* 84, 1211 (1951).

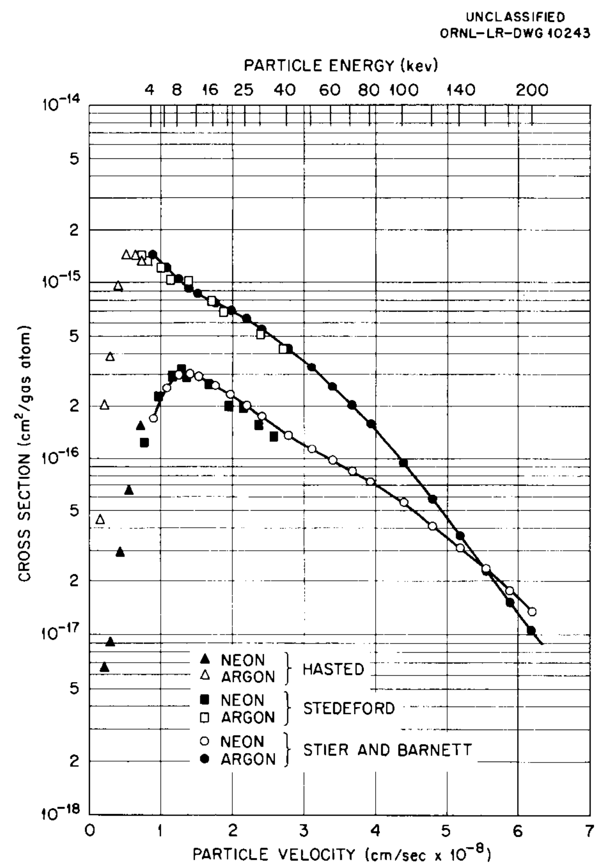

Fig. B.1.21. Electron-Capture Cross Section Per Atom of Gas Traversed: Protons in Neon and Argon Gases.

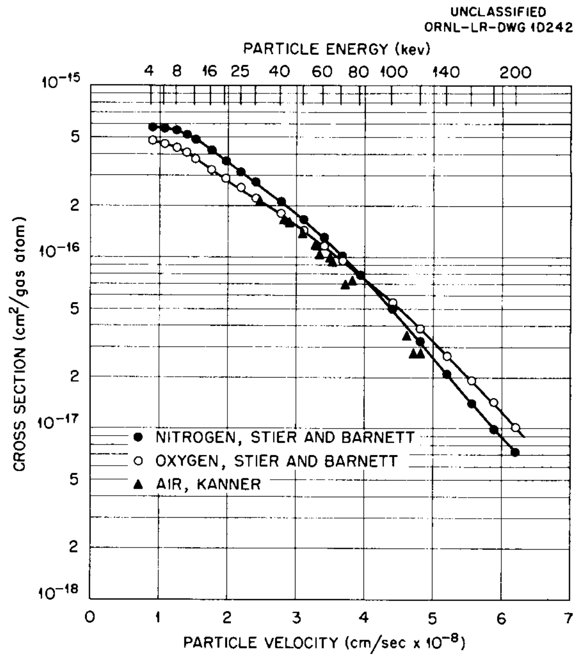

Fig. B.1.22. Electron-Capture Cross Section Per Atom of Gas Traversed: Comparison of Present Results for Protons in Nitrogen and Oxygen with Those of Kanner in Air.

cross sections, which are approximately 10% smaller than the values presented here. A few other results are to be found[33] but no exhaustive comparison will be made.

Stedeford and Hasted[28] have reported measurements of the detachment cross sections in the noble gases, and Whittier[26] has made similar measurements in hydrogen. Comparison of these data with the present work is made in Fig. B.1.23 for H^- in hydrogen and helium. Each of the σ_{-10} determinations was made much less precise than the corresponding σ_{10} measurement by the very small intensity of the H^- ion beam available. In view of this the relatively poor agreement may be considered satisfactory.

It should be pointed out again that these results have been treated as though in a single collision only one electron may be transferred. No quantitative determination of the two-electron-transfer cross sections has been possible. It seems likely that these cross sections must be considerably smaller than the single-electron-transfer cross

[33]H. S. W. Massey and E. H. S. Burhop, *Electronic and Ionic Impact Phenomena*, Clarendon Press, Oxford, 1952.

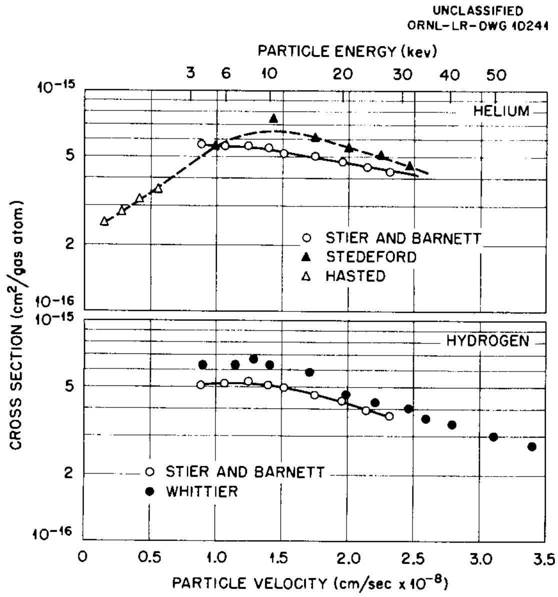

Fig. B.1.23. Electron-Detachment Cross Section Per Atom of Gas Traversed for H⁻ in Hydrogen and Helium Gases.

sections. This conclusion has been reached for the following experimental reasons. (1) In this rather extensive experimental program, no indication was ever present that double transitions were taking place. (2) The consistency of the results, interpreted in terms of single transitions, would indicate relatively few double transitions. (3) The present measurements of σ_{10} are in such excellent agreement with those of Stedeford and Hasted, in spite of the fact that the experiment described in Sec B.1.3d measures $\sigma_{10} + \sigma_{1-1}$ while the Stedeford and Hasted[28] method measures $\sigma_{10} + 2\sigma_{1-1}$. In the present work the cross section was computed from the attenuation of a transmitted beam due to all charge-changing collisions. In the Stedeford and Hasted experiment, the number of slow ions formed in the target gas was measured per incident ion, and the cross section was computed from this slow-ion current and the pressure according to the relation $\sigma = I'/Inl$, where I' is the slow-ion current, I the incident current, n the gas density in atoms per cubic centimeter, and l the path length in centimeters. If two-electron-transfer collisions occur, for example, $H^+ + A^0 \longrightarrow H^- + A^{++}$, the doubly charged slow ion will be "counted twice," and the equation should be rewritten in terms of the particle fluxes j as

$$\sigma_{10} + \sigma_{1-1} = \left(\frac{j_1}{j_0} + \frac{j_2}{j_0} \right) \frac{1}{nl} ,$$

where j_1 is the flux of singly charged slow ions, j_2 the flux of doubly charged ions, and j_0 the incident flux. In this notation their recorded currents are $I = ej_0$ and $I' = e(j_1 + 2j_2)$. Thus, the cross section given by Stedeford and Hasted is $\sigma_{10} + 2\sigma_{1-1}$. In view of the excellent agreement between the results of these authors and the present work, one must conclude that σ_{1-1} is small compared to σ_{10}.

The authors wish to acknowledge helpful discussions with Dr. A. H. Snell of the Oak Ridge National Laboratory and with Prof. S. K. Allison of the University of Chicago.

B.2 CROSS SECTIONS FOR ELECTRON LOSS BY HYDROGEN ATOMS AND THE EQUILIBRIUM CHARGE DISTRIBUTION OF A HYDROGEN BEAM[1]

C. F. Barnett H. K. Reynolds

Abstract

Cross sections were determined for electron loss by fast hydrogen atoms in various stopping gases in the energy range 250 kev to 1 Mev. Also, determinations were made of the equilibrium charge distribution of a hydrogen beam after passage through a thick gas target.

A previous report[2] included descriptions and results of a number of experiments in which were investigated the cross sections for electron capture and loss by fast hydrogen atoms and ions in gases. The particle energy ranged from 3 to 200 kev. Present results include measurements of the electron-loss cross sections of hydrogen and the equilibrium charge distribution in a thick gas target. From these two measurements, the electron-capture cross sections may be computed. The particle energy interval was 250 kev to 1 Mev for target gases of hydrogen, helium, nitrogen, and argon.

The apparatus used for these measurements consisted of two charge-exchange chambers, shown schematically in Fig. B.2.1. The ion beam from the 3-Mv Van de Graaff accelerator was incident upon the first differentially pumped gas cell, designated as the neutralizer. Since the Van de Graaff does not operate stably below 500 kev, it was necessary in the energy region of 250–500 kev to accelerate molecular hydrogen ions at higher energies and dissociate them in the neutralizer by impact with gas molecules, resulting in particles of half energy. For higher energies, protons were accelerated and a small fraction was converted into neutral particles in the neutralizer by charge exchange. The electrostatic deflection plates (electrostatic analyzer No. 1) removed all ions from the emergent beam, so that only neutral particles were incident on the second gas cell. Ions formed by electron-loss collisions in this second gas cell were removed from the beam by the applied transverse electric field. The geometrical path length was determined by measuring the attenuation of the neutral beam with voltage applied to all four analyzers and then only to the center two. Beam intensity was measured by use of secondary-electron emission from a brass target

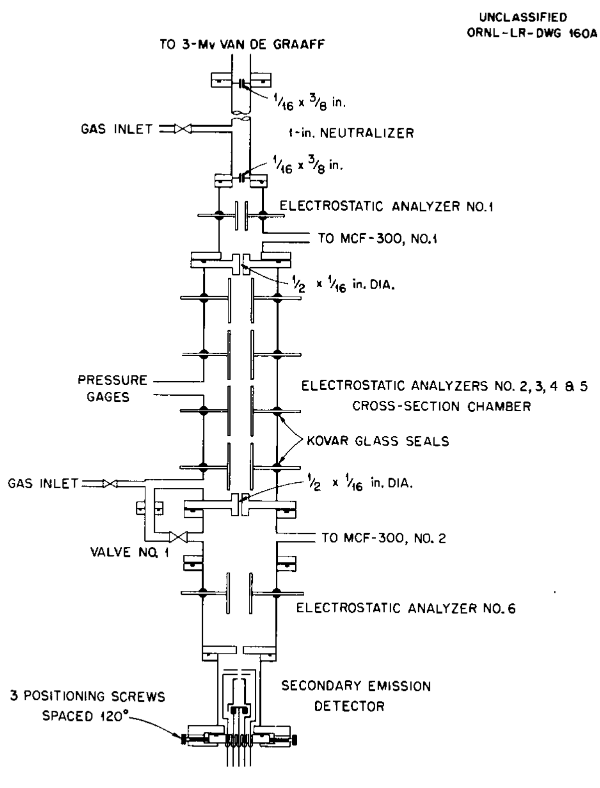

Fig. B.2.1. Schematic Diagram of Apparatus for Measurement of Electron-Loss Cross Section.

---

[1] C. F. Barnett, H. K. Reynolds, and R. G. Reinhardt, *Phys. Semiann. Prog. Rep. Sept. 10, 1956*, ORNL-2204, p 39–41.

[2] P. M. Stier and C. F. Barnett, *Phys. Rev.* 103, 896–907 (1956) (Appendix B.1 of this report).

and was corrected for the effect of the relative secondary-electron emission for hydrogen ions and atoms. This correction was determined by measuring with a thermocouple the rise in temperature of the target with only ions or atoms impinging. The ratio of the relative secondary-electron emission for hydrogen atoms to ions increased from 1.36 at 250 kev to 1.59 at 1 Mev.

The ratio of the electron-loss cross section to the electron-capture cross section, σ_{01}/σ_{10}, was determined by observing the charge distribution in the particle beam after passage through a gas target which was thick enough for equilibrium to be established between competing capture and loss processes. This equilibrium is independent of the initial charge state. For higher energies (500 kev to 1 Mev), the equilibrium charge distribution was determined for a proton beam incident on the first gas cell (the neutralizer). For lower energies (250 to 500 kev), the charge distribution was determined by first dissociating H_2^+ in the first gas cell, then removing all emergent ions by the electrostatic deflecting plates, so that only neutral atoms were incident on the second cell. This was necessary to eliminate any H_2^+ ions not dissociated in the neutralizer, although the presence of H^+ would not have altered the charge distribution. The measurements of equilibrium charge distribution, with a 500-kev proton beam or with a 1-Mev molecular ion beam which is dissociated, yielded results which are identical within the accuracy of the experiment. To obtain the sufficiently thick gas target, it was necessary to increase the pressure in the appropriate gas cell until no further change was noticed in the ion-to-atom ratio.

From the measurements of electron-loss cross sections, σ_{01}, and the equilibrium charge distribution, $n_1/n_0 = \sigma_{01}/\sigma_{10}$, the electron-capture cross sections may be readily computed. Shown in Figs. B.2.2–B.2.5 are the experimental determinations of the electron-loss cross sections and the computed electron-capture cross sections as a function of energy or velocity. The present results agree well with those obtained with the Cockcroft-Walton accelerator in the adjoining region, and, for completeness, these results are plotted for energies less than 250 kev.

For the case of hydrogen target gas, we can compare our result with theoretical predictions. Plotted in Fig. B.2.2 are the theoretical results of Dalgarno and Griffing[3] and of Jackson and Schiff.[4] The capture cross sections reported are the computed cross sections for the transition to the ground state only. If transitions to excited states are considered, then the cross section will be larger. The value of the theoretical electron-capture cross section deviates from the experimental points at higher energies. It had been expected from theoretical predictions that the calculated cross sections should agree closely with the measured values at the higher energies. On the other hand, the theoretical electron-loss cross sections of Dalgarno and Griffing[3] agree with the present experimental values to within 10% throughout the energy range.

At the present time, the theoretical calculations for cross sections of hydrogen atoms and ions in gases heavier than hydrogen are not satisfactory. This arises from the strong dependence of the cross sections on the effective charge of the target atom. Therefore, we cannot adequately compare the predicted values with the present measurements.

For the case of argon, it is to be noted that the slope of the capture cross section is rapidly decreasing in the energy range 300 kev to 1 Mev. In contrast, the electron-loss cross sections decrease by less than an order of magnitude throughout the high-energy range.

---

[3] A. Dalgarno and G. W. Griffing, *Proc. Roy. Soc.* (*London*) A232, 423 (1955).

[4] J. D. Jackson and H. Schiff, *Phys. Rev.* 89, 359 (1953).

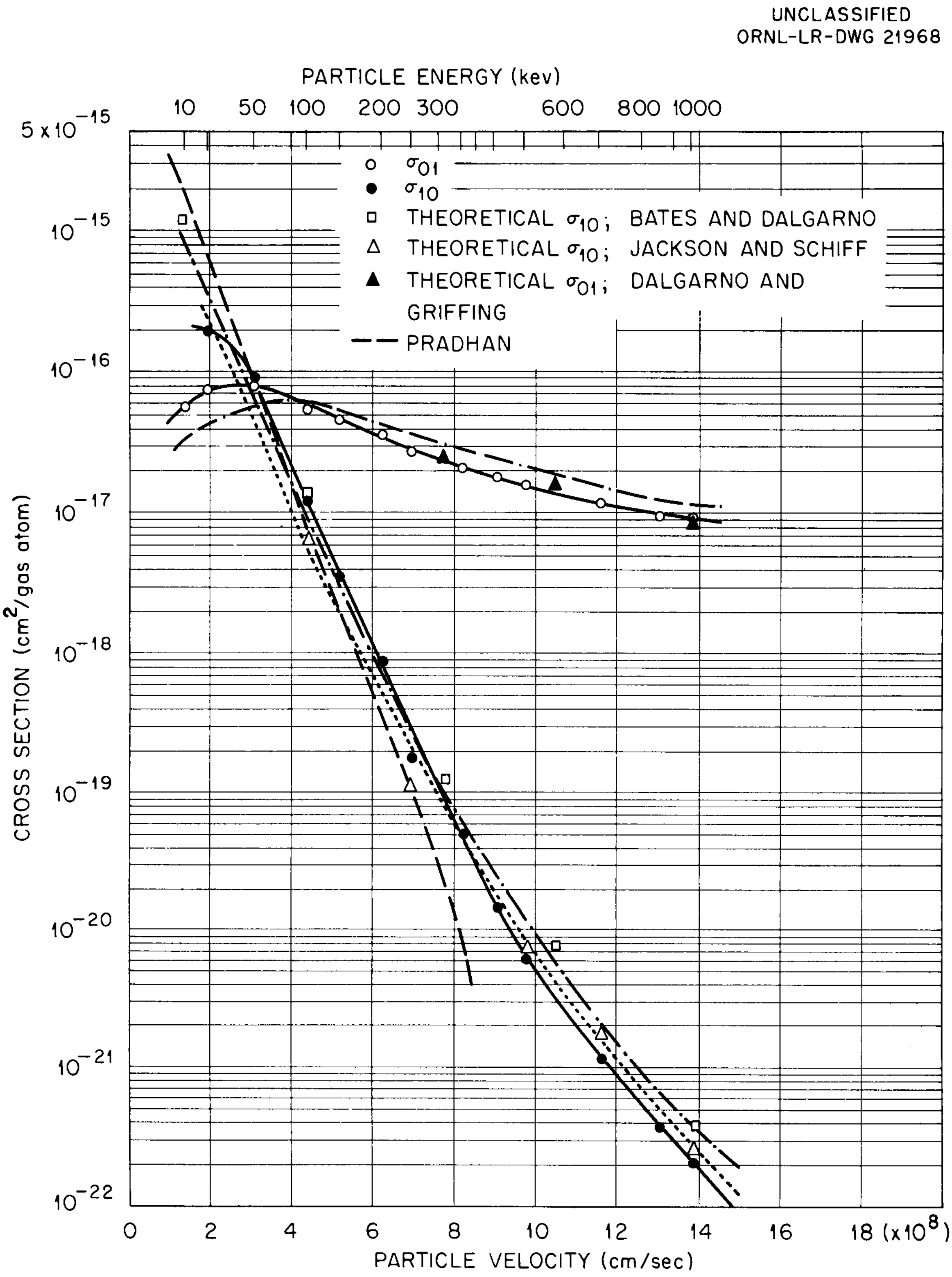

Fig. B.2.2. Charge-Transfer Cross Section Per Atom of Gas Traversed as a Function of Particle Velocity and Energy: Hydrogen Atoms and Ions in Hydrogen Gas.

UNCLASSIFIED
ORNL-LR-DWG 15938A

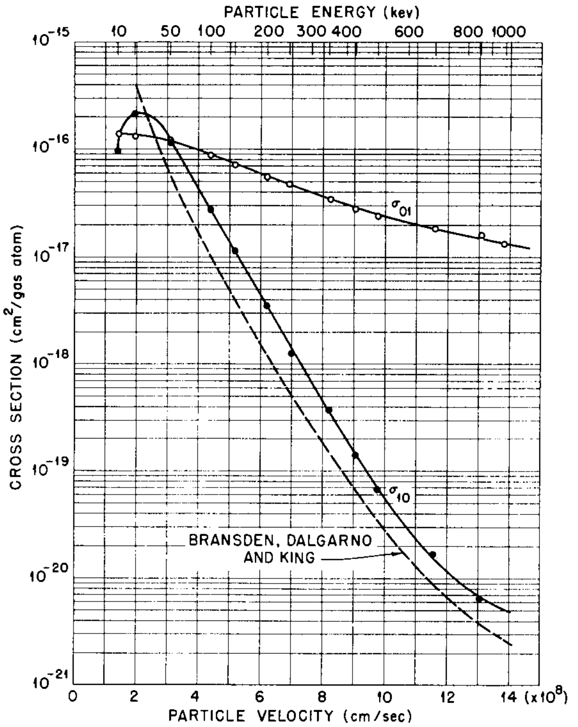

Fig. B.2.3. Charge-Transfer Cross Section Per Atom of Gas Traversed as a Function of Particle Velocity and Energy: Hydrogen Atoms and Ions in Helium Gas.

UNCLASSIFIED
ORNL-LR-DWG 15937

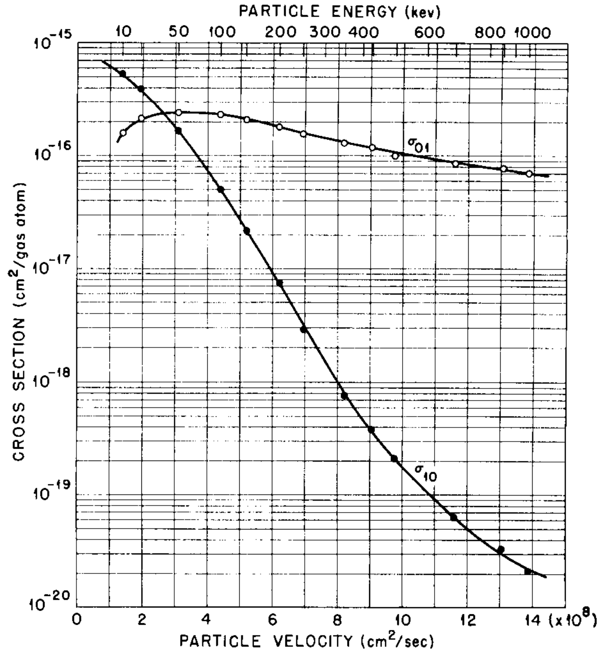

Fig. B.2.4. Charge-Transfer Cross Section Per Atom of Gas Traversed as a Function of Particle Velocity and Energy: Hydrogen Atoms and Ions in Nitrogen Gas.

UNCLASSIFIED
ORNL-LR-DWG 15936

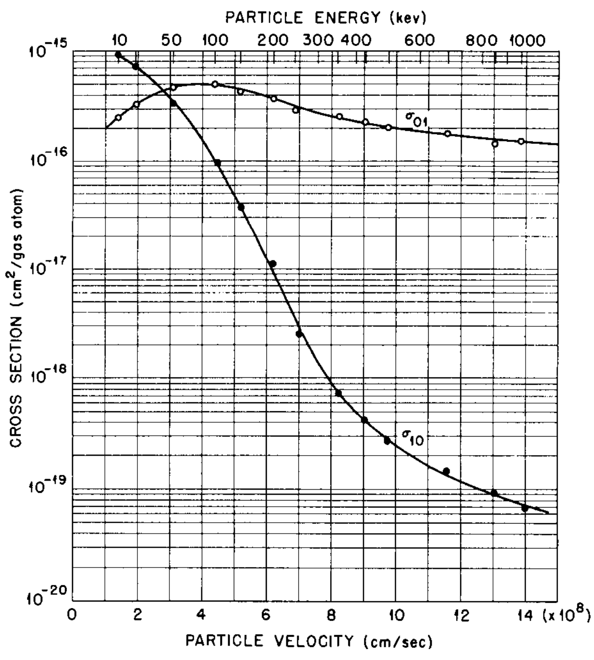

Fig. B.2.5. Charge-Transfer Cross Section Per Atom of Gas Traversed as a Function of Particle Velocity and Energy: Hydrogen Atoms and Ions in Argon Gas.

B.3 ELECTRON-LOSS CROSS SECTION FOR FAST HELIUM ATOMS[1]

C. F. Barnett P. M. Stier

As a continuation of the study of electron capture and loss, the cross section for loss of an electron by fast helium atoms has been studied. The energy range was from 30 to 200 kev. The target gases were hydrogen, helium, nitrogen, oxygen, neon, and argon.

Measurements were made in the apparatus[2] used to determine the electron-loss cross sections for hydrogen atoms. The schematic diagram of the target chambers is reproduced in Fig. B.3.1. Briefly, the procedure was as follows. With helium atoms incident on the cross-section chamber, voltage was applied to successive pairs of electrostatic plates. Ions formed by electron loss within the field were deflected from the initial path. The cross section was determined from the attenuation observed as the potential was applied. In preliminary experiments, it was found that the data were nonreproducible. The cross section was a function of the chamber pressure and also of the particular electrostatic plate used in the determination. To eliminate the effects of elastic scattering, the lower aperture of the cross-section chamber was replaced by a movable 0.005-in. slit. This slit was moved linearly across the beam, and the emergent flux of particles was integrated. The cross sections determined by this integration method were found to vary in the same manner as the data obtained with the aperture, indicating that elastic scattering played little or no role in the cross-section measurement. These variations in the cross sections were traced to differences in the pressure established in the neutralizer. Figure B.3.2 shows the dependence of the cross section on the neutralizer pressure for a 100-kev He^0 beam in hydrogen. Since only neutral helium atoms are incident on the charge-exchange chamber, it must be concluded that the character of the neutral beam was dependent on the amount of gas in the neutralizer. The conclusion drawn from the observations was that an appreciable number of electron-capture collisions in the neutralizer leave the fast helium atom in the metastable state. For low neutralizer pressures, when the mean free path is comparable to the dimensions, there is a high probability of the fast helium atoms emerging in the metastable state. As the pressure is increased, the small-angle elastic collisions subsequent to the capture collision may de-excite the helium atoms.

This explanation is supported by the curves (Fig. B.3.2) for the fast H, N, and Ne atoms. The measured cross section depends on the neutralizer pressure for Ne and He but not for H and N. This corresponds to the existence of strong metastable states for He and Ne atoms and to there being no highly populated metastable states in H and N.

At higher pressures, equilibrium is established between the flux of ions, atoms in the ground state, and atoms in the metastable state. The cross sections reported are for electron loss by this equilibrium distribution of metastable-state and ground-state atoms. The energy dependence of the electron-loss cross sections determined in these experiments is shown in Fig. B.3.3. The much more rapid variation of the cross section with energy is conspicuous for the heavier stopping gases.

The data from the present experiment also allow calculation of the fraction F_0 of the helium beam which is neutral after passage through a "thick" gas target. The values obtained agree well with the previously reported measurements.[3]

---

[1]P. M. Stier and C. F. Barnett, *Phys. Semiann. Prog. Rep. Sept. 10, 1955*, ORNL-1975, p 49–51.

[2]P. M. Stier *et al.*, *Phys. Semiann. Prog. Rep. Sept. 10, 1954*, ORNL-1798, p 64–65; Appendix B.1.3b of this report.

[3]P. M. Stier, C. F. Barnett, and G. E. Evans, *Phys. Rev.* 96, 973 (1954).

UNCLASSIFIED
ORNL-LR-DWG 160

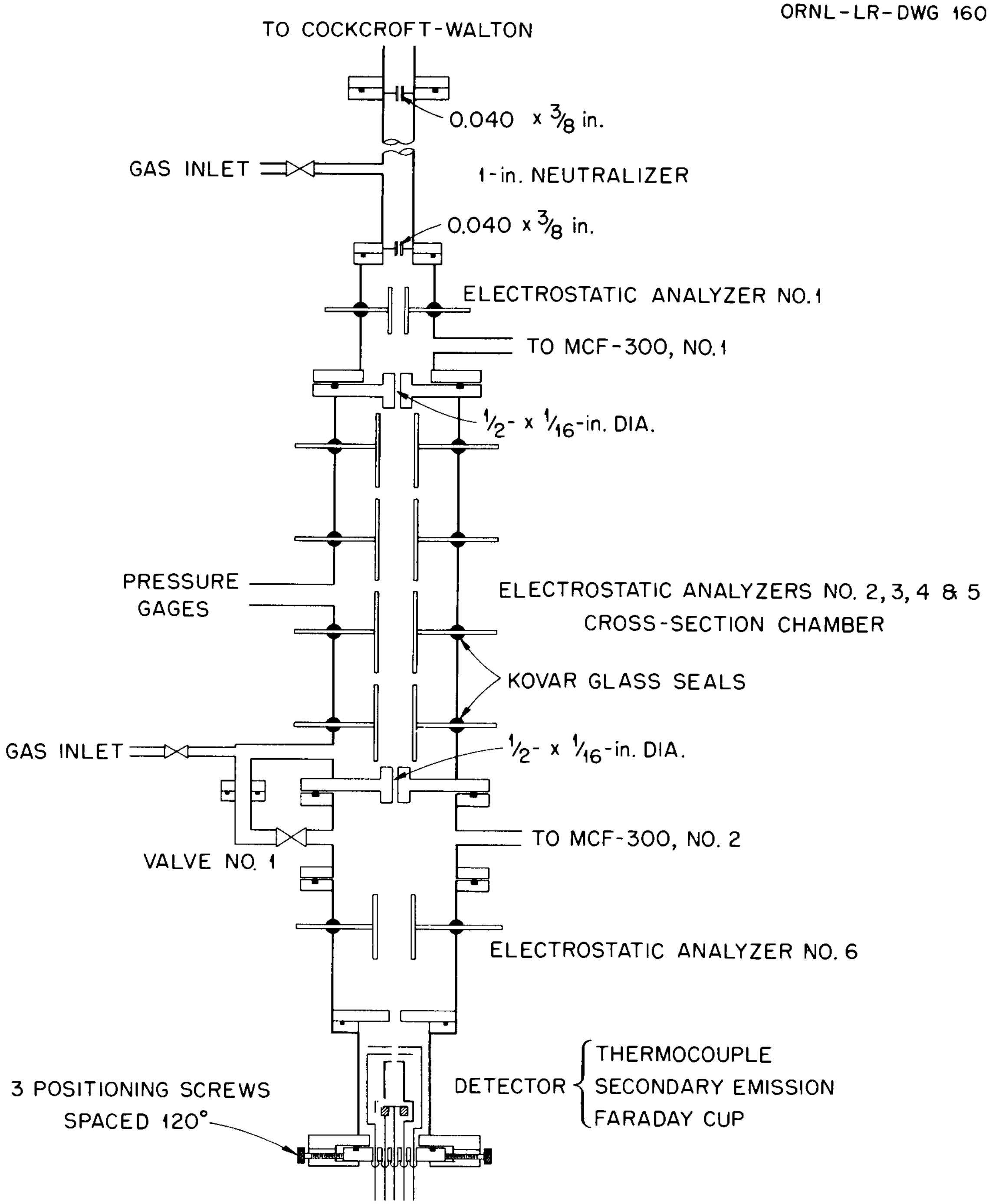

Fig. B.3.1. Schematic Drawing of Electron-Loss Apparatus.

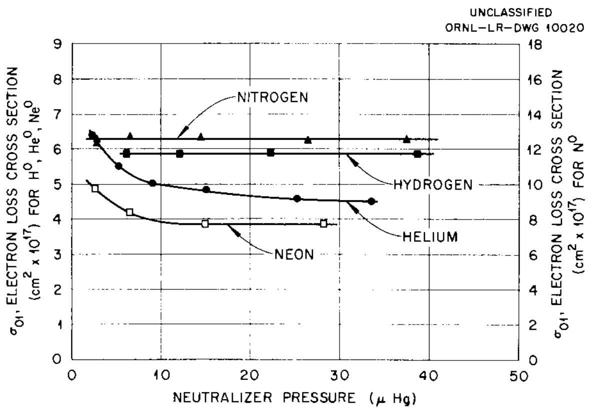

Fig. B.3.2. Dependence of Apparent Electron-Loss Cross Section on Neutralizer Pressure.

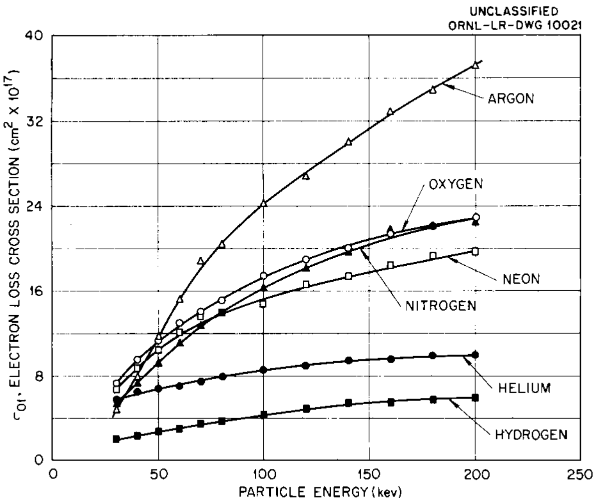

Fig. B.3.3. Energy Dependence of Electron-Loss Cross Sections.

B.4. DISSOCIATION CROSS SECTION OF H_2^+ IN THE ENERGY RANGE 500 kev TO 2.25 Mev[1]

C. F. Barnett

The cross section for dissociation of the diatomic hydrogen ion has been determined in the energy range of 500 kev to 2.25 Mev in target gases of hydrogen, helium, nitrogen, and argon. At energies less than 500 kev, the measurements become difficult due to the competing process of charge exchange. The apparatus used was essentially the same as that used for the charge-exchange experiments.[2] The principal differences are that the first gas cell was eliminated and an additional detector was installed to measure the deflected charge beam.

An H_2^+ beam was incident on the differentially pumped gas cell, in which the pressure was sufficiently low to prevent multiple collisions. Emerging from the gas cell was a mixture of H^0, H^+, and H_2^+. By use of the set of electrostatic deflection plates, the beam was analyzed into its various components. The axial detector was used as a secondary-electron detector to measure both the neutral component and total charge component of the beam. The other detector was used both as a secondary-electron detector and a Faraday cup to measure the individual charged beams.

The total beam available for dissociation was found by summing the emergent H_2^+ with the number of reactions occurring, found by a charge or particle balance between H^0 and H^+. By using such a balance, the per cent of the reactions going by simple dissociation (i.e., $H_2^+ \longrightarrow H^0 + H^+$) or by an ionizing dissociation (i.e., $H_2^+ \longrightarrow 2H^+ + e$) can be determined. From these measurements, the cross section is calculated from the following relation:

$$\frac{\text{total number of reactions}}{\text{total } H_2^+} = 1 - e^{n\sigma_d x} ,$$

where

n = target gas density,

x = particle path length in gas,

σ_d = dissociation cross section.

---

[1]C. F. Barnett, *Phys. Semiann. Prog. Rep. March 10, 1957*, ORNL-2302, p 33–34.

[2]P. M. Stier and C. F. Barnett, *Phys. Rev.* 103, 896–907 (1956) (Appendix B.1 of this report).

During a dissociating collision, momentum is imparted to the energetic particles, resulting in small-angle scattering. To estimate the magnitude of this scattering, the exit pinhole of the gas cell was enlarged. The measured cross section was independent of the defining geometry, indicating that the scattering is small.

In Fig. B.4.1 are shown the dissociation cross sections as a function of the particle velocity or energy. For gases of hydrogen and helium, the cross sections behave similarly to the electron-loss cross sections in that they have essentially a $1/v$ dependence. For the heavier gases of nitrogen and argon, the cross sections decrease only 15 to 20% over the velocity range studied. Shown in Fig. B.4.2 are the percentages of the total reactions going as simple dissociation for target gases of hydrogen and nitrogen. The mode of dissociation is independent of particle velocity and dependent on the target atom.

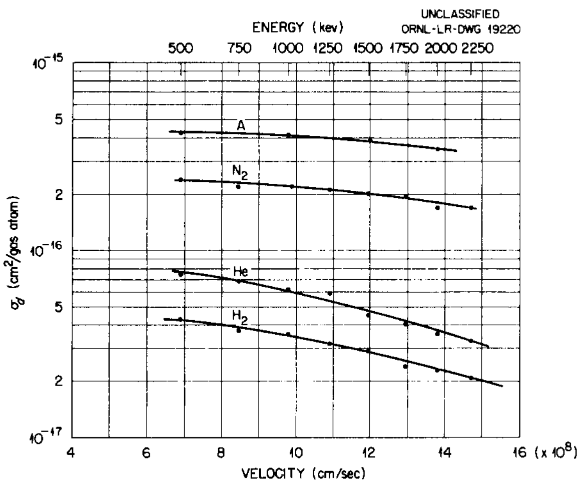

Fig. B.4.1. Dissociation Cross Section Per Atom of Gas Traversed as a Function of Particle Velocity or Energy: H_2^+ in Hydrogen, Helium, Nitrogen, and Argon Gases.

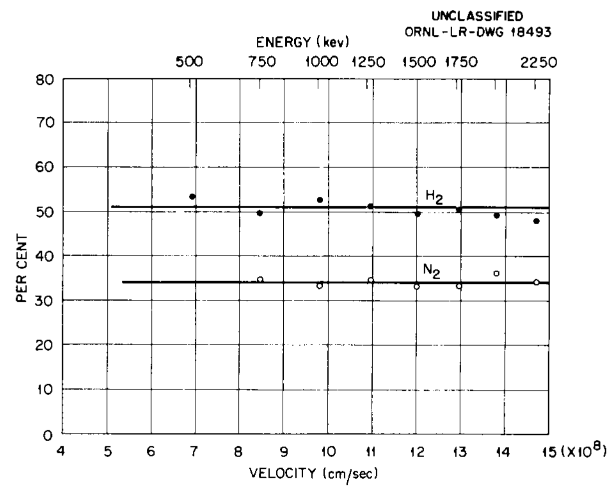

Fig. B.4.2. Per Cent of Dissociation by the Reaction $H_2^+ + M \rightarrow H^+ + H^0 + M$.

Appendix C

DISSOCIATION OF H_2^+ AND D_2^+ BY A VACUUM CARBON ARC[1]

C. F. Barnett R. J. Mackin, Jr. J. A. Ray

ABSTRACT

The efficiency of the carbon arc to dissociate diatomic hydrogen and deuterium ions has been measured for ion energies of 600 kev. The measured dissociation efficiency for hydrogen was $\left(10.6^{+2.1}_{-0.9}\right)$ % and for deuterium $\left(16.4^{+1.6}_{-1.2}\right)$ %. It was found that the dissociation was dependent upon the electrode geometry, the distance of dissociation from the anode, and the measured arc current.

INTRODUCTION

Previous measurements[2] have indicated that the cross section for dissociation of the diatomic hydrogen ion by impact with a gas atom is a slowly varying function of the particle velocity. In the energy interval between 500 kev and 2.25 Mev the cross section has a $1/v$ dependence for the light target gases hydrogen and helium; however, for the heavier gases nitrogen and argon, the cross section decreases only 10–20% throughout the energy range. Salpeter,[3] using a Born approximation, predicts the cross section to have a $1/v^2$ dependence in gases. Since no adequate explanation has been advanced for the high efficiency of the carbon arc[4] to dissociate H_2^+ at energies of 30 kev, it was believed advisable to extend the dissociation efficiency measurements to particle energies up to 600 kev. With the efficiency of the carbon arc and the cross sections for various loss processes known, a calculation may be made to determine the rate of entrapment of protons in DCX.[5]

If it is assumed that dissociation of the diatomic ions is the result of particle interaction (although electron and photon reactions are not certainly excluded), then one may write the following probable reactions leading to dissociation:

$$H_2^+ + C^{n+} \longrightarrow H^0 + H^+ + C^{n+} \quad (1)$$

$$H_2^+ + C^{n+} \longrightarrow 2H^+ + e + C^{n+} \quad (2)$$

$$H_2^+ + C^{n+} \longrightarrow 2H^+ + C^{(n-1)+} \quad (3)$$

where n may vary from zero to the highest states of ionization in the arc. The first two reactions involve electronic excitation, while reaction (3) is a charge-exchange reaction with the carbon ion capturing the electron from the diatomic ion. The present experiment cannot distinguish between (2) and (3); however, by using a charge balance between H^0 and H^+ one can determine roughly the fraction of the reaction proceeding by (1) and the fraction proceeding by (2) plus (3). The terminology used in this paper will be that (1) is a simple dissociation reaction, (2) is an ionizing dissociation reaction, and (3) is a charge-exchange reaction. One cannot exclude entirely dissociation that is due to excitation of the vibrational levels of the molecule upon collision with arc electrons. For simplicity, the dissociation efficiency will be defined as the ratio of the H^+ current to the sum of the H^+ and the H_2^+ currents.

---

[1] C. F. Barnett, R. J. Mackin, Jr., and J. A. Ray, *Dissociation of H_2^+ and D_2^+ by a Vacuum Carbon Arc*, ORNL-2420 (Dec. 6, 1957).

[2] C. F. Barnett, p 466 in *Controlled Thermonuclear Reactions: A Conference Held at Berkeley, California, Feb. 20–23, 1957*, TID-7536 (Part 2).

[3] E. E. Salpeter, *Proc. Phys. Soc.(London)* **A63**, 1295–1297 (1950).

[4] J. S. Luce, *Ionization and Dissociation of Energetic Ions by a Carbon Discharge – Status Report*, ORNL-2219 (Jan. 1957).

[5] A. Simon and M. Rankin, *Some Properties of a Steady State High-Energy Injection Device (DCX)*, ORNL-2354 (Aug. 26, 1957) (Appendix A of this report).

APPARATUS AND PROCEDURE

A schematic diagram is shown in Fig. C.1.1. The ions were formed in a conventional r-f ion source and accelerated to 600 kev by the ORNL cascade accelerator. Mass analysis was accomplished by means of a 90-deg magnetic analyzer. The analyzed ion beam was defined by a movable $\frac{1}{8}$-in. aperture placed directly in front of the solenoid containing the carbon-arc chamber. On the exit side of the arc chamber was a fan-shaped vacuum chamber in which an ion detector could be moved vertically to measure the various beams emerging from the chamber. The backing plate of the chamber consisted of quartz windows so that the various beams could be observed visually.

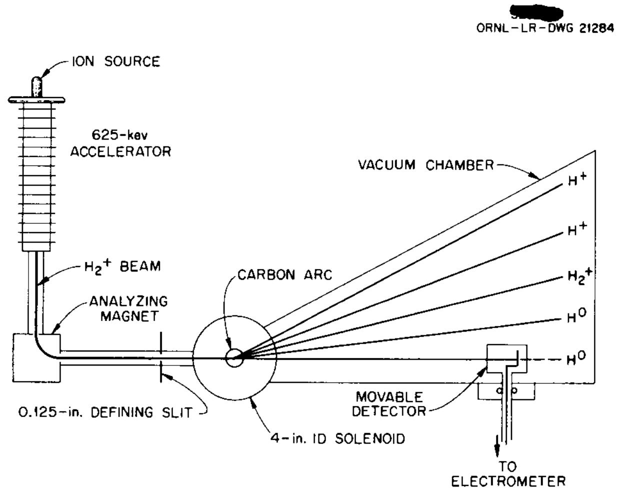

Fig. C.1.1. Apparatus for Measurement of Dissociation Efficiency.

The initial beam was analyzed into five separate beams by passage through the solenoid. In the region between the solenoid and the analyzing magnet, a fraction of the diatomic ions was dissociated into protons and neutral atoms. The protons from this dissociation were deflected through a large angle by the solenoid field, whereas the neutral particles traveled in an undeflected trajectory. In addition to these two beams, there were also a proton beam and a neutral-particle beam resulting from dissociation in the arc. The latter neutral beam was separated from the previously dissociated beam, since the H_2^+ was deflected by the magnetic field before suffering a dissociation collision in the arc. There was also present the beam of H_2^+ which had not been dissociated.

The dissociation process was found to take place along the diameter of the arc, resulting in the protons and atoms being formed at different positions in the magnetic field. This caused a vertical spread of the proton and neutral beam of approximately 1 in., which was larger than the detector aperture. In measuring ion beam intensities, the detector was moved at a constant linear rate across each beam by a synchronous motor, and the beam current was measured by an electrometer whose output was plotted by a Brown recorder. The area under the recorder trace was integrated with a planimeter to determine the beam intensity. The procedure consisted of measuring, in turn, H_2^+, H^+, H^0, and H_2^+. When the two H_2^+ recordings differed by more than 10%, the run was discarded.

A more detailed diagram of the solenoid and arc chamber is shown in Fig. C.1.2. The chamber was an evacuated stainless steel tube 6 ft long and 4 in. in diameter. Surrounding this tube was the magnetic coil consisting of seven layers of water-cooled copper tubing, each layer containing 3.2 turns per inch. The coil was broken in the center to provide a gap of 2 in. for the beam entrance and exit ports. Inside the tube was a 3-in.-dia water-cooled copper liner to dissipate the power radiated from the arc. The arc electrodes were Union Carbide grade C-18 graphite pressed into water-cooled copper sleeves. Quartz tubing was placed around the cathode assembly to prevent arc-over in the fringing magnetic field region. Various configurations of anodes were used, and these will be discussed below. The

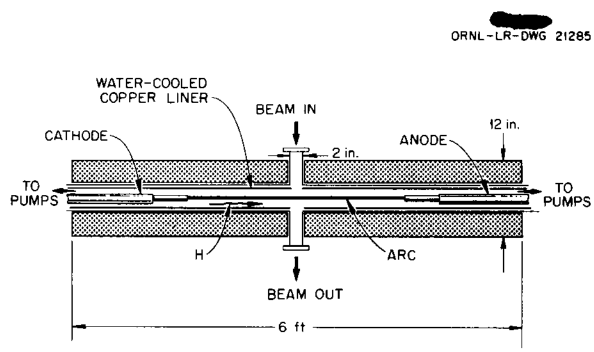

Fig. C.1.2. Solenoid and Arc Chamber.

anode and cathode assemblies were mounted so that the arc length could be varied between 6 in. and 4 ft.

The detection of the energetic particles was complicated by high r-f fields produced by the arc, and also by a copious supply of photoelectrons ejected from the detector and from walls surrounding the detector region by the intense ultraviolet radiation from the arc. The detector found most feasible (Fig. C.1.3) consisted of a Faraday cup and biased suppressor ring mounted inside a completely shielded box which the beam entered through a 25-microinch nickel foil soldered over a $\frac{3}{8}$-in. aperture. The foil was sufficiently thick to ensure an equilibrium charge distribution between energetic positive ions and neutral particles emerging from the back surface. The characteristic charge distribution was independent[6] of the initial charge state and dependent only on the particle energy and foil thickness. The incident H_2^+ beam was immediately dissociated at the surface of the foil, resulting in two particles of half the initial energy, each of which registered with the same efficiency as the H^0 and H^+.

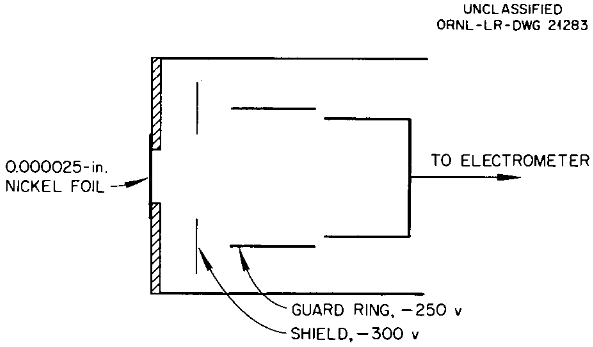

Fig. C.1.3. Particle Detector.

The procedure used in striking the carbon arc was the one customary with shorter d-c arcs.[7] To the arc electrodes were applied 250 v dc (open-circuit voltage of the four series-connected welding generators which supplied arc power) and a comparable r-f voltage. When gas was admitted through a passage in the cathode, an r-f arc appeared, followed immediately by the main discharge. The r-f voltage and the gas input were removed as soon as the d-c arc had fired. Thereafter, the arc was supported solely by carbon vaporized from the electrodes. Three hundred amperes was the customary arc current, and voltages ranged from 70 to 100 v, depending upon arc length. The relationship is shown in Fig. C.1.4, in which the slope of the curve is found to be 1.0 v/in.

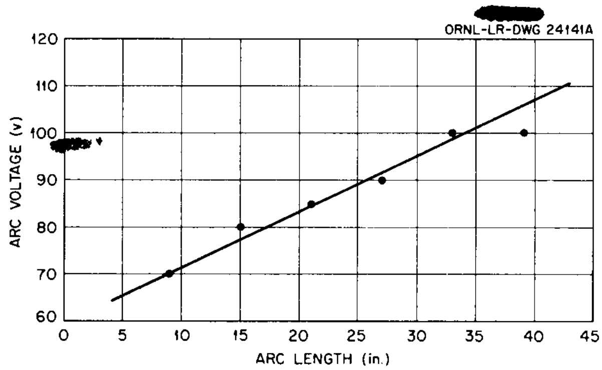

Fig. C.1.4. Carbon Arc Voltage as a Function of Arc Length.

RESULTS

For a 600-kev H_2^+ particle the average efficiency obtained was $\left(10.6^{+2.1}_{-0.9}\right)$ %, which may be compared with an average efficiency of $\left(16.4^{+1.6}_{-1.2}\right)$ % for a D_2^+ particle of the same kinetic energy. These efficiencies were measured at a distance of 6 in. from the arc anode. The arc conditions were (1) 300-amp arc current, (2) $\frac{3}{8}$-in.-dia cathode, and (3) $\frac{3}{4}$-in.-dia anode. The errors are the maximum deviations from the average value. Attempts to measure the velocity dependence of the efficiency with an H_2^+ beam were unsuccessful due to difficulties encountered with the detector at lower particle energies. If it is assumed that the deuterium ion and hydrogen ion will have the same inelastic-collision cross section at identical velocities, then the above values are consistent with a $1/v$ dependence for the efficiency. It is not readily possible to compare these figures with those measured at lower energies in another

[6] P. M. Stier and C. F. Barnett, *Phys. Rev.* 103, 896–907 (1956) (Appendix B-1 of this report).

[7] J. S. Luce, *Ionization and Dissociation of Energetic Ions by a Carbon Discharge – Status Report*, ORNL-2219 (Jan. 1957).

geometry[7] because the distance from the anode is a critical factor, as will be seen.

By making a charge or particle balance between the dissociated beams of H^0 and H^+ and the undissociated H_2^+, it is possible to determine the fraction of the reactions proceeding by simple dissociation or by ionizing dissociation and charge exchange. For the H_2^+ particles, the fraction going as simple dissociation was found to be 80% for a 600-kev beam. For a deuterium particle, this percentage decreased to 65%. This may be contrasted with dissociation of H_2^+ by gas impact, where it was found[8] that the fraction of the reactions going by simple dissociation was independent of the particle velocity in the energy range of 500 kev to 2.25 Mev. However, the fraction was dependent on the nature of the target atom or molecule. In the present experiment, there could not be excluded the possibility of the ionization in the arc of some of the H^0 produced by dissociation in the arc.

In a device such as DCX, it is desirable that the dissociated H^+ particle, with its multiple traversals of the arc, does not capture an electron from either the free electrons or the charged or neutral components of the arc. To determine the magnitude of the electron capture, a 300-kev proton beam was passed through the arc, and the appropriate region was scanned for the presence of neutral particles. It was possible to place an upper limit of less than one part in 10^5 for the electron capture. This upper limit was determined by the sensitivity of the detector and the background in the detector circuit.

Numerous changes were made in the geometry of the electrodes to determine optimum conditions. The initial geometry consisted of a cathode $\frac{1}{2}$ in. in diameter and 10 in. long, with a $\frac{1}{8}$-in. longitudinal bore to admit gas to the arc. The anode was $1\frac{1}{2}$ in. in diameter and $1\frac{1}{2}$ in. long. Visual observation showed the arc to be diverging to approximately 1 in. in the center of the solenoid. This divergence was the result of bowing of the magnetic field in the 2-in. solenoid gap which was necessary to provide an entrance and exit aperture for the particle beam. This visual observation was confirmed by placing a carbon disk in the center of the solenoid and measuring the diameter of the hole burned through it. If the dissociation of the carbon arc was the result of particle interactions, which would be proportional to the density, then the density of particles would be smaller in the bowed region, which would result in decreased dissociation. To decrease the diameter of the arc, the cathode diameter was decreased to $\frac{3}{8}$ in. With this smaller cathode, the diameter of the arc in the central region was $\frac{3}{4}$ in. Attempts to decrease the diameter of the cathode to $\frac{1}{4}$ in. were unsuccessful; the cathodes shattered when current was passed through them. Previous experiments[9] have indicated that the efficiency for dissociation at low particle energies is dependent on the temperature of the anode. By decreasing the anode diameter to $\frac{3}{4}$ in., the radiant heat was decreased, with a gain of a factor of 1.3 in the dissociation efficiency.

The efficiency of dissociation was found to be dependent upon the distance of the anode from the axial position of the beam path. In Fig. C.1.5 is shown the efficiency as a function of this distance to the anode (for a 1.5-in. anode diameter). In moving the anode from a position 3 in. from the H_2^+ beam to 21 in., the efficiency decreased from 10.1 to 4.9%. Also shown in Fig. C.1.5 is the total radiant energy as a function of the anode distance. This was measured by a thermal detector placed in the same position as the particle detector. This thermal detector

[8] C. F. Barnett, p 466 in *Controlled Thermonuclear Reactions: a Conference Held at Berkeley, California, Feb. 20–23, 1957*, TID-7536 (Part 2).

[9] J. S. Luce, private communication.

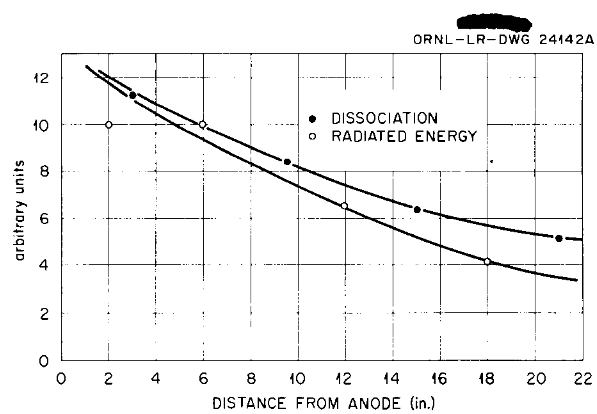

Fig. C.1.5. Efficiency of Dissociation of H_2^+ and Energy Radiated from the Arc as a Function of the Distance from the Anode.

consisted of a copper ring with a 25-microinch nickel foil soldered to the front surface. Soldered to the center of the nickel foil was a fine copper wire, which formed a thermocouple indicator with low heat loss, short time constant, and sensitivity of the order of microwatts. Absorbers of glass, quartz, and fluorite all absorbed more than 95% of the radiant energy emitted by the arc. It will be noticed in Fig. C.1.5 that the slope of the radiant energy curve is similar to the slope of the dissociation efficiency. Both the efficiency and the radiant energy were independent of the cathode position. It may be inferred from the radiant energy curve either that the density of radiating particles is increasing or that the state of excitation of the particles is increasing as regions closer to the anode are examined.

In Fig. C.1.6 is plotted the dissociated H^+ current as a function of the measured arc current.

[redacted]

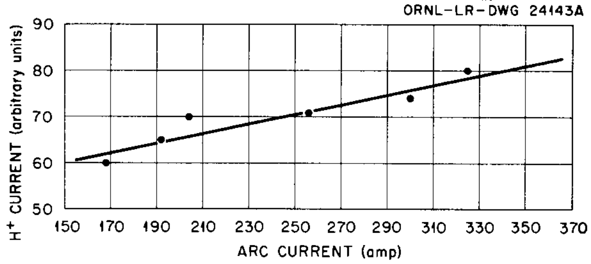

Fig. C.1.6. Proton Current Resulting from Dissociation in the Carbon Arc as a Function of the Measured Arc Current.

[redacted]

The arc current was varied from 160 to 325 amp with a corresponding 1.3-fold increase in the H^+ current.

Attempts to measure the attenuation of various beams by measuring currents with and without the arc were unsuccessful due to the pumping action of the carbon arc. The pressure in the solenoid was reduced by a factor of 3 with the carbon arc operating, following an initial outgassing period. The lowest pressure obtained in the vacuum system was 4×10^{-6} mm Hg as measured by a VG-1A ionization gage placed 8 in. from the arc along the beam tube.

Experiments are continuing on the dissociation produced by the carbon arc at lower particle energies. Also, various energetic particles are being studied to learn more about the nature of the processes taking place.

ACKNOWLEDGMENTS

It is a pleasure to acknowledge the help and comments of various members of the Thermonuclear Experimental Division. Special acknowledgment is made to J. S. Luce for suggesting the work and for his help in leading the design group of H. C. Hoy, G. F. Leichsenring, and R. L. Knight in designing the arc assembly and solenoid. The many helpful comments and suggestions of Drs. E. D. Shipley, P. R. Bell, C. D. Moak, and R. A. Dandl are greatly appreciated.

Appendix D

SPUTTERING

D.1 THEORY OF SPUTTERING BY HIGH-SPEED IONS

David T. Goldman[1] Albert Simon

Abstract

The theoretical treatment of sputtering by ions at energies above about 50 kev is simplified by the fact that the emergent particles originate at depths in the material which are small as compared with the range of the incident particles. The displacement rate is nearly constant over this region, and this makes it possible to obtain relatively simple solutions of the diffusion problem for emission.

The emission problem is in effect reduced to a one-velocity diffusion calculation by an artifice. The volume displacement rate is increased by the facto $\bar{\nu}$, where $\bar{\nu}$ is the average number of secondaries, and the macroscopic absorption and scattering cross sections are adjusted to make the average number of collisions of each particle equal to the actual average over the secondaries. The resultant sputtering ratio $\mathcal{R}$ varies with incident energy E, incident angle ψ, and mass ratio $\mu = M_1/M_2$ as

$$\mathcal{R} \sim \frac{\mu \ln E}{E \cos \psi} .$$

D.1.1 Introduction

Most of the theoretical treatments of sputtering by ions appear to be limited to the energy region below a few kiloelectron volts.[2,3] In this case, the ions have a mean free path of only a few atomic layers, and the phenomenon involves a complicated analysis of surface interactions. As the energy of the bombarding ion increases above about 50 kev, however, a simplifying feature emerges. The range of the incident particle increases greatly ($\cong 10^{-4}$ cm at 500 kev), while the knock-on particles maintain an approximately constant mean free path ($\cong 10^{-7}$ cm). Hence, only a small portion of the initial track length of the incident particle produces knock-on particles which can re-emerge from the surface. The displacement rate is nearly constant over this region, and this makes it possible to obtain relatively simple solutions of the diffusion problem for emission.

In Sec D.1.2 an expression is obtained for the volume density of primary particles produced by the incident beam. The mean free path for primary production is calculated in Sec D.1.3, as well as the average energy of the primaries. The average number of secondaries is calculated in Sec D.1.4, the diffusion problem for re-emission is solved in Sec D.1.5, and the results are summarized in Sec D.1.6.

D.1.2 Volume Density of Primary Sources; Sputtering Ratio

Consider an initial beam of monoenergetic ions incident at an angle ψ to a solid surface, as shown in Fig. D.1.1. The particle flux in the beam is denoted by I, and the cross-sectional area of the beam, measured normal to its direction, is denoted by A. The number of primaries produced per unit volume in the solid is then given by

$$q \cong \frac{I\, S(R)}{A\, \lambda_i(E)} , \qquad \text{(D.1.1)}$$

where $S(R)$ is a step function which is equal to unity from 0 (the surface) down to R (the incident

---

[1]Now at Department of Physics, University of Maryland, College Park, Maryland.

[2]D. E. Harrison, *Phys. Rev.* 102, 1473 (1956).

[3]E. B. Henschke, *Phys. Rev.* 106, 737 (1957).

particle's range) and is zero thereafter. The mean free path for production of a primary by an ion of energy E is denoted by $\lambda_i(E)$, and E is the energy at a given depth r. The basic assumption is that the displaced particles which emerge originate from a depth which is small as compared with R. Hence, q is effectively a constant over this region, with E equal to the incident energy E_i. Thus

(D.1.2) $$q \cong \frac{I}{A\,\lambda_i(E_i)} .$$

Owing to the linear nature of the problem, the current density of sputtered atoms leaving the surface will be directly proportional to the volume source strength. Hence

(D.1.3) $$J = \gamma q ,$$

where J is the emitted current density normal to the surface and γ is to be determined later. The total emitted current is then (see Fig. D.1.1)

(D.1.4) $$J_{tot} = \gamma q A_s .$$

The sputtering ratio $\mathcal{R}$, defined as the ratio of the total current of sputtered atoms to the incident

UNCLASSIFIED
ORNL-LR-DWG 26303

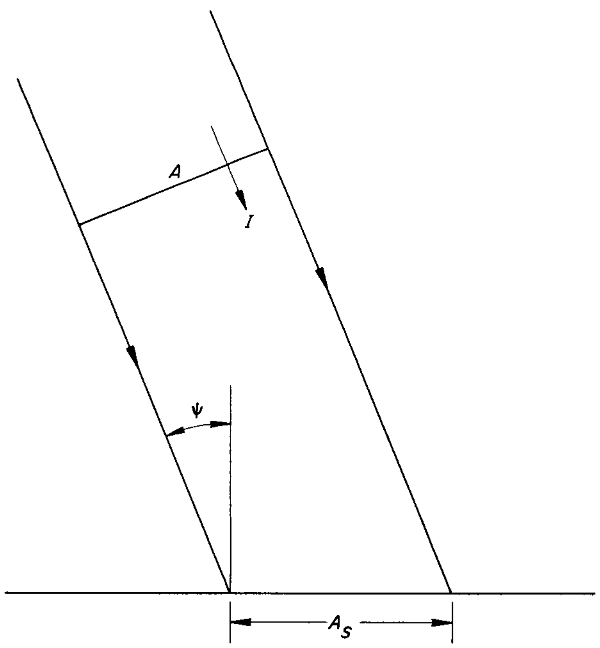

Fig. D.1.1. Incident Ion Beam.

current, is obtained by dividing Eq. D.1.4 by the incident current I and substituting from Eq. D.1.2. The result is

(D.1.5) $$\mathcal{R} = \frac{\gamma A_s}{A\,\lambda_i(E_i)} = \gamma[\lambda_i(E_i)\cos\psi]^{-1} .$$

The mean free path for primary production, λ_i, will be evaluated in the next section.

D.1.3 Mean Free Path for Primary Production

Following Seitz and Koehler[4] the differential cross section for a Coulomb collision in which an energy between T and $T + dT$ is transferred is given by

(D.1.6) $$d\sigma = \frac{\pi b^2}{4} T_m \frac{dT}{T^2} ,$$

where the maximum energy transferable, denoted by T_m, is

(D.1.7) $$T_m = \frac{4M_1M_2E}{(M_1 + M_2)^2} .$$

The energy of the incident particle of mass M_1 is denoted by E, M_2 is the target mass, b is the classical distance of closest approach defined by

(D.1.8) $$b = \frac{z_1 z_2 e^2}{E_r} ,$$

and E_r is the relative energy in the center-of-mass system. We assume that the screening is weak, as it will be for energetic ions. The total cross section for producing a displacement, σ_d, is the integral of $d\sigma$ between E_d and T_m, where E_d is the energy which must be transmitted to the struck particle to cause it to be removed from the lattice structure. Hence

(D.1.9) $$\sigma_d = \frac{\pi b^2}{4}\left(\frac{T_m}{E_d} - 1\right)$$

$$= \frac{\pi b^2 T_m}{4E_d} ,$$

[4]F. Seitz and J. S. Koehler, p 321, vol 2, *Solid State Physics; Advances in Research and Applications*, ed. by F. Seitz and D. Turnbull, Academic Press, New York, 1956.

since E_d ($\cong 25$ ev) is much smaller than T_m. Substituting in Eq. D.1.9 from Eqs. D.1.7 and D.1.8, we obtain

$$(D.1.10) \qquad \sigma_d = \frac{\pi M_1 z_1^2 z_2^2 e^4}{M_2 E E_d} .$$

The mean free path for primary production is then

$$(D.1.11) \qquad \lambda_i = (n_0 \sigma_d)^{-1} ,$$

where n_0 is the particle density in the medium.

For illustration in this and succeeding sections, we shall consider the case of a beam of 500-kev deuterons striking a copper target. Then

$$\sigma_d = \frac{6.95 \times 10^{-14}}{E} = 1.4 \times 10^{-19}\,\text{cm}^2 ,$$

and

$$\lambda_i = 0.86 \times 10^{-4}\,\text{cm} .$$

The mean energy transferred to the primary particle is readily obtained from Eq. D.1.6. The result is

$$\bar{T}_d = E_d \ln \frac{T_m}{E_d} , \qquad T_m >> E_d .$$

In our illustrative case, $\bar{T}_d = 195$ ev. In fact, owing to the slow variation of the logarithm, the mean energy transferred is less than 500 ev at all energies of interest.

Since the incident particle loses on the average only a small portion of its kinetic energy, the direction of the primary recoil after the collision will be almost perpendicular to the direction of the incident particle. This follows from the relationship between the center-of-mass scattering angle θ and the energy transferred:

$$\sin^2 \frac{\theta}{2} = \frac{T}{T_m} ,$$

together with the definition of the recoil angle ψ in the laboratory system,

$$\psi = \frac{\pi - \theta}{2} .$$

In our illustrative case, $\psi = 86.6$ deg.

D.1.4 Average Number of Secondaries Produced

Since the primary particles are not very energetic, their interaction with the lattice ions reduces to hard-sphere collisions. The total cross section is πR^2, where R is determined from the relationship:

$$(D.1.12) \qquad \frac{z_2^2 e^2 \exp(-R/a')}{R} = E' ,$$

and where, after Seitz,

$$a' = \frac{a_0}{z_2^{1/3}} ,$$

with a_0 being the Bohr radius. The radius R is not a very sensitive function of the energy E'. In our illustrative case,

$$R \cong 1.35 a_0 = 0.7 \times 10^{-8}\,\text{cm} .$$

The corresponding mean free path in copper is then 7.4×10^{-8} cm.

The average number of all secondary atoms dislodged from the lattice by the primary atom may be determined by the method described by Seitz and Koehler.[5] The result is

$$(D.1.13) \qquad \bar{\nu} = \left(0.885 + 0.561 \ln \frac{x_m + 1}{4} \right) \frac{x_m + 1}{x_m} ,$$

where

$$(D.1.14) \qquad x_m + 1 = \frac{4 M_1 M_2}{(M_1 + M_2)^2} \cdot \frac{E}{E_d} .$$

For 500-kev deuterons impinging on copper, $x_m = 2.4 \times 10^3$ and $\bar{\nu} = 4.5$.

D.1.5 Diffusion Solution for the Return Current

The exact solution of the propagation of knock-on particles through the material to the surface involves a complex multiplication problem which cannot easily be solved by analytic means. Instead, we shall replace the correct source term q, of Eq. D.1.2, by an effective source $\bar{\nu} q$, where $\bar{\nu}$ is given by Eq. D.1.13, thus accounting for the multiplication process directly at the primary

[5] *Ibid.*, p 380.

source. In addition, the angular distribution of primaries is considered to be isotropic, instead of peaked at right angles to the incident particle's direction. This artifice in effect allows us to deal with a one-velocity diffusion problem. The mean free paths for absorption and scattering, λ_a and λ_s, will be adjusted so that the average number of collisions made by the source particles will be equal to the average number of collisions suffered by all the knock-ons.

Since the collision of a secondary particle with a lattice particle is an isotropic hard-sphere scattering, there will be equal probability for all possible energy transfers. Hence, the ratio of scattering with displacement to scattering without displacement will be approximately

$$R \cong \frac{E - E_d}{E} .$$

When E is large as compared with E_d, there are very few scatterings without displacement. On the other hand, when E approaches E_d, it takes only one or two collisions for the particle itself to become trapped and effectively absorbed. It seems reasonable to assume that the number of scatterings without either displacement or absorption can be neglected in comparison with those that result in either a knock-on or absorption.

The average number of collisions (including absorption) of the knock-ons, $\bar{N}$, is equal to the sum of the number of scatterings without displacement, N_s, plus the number of displacement collisions, N_d, plus the total number of absorptions, N_a, all divided by the mean number of secondaries. Thus

$$\bar{N} = \frac{N_s + N_d + N_a}{\bar{\nu}} .$$

However, in accordance with the discussion in the previous paragraph, N_s may be neglected. In addition

$$N_d = \bar{\nu} - 1$$

and

$$N_a = \bar{\nu} .$$

Hence

$$\bar{N} = 2 - \frac{1}{\bar{\nu}} \cong 2 .$$

It is quite unlikely that $\bar{N}$ can be much larger than this value. It will be shown at the end of this section that a value of $\bar{N} = 3$ does not change the numerical results by a large factor.

This value of $\bar{N}$ may now be used to determine the ratio of scattering to absorption. It is clear that the average number of collisions, $\bar{N}$, including absorptions, is

$$\bar{N} = \frac{\Sigma_s + \Sigma_a}{\Sigma_a} .$$

If $\bar{N} = 2$, this requires that $\Sigma_s = \Sigma_a$, and this is the choice that is made in the diffusion calculation which follows.

The diffusion equation in plane geometry for a constant volume source $\bar{\nu}q$ is:

$$\text{(D.1.15)} \qquad - D \frac{d^2\phi}{dx^2} + \Sigma_a\phi = \bar{\nu}q ,$$

where ϕ is the particle flux and where the diffusion coefficient D is

$$\text{(D.1.16)} \qquad D = [3\Sigma_s(1 - \bar{\mu})]^{-1} .$$

Here $\bar{\mu}$ is the average cosine of the scattering angle in the laboratory system. For isotropic scattering in the center-of-mass system,

$$\bar{\mu} = \frac{2}{3A} << 1$$

for all but the lightest elements. Hence

$$D \cong (3\Sigma_s)^{-1} .$$

The solution of Eq. D.1.15 is:

$$\text{(D.1.17)} \qquad \phi = \frac{\bar{\nu}q}{\Sigma_a} + Ae^{\kappa x} ,$$

where $\kappa = [\Sigma_a/D]^{1/2}$, A is a constant of integration, and the negative solution is thrown out by the boundary condition at $x = - \infty$. The usual diffusion-theory boundary condition at a vacuum interface is the vanishing of the flux at the extrapolated end point, $x = d$, where in our case $d = 0.71\Sigma_s^{-1}$. Hence

$$\text{(D.1.18)} \qquad \phi = \frac{\bar{\nu} q}{\Sigma_a} [1 - e^{\kappa(x-d)}] \ .$$

The surface current density is now

$$J = - D \left. \frac{d\phi}{dx} \right|_{x=0} \ .$$

Hence

$$\text{(D.1.19)} \qquad J = \bar{\nu} q \frac{D}{\Sigma_a} \kappa e^{-\kappa d}$$

$$= \bar{\nu} q \left(\frac{D}{\Sigma_a} \right)^{1/2} e^{-\kappa d} \ .$$

By use of Eq. D.1.3,

$$\text{(D.1.20)} \qquad \gamma = \bar{\nu} \left(\frac{D}{\Sigma_a} \right)^{1/2} e^{-\kappa d} \ .$$

Finally, since $\Sigma_a = \Sigma_s$ in our case,

$$\text{(D.1.21)} \qquad \gamma = \frac{\bar{\nu}}{\sqrt{3}\ \Sigma_s} e^{-0.71\sqrt{3}}$$

$$= \frac{0.17\bar{\nu}}{\Sigma_s} \ .$$

It should be noted that if $\bar{N} = 3$ this result is changed to $0.34\bar{\nu}/\Sigma_s$, which is larger by a factor of 2.

D.1.6 Summary

By combination of the results in Eqs. D.1.5, D.1.10, D.1.11, and D.1.21, the following expression for the sputtering ratio is obtained:

$$\mathcal{R} = \frac{0.17\bar{\nu}}{\Sigma_s} \cdot \frac{n_0}{\cos\psi} \cdot \frac{\pi M_1 z_1^2 z_2^2 e^4}{M_2 E E_d} \ .$$

The macroscopic scattering cross section for the secondaries is hard-sphere scattering and is equal to $n_0 \pi R^2$, with R given by Eq. D.1.12. Hence,

$$\text{(D.1.22)} \qquad \mathcal{R} = \frac{0.17\bar{\nu} M_1 z_1^2 z_2^2 e^4}{M_2 E E_d R^2 \cos\psi} \ ,$$

with

$$\bar{\nu} = \left(0.885 + 0.561 \ln \frac{x+1}{4} \right) \frac{x+1}{x} \ ,$$

$$x = \frac{4 M_1 M_2}{(M_1 + M_2)^2} \cdot \frac{E}{E_d} \ ,$$

and with R the solution of the transcendental equation D.1.12. Equation D.1.12 is not very sensitive to the energy E', which should be chosen equal to some value between E_d and $E_d \ln x$.

At high energies, x is large as compared with unity, and the general behavior of the sputtering ratio is

$$\text{(D.1.23)} \qquad \mathcal{R} \sim \frac{M_1}{M_2} \cdot \frac{\ln E}{E} \cdot \frac{1}{\cos\psi} \ .$$

In our illustrative case, 500-kev deuterons striking a copper target at normal incidence, the numerical value of the sputtering ratio given by Eq. D.1.22 is

$$\mathcal{R} = 6.5 \times 10^{-4} \ .$$

Experimental data in this energy range seem to be unavailable.

The numerical results obtained from the general formula, Eq. D.1.22, are probably trustworthy only in their order of magnitude. The dependence on incident energy, angle, and mass ratio may be more reliable.

D.2 SPUTTERING OF COPPER BY MONOENERGETIC IONS

O. C. Yonts

The breakdown of a metallic surface due to positive-ion bombardment has been observed since the earliest experimental investigations in the field of gaseous electronics. Investigations of this breakdown, now called "sputtering," have for the most part been made with a glow discharge as a source of ions. As a consequence, experimental results in many cases were strongly dependent on the gas pressure and on the geometry of the discharge tube. Also, the rate of sputtering was measured by indirect means, such as the change of resistance of a pure tungsten wire as its cross section decreased.

Sputtering studies were undertaken at ORNL because of the lack of information on sputtering rates in a magnetic field, the general need for just such information in the development of thermonuclear devices, and the ready adaptibility of Calutron equipment to these studies.

In order to make direct measurements of the number of atoms sputtered per incident ion, it is necessary to fulfill the following conditions:

1. The mean free path near the metallic surface must be sufficiently large to allow the escape of all sputtered atoms. In practice, this means pressures below 10 μ.

2. The incident ion current must be accurately known.

3. The source of ions must have a sharply defined energy.

4. The loss of target material must be measured directly.

Guntherschultz and Meyer, working in the range from 100 to 1200 v, and Keywell, working in the range from 1000 to 6000 v, were able to satisfy all of the above requirements with the possible exception of 3. All of these requirements can be satisfied by use of the Calutron.

1. The pressure in the tank during operation is 0.02 to 0.04 μ, which makes the mean free path longer than any dimension of the vacuum tank, and sputtered material deposits on the tank walls at a distance varying from a few inches to several feet.

2. The magnetic field returns secondary electrons to the target. This ensures that the target current is an accurate measurement of the incident ions.

3. The ion energy is constant to ~ 1 part in 2500.

4. The large ion currents that are available permit the removal of an appreciable amount of material from the target in a reasonable length of time.

For sputtering work, the degree of modification of the Calutron depends on the mass of the ion that is used. In the case of argon, it was only necessary to replace the usual receiver "pocket" with a weighed copper target mounted in good thermal contact with a water-cooled plate.

Because of the minimum magnetic field required by the source for efficient operation, it was necessary to make more extensive modification for the work with hydrogen, deuterium, and helium. The radius of the ion orbit was decreased from the standard 24 in. to 7 in.

Because of the large ion currents required with H, D, and He for removal of appreciable amounts of material, it was necessary to use direct water-cooling on the target. The seal was made by using an O-ring in a groove around the edge of the rectangular water baffle. Beam currents as high as 600 ma at 20 kev were easily handled by this target.

The 7-in.-radius unit described above was unsatisfactory for use with hydrogen below 20 kev. A third unit operating on a $2\frac{3}{4}$-in. radius was constructed for hydrogen in the energy range from 10 to 20 kev. This unit is a complete departure from the usual Calutron source configuration. The ion-exit port faces in the downward direction and is so arranged that the primary focus is in the 90-deg position. A baffle at this point intercepts all but the desired ion beam, which passes through a ¼-in. slit and strikes the target at the 180-deg position.

The experimental procedure used in all cases consisted in cleaning, drying, and weighing the copper plate both before and after exposure to the ion beam. Exposure to the beam was on the following approximate schedule: A^+, 100 ma-hr; He^+, 500 ma-hr; and H^+ and D^+, 1000 ma-hr. Data were recorded as milligrams of weight loss by the target per milliampere-hour of received current. The sputtering ratio, which is the ratio of atoms sputtered out to ions incident, was calculated and is given in Table D.2.1.

The hydrogen data should be considered as order of magnitude only. Since the weight losses were small (10 to 20 mg in 400 g), the error was estimated to be as large as 20%.

One hydrogen-bombarded target was chemically analyzed for dissolved hydrogen after bombardment. This target had been bombarded for 1152 ma-hr by 42-kev H^+ ions. This corresponds to 41 mg of H^+ hitting the target. The analysis showed less than 1 ppm of hydrogen in the bombarded area. This was identical with that in the unbombarded area.

At present, the experimental work is being continued to give more consistent results. The present equipment can be used to extend the range of sputtering measurements to 80–90 kv. Units for this work have been designed and are under construction at present.

Table D.2.1. Sputtering of Copper by Monoenergetic Ions

Ion Energy (kev)	Sputtering Ratio	Ion Energy (kev)	Sputtering Ratio
A^+ ions[a]		He^+ ions[b]	
6.0	6.6	15.0	0.212
10.0	7.9	19.5	0.161
15.0	9.3	23.0	0.210
20.0	9.4	30.0	0.126
25.0	9.2	39.0	0.086
25.0	8.6		
30.0	8.6		
38.8	8.5		
40.0	8.9		
D^+ ions[c]		H^+ ions[c]	
10.0	0.0501	10.0	0.0049
11.0	0.046	19.5	0.0048
20.0	0.032	22.0	0.0047
30.5	0.035	30.5	0.011
30.0	0.029	42.0	0.0095
42.0	0.021		

[a]100 ma-hr per target.
[b]500 ma-hr per target.
[c]1000 ma-hr per target.

Appendix E

IONIZATION AND DISSOCIATION OF ENERGETIC IONS BY A CARBON DISCHARGE: STATUS REPORT NO. 2

J. S. Luce

ABSTRACT

Self-sustained carbon arcs varying in length from 2 in. to 6 ft have been operated continuously in longitudinal magnetic fields at pressures of approximately 10^{-5} mm. These arcs have been studied in several facilities under varying conditions. Some of their characteristics are described. Spectrographic analysis showed the ions to be predominantly C^{+} and C^{++}, with measurable amounts of C^{+++}. No trace of excited neutral carbon atoms could be observed; it is assumed that the carbon was essentially completely ionized. Ionization was measured ($N^{+} \rightarrow N^{++} + e$) when a 24-kev N^{+} beam was passed through the discharge. Forty per cent of a 27-kev D_2^{+} beam was continuously dissociated ($D_2^{+} \rightarrow D^{+} + D^{0}$) without any measurable losses when passed through the discharge. Approximately 90% dissociation has been measured with an arc current of 700 amp. Electrical and calorimetric measurements of the resultant beams (D^{+} and D^{0}) were made. Characteristics of the trapped half-radius atomic beam were studied. Application of this discharge to accelerators is mentioned.

THE CARBON ARC

During the first months of 1956, an investigation to determine the characteristics of d-c arcs in a longitudinal magnetic field and under a high vacuum was conducted at the Oak Ridge National Laboratory. During the course of these experiments, it was found that a self-sustained energetic carbon discharge could be operated over long gaps if the proper conditions were achieved. The discharge has many interesting characteristics. It is not a true arc, in that no stable homogeneous structure exists. The discharge constantly undergoes segmentation, each section appearing as a filament of discharge. The filaments are in constant motion and readily cross a strong magnetic field. The life of each section appears to be limited, and new ones are constantly forming. These dynamic conditions induce appreciable impacts and/or thermal gradients at the cathode, which cause hot carbon pieces of small size to be torn from the cathode and ejected at high speed in wide angles toward the anode. These particles make many collisions with the walls of the volume without disintegrating or changing their shape. A photograph of some of these particles is shown in Fig. E.1.1. These carbon pieces adsorb neutral gas as they cool, and act as a pumping system.[1] In addition to these particles, carbon ions also reach the walls and assist in occluding neutral gas. Some studies have been made of the pumping characteristics of this arc and have been reported.[2]

A gas-fed radio-frequency arc is used to strike the discharge. After the discharge has been established, the gas flow is completely stopped, and the carbon arc is self-sustained. When first struck, the discharge is surrounded by an atmosphere of carbon and other neutrals. In this phase, its basic characteristics are essentially the same as those of a large d-c gas arc in a magnetic field. Under these conditions, a secondary plasma is observed around the arc. As the pressure drops, the discharge separates into segments, which move continuously across the magnetic field. The secondary plasma decreases in intensity as the pressure drops, while the light emitted by the anode increases. These changes indicate greater energy and fewer collisions of the electrons reaching the anode. It is assumed that the average energy of the electrons increases as the pressure decreases, and this explains, in part, the unusual characteristics of the discharge.

[1] R. H. Savage, *J. Appl. Phy.* 19, 1 (1948).

[2] C. E. Normand, O. C. Yants, and C. W. Blue, p 462 in *Controlled Thermonuclear Reactions: a Conference Held at Berkeley, California, Feb. 20–23, 1957*, TID-7536 (Part 2).

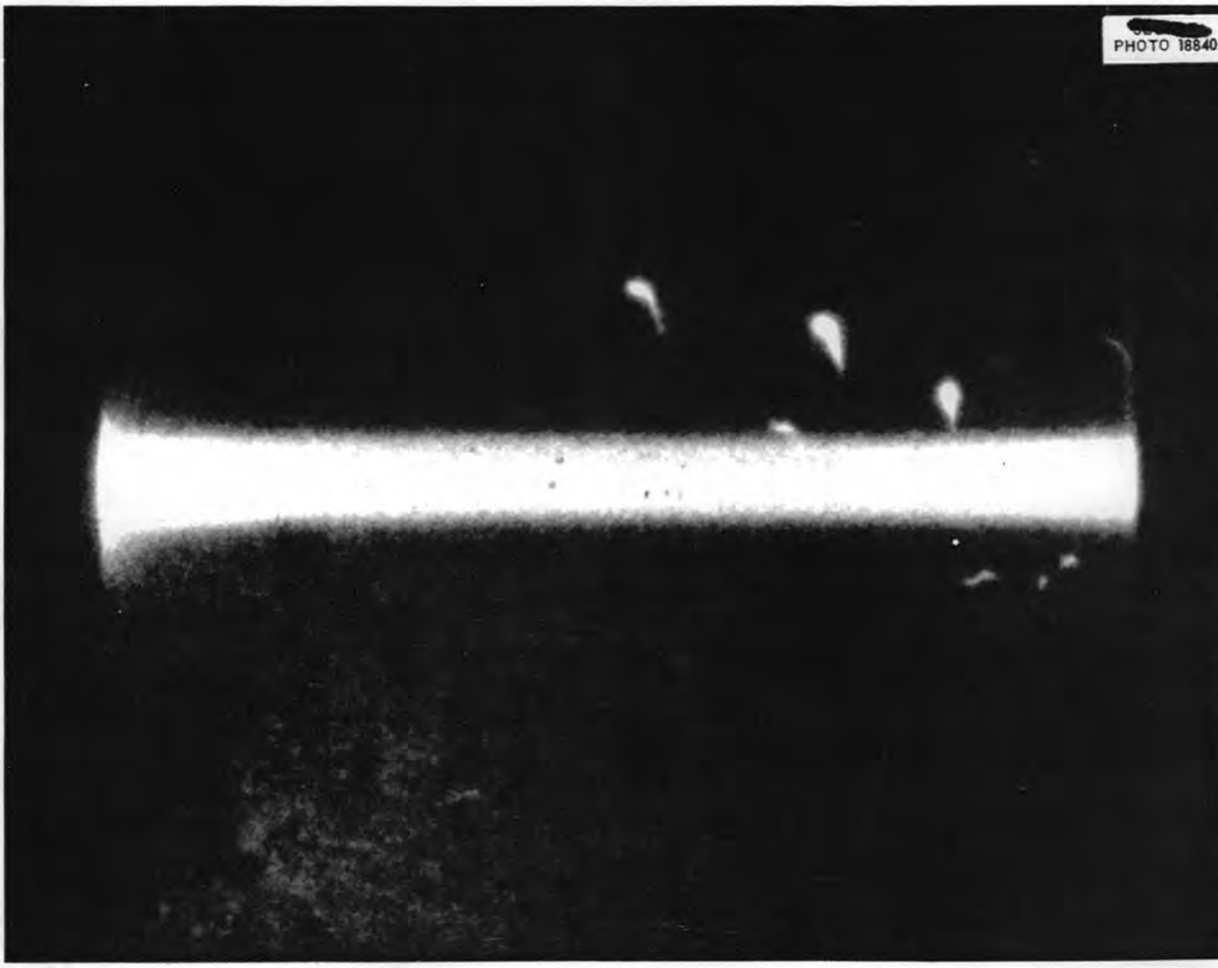

Fig. E.1.1. Motion of Large Charged Carbon Particles.

Some phenomena related to those described above have been observed in mercury arc rectifiers and in atmospheric carbon arcs. The techniques developed[3] at ORNL, however, permit the operation of carbon arcs with wide gaps in strong magnetic fields and under a high vacuum (Figs. E.1.2 and E.1.3). The resultant discharge has characteristics radically different from those normally encountered.

This discharge was observed during the first months of 1956. In August of the same year, operation had become stable enough to permit preliminary measurements. These studies included pumping speed measurements, calorimetric measurements of the power dissipated by radiation, oscillographic measurements of electric fields present, and spectrographic analysis of the arc constituents. In addition to these studies, energetic ion beams of He^+, N^+, H_2^+, and D_2^+ were passed through the discharge, and ionization and dissociation were measured. Arc currents of approximately 300 amp were used for these experiments. The original experiments were done in a magnetic track of the former electromagnetic separation plant, which imposes several limitations. The vacuum volumes available in this track are only 16 in. wide, and so the arc length was restricted to about 8 in. Outgassing and pumping conditions in these tanks are poor. Also, the magnetic field is uniform and allows little opportunity to produce containing geometries, such as magnetic mirrors. For these and other reasons, three other facilities have been constructed in which a carbon arc can be used. In each, the operating conditions and geometries

[3]J. S. Luce, p 448 in *Conference on Controlled Thermonuclear Reactions, June 4–7, 1956, Gatlinburg, Tenn.*, TID-7520 (Part 2).

[redacted]

[redacted]
ORNL—LR—DWG 25999

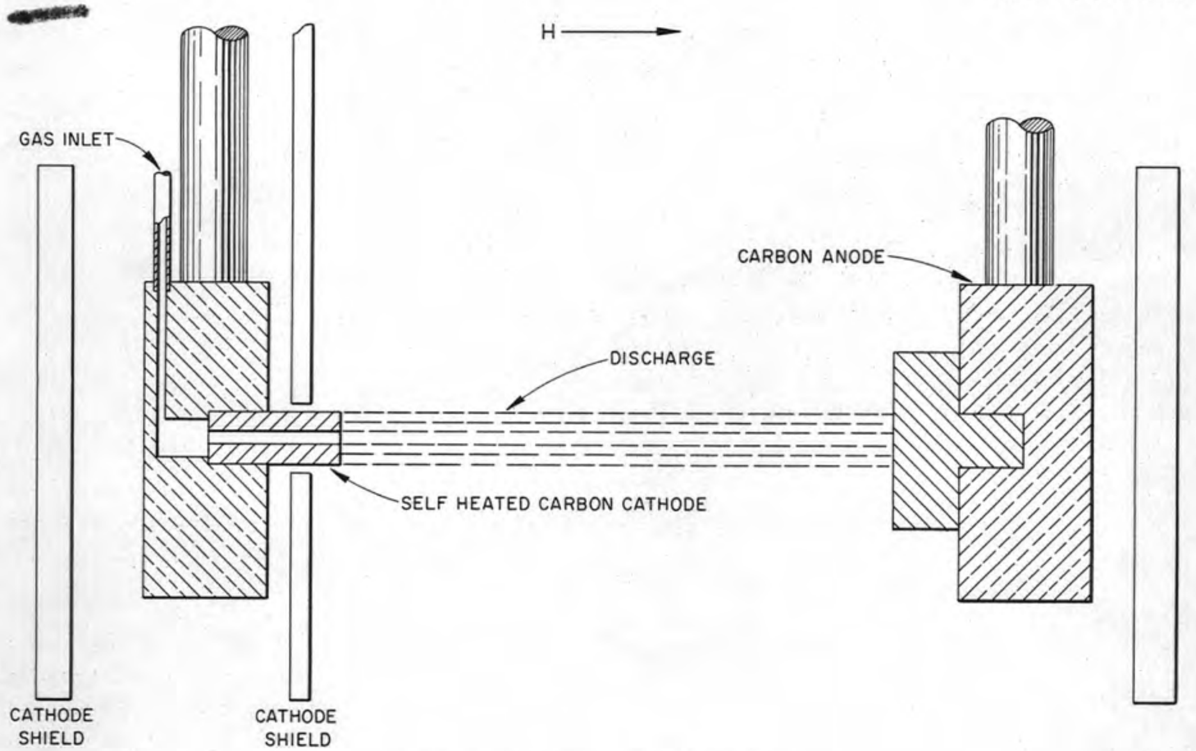

Fig. E.1.2. High-Current Carbon Arc.

[redacted]
PHOTO 27531

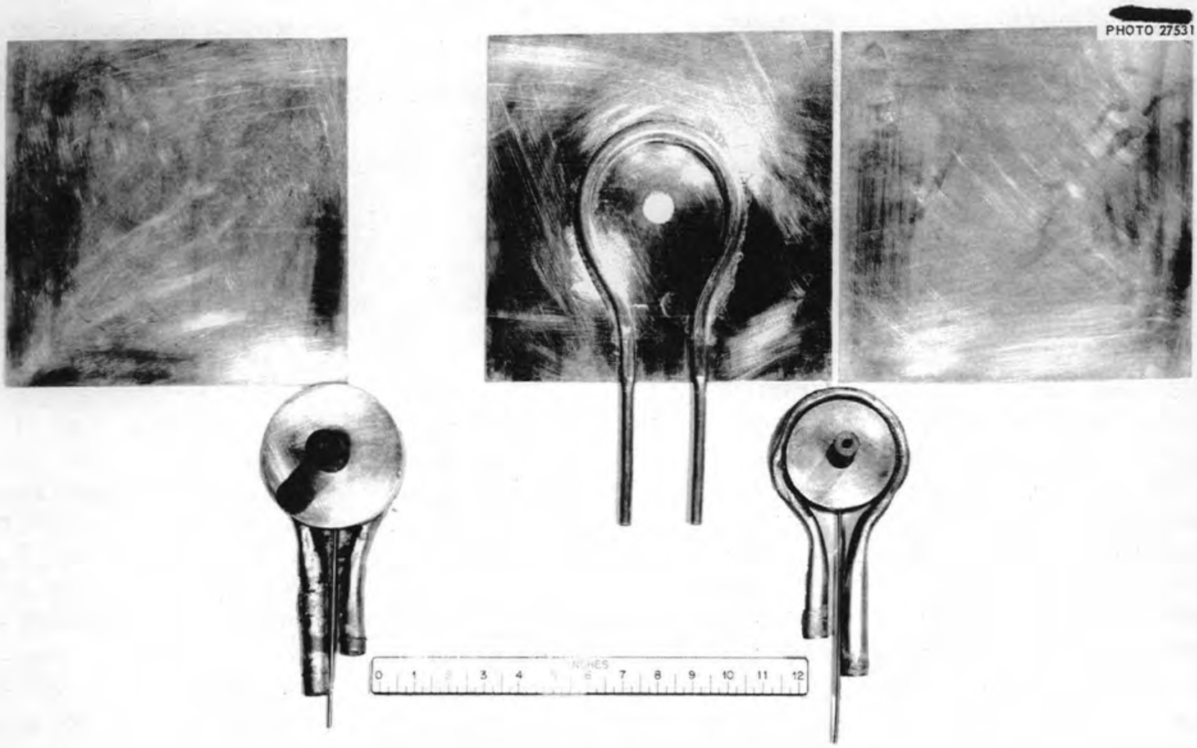

Fig. E.1.3. Carbon Discharge Components.

are different. These three facilities are the long solenoid facility in Building 9204-3, the carbon arc assembly in Building 5500, and DCX.

MAGNETIC TRACK EXPERIMENTS

Electric Field Measurements

Oscillographic measurements of the carbon arc show the presence of oscillations in the radio-frequency range. Due to the internal impedance of the power supply, it has been difficult to measure accurately oscillations originating in the discharge. The work is being continued, however, and it is hoped that by the use of a more suitable power supply, or by proper filtering circuits, more exact results may be achieved.

Spectrographic Measurements

The spectrographic group observed the carbon discharge at short wavelengths, using a quartz window to permit study of the carbon resonance line at 2478 Å. With discharges of 170, 270, and 425 amp, reasonably strong spectra of C^+ and C^{++} were observed. The ratio of C^{++} spectra to C^+ increased with increasing current. No trace of the resonance line of neutral carbon was observed in the center of the arcs for these exposures; it was concluded that the center section of the high-current carbon discharge is more than 99% ionized.

Neutral argon gas was introduced into the discharge at both the cathode and the anode ends. Complete ionization of the argon into A^+, A^{++}, and A^{+++} ions was observed in the pressure range of 2×10^{-5} to 5×10^{-4} mm Hg. The introduction of neutral[redacted]caused a large decrease in the number of C^{++} ions. It appeared that the introduction of neutrals into the discharge caused collision processes that reduced the average energy of the particles in the discharge.

During the course of these experiments, excitation levels requiring 43-v electrons were observed. More detailed descriptions of the spectrographic measurements are given in Appendix F.

Ionization of Energetic Ions

A single test was made with a beam of N^+ ions to see whether additional electrons could be stripped from the N^+ ion when it was passed through the discharge. A schematic outline of the experimental setup, showing the beam paths, is given below.

[redacted]
ORNL–LR–DWG 26000

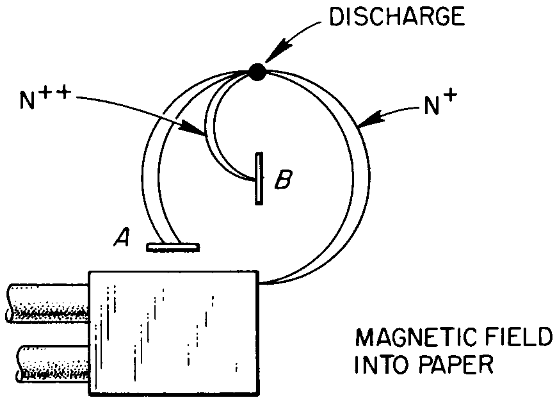

Removal of electrons from the ions causes a change in the charge-to-mass ratio, resulting in smaller radii for the stripped ions.

If it is assumed that the reaction involved here is $N^+ \longrightarrow N^{++} + e$, then the current reading on plate B, due to the doubly charged ions, must be divided by 2. The removal of a single electron is probably a good assumption, since the energy required for double ionization is 29.47 v, whereas the removal of the third electron requires 47.49 v. When He^+ was passed through the discharge, very little ionization occurred; this seemed to indicate that stripping under the conditions of this experiment is confined to ions whose ionization potential is below 47 v. This assumption is strengthened by the spectrographic analysis, where strong excitation of levels up to 43 v was observed.

If the current to plate B is divided by 2, the ionization efficiency appears to be about 12%. When discharges of higher current are available, the energy of the discharge will be increased, and more efficient stripping of energetic ions may be possible.

These results show that ionization of energetic particles can be achieved in a carbon arc. This is a useful tool for several reasons. For example, energetic D^0 could be passed through the arc in a containing magnetic field, and the ionized particles would be trapped. Since the energetic neutral is not affected by the magnetic field, it is free to move across the field until it is ionized. This is a distinct advantage where high magnetic fields are used.

The nee[redacted]tudying trapped D^+ beams necessitated postponement of electron-stripping experiments, but in the future it is planned to identify the stripped ion beams by the use of a scanning probe.

Dissociation Experiments ($D_2^+ \rightarrow D^+ + D^0$)

The phenomenon of dissociation (and ionization) of energetic ions[4–6] is pertinent to Project Sherwood, since it provides a means of trapping energetic ions in a magnetic field and produces an energetic neutral beam. Twenty-five per cent of a 60-ma D_2^+ beam has been continuously dissociated for 50 min when the beam was passed through the discharge; 40% dissociation has been maintained for 10 min. Complete dissociation could probably be achieved by using higher current, or two or more discharges.

In these experiments, a narrow source slit was used to provide 180-deg focusing. The carbon discharge was placed so that it intersected the beam at 180 deg. The dissociated atomic ion beam (referred to as the *R*/2 beam) was measured on a water-cooled target which was well shielded by a water-cooled copper box. The neutral beam was measured 10 in. from the carbon discharge on a water-cooled copper plate.

Both calorimetric and electrical measurements of the atomic (*R*/2) beam were made, and good correlation was achieved. The following data are typical of the calorimetric measurements. With an *R*/2 beam of 0.010 amp at 13 kv, or a power rate of *130* w, the temperature increase of the cooling water was 3.9°C. With a water flow of 0.473 kg/min, an increase of 3.9°C is equal to a power rate of *129* w. No metered loss of ions was detected in the electrical measurements. Adding the *R*/2 and the residual D_2^+ beam (plates *A* and *B*) always gave the same current reading as the total D_2^+ beam before dissociation (see sketch below).

Measurements of the energetic neutral beam were less successful, because it was impossible to shield the neutral target as adequately as the *R*/2 target. The neutral target is exposed to the carbon discharge, which causes thermal fluctuations. It was possible, however, to identify the energetic neutral beam despite a large variation in the readings.

Neutral argon gas fed into the carbon discharge during the course of these experiments caused attenuation and losses in all the ion beams. This may be due to higher neutral pressure. However, the argon lines were studied spectroscopically during the tests, and the neutral argon lines were not observed. It is assumed that the argon gas in the arc was completely ionized, but that the pressure in the working volume was increased by recombination.

Approximately 90% of the D_2^+ beam has been dissociated by using an arc current of 700 amp. High pressure, due to outgassing surfaces, caused

[4] J. S. Luce, *Proposed Sherwood Experiment*, ORNL CF-55-4-73 (April 11, 1955).

[5] J. S. Luce, *Molecular Ion Source*, ORNL CF-55-11-160 (Nov. 30, 1955); p 335–38 in *Conference on Controlled Thermonuclear Reactions Held at Princeton University, Oct. 17–20, 1955*, TID-7503.

[6] A. E. Ruark and M. Rankin, *Beam Degeneration and Thermalization Problems* (unpublished).

[redacted]
ORNL-LR-DWG 26001

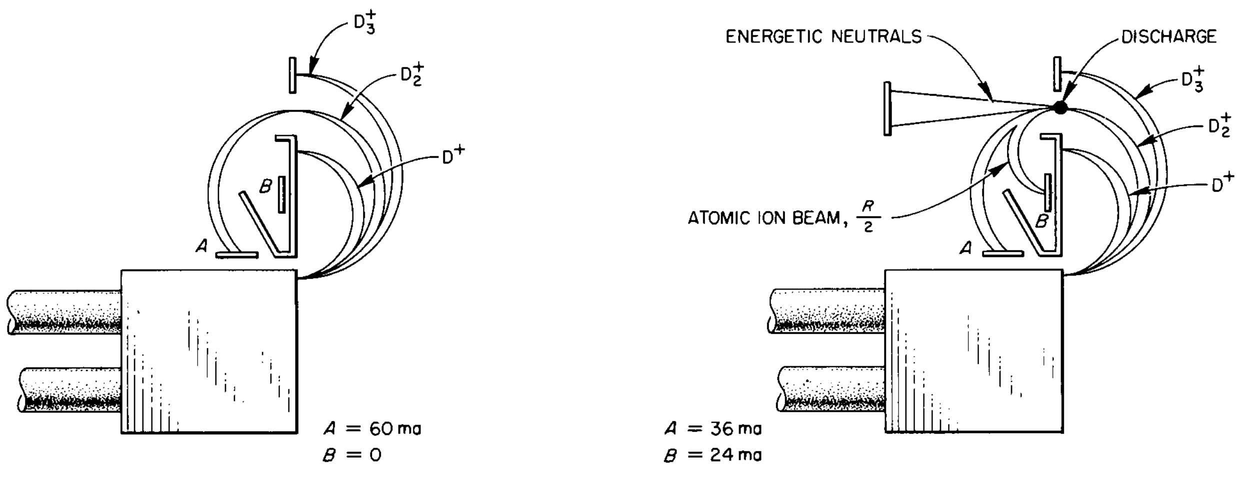

beam losses which made an exact measurement impossible. With a larger power supply, proper bakeout, and differential pumping, complete dissociation of the D_2^+ beam may be possible.

Measurements of Trapped Energetic Ions

Due to the difficulty of operating in the old electromagnetic equipment, only brief studies were made of the trapped circulating beam. Probe measurements show plainly that a circulating current of energetic ions does exist. It is extremely difficult, however, to make accurate probe measurements in the presence of the carbon discharge, since the probes read some current from the discharge.

Despite these difficulties, qualitative measurements were made with small tungsten probes when the $R/2$ beam was intercepted at 180 deg, and these measurements were compared with $R/2$ readings made with the circulating beam. The $R/2$ current readings per unit area of beam increased by at least a factor of 5 with the circulating beam. By using multiple probes, it was also shown that the circulating beam occupied a larger area than the intercepted beam. While it is impossible to show accurately from these experiments the magnitude of the beam multiplication, it is certain that conversion of energetic molecular ions into a circulating atomic beam was achieved.

An indication of the shape of the trapped beams was obtained by passing them through foils. In one test, the $R/2$ beam was intercepted at 180 deg after passing through a foil. A second test was

[redacted]
ORNL-LR-DWG 26002

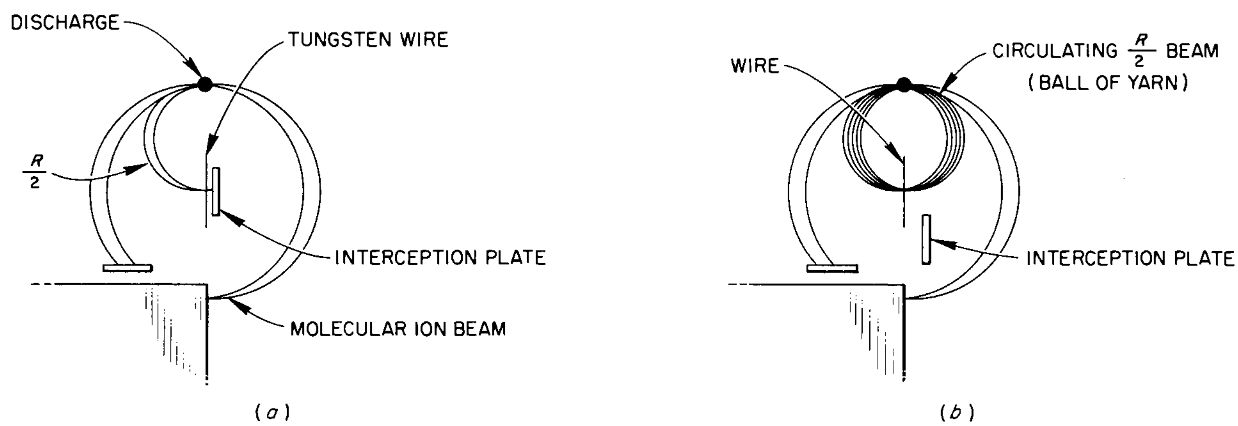

[redacted]
ORNL-LR-DWG 26003

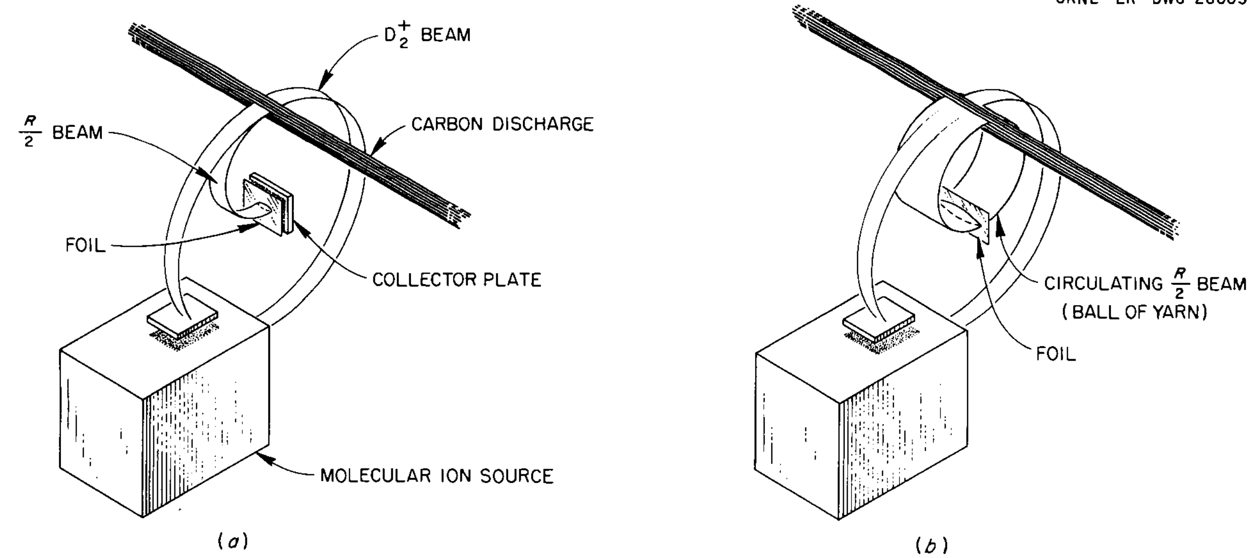

made under the same operating conditions except that the $R/2$ beam was allowed to circulate.

Reference to Fig. E.1.4 will show the difference in burn-through in the two cases.

LONG SOLENOID FACILITY

Description

The long solenoid facility (Fig. E.1.5) was first constructed to study injection of energetic ions

SECRET
PHOTO 27269

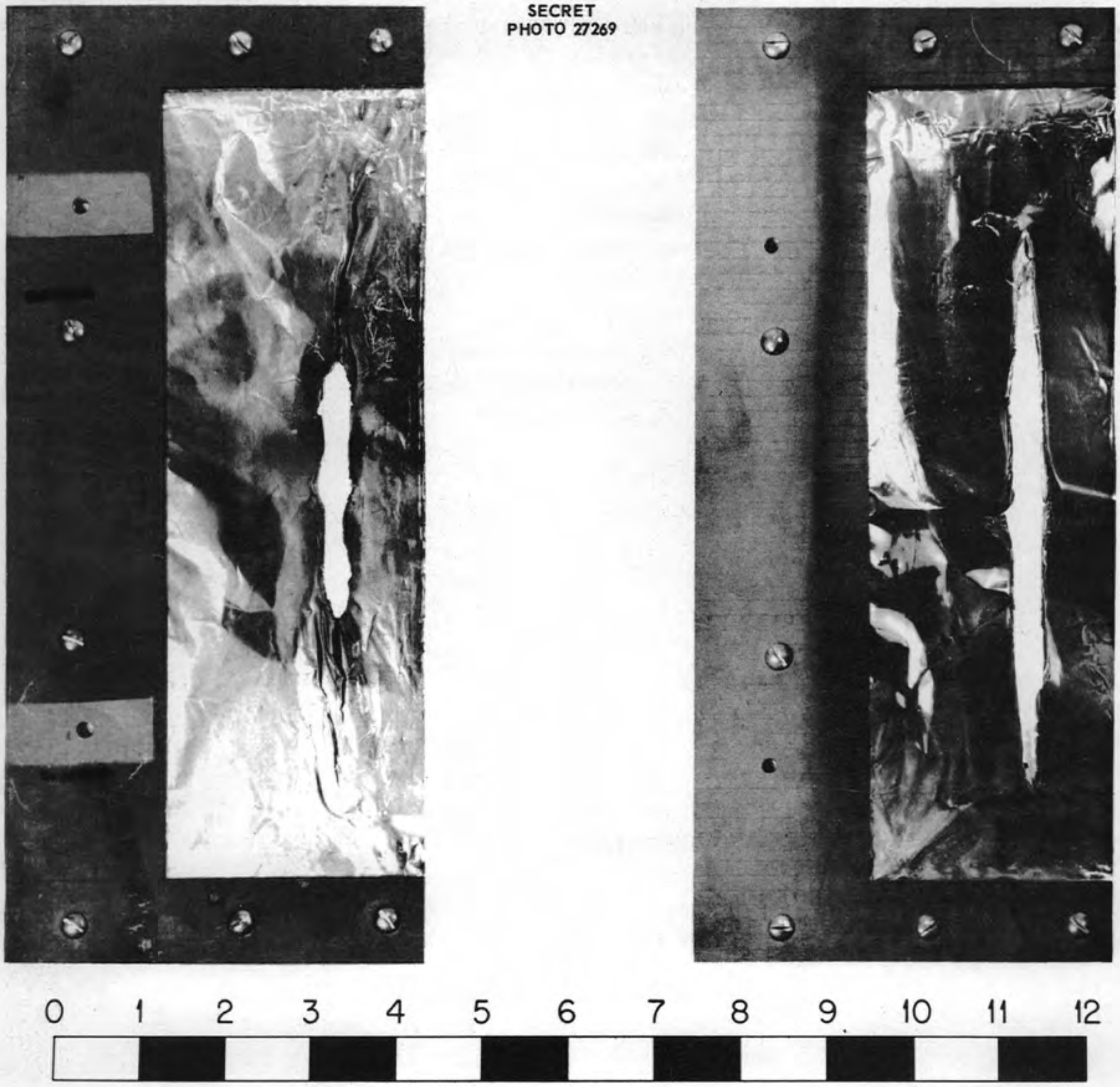

Fig. E.1.4. Foils Burned Through by Ion Beam.

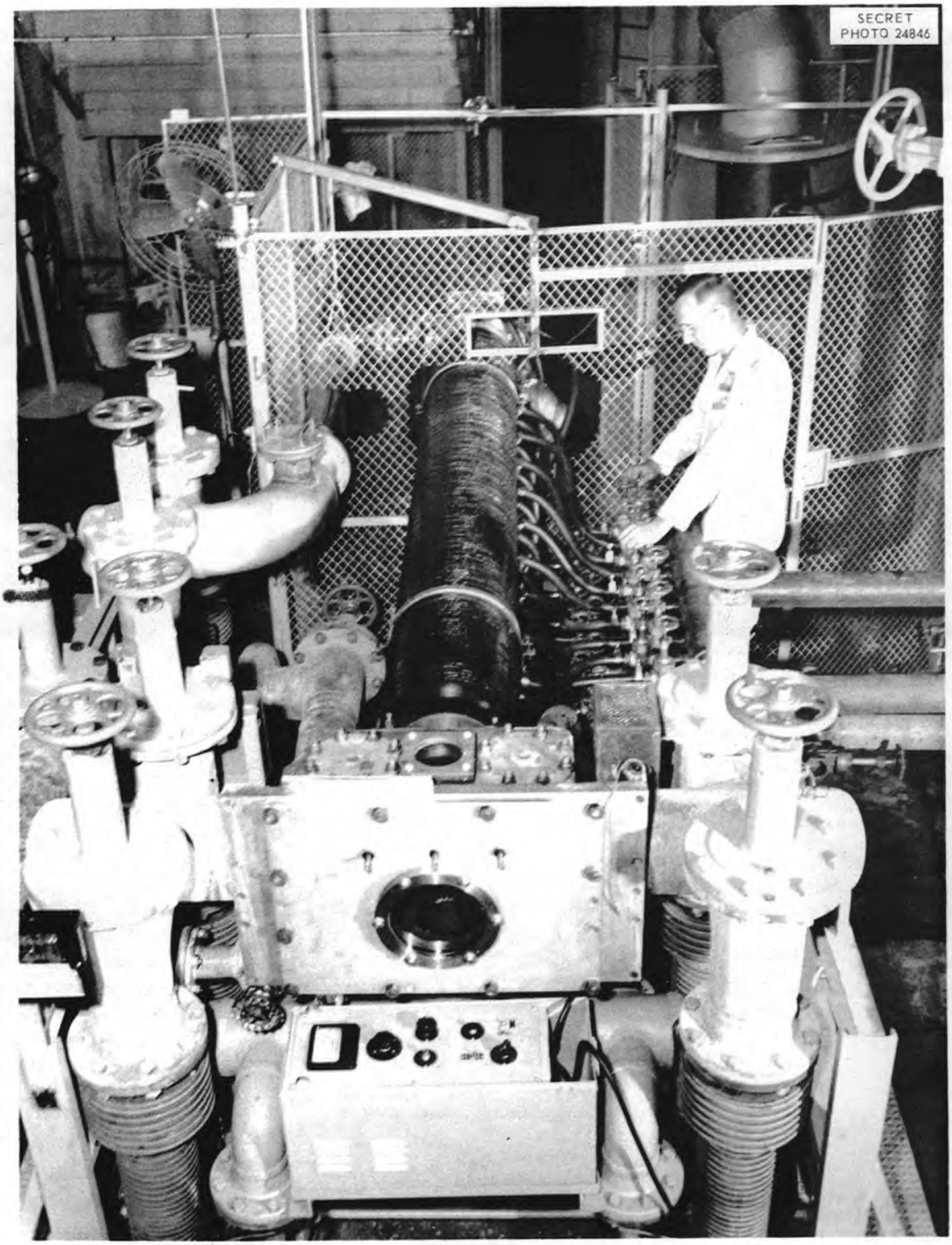

Fig. E.1.5. Long Solenoid Research Facility.

through a magnetic mirror. The machine has been rebuilt to facilitate a more comprehensive study of high-energy arcs. It was in this facility that the feasibility of operating a long (6-ft) carbon arc was first determined. A typical cathode and anode assembly is shown in Fig. E.1.6. Experiments were done in which all the floating cathode shields shown in Figs. E.1.2 and E.1.3 were replaced by two pieces of quartz tubing as shown in the following sketch.

Other experiments were done to show that the carbon arc could operate with the vacuum pumps closed off, showing that the arc itself was indeed a vacuum pump.[7]

[7] C. E. Normand, O. C. Yonts, and C. W. Blue, p 462 in *Controlled Thermonuclear Reactions: a Conference Held at Berkeley, California, Feb. 20–23, 1957,* TID-7536 (Part 2).

[redacted]

ORNL-LR-DWG 26184

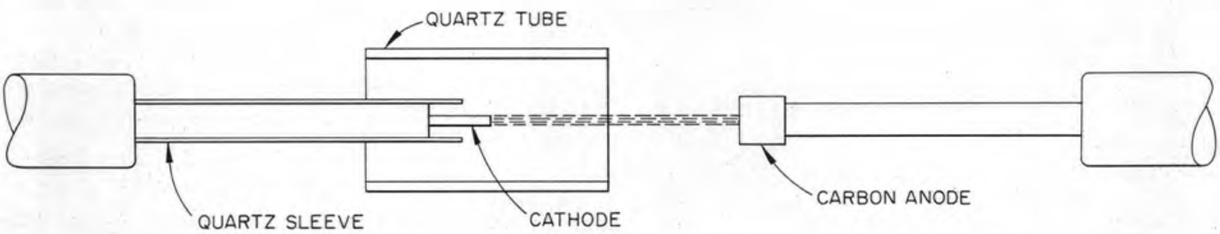

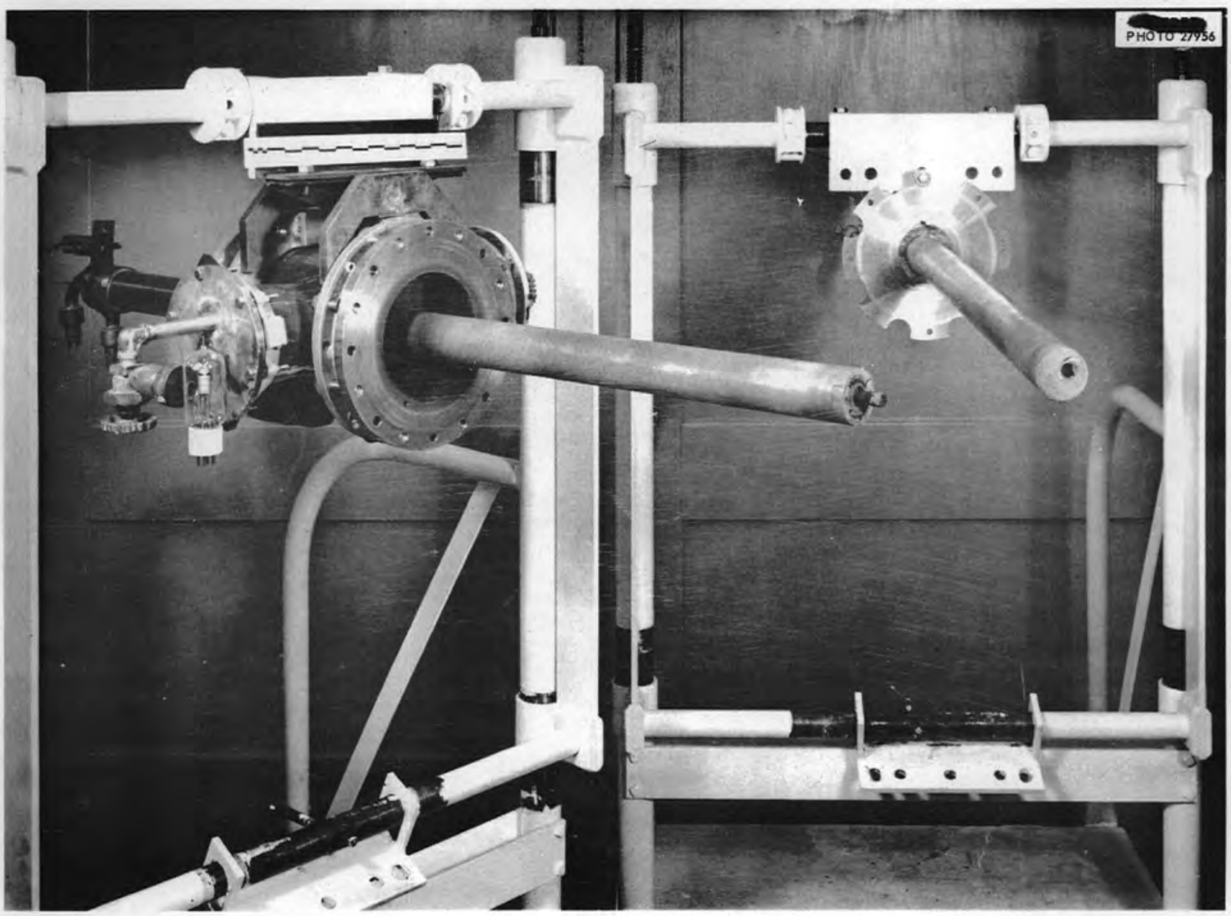

Fig. E.1.6. Typical Electrode Assembly for Carbon Arc.

Calorimetric Measurements of the Carbon Arc

A series of experiments were done to determine the amount of energy radiated from the arc column. For this purpose, a 6-ft arc was operated between carbon electrodes at a pressure of about 10^{-5} mm Hg. Collimation of the arc was achieved by a magnetic field of 3000 gauss maintained parallel to the axis of the arc. The following sketch shows the arrangement of the apparatus used inside the long solenoid for these measurements. A carbon

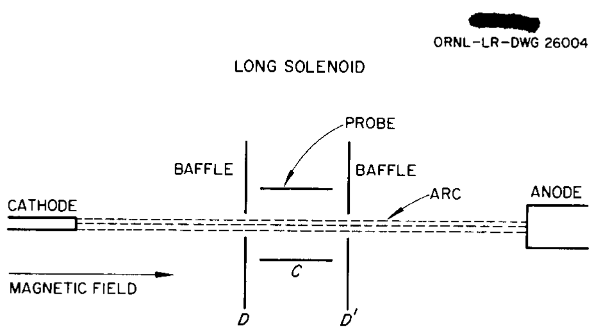

arc was operated between the electrodes, as indicated. No gas was used in this system, the carbon feed coming directly from the anode. A cylindrical probe was placed around the center 12-in. section of the arc, which was shielded from electrode radiation by the water-cooled baffles *D* and *D′*. This arrangement assured that the probe would measure power from the main body of the arc only. The power to the probe was measured calorimetrically. With an arc of 240 amp it was found that the energy transferred to the probe was 2500 to 3000 w[redacted]ower varying somewhat with pressure.

The power reaching the probe was attributed to one or more of three sources: photons, charged particles, and energetic neutral particles. A study of probe characteristics showed that the energy reaching the cylindrical probe by means of charged particles was at most very small. For all practical purposes it could be neglected. No measurements were made of energetic neutrals, but means of doing this are being devised. It is believed that the amount of power reaching the probe by means of energetic neutrals is also small.

Miscellaneous Studies

Several studies of other types were made in the long solenoid. Among these experiments, some were done to determine whether the carbon arc could pass through magnetic mirrors without difficulty. Experiments were also done with off-axis operation to facilitate carbon arc work in DCX. These studies will not be reported here, since experiments in DCX led to a new system which made arc operation much simpler than had been anticipated.

Other experiments were done to determine the feasibility of operating a carbon arc in the ORNL High Voltage Laboratory at the X-10 site. The available power at this site was such as to limit the solenoid magnet to a 3-in. bore. To operate in the 3-in.-dia tube, it was necessary to reduce the diameter of the cathode assembly from $2\frac{1}{2}$ in. to 1 in. The floating shields were replaced by quartz tubes, as indicated earlier. It was necessary to insulate the entire cathode assembly where it could "see" a positive potential along a magnetic flux line. This insulation was needed to prevent back-streaming ions from striking the cathode assembly. When these ions do strike the cathode assembly, they cause arcing along the lines of force where a difference in potential exists.

These studies demonstrated the feasibility of operating a 6-ft arc in a 3-in.-dia tube. Consequently, a new solenoid facility was constructed and was installed at the High Voltage Laboratory.

CARBON ARC ASSEMBLY (HIGH VOLTAGE LABORATORY)

The carbon arc assembly in the High Voltage Laboratory is shown in Fig. E.1.7. Movable cathodes and anodes were provided so that breakup of D_2^+ ions could be determined as a function of distance from the electrodes. Striking of the arc was done by two methods: (1) by means of the usual r-f discharge described earlier and (2) by touching the cathode and anode together and then pulling them apart. A debugging period of about two weeks was used to place this unit in operation. Since that time, stable operation has been consistently maintained. A schematic sketch of this facility is shown in Fig. E.1.8. This assembly was attached to a 600-kv cascade accelerator. A beam of D_2^+ ions was passed through the carbon arc, and dissociation was measured. These and other experiments are reported elsewhere.[8]

[8] C. F. Barnett, R. J. Mackin, Jr., and J. A. Ray, *Dissociation of H_2^+ and D_2^+ by a Vacuum Carbon Arc*, ORNL-2420 (Dec. 6, 1957) (Appendix C of this report).

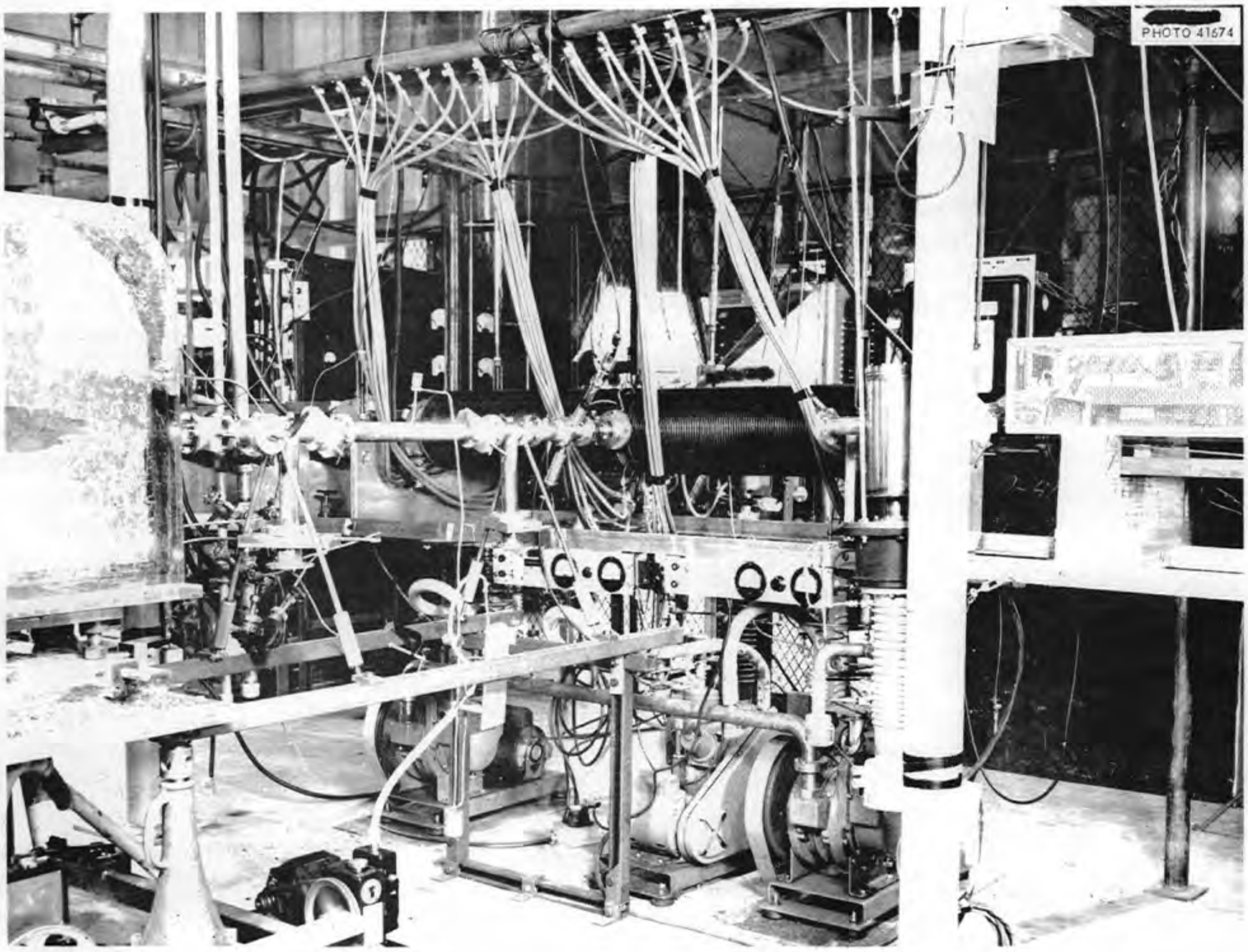

Fig. E.1.7. Carbon Arc Facility in the High Voltage Laboratory.

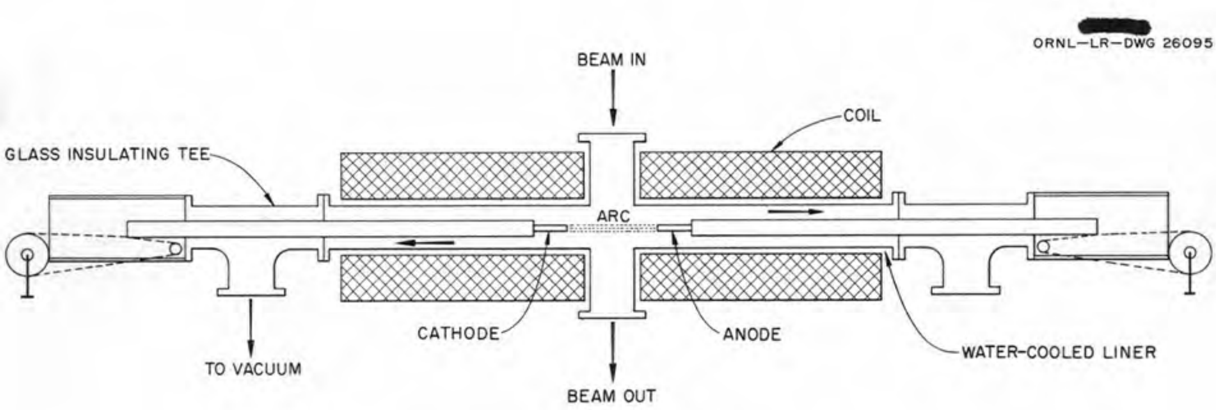

Fig. E.1.8. Carbon Arc Assembly.

CARBON ARC EXPERIMENTS IN DCX

The carbon arc in DCX was first operated on the axis of the machine. No difficulty was encountered, the arc operating the first time it was turned on. Stable operation was achieved with both the cathode and the anode located 10 in. beyond the peak of the mirror magnetic field. The operation was more stable than that obtained in any of the other facilities. This was attributed to the higher magnetic field in DCX, although the direction of the magnetic field was also different from that in the other facilities. Due to the high momentum of the trapped atomic ions relative to the available magnetic field, operation of DCX with the arc on the axis was not practical. With the arc on the axis, the trapped ions are off center and escape from the system. Proper placement of the arc off the axis causes the atomic ions to be trapped in the center of the machine. Consequently, off-axis operation of the arc was necessary. This was first achieved by simply bending the cathode and the anode assemblies. With the arc off center, it was found that the back-streaming ions no longer struck the cathode assembly. It was thus possible to eliminate the quartz tubing which had formerly been necessary. This method of operation also made it possible to study the back-streaming ions that miss the cathode. When these ions were allowed to strike an insulated plate, it became charged up to 50 v. When this plate was grounded, it was found to draw a current of 20 amp. The carbon arc is now operated in DCX on a routine basis.

OTHER APPLICATIONS

The availability of trapped, circulating ion beams and large high-energy neutral beams opens several new possibilities in accelerators. The University of California has considered the breakup of H_2^+ as a method of injection in proton synchrotrons.[9] A gas target was considered in this study. Several advantages accrue from using the carbon discharge described in this report.

Under proper conditions, all the H_2^+ could very probably be dissociated. Dissociation occurs in a small area, as shown by the sharp focus of the dissociated beam. Scanning of the 180-deg focal line of the H_2^+ beam and the 180-deg line of the trapped H^+ shows no difference in width of focus. Stainless steel strips placed at the focal line of the trapped H^+ beam can be melted through with ease even when small beams (10 to 15 ma) are used, indicating sharp focus (Fig. E.1.9).

Another advantage is the low pressure associated with these discharges, due to the pumping effect of the small particles as well as to the pumping action of the discharge itself. Thus, losses from scattering and degradation of energy are reduced because of low background pressure; this enhances the possibility of "storing" ions in a ring for longer periods of time.

Application of this discharge to heavy-ion accelerators may make a higher degree of ionization possible. In addition, the obvious advantages of stripping at low pressure in a small area could be exploited.

The dissociation experiments described in this report show the feasibility of producing large, well-defined neutral beams ($H_2^+ \longrightarrow H^+ + H^0$). High-energy neutral beams should be easy to obtain since the cross section for dissociation decreases slowly as the energy increases. These neutral particles could be injected into accelerators, where the neutrals would be converted into ions.

ACKNOWLEDGMENTS

The writer was assisted by members of the Thermonuclear Experimental Division of the Oak Ridge National Laboratory and several consultants. Power measurements were made by C. W. Blue, and spectrographic measurements were made by the Spectroscopy Research Laboratory. Construction work was done by a group led by O. D. Matlock. P. R. Bell, E. D. Shipley, C. F. Barnett, and many others have contributed to the program. Their assistance and encouragement are gratefully acknowledged.

[9] C. Van Atta, private communication.

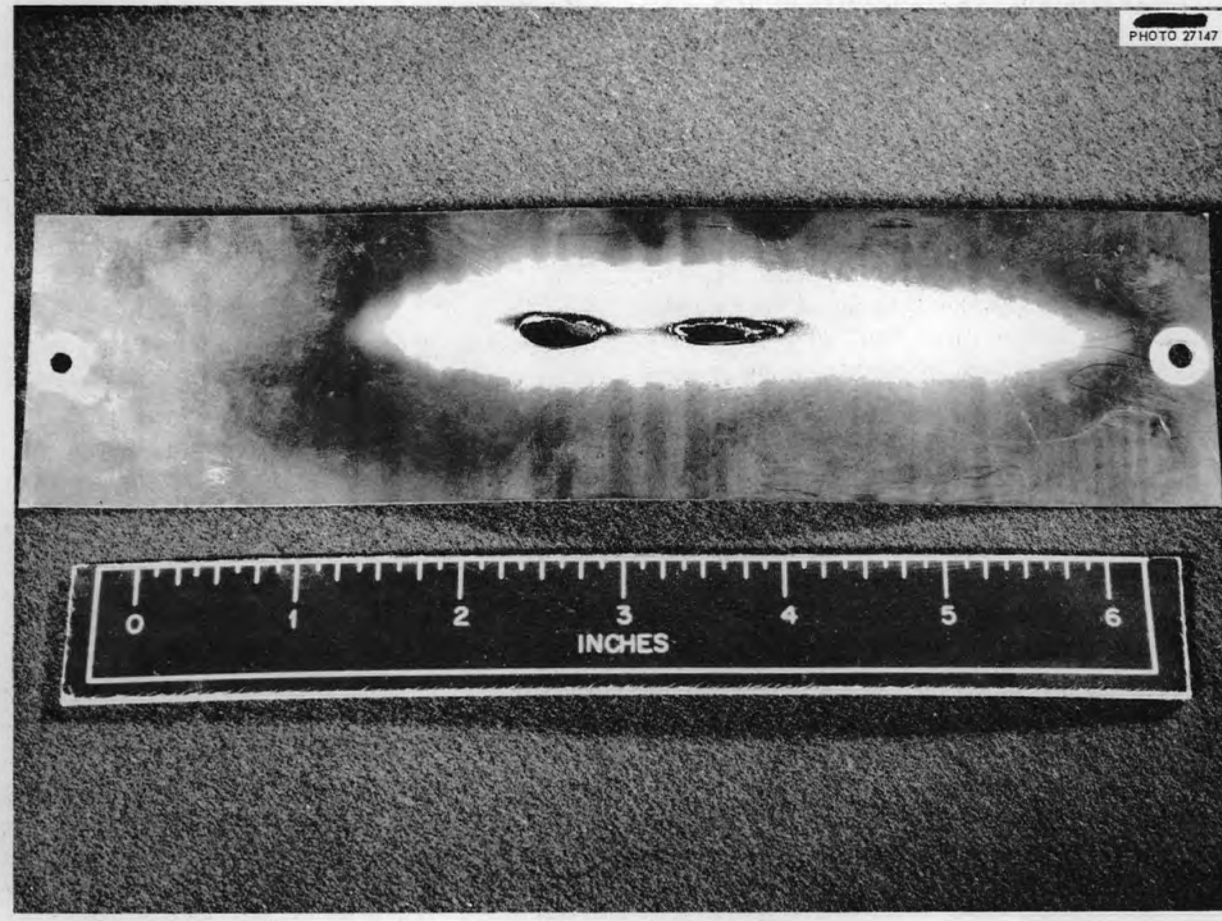

Fig. E.1.9. Stainless Steel Foil Burned Through by Dissociated Beam. (Secret with caption)

Appendix F

SPECTROSCOPIC STUDIES OF THE HIGH-CURRENT VACUUM CARBON ARC

J. R. McNally, Jr.

Spectra have been obtained of the high-current vacuum carbon arc in a magnetic field and in a vacuum of $\sim 3 \times 10^{-5}$ mm Hg, quartz optics being used in order to permit study of the resonance line of neutral carbon at 2478 Å. Arcs of 170, 270, and 425 amp were studied. The spectra show increasing excitation and ionization (C^{++}/C^{+}) as the current is increased, indicating either increased collision rates, higher temperatures, or higher electron energies.

Investigations of the 2478-Å neutral-carbon line showed no trace in these discharges of this normally intense resonance line. From this, it was concluded that the degree of ionization was extremely high, probably exceeding 99%. Recent investigations, in which an image rotator was used to permit ready observation either along or transverse to the arc, have shown this neutral-atom line at 350 amp in fields of a few kilogauss, but only for heavy exposures. The neutral species is relatively weak in the main arc column and of moderate to weak intensity in the anode region. In addition, high-intensity bands of molecular carbon, C_2, known as the Fox-Herzberg bands and the Deslandres-Azambuja bands, have been observed, but only in the anode region. This enhancement of neutral C and C_2 near the anode is increased at the higher base tank pressures (0.12 μ); the lower the pressure, the weaker the 2478-Å line and the C_2 bands. A section of the spectrum along the arc is shown in Fig. F.1.1, in which the absence of neutral-carbon lines in the central region of the arc and the growth of C^{++} lines away from the anode can be noted.

No unique optical definition of the anode edge on the spectrograms can, at present, be claimed because of wandering of the arc and erosion of the electrode; however, the spectrograms show that the neutrals are prominent, though weak, only at the anode edge. This shows that carbon is evaporated from the anode and rapidly becomes ionized. The region of the column in which ionization takes place is approximately ½ in. wide.

Strong Si^{++} lines, especially the line at 3590 Å, appear in the main arc column and, like the spectra of ionized carbon, are weak near the anode. It has been suggested that this may be due to a binder used in the fabrication of the carbon. Lines of O^{+}, due to residual impurity gas, have also been observed.

Regarding neutral-silicon spectrum lines, the spectrochemically most sensitive line at 2881 Å is observed and is excited analogously to the neutral-carbon line at 2478 Å. The usually relatively strong triplet transition at 2500 Å is not observed in these exposures to the 350-amp arc.

An electron energy of 11.26 v is required for the ionization of neutral carbon to C^{+}, 24.38 v is needed to ionize C^{+} to C^{++}, and 47.76 v to ionize C^{++} to C^{+++}. No trace of C^{+++} was observed, but only weak lines are available in this region of spectra; however, levels requiring up to 43 v excitation energy were observed, and C^{+++} spectra have been observed in an arc with a rotating carbon anode. The mechanism of excitation is probably largely electronic in origin, although ion energies measured by the slant effect previously observed in this type of arc were of the order of 10 v for motion transverse to the magnetic field.

A crude measure of the ion density in the arc has been attempted on the basis of photon losses resulting from collision excitation and with utilization of the radiation balance existing in the carbon arc. Inasmuch as the density is obtained as a square root of certain basic physical parameters, such as the cross section for electron excitation and the assumed electron velocity distribution, it is not as sensitive to errors in these parameters. The density is given by

$$n_+^2 \cong n_-^2 = \frac{Pm\bar{E}_i}{h^2 E_i v_i A \pi} ,$$

where P is the power radiated per unit length of the carbon arc in ergs/cm·sec, $\bar{E}_i$ is the average energy of the ith class of electrons ($\gtrsim E_i$), E_i is the quantum energy radiated, A is the arc cross section, and v_i is the velocity of the ith class of electrons. The electron-excitation cross section σ_i is chosen as not greater than the De Broglie

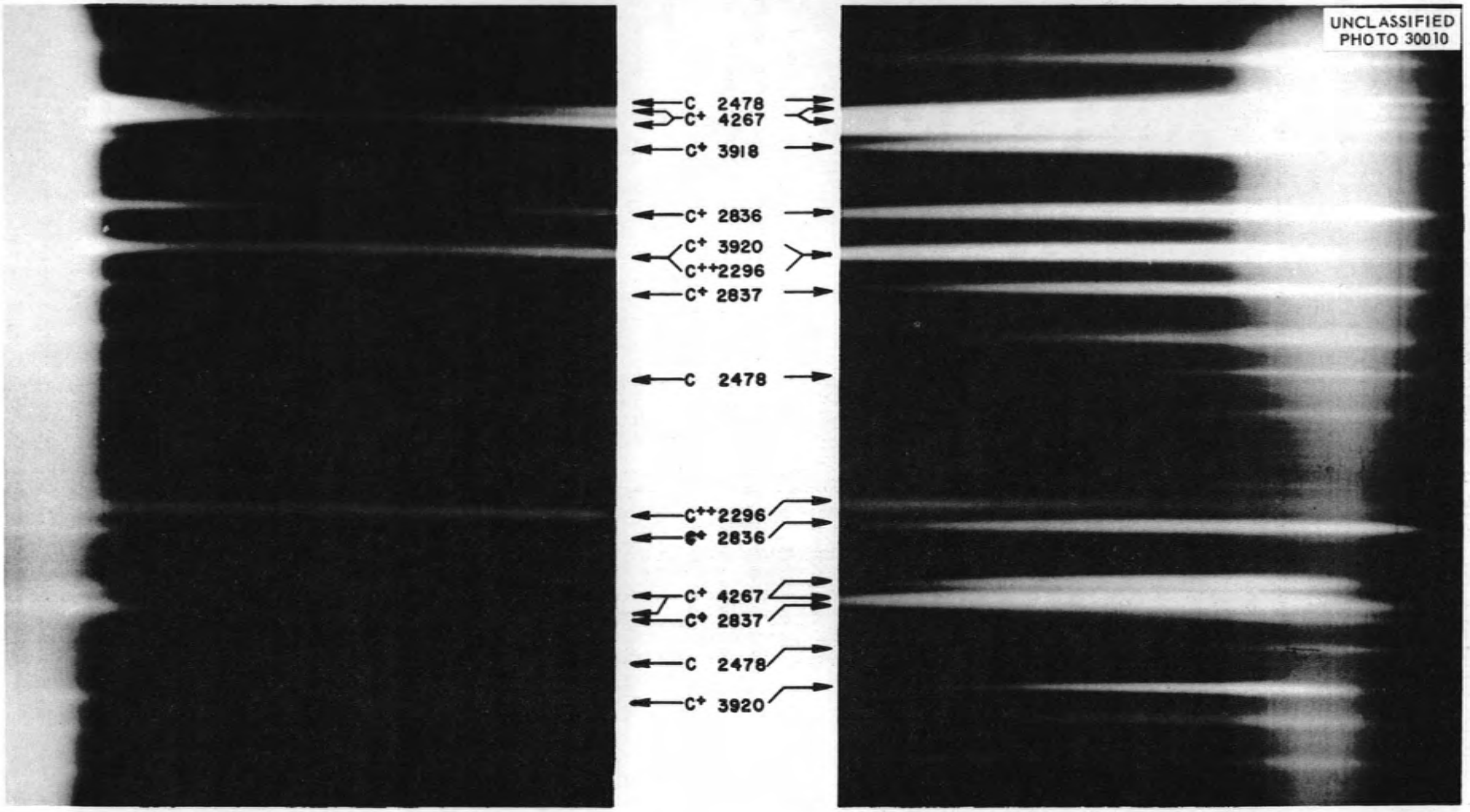

Fig. F.1.1. Portion of the Spectrum of the High-Current Vacuum Carbon Arc. (Secret with caption)

cross section ($\pi\hbar^2/2m\bar{E}_i$). This can be expressed as

$$n_+ \cong n_- \geq \frac{0.85 \times 10^{18}}{\sqrt{v_i}} ,$$

since $\bar{E}_i \gtrsim E_i$ and $A \cong 1$ cm^2. More precise radiation measurements will be necessary to firm up the constant used in this expression. The predicted ion density of the high-current vacuum carbon arc, used in the magnetic track facility, as a function of various assumed energy classes of electrons is given in Table F.1.1. The average value predicted by this radiation-balance approach is at least ten times that predicted from the electron current equation on the assumption that all electrons have the energy equivalent of the total arc voltage.

The Stark broadening of the Balmer H_β line as measured in such arcs is comparable with that expected from Doppler, magnetic, and fine-structure broadening. However, by using the fourth member of the Balmer series, H_δ, the density is computed as 8×10^{13} ions per cubic centimeter. The actual value of the density as a function of arc length, cross section, filamentary structure, magnetic field, feed gas, current, and voltage will be investigated further in DCX and the solenoid facility.

Table F.1.1. Minimum Ion Density from Radiation Measurements in the High-Current Vacuum Carbon Arc

E_i (v)	v_i (cm/sec)	Minimum n_+ (cm^{-3})
	$\times 10^8$	$\times 10^{13}$
50	4.4	4.0
25	3.1	4.8
10	2.0	6.0
5	1.4	7.2
1	0.61	10.9

Appendix G

ION BEAM ENTRY CALCULATIONS

R. J. Mackin, Jr.

G.1 INTRODUCTION AND SUMMARY

It has been found possible to make the calculations necessary to prescribe how the high-energy ion beam shall be led into DCX, without following explicitly the path of the ions through the fringing magnetic field. The problem is a two-dimensional one, motion being in the mid-plane of the mirror configuration. Its simplification results from the circular symmetry of the field. Focusing calculations and an analysis of certain aspects of the containment problem have been made with the use of the same approach.

Figure G.1.1 shows the experimental geometry and specifies the coordinates of interest. The origin is on the symmetry axis of the magnetic field. The positions of the accelerator column and the bending magnet are fixed, and it is proposed to move the beam by varying the bending angle. The distance R, in initial experiments, was taken to correspond to a point 2 or 3 in. outside the DCX vacuum chamber, for convenience. As it turned out, the field in this region and beyond was so weak as to make unnecessary the use of magnetic shielding.

The calculation proceeded as follows. Upon specifying that the beam pass through the arc at a distance r_0 from the axis and with a specified inclination (for instance, tangent to the circle of radius r_0), it was possible, as will be shown below, to calculate the inclination α at radius R. With the use of a layout drawing of the apparatus, this angle α was then used to determine the necessary bending angle and point of entry into the DCX vacuum chamber. The angle θ was then calculated and was used to locate the arc on the circle at r_0.

[redacted]
ORNL-LR-DWG 26005

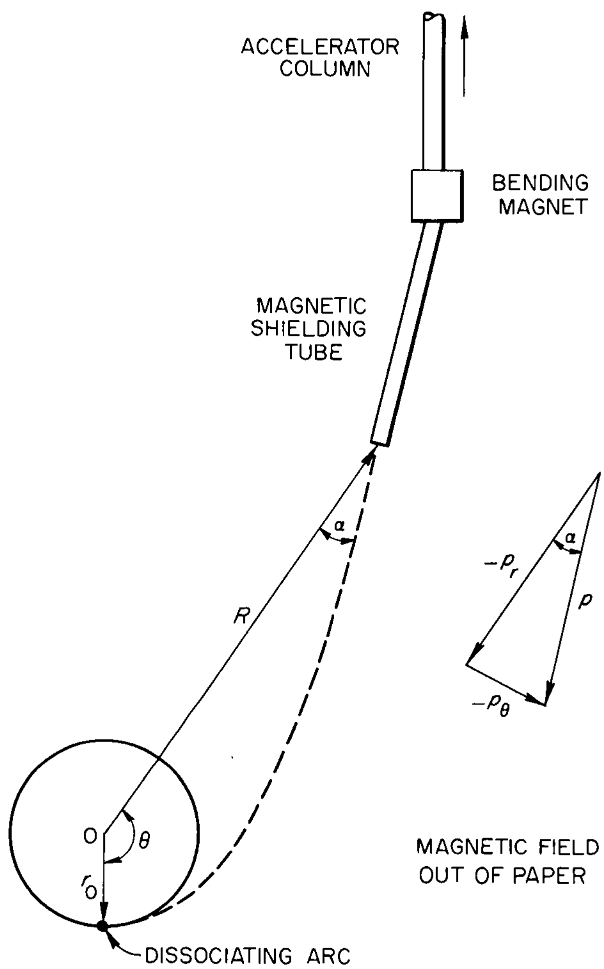

Fig. G.1.1. Entry of Molecular Ion Beam Into DCX.

G.2 GENERAL DEVELOPMENT

We use cylindrical coordinates and introduce the vector potential (which has only an azimuthal component and will be denoted simply by A, just as the magnetic field has only an axial component and will be denoted by B):

(G.2.1) $$A(r) = \frac{1}{r} \int_0^r r' B(r')\, dr' \; .$$

The expression has been evaluated by numerical integration over measured field values. Plots of $A(r)$ and $B(r)$, both normalized by the value of B on the axis, $B(0)$, are shown in Fig. G.2.1.

Recalling the expression relating momentum, magnetic field strength, and radius of curvature for a charged particle in a magnetic field,

(G.2.2) $$Br = \frac{cp}{e} \; ,$$

UNCLASSIFIED
ORNL-LR-DWG 26006

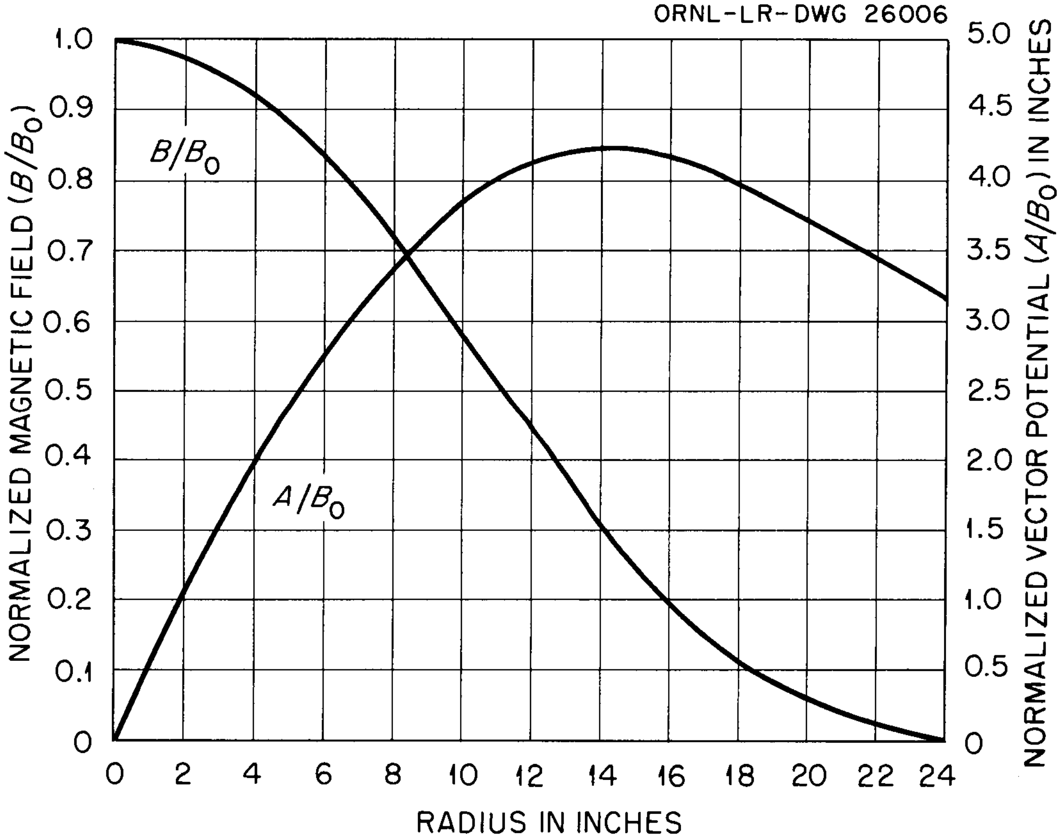

Fig. G.2.1. DCX Midplane Field.

we specify momentum in units of field strength times length. A convenient relationship for a deuteron is

$$p = 2.54\sqrt{E} \ , \tag{G.2.3}$$

where p is in kilogauss-inches and E is in kilo-electron volts.

Useful constants of the particle's motion are the magnitude of the momentum p and the canonical angular momentum C,

$$C = r\,A(r) + rp_{\theta} \ , \tag{G.2.4}$$

where p_{θ} is the azimuthal component of total momentum, with the positive sense defined by the direction of A.

We can now specify α (see Fig. G.1.1), the angle between r and the direction of motion of the particle:

$$\sin\alpha(r) = \frac{-p_{\theta}}{p} = \frac{-(C/r) + A(r)}{p} \ . \tag{G.2.5}$$

The important point in the argument is that $\sin\alpha$ is a function only of r. Thus, the values of C and p may be specified by the conditions of dissociation, and Eq. G.2.5 may then be used to determine α at the exit of the magnetic shielding tube.

The dissociation azimuth may be calculated by noting that

$$\frac{r\,d\theta}{dr} = \tan\alpha(r) \ , \tag{G.2.6}$$

which leads to

$$\theta(R) - \theta(r_0) = \int_{r_0}^{R} \tan\alpha(r)\,\frac{dr}{r} \ . \tag{G.2.7}$$

Once more the integration is numerical.

The integrand has a singularity for the case of tangential approach to the circle at r_0. The portion of the integral near r_0 must then be computed by a series expansion. For the special case of dissociation that leads to a deuteron with orbit concentric with the magnetic axis, for which $B(r_0)r_0 = \frac{1}{2}\,p_{\text{mol ion}}$,

$$\theta(r_0[1+\epsilon]) - \theta(r_0) = 2\sqrt{\epsilon}\left(1 - \frac{5+2n}{24}\,\epsilon + \frac{369 - 124n + 36n^2}{1920}\,\epsilon^2 + \ldots\right) \ , \tag{G.2.8}$$

where

$$n = -\frac{r_0}{B(r_0)}\left.\frac{dB}{dr}\right|_{r=r_0}$$

G.3 EXAMPLES

Example 1. – For an orbit through the axis, $C = 0$, and Eq. G.2.5 reduces to

(G.3.1)
$$\sin \alpha = \frac{A(r)}{p} \; .$$

The momentum may be specified by either the desired injection energy or the distance of maximum departure of the residual deuteron from the axis. At this distance, r_m,

(G.3.2)
$$p_d = A(r_m) \; .$$

Thus for the incoming ion

(G.3.3)
$$\sin \alpha (R) = \frac{A(R)}{2A(r_m)} \; .$$

It will be noted in Fig. G.2.1 that $A(r)$ is peaked in the vicinity of the mean coil radius. The position of the peak is a point of no return; particles passing through the origin with $p > A_{max}$ will not be contained by the field.

Example 2. – If dissociation takes place at the point of closest approach to the axis ($r = r_0$), for which $p_r = 0$,

(G.3.4)
$$\frac{C}{r_0} - A(r_0) = p_{\text{mol ion}} = -2p_d \; .$$

Thus

(G.3.5)
$$\sin \alpha (R) = \frac{r_0}{R} + \frac{1}{2p_d} \left[A(R) - \frac{r_0}{R} A(r_0) \right] \; .$$

For deuteron orbits concentric with the axis,

(G.3.6)
$$p_d = B(r_0) r_0$$

and

(G.3.7)
$$\sin \alpha = \frac{r_0}{R} + \frac{1}{2B(r_0)} \left[\frac{A(R)}{r_0} - \frac{A(r_0)}{R} \right] \; .$$

For an injection energy of 600 kev and for a mid-point field of 9.6 kilogauss, Eqs. G.2.3 and G.3.6 and Fig. G.2.1 give $r_0 = 5.4$ in., and Eq. G.3.7 gives $\alpha = 23$ deg. The configuration looks roughly like Fig. G.1.1.

G.4 FOCUSING

We consider two orbits which originate at a distance R from the axis with inclinations α and $\alpha + \Delta\alpha$, parallel and separated by a small distance d (see Fig. G.4.1a). These will represent extreme rays of an initially parallel beam whose separation at the point of dissociation will be computed. From Eq. G.2.4,

(G.4.1) $$\Delta C = -pd \ .$$

For tangential approach at the dissociation point, that is, $p_r(r_0) = 0$,

(G.4.2) $$\Delta C = -p \ \Delta r + \frac{\delta}{\delta r}(rA) \ \Delta r \ ,$$

or

(G.4.3) $$= (-p + r_0 B) \ \Delta r \ .$$

Thus, the ultimate separation of the extreme beams is

(G.4.4) $$\Delta r = \frac{d}{1 - r_0 B(r_0)/p} \ .$$

Injecting the residual deuteron into a concentric orbit permits use of Eq. G.3.6 and leads to

(G.4.5) $$\Delta r = 2d \ .$$

That is, the beam size for a parallel beam may be expected to be doubled, radially. There will be some z-wise compression. The difference in azimuth between the respective points of closest approach affects only higher orders in the calculation.

We may also calculate the convergence necessary for a beam to be focused at the dissociation point. For two orbits, one with $p_r = 0$ at $r = r_0$ and the other rotated through an infinitesimal angle ϵ (see Fig. G.4.1b),

(G.4.6) $$\begin{aligned} \Delta C &= p r_0 \, (1 - \cos \epsilon) \\ &\cong \tfrac{1}{2} \, p r_0 \, \epsilon^2 \\ &\cong 0 \ . \end{aligned}$$

At R, the orbits will have a separation d and a relative inclination δ:

$$\Delta C \cong -pd + pR \ \delta \cos \alpha = 0 \ ,$$

giving

(G.4.7) $$\delta = \frac{d}{R \cos \alpha} = \Delta\alpha \ .$$

This equation may be expressed as a theorem: If an ion beam entering a circularly symmetrical axial magnetic field is to be focused (radially) at its distance of closest approach to the axis, its convergence must be such as to focus it at its distance of closest approach in the absence of a field.

The case of a beam which cuts the axis may be treated in the same way; the conclusions are that an initially parallel beam remains the same size where it crosses the axis, and that the focusing theorem still holds.

[redacted]
ORNL-LR-DWG 26167

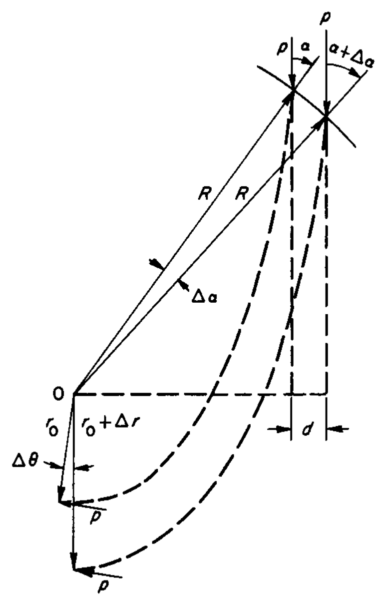

(a) RADIAL SEPARATION OF INITIALLY PARALLEL ION PATHS

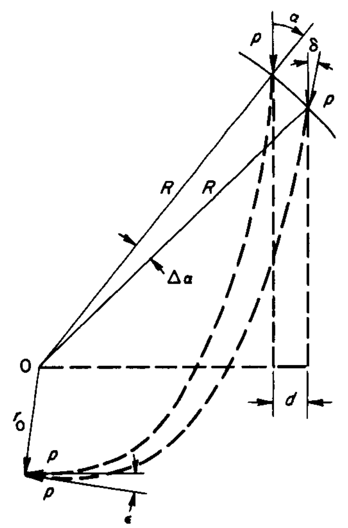

(b) CONVERGENCE NECESSARY TO GIVE A RADIALLY FOCUSED BEAM

Fig. G.4.1. Diagram To Illustrate Focusing Calculations.

G.5 REMARKS ON CONTAINMENT

The magnetic field necessary to contain a circulating concentric ring of 300-kev deuterons in the DCX mid-plane corresponds to an axial field value not much under 8 kilogauss. However, for a marginal field, we may expect that the very gentlest of scattering collisions will cause an ion to be lost. It is, therefore, of some interest to calculate the size of a (mid-plane) scattering angle which can be tolerated.

A bound eccentric orbit will be characterized by apsidal points. At these points, $p_r = 0$, $p_\theta = -p$, and Eq. G.2.4 gives:

$$\frac{C}{p} = \pm r + r\frac{A}{p} , \tag{G.5.1}$$

in which the minus sign pertains to a point at which the orbit is concave toward the axis, that is, for both apses of an orbit which encircles the axis. For such an orbit, for the DCX field, C is negative.

Plots of Eq. G.5.1 for three different values of $B(0)/p$ are shown in Fig. G.5.1. These correspond, for 300-kev deuterons, to values of $B(0)$ of 8, 9.6, and 12 kilogauss. Clearly, containment of an ion requires that its C/p fall on an ordinate which is cut three times by the appropriate curve. The turning points are specified by the inner two intersections, while the outer one gives the distance of closest approach for a particle entering from outside. The constraint, Eq. G.3.2, on orbits which cut the axis is a special case of Eq. G.5.1.

We may now determine the permissible scattering angle for a concentric orbit (minimum C/p) by calculating the change in C corresponding to a scattering angle θ. Using Eq. G.2.5 and noting that θ is the complement of α as defined there, we obtain

$$\frac{\Delta C}{p} = r(1 - \cos\theta) . \tag{G.5.2}$$

The maximum permissible $\Delta C/p$ for 8 kilogauss is seen in Fig. G.5.1 to be 0.15 in., corresponding to a scattering angle of 12 deg. A 20% increase in the field brings the permissible scattering angle up to 58 deg. This is comparable with the scattering angle necessary for entering the mirror cone, suggesting that a further field increase would be less profitable.

UNCLASSIFIED
ORNL-LR-DWG 26007

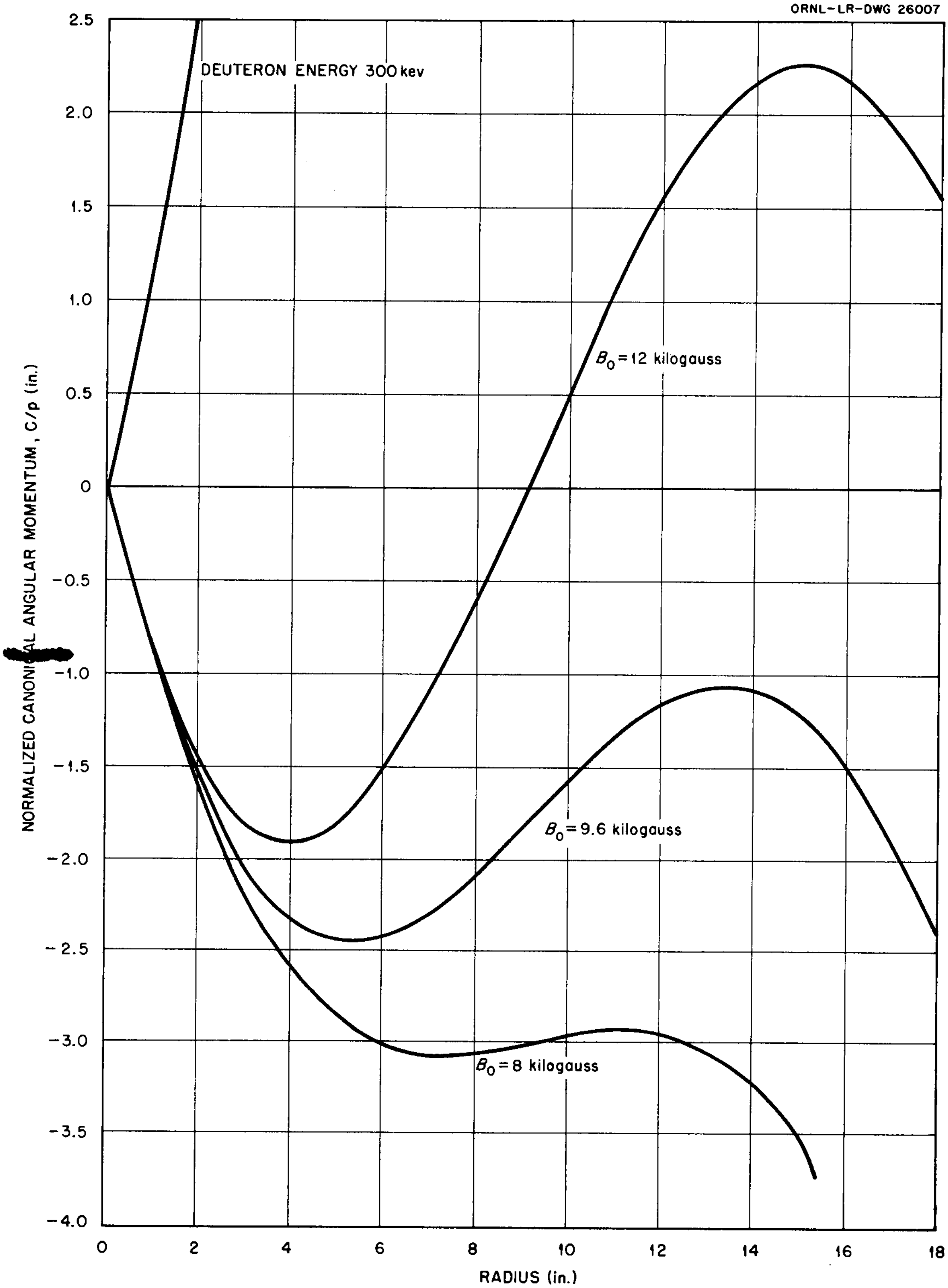

Fig. G.5.1. Normalized Canonical Angular Momentum.

Appendix H

MODE II IN A MIRROR GEOMETRY

R. V. Neidigh

As a result of consideration of the use of Mode II (see Sec 12.1) to fill a thermonuclear container, an experiment has been conducted to test the basic feasibility of Mode II injection into a mirror field. A hollow iron cylinder, placed as shown in a normally uniform magnetic field, will distort the flux lines as shown in Fig. H.1.1. With this apparatus, it was possible to obtain a magnetic field strength at the vacuum chamber wall approximately twice that within the iron cylinder.

The position of the Mode II arc was adjusted so that the origin of the energetic ions was between the mirrors. From the sputtering patterns on the end walls and on the iron, it appeared that some of the ions were multiply reflected by the mirrors. The ion current to a probe just inside the iron cylinder, but just outside the orbit of the most energetic ions, was used to record the decay of the plasma. The decay time could be determined by establishing a zero (the time when the Mode II arc forming the energetic ions was extinguished). For the conditions of the experiment, the decay time was found to vary from 50 to 250 μsec (see Fig. H.1.2). The upper trace in each photograph is from a probe in the arc which determined when the arc was turned off. The lower trace indicates the ion current to the probe just outside the plasma. Although the calculated and the measured values for the decay time are not in good agreement, the decay time does vary inversely with the density of neutral gas, as expected. Incandescent carbon particles could be seen when the plasma was at maximum density.

[redacted] ORNL-LR-DWG 26008

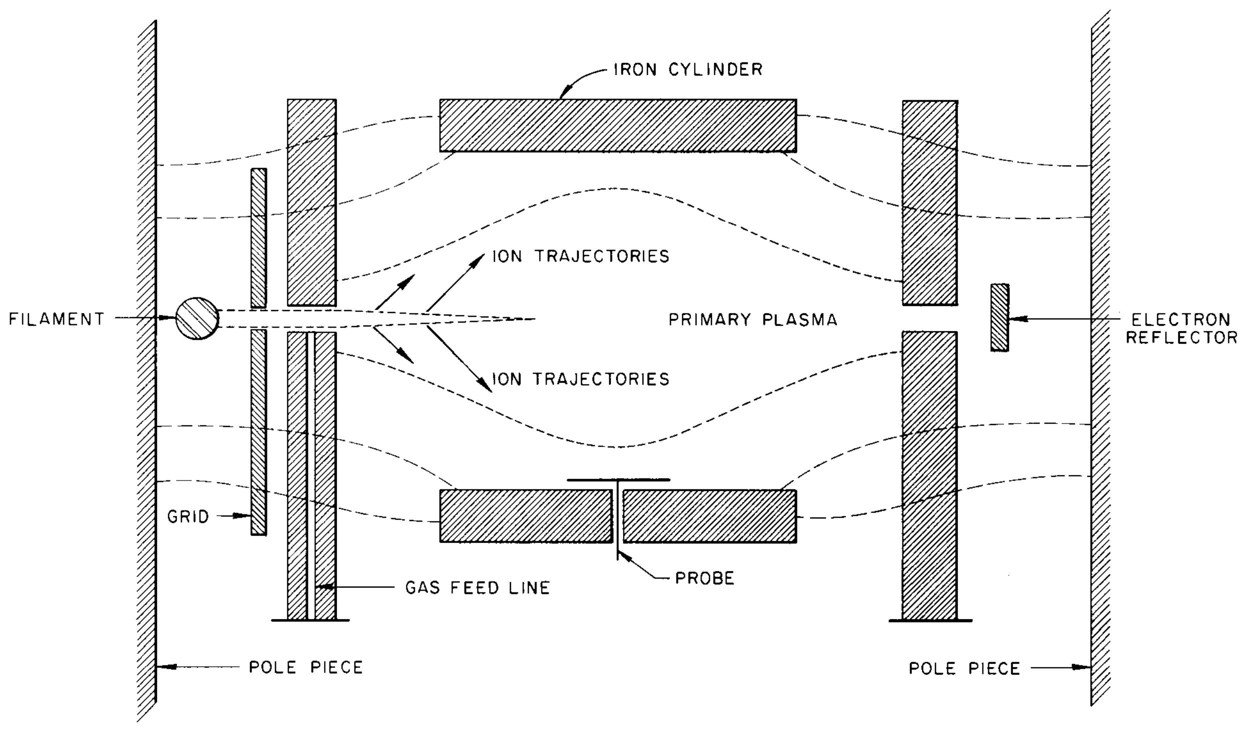

Fig. H.1.1. The Mode II Arc Between Magnetic Mirrors.

[redacted]

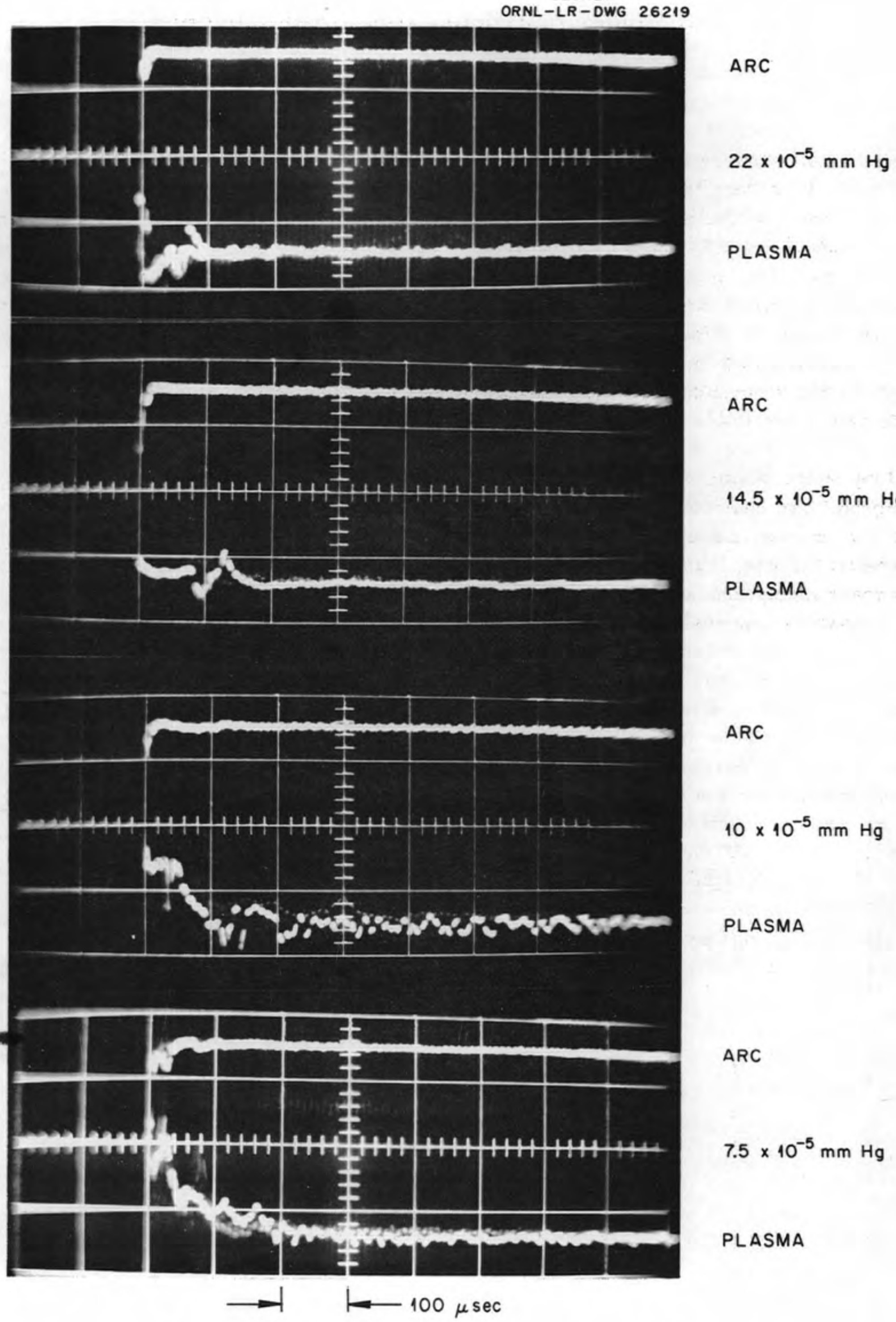

MAGNETIC FIELD APPROXIMATELY 7700—5000—7700 gauss

Fig. H.1.2. Decay of Plasma Formed by Mode II Arc in Mirror Field.

Appendix I

[redacted]

A HIGH-ENERGY DEUTERIUM ARC: INTERIM REPORT

P. R. Bell J. S. Luce

ABSTRACT

A 150-amp deuterium arc using a "cup" anode has been operated at a pressure of 5×10^{-5} mm Hg. Several impurities were present. Fifteen per cent of a 20-kev D_2^+ beam was dissociated ($D_2^+ \longrightarrow D^+ + D^0$) when it was passed through the arc.

A carbon arc is used at Oak Ridge National Laboratory to "break up" (dissociate and/or ionize) D_2^+ ions[1-3] and create a hot plasma. Despite the many desirable characteristics of the carbon arc, a basic disadvantage exists. Bremsstrahlung losses are a serious handicap in any thermonuclear device. Material having a high atomic number, such as carbon, will certainly increase these losses. Early experiments in which deuterium arcs were used to dissociate energetic molecular ions were unsuccessful. It was not possible to measure any dissociated ($R/2$) beam, and losses in the D_2^+ beam were large. The effective breakup and low pressure achieved with the carbon arc[1] caused curtailment of work on deuterium arcs. Recent modification of the anodes used with deuterium arcs has permitted operation at much lower pressure (5×10^{-5} mm Hg) than was formerly possible, and 15% dissociation of a 20-kev D_2^+ beam was immediately achieved. A long cylindrical tungsten anode was used, and the gas was fed directly into the end of the anode.

In operation, the arc fills the inside of the cylinder and impedes the flow of gas. It is this anode design that permits operation of the arc at low pressure. Since all the gas must pass through the section of the arc inside the anode, ionization is essentially complete.

Even with complete ionization, the diffusion and recombination of positive ions usually causes an untenable high pressure of neutral gas in the working volume. In the high-energy deuterium arc, there is an electrical gradient which accelerates the ions along the magnetic field toward the cathode. Since the motion of the ions is not random but carries them rapidly toward the

---

[1] J. S. Luce, *Ionization and Dissociation of Energetic Ions by a Carbon Discharge – Status Report*, ORNL-2219 (Jan. 1957).

[2] C. F. Barnett, R. J. Mackin, Jr., and J. A. Ray, *Dissociation of H_2^+ and D_2^+ by a Vacuum Carbon Arc*, ORNL-2420 (Dec. 6, 1957) (this report, Appendix C).

[3] A. Simon and M. Rankin, *Some Properties of a Steady State High-Energy Injection Device (DCX)*, ORNL-2354 (Aug. 26, 1957) (this report, Appendix A).

[redacted]

ORNL-LR-DWG 26304

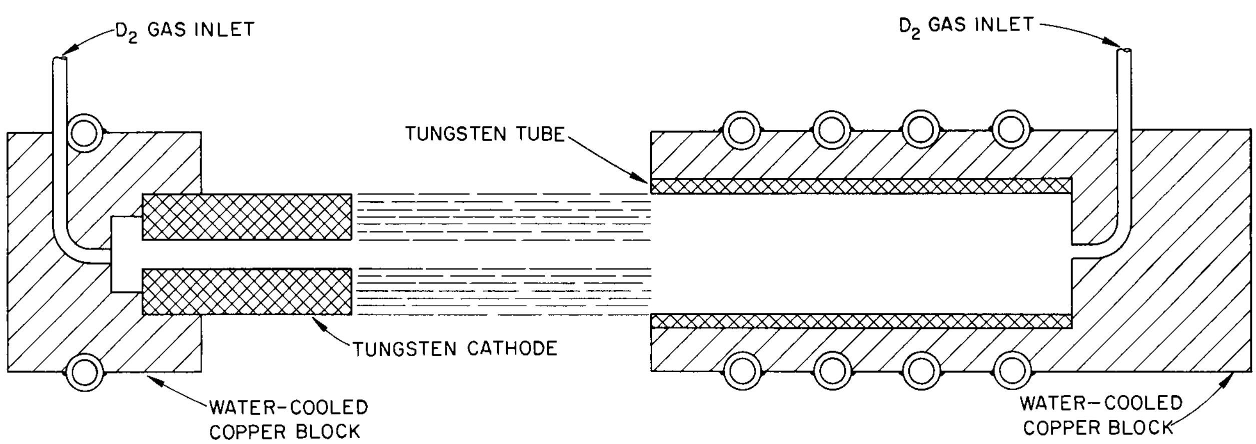

cathode, diffusion and recombination will be greatly reduced. To exploit this advantage, it will be necessary to move the cathode and to install baffles between it and the working volume. A large number of the ions that are accelerated into the cathode and that recombine will then be prevented from flowing back as neutral particles. Differential pumping must be provided to remove the neutrals formed at the cathode. It may be necessary to install a similar baffle system at the anode.

While very little work has been done on this arc, a few of its characteristics have been observed. The arc color oscillates between blue and red. It is thought that the arc is changing between the molecular and atomic states. At high pressure, the anode becomes heated at the end nearest the cathode. As the pressure decreases, the hot spot moves down the barrel of the anode. It has been postulated that this hot region results from electrons slowing down in the gas, causing an increase in the space potential at that point. The heating is so severe that in one test a hole was melted in the side of the anode and molten tungsten was spewed in the tank (Fig. I.1.1). It is interesting to note that primary electrons must cross the magnetic field to reach the walls of the anode. Very little wear was found at the end of the anode, indicating that most of the electrons were stopped in the region of high space potential. It is necessary to use relatively high pressure to strike the arc. As the pressure is decreased, the arc voltage rises and the current falls. At a critical point, the voltage jumps and the current falls rapidly. In this high-voltage stage, the arc is unstable. Figures I.1.2 and I.1.3 show the current and voltage characteristics as a function of pressure. An arc current of 150 amp was required in order to achieve 15% breakup of

UNCLASSIFIED
T-13586

Fig. I.1.1. Damaged Tungsten Anode. (Secret with caption)

[redacted]
ORNL-LR-DWG 26083

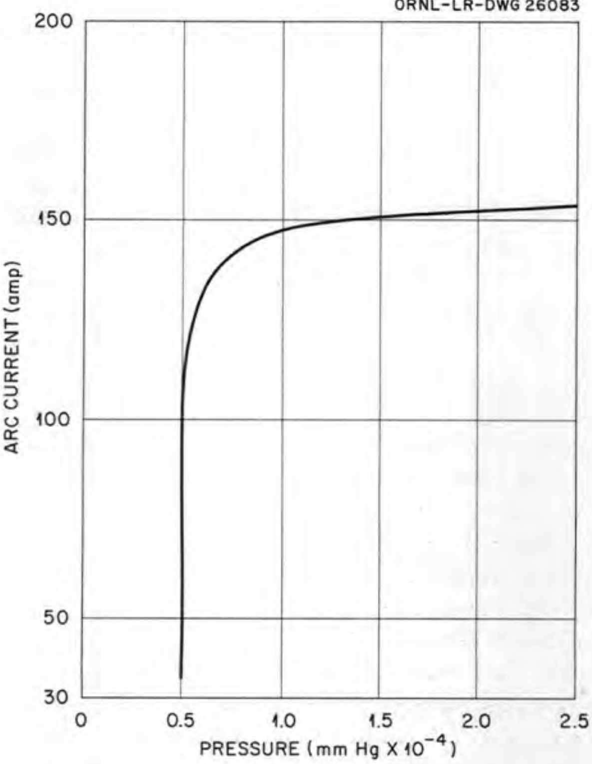

Fig. I.1.2. Current Characteristics of Deuterium Arc.

[redacted]
ORNL-LR-DWG 26084

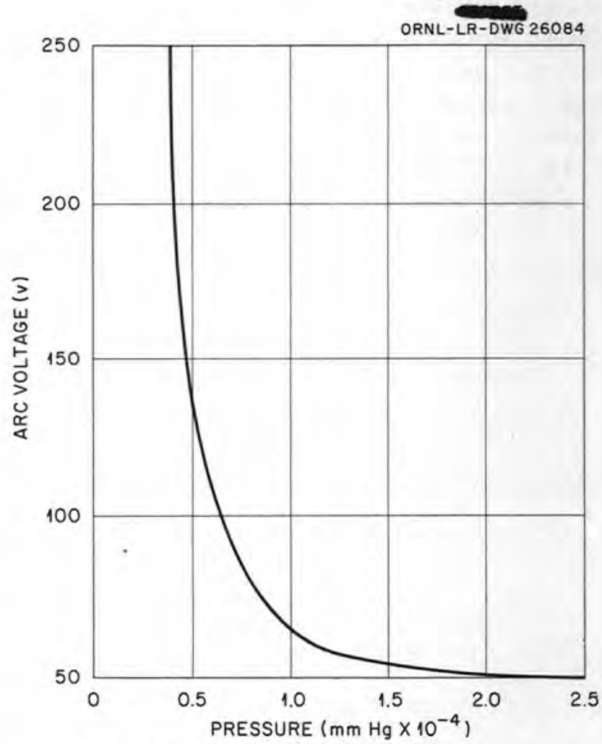

Fig. I.1.3. Voltage Characteristics of Deuterium Arc.

20-kev D_2^+ ions that were passed through the arc.

Several improvements are planned for the near future. The anode will be water-cooled to reduce impurities and prevent burning through the anode wall. An axial coil will be installed around the base of the anode to produce a mirror magnetic field. This geometry should reduce the number of electrons that reach the walls of the anode. Better electron utilization and reduced heating should result from this magnetic configuration.